REPORT DOCUMENTATION PAGE

Form Approved
OMB No. 0704-0188

1. REPORT DATE *(DD-MM-YYYY)*	**2. REPORT TYPE**	**3. DATES COVERED** *(From - To)*
23-02-2011	Final Performance Report	From 09-02-2009 To 23-02-2011

4. TITLE AND SUBTITLE

(NANOSAT FY09) MIT ORBITAL TRANSFER VEHICLE (MOTV)
(CASTOR Satellite: Design Document)

5a. CONTRACT NUMBER

5b. GRANT NUMBER
FA9550-09-1-0056

5c. PROGRAM ELEMENT NUMBER

6. AUTHOR(S)

Dr. David W. Miller

5d. PROJECT NUMBER

5e. TASK NUMBER

5f. WORK UNIT NUMBER

7. PERFORMING ORGANIZATION NAME(S) AND ADDRESS(ES)

MASSACHUSETTS INSTITUTE OF TECHNOLOGY
77 Massachusetts Avenue
Cambridge, MA 02139-4307

8. PERFORMING ORGANIZATION REPORT NUMBER

9. SPONSORING / MONITORING AGENCY NAME(S) AND ADDRESS(ES)

AFOSR / RSE
875 North Randolph Street, Suit 325
Room 3112
Arlington, Virginia 22203-1768

10. SPONSOR/MONITOR'S ACRONYM(S)

AFORS/RSE

11. SPONSOR/MONITOR'S REPORT NUMBER(S)
AFRL-OSR-VA-TR-2012-0507

12. DISTRIBUTION / AVAILABILITY STATEMENT

1) DISTRIBUTION STATEMENT A: Approved for public release; distribution is unlimited

13. SUPPLEMENTARY NOTES

14. ABSTRACT

This design document describes the current status of the Cathode/Anode Satellite Thruster for Orbital Repositioning (CASTOR), which is at the Critical Design Level.

The mission of CASTOR is to validate the performance and application of Diverging Cusped Field Thruster (DCFT) technology. The mission will be achieved by taking on- orbit state data to compare the degradation experienced by the DCFT to that of similar technologies. Specifically, the mission objects, with corresponding minimum success criteria are shown below:

- Operate the DCFT on orbit for 1500 hours, which is comparable to similar technologies
- Minimum Success: Demonstrate that the DCFT will operate on-orbit
- Measure the on-orbit performance, efficiency, and degradation of the DCFT during orbital maneuvers
- Minimum Success: Use the DCFT to provide a measurable change in velocity

15. SUBJECT TERMS

CASTOR, Cathode/Anode Satellite Thruster for Orbital Repositioning, Power, Propulsion, Science and Payload, ADCS, Communication, Avionics, Structures, Thermal

16. SECURITY CLASSIFICATION OF:			**17. LIMITATION OF ABSTRACT**	**18. NUMBER OF PAGES**	**19a. NAME OF RESPONSIBLE PERSON**
a. REPORT	**b. ABSTRACT**	**c. THIS PAGE**			Kent Miller, RSE (Program Manager)
U	U	U	UU		**19b. TELEPHONE NUMBER** *(include area code)* 703.696.8573

Standard Form 298 (Rev. 8-98)
Prescribed by ANSI Std. Z39.18

CASTOR Satellite

Design Document

16.83x Class

November 18, 2010

TABLE OF CONTENTS

LIST OF FIGURES

LIST OF TABLES

1 SYSTEMS LEVEL DESIGN SUMMARY

1.1 CASTOR OVERVIEW (J. JAMES AND J. ROBINSON)

This design document describes the current status of the Cathode/Anode Satellite Thruster for Orbital Repositioning (CASTOR), which is at the Critical Design Level.

The mission of CASTOR is to validate the performance and application of Diverging Cusped Field Thruster (DCFT) technology. The mission will be achieved by taking on-orbit state data to compare the degradation experienced by the DCFT to that of similar technologies. Specifically, the mission objects, with corresponding minimum success criteria are shown below:

- Operate the DCFT on orbit for 1500 hours, which is comparable to similar technologies
    - Minimum Success: Demonstrate that the DCFT will operate on-orbit
- Measure the on-orbit performance, efficiency, and degradation of the DCFT during orbital maneuvers
    - Minimum Success: Use the DCFT to provide a measurable change in velocity

1.2 UNIVERSITY NANOSAT PROGRAM (UNP) (C. CROWELL)

The CASTOR satellite is being designed with the support of the AFOSR University Nanosat Program (UNP) and the Air Force Research Lab Space Vehicles Directorate (AFRL/RV). The UNP office provides support in terms of expert telecons, design reviews, workshops, funding, and a sponsorship for a launch (through the Space Test Program‘s (STP‘s) SERB process) to the winning university. MIT is one of 11 universities participating in UNP-6. The UNP competition began in January 2009 and will conclude in January 2011. Inside of these terms, the UNP timeline includes the following major design reviews:

- SCR – Systems Concept Review (March 2009 via Telecon)
- SRR – Systems Requirement Review (April 2009 via Telecon)
- PDR – Preliminary Design Review (August 2009, Logan, UT)
- CDR – Critical Design Review (April 2010, MIT)
- PQR – Proto-Qualification Review (August 2010, Logan, UT)
- FCR – Flight Competition Review (January 2011, Albuquerque, NM)

At FCR, each university will have a 15 minute presentation and then a hardware station afterwards and groups of judges will evaluate the final design and choose the winner. All previous reviews can be found in section 4.2 in the fileshare. Additional UNP activities include the Student Hands-on Training (SHOT) workshops in the summer of 2009 and 2010 at the University of Colorado-Boulder. This consisted of building a small payload for a high

altitude balloon flight. Another UNP event is the fabrication class, which occurred in January 2010 at Kirtland AFB, NM. UNP provided resources, expertise, and experience for the design of CASTOR. Additionally, the UNP User's Guide outlines several requirements and guidelines that the satellite needs to be built to. Any departure from the requirements outlined by the UNP office will require waivers to be submitted and approved.

1.3 OVERALL ARCHITECTURE (J. JAMES AND R. MCLINKO)

Eight subsystems comprise the satellite. These are Power, Propulsion, Science and Payload, ADCS, Communication, Avionics, Structures, and Thermal. Each subsystem has a team of students who work on improving and testing that system. A ninth team, known as the Systems team, acts to unify the subsystems.

1.3.1 APPROACH

The Systems team is responsible for determining the overall architecture of the CASTOR system. The optimal shape, size, mass, and other driving factors of the spacecraft are determined from the University Nanosatellite Program guidelines, the 16.83 designs of the subteams, UNP PDR and CDR feedback, and constraints provided by the faculty. Furthermore, as it becomes necessary to decide between two conflicting subsystem choices, the Systems team is responsible for negotiating a solution between the conflicting subsystems. The design presented below is the current architecture of CASTOR.

1.3.2 CURRENT ARCHITECTURE

Figure 1.3-1 shows the overall structure. A central propellant tank is surrounded by structural trusses to which CASTOR's other components are mounted. The spacecraft is then mounted with the ESPA ring to the fore end of the spacecraft (inside for launch configuration) and attached inside a volume that marginally exceeds UNP constraints (allowing for a 50 cm x 50 cm x 60 cm satellite). The maximum wet mass of the satellite is 50 kg, meeting UNP mass constraints.

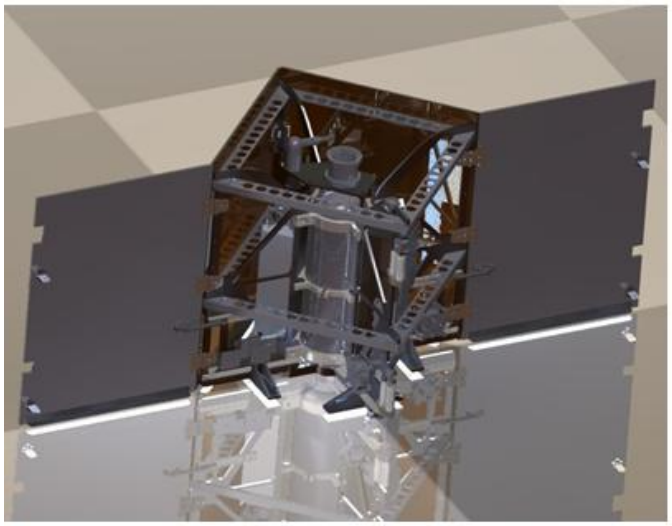

FIGURE 1.3-1: CONFIGURATION (DEPLOYED) WITH MASS MOCKUPS

Subsystem architectures for the current system are outlined below:

- **Structures:** Four trusses mount around the propellant tank using three tank clamps. The ESPA ring mount attaches to the bottom of the trusses; two of the solar array panels are body-mounted directly to the trusses, and the other two solar panels mount to opposing trusses with a hinge. The solar arrays deploy using linear actuators that release pins in the panels.
- **Thermal:** A number of components require surface treatments of Z93 (a white paint) in order to maintain operational temperatures. Temperature sensors will also be used to track the thermal state of the satellite, though passive control shall be the primary mode of operation.
- **Operations:** The HETE ground station at Cayenne will be used. Pre-launch and launch operations are compiled in the Concept of Operations Document (ConOps). The on-orbit operations will be performed as follows: detumble, solar panel deployment, commissioning, system verification (standard orbit operations), decommissioning, and finally end of life via uncontrolled re-entry. Orbital maneuvers will be performed in LEO to demonstrate high delta-v capability via orbital altitude changes.
- **ADCS:** Attitude determination will be performed with four Sinclair sun sensors, two PNI Corporation 3-axis magnetometers, and a 3-axis gyro. Attitude control will be performed with three reaction wheel assemblies in each orthogonal thrust axis and three torque coils in each orthogonal axis. GPS navigation will be used for GNC using a space-rated SSTL GPS receiver. Furthermore, a NORAD TLE is provided for free on a daily basis for a cross check. Furthermore, a magnet will be placed opposite the engine to cancel the engine dipole.
- **Avionics:** The backbone of the avionics subsystem consists of three Microchip dsPIC33F 16-bit microcontrollers and a FLASH memory device.

These components are accompanied by sensors and actuators, while running FreeRTOS.

- **Communications:** Two Microhard S-band modems will support two patch antennas to provide 115 Kbps data rate capability.
- **Propulsion:** A modified field thruster built in-house will operate in either high power mode, providing about 4 mN of thrust, or in off mode, in which the cathode will remain heated. The propulsion system will also consist of the tank and various plumbing components. The thruster will be mounted on the opposite end from the ESPA ring mount. Plumbing will be provided largely by a NASA-provided flow controller, the Xenon Feed System (XFS).
- **Power:** Donated Loral cells with an area of 1.1 m^2 will provide a maximum of 160 W to the Maximum Peak Power Tracker, which will provide power to the various components as needed and to Nickel-Cadmium batteries for storage during eclipse. Furthermore, in-house assembled Power Processing Unit and Power Distribution Unit will provide power to propulsion and all other systems, respectively.
- **Science and Payload:** A camera pointed at the cathode and thruster provides critical information on degradation of the thruster and performance of the cathode during the firing phase. A shutter protects the lens from damage when the camera is not taking photos. The color of the plume in the image provides information on thruster efficiency.

1.4 MISSION REQUIREMENTS (K. ANDERSON)

CASTOR's requirement verification matrix (RVM) provides the list of requirements that CASTOR needs to fulfill and which provide direction when deciding upon a design. In addition to this function, the RVM provides an understanding between all parties involved, mainly the CASTOR group and UNP, of what exactly the satellite will do.

The requirements come from UNP guideline, interfacing requirements, or requirements needed in order to fulfill the mission statement. The requirements that originate from the mission statement should carry through all of the subsystems to allow for requirement traceability and ensure that the overarching requirements are met by all the smaller more detailed requirements that it encompasses.

The mission requirements are stated as follows:

- Measure the on-orbit performance, efficiency, and degradation of the DCFT during orbital maneuvers
- Operate the DCFT simultaneously in the operational space environment and a vacuum chamber

The system requirements stem from the mission requirements and are stated as follows:

- CASTOR shall have a DCFT as the primary propulsion system, which shall operate throughout the mission lifetime
- The CASTOR bus must be able to support on-orbit mission operations for the mission lifetime of at least 6 months
- CASTOR shall provide sufficient state data to measure the change of performance, efficiency, and degradation over the DCFT's operational lifetime

In addition to stating each of the requirements, the requirements verification matrix lists the document that shows how that requirement was met and the test that verified it was met. For instance, the requirement: "EPS must be able to generate 113.7W in a fully operational state"; is met in the Design Documentation and tested in the solar panel test.

The requirements verification matrix also states the status of meeting a particular requirement. If the satellite has been designed in a way that the requirement should be met, and not tested it is yellow. If it has been tested and verified it is green. If it hasn't been designed or the current design doesn't meet the requirement, the column is red. The RVM currently is all green and yellow meaning that the current design meets all of the requirements, but hasn't been fully verified, the appropriate status for CDR.

The RVM has all of the requirements listed, and each of these requirements is met through the design. All of the requirements have a verification document listed, and the tests that have been performed and the results have been written, the entire requirement row is filled. The RVM is listed in Appendix **Error! Reference source not found.**.

1.5 TEAM ORGANIZATION (J. JAMES)

In order to allow specialization, work on CASTOR is divided into teams. The organizational structure of teams shown in Figure 1.5-1 allows for the efficient flow of information between these subsystems. The chart outlines the Spring 2010 personnel as well as indicating their involvement in various teams. Lines linking the members of the Systems Team to sub-teams show how systems members act as liaisons to the various teams.

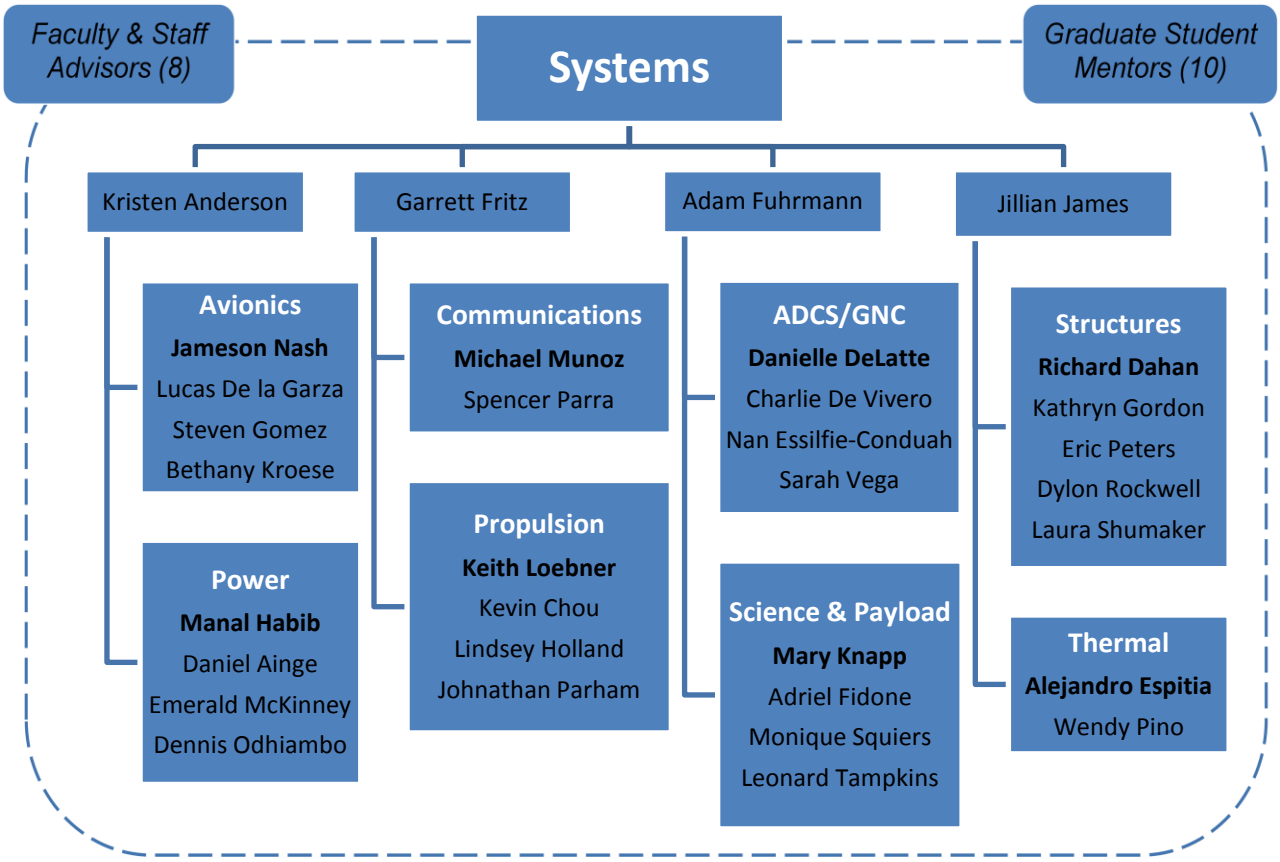

FIGURE 1.5-1: CASTOR ORGANIZATION

Figure 1.5-1 highlights the nine CASTOR sub-systems. These teams specialize in various technical aspects of the project. The Systems team, consisting of four primary members, provides the leading management and system interfacing. Additionally, each member of the Systems team acts as a liaison to two sub-teams (illustrated in Figure 1.5-1 by a connecting line). Each sub-team has a team lead (shown in bold), who is held responsible for the deliverables for that team. Both students enrolled in 16.83 and UROPs are included in this diagram. Ten graduate students and eight faculty and staff are spread among the teams providing continual mentorship. Organizational structure allows efficient flow of information from the systems team down to subsystem team, and from subsystems directly to the systems team which can call all subsystems to action. Communication between subsystems is facilitated during weekly team leads meetings (with the systems team) where inter-team issues are addressed. Subsystems are also encouraged to work directly with other subsystems on relevant tasks.

1.6 BUDGET (G. FRITZ)

1.6.1 APPROACH

The Systems team is responsible for tracking CASTOR's mass and cost budget. The goal with this tracking is to ensure that every team is aware of the current state of the satellite and how much funding is still available for purchasing and manufacturing.

1.6.2 ORGANIZATION

The cost and mass budgets for CASTOR are tracked through the use of the Master Equipment List or MEL. This list is an Excel Spreadsheet documenting is component either on the flight model of the satellite or used for testing. It also tracks components that still need to be acquired.

Each subteam has a section of the MEL dedicated to them. Through regular meetings with Systems and the team leads, the MEL is always an up to date representation of the components on the satellite. When any component is updated on the MEL the person responsible for the change will document his name and the date onto that component's row so that others can verify the change in the future. Each team can use the MEL to identify particular part numbers or types of components used by other teams should they need to interface with them in their designs.

Due to the high density of presentations over the past few months, the MEL has been equipped with the functionality of rapidly and easily producing charts and tables to represent the components on the list on a team-by-team basis. The new tab labeled "Graphs and Tables" only requires the user input of changing a drop down box to represent the appropriate team and the table and graph will automatically update. This will continue to be a useful tool as CASTOR moves forward to document and present the data.

The MEL has the ability to hold independent margins for both cost and mass for every component listed. This allows greater flexibility and accuracy when margining components since there may be better knowledge on one characteristic over the other. For example, a part may have been bought, so cost is exact, but the component has not yet been received and measured in the lab, so mass and power are estimates. The margining scheme is:

Exact (0-5%)

Mass: component has been weighed and integrated into the satellite

Cost: component has been purchased

Fine Estimate (5%-10%)

The mass or cost has been quoted by the manufacturer or found on a specification sheet.

Coarse Estimate (15% - 35%)

Number based on SMAD or other approximation not yet verified by manufacturer.

Guess (35% +)

The component is still largely unknown, such as bolts/nuts in the current design.

1.6.3 BUDGET TRACKING

Systems with the assistance of G. Sondecker also tracks the purchase orders that Professor Bauer receives and updates the MEL part status to "delivered". Furthermore, all purchases must be approved by G. Sondecker and (for purchases over $100) R. McLinko before being submitted to Paul Bauer. Purchases are approved only if the component is listed on the MEL.

The accrued costs of all purchased items are being tracked, not just those of flight hardware. An item is added to the spending tracking sheet once the purchase order has been approved, not when the actual debt has been incurred. This will allow the team to anticipate the need to request more funding in a timely manner, should it become necessary. Purchase orders must be approved by the Systems team in order to prevent unauthorized purchases. A student who wishes to purchase hardware must completely fill out a standardized Purchase Order or PO form. This PO is then sent to G. Sondecker, who then checks the MEL to verify the part is accounted for. If it is, then the PO is submitted to Paul Bauer for purchasing. If the part is not accounted for in the MEL, then it must first be submitted for approval to the MEL before being approved for purchase. If it is subsequently added to the MEL, the PO will then be accepted.

This past March each subteam provided a list of components that still need to be purchased before FCR next January. An estimated $101,108.64 of hardware and test expenditures is anticipated through FCR.

1.6.4 BUDGET ALLOCATIONS

The Systems team uses the allocations assigned to subsystems to hold them accountable for their budgets. Allocations were initially defined based on the preliminary design developed in spring 2008 during the first 16.83x sequence. These allocations have been constantly updated by Systems to allow the design to move forward. Since the design has been actively holding the margined mass constraint of 50 kg, providing additional allocation to one team always meant removing allocation from another. As such, the

Systems team often had to manage trade studies between subteams and negotiate the latest allocations and resulting architecture. At this point in the program, final allocation changes are being determined toward the final design. As such, the masses between subteams are relatively solid and there has been very little fluctuation this term.

1.6.5 CURRENT BUDGET

A summary of the current budget is shown in Table 1.6-1.

	Mass (Kg)	Margined Mass (Kg)	Cost	Margined Cost
ACS & GNC	1.91	2.21	$132,850.00	$148,236.00
Avionics	2.59	3.83	$ 23,010.00	$ 25,311.00
Communications	0.36	0.43	$ 1,255.80	$ 1,400.96
Propulsion	12.23	13.09	$ 1,702.00	$ 1,794.60
Power	9.41	10.10	$ 39,644.50	$ 43,928.95
Thermal	0.34	0.38	$ 4,267.18	$ 4,750.18
Structures	16.70	19.36	$ 1,473.18	$ 1,911.65
Science and Payload	0.10	0.13	$ 7,926.33	$ 8,865.21
Total	43.62	49.54	$212,128.99	$236,198.54

TABLE 1.6-1: CURRENT BUDGET

As is evident from the table, the current CASTOR design is at the margined mass constraint and within the margined cost constraint.

1.7 SCHEDULE (G. FRITZ)

Due to the segment sub-team structure of the CASTOR project it is important to track progress among individual teams. Scheduling is a constantly evolving process with each team developing goals and action items, submitting them to Systems and then getting feedback. This back and forth of checking scheduling allows for a cohesive structure that spans all teams and enhances accountability among the teams.

A representation of the flow of schedule tracking as it is done at CASTOR is represented by Figure 1.7-1.

.

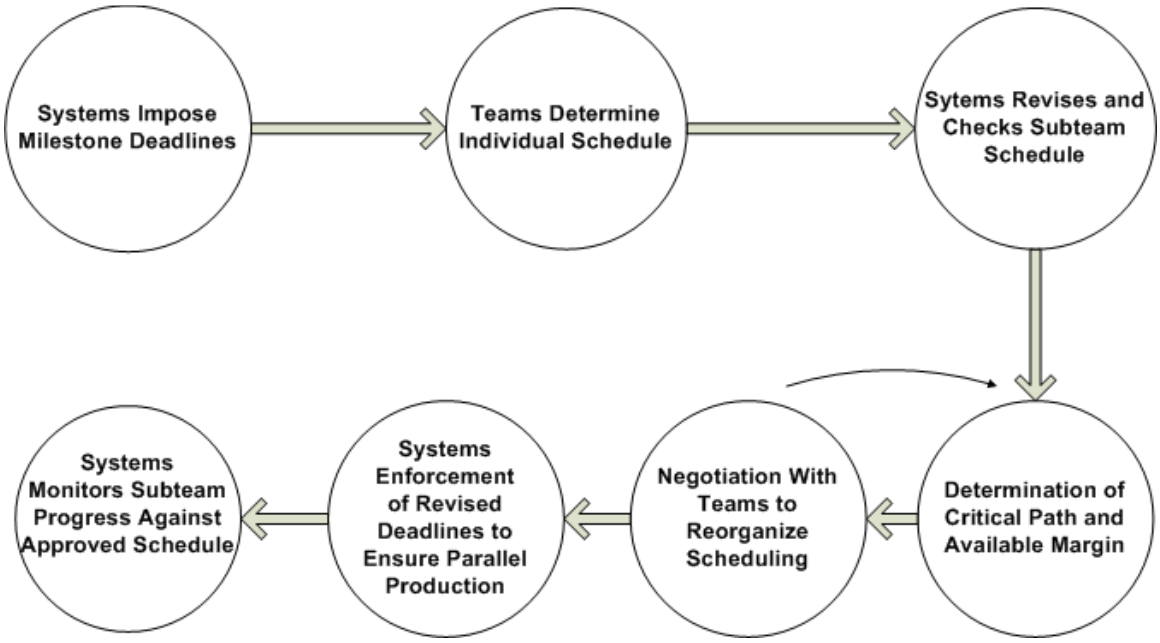

FIGURE 1.7-1: SCHEDULING FLOW CHART

The Systems team is currently operating in the last two bubbles of the flow chart. There has been a recent update to the schedule conducted in March where all predecessor tasks have been identified at a team leads meeting. Now that critical paths have been identified, Systems now needs to ensure that deadlines are being met, and if they are subject to schedule slip, re allocate personnel to help meet the deadline.

The current schedule takes form of a Gantt chart developed as a Microsoft Project. This full schedule can be found under section 1.1 of the fileshare [1]. The basic organization of the chart is by each team sub ordered by start date. The arrows connecting tasks to each other represent tasks that require completion of a previous task before they can begin. These are particularly important for the Systems team to monitor if a predecessor task is going to slip schedule and what tasks will be effected by that. Checks for schedule slip occur at each team leads meeting.

1.8 INTERFACE CONTROL DOCUMENTS (A. FUHRMANN)

The purpose of an ICD is to document and explain all of the possible inputs to and all potential outputs from a system or subsystem. This documentation is helpful not only for the future user of the system, but also for each sub team designing the system. These documents help the designers determine what information they need to request from each team as well as how their design changes may affect the other teams.

Below is a template for the MIT format ICD as well as explanations for each component. Formatting is often times just as important as the technical content because improper formatting can easily make the technical message confusing or completely not interpretable.

The title page gives basic information such as which two components are being discussed.

It may also have instructions for distribution of the information contained in this document.

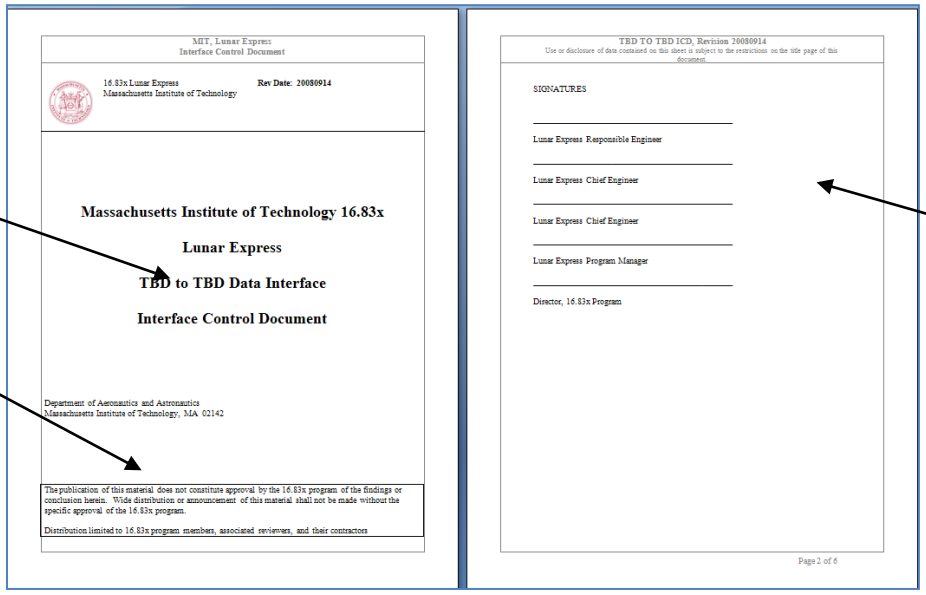

MIT, Lunar Express
Interface Control Document

16.83x Lunar Express
Massachusetts Institute of Technology

Rev Date: 20080914

Massachusetts Institute of Technology 16.83x

Lunar Express

TBD to TBD Data Interface

Interface Control Document

Department of Aeronautics and Astronautics
Massachusetts Institute of Technology, MA 02142

The publication of this material does not constitute approval by the 16.83x program of the findings or conclusion herein. Wide distribution or announcement of this material shall not be made without the specific approval of the 16.83x program.

Distribution limited to 16.83x program members, associated reviewers, and their contractors

TBD TO TBD ICD, Revision 20080914
Use or disclosure of data contained on this sheet is subject to the restrictions on the title page of this document.

SIGNATURES

Lunar Express Responsible Engineer

Lunar Express Chief Engineer

Lunar Express Chief Engineer

Lunar Express Program Manager

Director, 16.83x Program

Page 2 of 6

The signature page needs to have the names of key persons relevant to this document.

These people may be the relevant subsystem team leads, systems lead, chief engineer, etc.

Make sure the table of contents is correct. ICDs are updated frequently and pages are constantly shifting.

List all of the figures and tables as well as their locations for quick reference

While ICD is being created there will be many TBR and TBDs during the system design process. Explicitly document these so that they will not be overlooked later on.

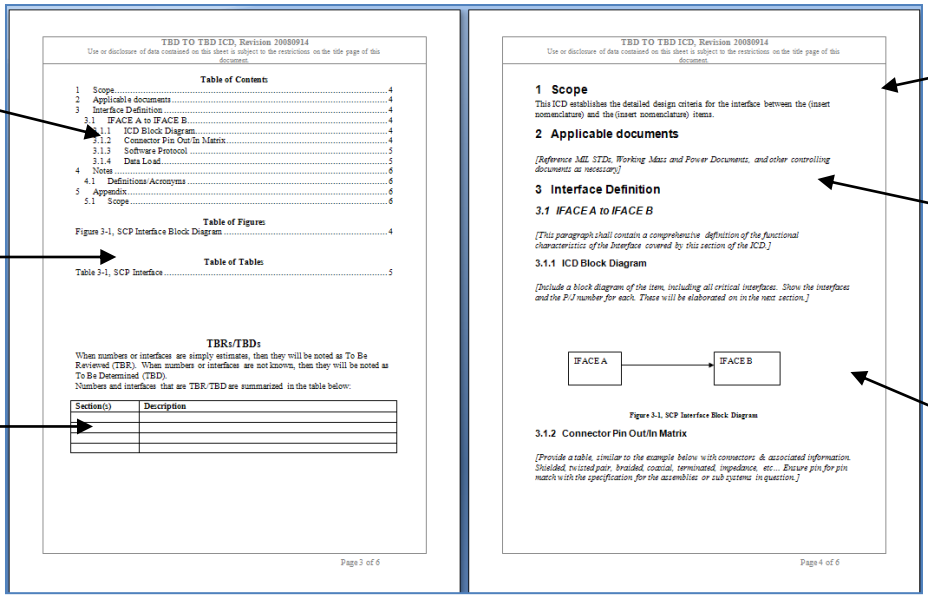

TBD TO TBD ICD, Revision 20080914
Use or disclosure of data contained on this sheet is subject to the restrictions on the title page of this document.

Table of Contents

Table of Figures

Table of Tables

TBRs/TBDs

When numbers or interfaces are simply estimates, then they will be noted as To Be Reviewed (TBR). When numbers or interfaces are not known, then they will be noted as To Be Determined (TBD).
Numbers and interfaces that are TBR/TBD are summarized in the table below:

Section(s)	Description

Page 3 of 6

TBD TO TBD ICD, Revision 20080914
Use or disclosure of data contained on this sheet is subject to the restrictions on the title page of this document.

1 Scope

This ICD establishes the detailed design criteria for the interface between the (insert nomenclature) and the (insert nomenclature) items.

2 Applicable documents

[Reference MIL STDs, Working Mass and Power Documents, and other controlling documents as necessary]

3 Interface Definition

3.1 IFACE A to IFACE B

[This paragraph shall contain a comprehensive definition of the functional characteristics of the Interface covered by this section of the ICD.]

3.1.1 ICD Block Diagram

[Include a block diagram of the item, including all critical interfaces. Show the interfaces and the P/J number for each. These will be elaborated on in the next section.]

IFACE A → IFACE B

Figure 3-1, SCP Interface Block Diagram

3.1.2 Connector Pin Out/In Matrix

[Provide a table, similar to the example below with connectors & associated information. Shielded, twisted pair, braided, coaxial, terminated, impedance, etc… Ensure pin for pin match with the specification for the assemblies or sub systems in question.]

Page 4 of 6

The Scope section should be a relatively short description of what systems this ICD covers

Applicable Documents are important to point out especially if the expected audience is not familiar with them or do not have explicit access to the reference documents

ICD block diagrams should be an extremely simple, non-technical diagram which eliminates any ambiguity about what system interfaces are being discussed.

Make sure to define all acronyms. Assume that the reader does not know any of them.

Here is an opportunity to add more diagrams, notes, etc. to help define the scope of this ICD in more detail.

Document all changes so that everyone working on the ICD knows who has made the change and when.

The specific sections of the ICD will be different for each type of subsystem. For example, avionics will have a section for Software Protocol while the Structures team would have no need for that section

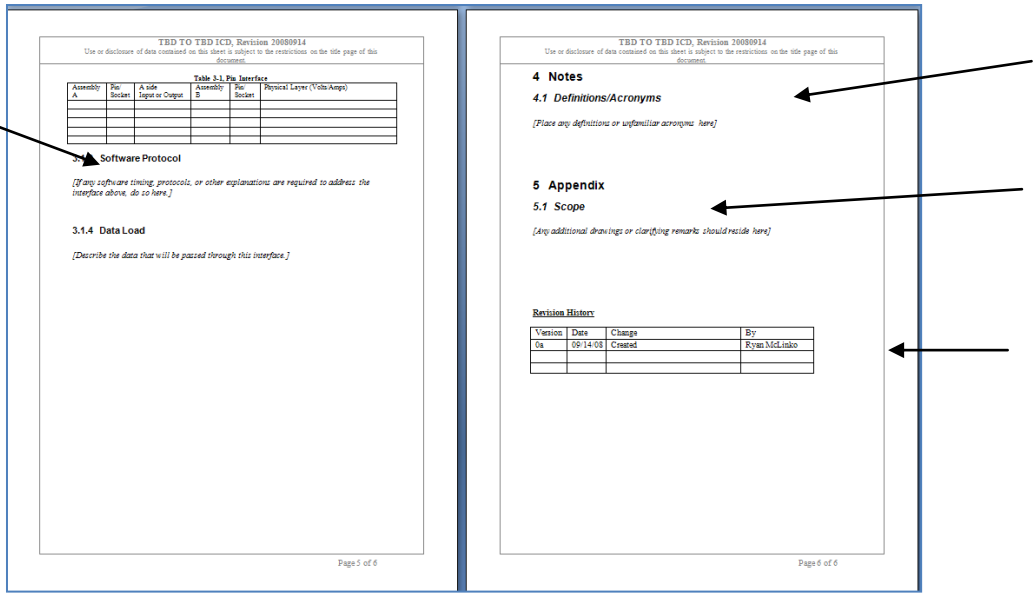

FIGURE 1.8-1: ICD EXAMPLE

ICD Management

Storage: The ICDs which are available for editing by the subteams are stored in the CASTOR fileshare under 2.2-Interfaces_Management [2]. This is where the sub teams can view their ICDs and make changes as they see fit. When they sub-teams want to submit these changed ICDs for approval they send them to their system liaison. We do an initial screening of the ICDs as well as pass them on to TAs who can point out mistakes we may have missed. Once the inconsistencies have been fixed, the ICDs are then placed in the UNP section under 4.2.4.2-Documenation-ICDs which will eventually be submitted to UNP.

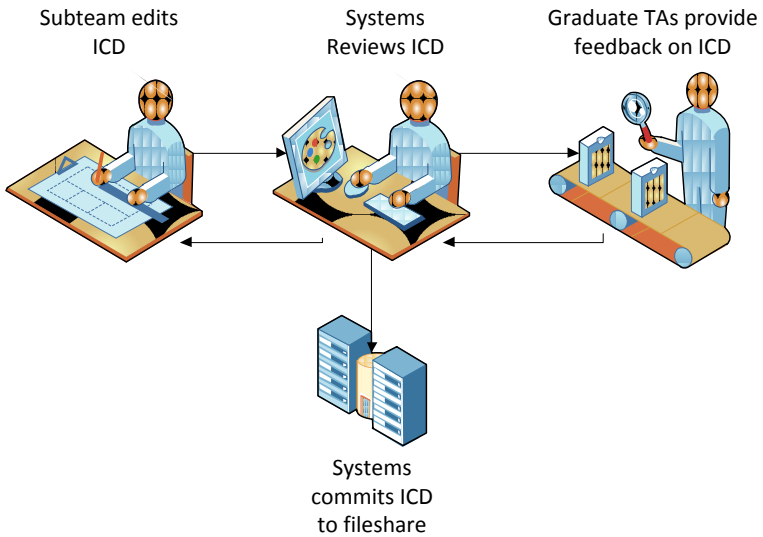

FIGURE 1.8-2: ICD MANAGEMENT FLOW

Tracking Changes: When an ICD is edited the author needs to list the date of change as well as the topic of change in the "Revision History" section of the ICD itself. This way, when the document is reviewed, any questions can be directed to the original author. This facilitates ease and speed of the ICD change approval process.

Types of ICDs

The Mechanical ICD identifies the hardware for the system or subsystem, and identifies to what it will be connected. For each piece of hardware, the ICD contains three main subsections: ICD Block Diagram, Physical Envelopes, and Hardware Mounting. The ICD Block Diagram identifies and shows all critical interfaces for the item. The Physical Envelopes section gives the initial (and, if applicable, final) current best estimate dimensions of the item: length, width, height, volume, and mass. The Hardware Mounting section provides a CAD drawing (if applicable) of each item, and describes the surface location, the hole locations, and the mounting hardware to be used. For many pieces of hardware, a fourth subsection, modeling, is included; this section describes any analysis (e.g. CAD drawings, finite element analysis) that was used.

The Power ICD identifies the hardware necessary to power each system or subsystem, and identifies to what the hardware will be connected. The ICD contains four subsections: ICD Block Diagram, Connector Pin Out/In Matrix, Grounding, and Load. The ICD Block Diagram identifies and shows all interfaces and connections for the hardware. The Connector Pin Out/In Matrix lists the in and out pins used for each connection, as well as the amount of amperage passing through the connections. Diagrams of the pin connections are included. The Grounding section identifies the type of grounding connections (i.e. analog, digital, or both). The Load section identifies the amount of power each piece of hardware will receive during the mission, and how often the power will be received.

The Thermal ICD identifies the surface connections (i.e. metal on metal contact) for each system or subsystem. The ICD contains four subsections: ICD Block Diagram, Heat Transfer Method, Thermal Path, Heat Loads and Fluxes, and Modeling. The ICD Block Diagram identifies the connections between the surfaces. The Heat Transfer Method section defines the method of heat transfer that will take place, the Thermal Path section identifies the path the heat load will travel, and the Heat Loads and Fluxes section identifies the amount of heat load that will be transferred during the mission, as well as the hardware limits. The Modeling section lists the types of analyses used.

The Data ICD identifies the hardware for each subsystem and to what it will be connected. For each piece of hardware, the ICD contains four sections: ICD Block Diagram, Connector Pin Out/In Matrix, Software Protocol, and Data Load. The ICD Block Diagram shows all interfaces and connections between the hardware. The Connector Pin Out/In Matrix lists the physical pin or socket connections for each piece of hardware, and whether the connection is in or out, as well as the voltage and amperage of each connection. The Software Protocol section describes how the software will interact

with the hardware, and the Data Load section lists the type and amount of data that will flow between the hardware, and how often, during the mission.

Interface Diagram

The following diagram provides a visual representation of the relationships between all of the subteams and the subsequent ICDs which need to be managed for each relationship.

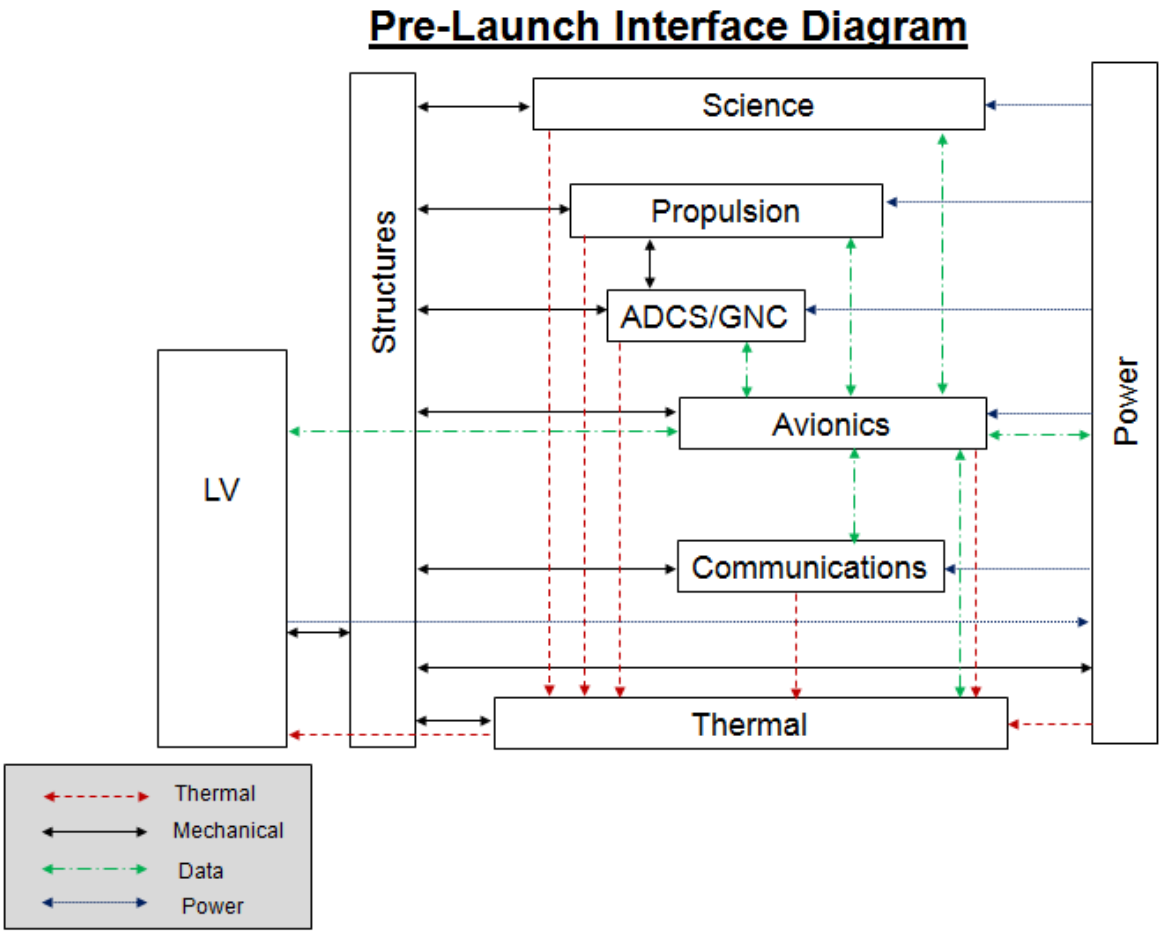

FIGURE 1.8-3: PRE-LAUNCH INTERFACE DIAGRAM

1.9 RISK MANAGEMENT (J.JAMES)

In order to mitigate risk, potential difficulties must be identified, quantified, tracked and analyzed. A risk tracking spreadsheet serves as the backbone of CASTOR's risk management system. Risk factors require continuous monitoring and thorough analysis for the purpose of risk reduction.

1.9.1 DEFINING RISK

Risk: The inability to achieve mission objectives - comprised of failure probability and consequences.

There are several types of risk. In order to consider them, a careful definition was determined by consulting NASA, Air Force, and MIT documentation [3]. *Programmatic* risk consists of any risk involving the program, including all external and internal risk. Subsets of programmatic risk include *technical* risk, *cost* risk, and *schedule* risk. Tradeoffs between the types of risk constitute risk management. Risks differ from issues in that they are problems that have not yet occurred. Once a risk becomes a reality, it is an issue and requires immediate action.

Successful risk management comes from continuous work. In order to mitigate risk, careful identification, analysis and tracking must be completed to ensure safety. The management process can be broken into four stages - planning, assessment, handling and monitoring.

Risk planning involves creating a framework to identify and track risks, along with their mitigation strategies. Documentation, such as the risk management file currently on the fileshare, falls under this category [4]. Planning also includes scheduled meetings with team leads to discuss risks.

Assessment consists of the actual identification and analysis of risks, including their likelihood and perceived consequence. Assessments are generally conducted by subsystem personnel, at the request of risk management managers. Updating the documentation created in the planning stage is a part of assessment.

Risk handling is the response to risk assessment. Operational backup plans fall into the category of handling. Risk handling also involves distribution of responsibility of risk mitigation, to team leads for instances, as well as a plan forward to reduce or respond to risks. . Higher risk items shall be brought to the attention of everyone in the systems team to increase involvement. Assessment also involves assigning a value to risks. For CASTOR, the current metric is *risk level*, measured as a function of likelihood and consequence. Each risk item receives a score from 1-5 for both likelihood and severity of consequence (5 being extremely likely or catastrophic). The *risk level* is low (green), medium (yellow), or high (red).

Finally, risk monitoring is the process by which the entire system risk is checked, allowing for a comparison to metrics to show improvement. This allows one to see the effectiveness of risk handling measures. Risks are considered improved as risk levels decrease.

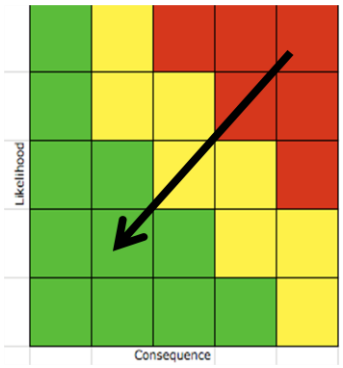

FIGURE 1.9-1: RISK LEVEL - LIKELIHOOD VS. CONSEQUENCE

The above chart depicts the five levels of likelihood and risk, and shows the breakdown into risk level. Green indicates low risk, yellow medium risk, and red shows high risk. By this point in the design, there should be no high risk items, as risk items should flow in the direction of the arrow. Monitoring helps in tracking this flow.

1.9.2 APPROACH

By improving CASTOR's management process, risk shall be reduced. The implemented system includes a tracking spreadsheet and a process of listing components and their technical risks. The last person to update the item is also tracked in the system.

An initial project-wide risk assessment was completed to determine where components stand and what areas needed additional focus. This involved contacting leaders of each subsystem and discussing risks and mitigation strategies. Next, further progress was made by discussing the list of risks with team leads to increase the robustness of the spreadsheet.

Further enhancement of the risk management spreadsheet is an ongoing process. Care must be taken not to overload the system by delving too deeply into compounded problems, and to focus on the most critical risks. While initially adding risks to the database was encouraged, feedback from CDR showed that risks should be limited to twenty or thirty important risks, rather than nearly a hundred detailed risks. As a response, higher level risks from the spreadsheet were categorized and combined in order to develop a concise, but comprehensive spreadsheet of risks. Thus the database was condensed to focus on the true concerns for the project.

1.9.3 ASSESSMENT MODEL

Various characteristics of risk are tracked to gain a sense of risks. These include the area of risk (hardware, software, operational, programmatic, manufacture, transport, etc.), the

risk dependency (what else must fail first), likelihood, consequence, mitigation, diagnostic, and repair or backup method. Subsystems are asked to self-report estimates of their risks and address these categories. In considering risks, personnel should be aware that critical changes that affect multiple systems can have far-reaching effects. These can cause other subsystems to make numerous changes to their system and thus increases risk level. Since the level of risk is measured by the likelihood and consequence, changes such as this increase the consequence level and thus are reflected in the tracking process.

Relationships between risks are shown as 'dependencies.' Direct links between subsystems can lead to similar probabilities.

In order to maintain consistency between subsystems, team members updating the spreadsheet are asked to consider the scheme in Table 1.9-1:

TABLE 1.9-1: RISK PROBABILITY VS. CONSEQUENCE

Likelihood or Consequence Level	Likelihood	Consequence
1	<< 1%	Inconvenience
2	~1%	Causes difficulties/delays, but can be corrected or handled
3	~10%	Compromises mission
4	~25%	Mission Failure or Partial Mission Failure
5	~50%	Injures people or harms launch vehicle & payloads; Total Mission Failure

Further work should involve tracking the assurance level of the evaluator (whether this is a tested likelihood or a complete guess).

1.9.4 TECHNICAL RISK

Technical risks are tracked in a spreadsheet. Each risk item is looked at individually and considered for thoroughness. Higher risk items are initially flagged so as to prioritize them. Currently medium-risk items include the anode (high voltage affecting system), camera lens degradation, and reaction wheel failure. The next set of high risk items includes magnetometer failure, schedule slips, reaction wheel malfunctions, torque coil failures, solar panel deployment failure, and others. Mitigations range from using the engine to de-saturate to modifying the duty cycle to account for low power input.

A meeting with the Power team took place to discover the relationship between power and voltage converter failures and various components. A single converter failure could cause an entire system, for instance ADCS, to become inoperable. Since most ADCS components work on 5V power, only the torque coils will operate should there be a failure. Thus analysis of the discussion also led to the discovery of unlisted risks, such as inhibits, and the difference between the battery charging circuit and the MPPT. Careful checking must be conducted to avoid errors, and to discover relationships between failures.

1.9.5 COST ESTIMATE

Assessment of costs is more straightforward, in that spending has been tracked over the last year and a spreadsheet has been implemented to track expenditures. Details regarding expenditures can be found in 2.1.4 of the fileshare. Income, or available funds, is constrained, and shall be determined based on a detailed cost projection plan. The current method for dealing with this limitation is to delay the purchase of expensive, high TRL components, and instead test with engineering mockups until funding can be secured. It has been noted that for FCR in January, according to UNP representative Abbie Stovall, UNP does not expect a flight-ready satellite, but a proto-flight satellite. Instead, high-cost flight hardware can be purchased later, as long as the interfaces and controllability can be modeled. For instance, purchase of one reaction wheel and a demonstration of functionality will suffice, rather than purchasing (and integrating) all three reaction wheels. Functionality of the other two reaction wheel should be verified by integrating engineering models into the system. This provides the advantage of reduced cost as well as sufficient testing.

Summary of Cost Risks:

- Limited Budget
    - Consequence: students spend excessive amounts of time re-creating COTS components to reduce costs; adverse effect on schedule adherence
    - Dependent on stringent monetary control and limited donations
    - Mitigation: Ask companies for material donations (such as solar cells) to reduce costs while not impacting student workload.
- Exceeding budget
    - Consequence: Strain on resources; could lead to lack of funding for testing and manufacture of satellite, as well as purchase of components
    - Dependant on insufficient tracking and spending policies; inability to accurately project costs

  - Mitigation: include margining in cost projections; outline of all large-cost items & cost estimates; delay purchase of expensive items until funding is secured; testing with less costly 'engineering units' avoids potential of damaging expensive hardware during testing and thus having to make replacement purchases

- Lack of funding for testing and manufacture of satellite
  - Consequence: serious delays which will adversely affect progress along UNP schedule
  - Dependencies: insufficient funds (lack of donors); going over budget
  - Mitigation: Promote satellite to potential donors; careful not to drastically exceed budget;

Other methods for dealing with cost risk that are already under implementation include cost margining and purchasing restrictions. Costly items must be approved by faculty and staff. Garrett Fritz has done some work on cost projection modeling for the future of the program.

1.9.6 SCHEDULE RISK

Schedule risk is high in this program, thus great attention has been given to compiling schedules from teams and integrating them with a systems master schedule. Freeze dates have been created to help track design phases and keep teams at the same stage in design. Essentially the chosen method for reducing schedule-slip risk involves early identification of slips, re-working of schedule to reflect realistic delays (and flow-down to other systems), and reallocation of labor and resources to meet changing demands. Margins in the schedule allow for improved schedule-tracking, along with advanced freeze dates and compilation deadlines. Subteams are additionally encouraged to adhere to the schedule by taking part in schedule creation and thus being held responsible.

1.10 DOCUMENTATION SUMMARY (A. FUHRMANN)

1.10.1 COMMAND MEDIA

Command Media refers to all the documentation that is actively managed and tracked by the systems teams. These documents are divided into easily accessible frozen sets so that modifications can be viewed over time. Generally a command media freeze occurs when documentation is due to UNP or for an internal review. Freezing the command media gives the systems team an opportunity to review it and make comments before final edits. In between these freezes the command media is often updated to reflect the most up to

date changes. Each type of document has a specific approval process for editing and submitting to systems during this inter-freeze period.

FIGURE 1.10-1: COMMAND MEDIA PHASES

The command media are tracked through phases A-E which closely corresponds to the NASA system used to track documentation throughout a program. Below are all of the command media listed with the project phases they most directly correspond to.

Document/Model	**Phases**
Requirements Verification Matrix (RVM)	A-B
Work Breakdown Structure (WBS)	A
Program Schedule	A-C
Budgets (MEL, Data, Power, Communications)	A-C
CONOPS	A-C
Risk Mitigation and Safety	A-C
Integrated Systems Model	A-E
Interface Control Documents	B-C
CAD Models	B-C
Systems Diagram	B-D
Electrical Schematic Diagrams	B-D
Manufacturing, Assembly, and Integration Plan	B-D
Testing Plans and Reports	B-D
Design Document	B-D
On-Orbit Handbook	D-E

TABLE 1.10-1: CASTOR COMMAND MEDIA

1.10.2 SUBVERSION REPOSITORY

All of the CASTOR Command Media is stored on a subversion repository which is broken down as follows:

- Management
- Systems
- Subteams
- Shared
-

Each of these sections has different levels of access. Subteam folders, for example, offer space for each of the systems to work on their command media before submitting it to systems for approval. The systems team then makes the determination of whether or not

that document is ready for submission to UNP. Those final documents are then stored in a systems level folder.

The structure of the repository prevents multiple editors from overwriting changes if they are working on a document at the same time. If there is a conflicted copy then the repository will advise the author to update to the newest version before submitting their changes.

1.10.3 ENGINEERING CHANGE ORDERS

An Engineering Change Order (ECO) is the documentation process followed to implement significant changes that affect multiple subsystems. Its purpose is to ensure continuity of design and to resolve potential conflicts which may arise from the design changes. The ECO creation process serves as a mini-review for significant changes so that all the subteams are on the same page. This process is to:

- Deliver the proposed ECO to all directly affected subsystems for review
- Subsystems change specifics and inform the systems team
- Deliver the current proposed ECO to all other teams for review
- Check with systems team again
- Perform a sign-off of the ECO at a team leads meeting

This process managed by "ECO Manager" member of Systems Team who is responsible for making sure that all relevant parties are committed to the new design change before it is signed off. There have been six ECOs throughout the CASTOR program and there have been none so far this semester. However, the process is still in place in case significant changes still need to be made.

CASTOR ENGINEERING CHANGE ORDER			ECO # 002
Originator	**Date Submitted**	**ECO Status**	**Revision**
R. McLinko	2009/11/03	Submitted	01

Changing Elements

ADCS System Design

Reason For Change

The current nitrogen gas system has been shown to be inadequate to correct for disturbance torques throughout the operational life of the satellite. Furthermore, it is much heavier and more complicated than other options.

Description of Change

The key elements of the change are as follows:
-The nitrogen gas system of the satellite is removed
-Two reaction wheels are added to the satellite, orthogonal to the existing one
-Three torque coils are added to the satellite in mutually orthogonal directions
-The spacecraft is allowed to "tumble" during eclipse
-The engine gimbal system is removed
-A magnet is added opposite the structure
-The magnet and reaction wheels will be used to replace the engine gimbal system

ECO Board Members	Signature	Date	Comments
ECO Manager			
Operations Lead			
ADCS Lead			
Avionics Lead			
Communications Lead			
Propulsion Lead			
Power Lead			
Thermal Lead			
Structures Lead			

ECO Manager Notes

FIGURE 1.10-2: ENGINEERING CHANGE ORDER

1.11 OUTREACH SUMMARY (J. JAMES)

Reaching out to the community is an important goal of CASTOR. In order to encourage enthusiasm for the sciences and exploration of the frontier beyond Earth, CASTOR has been involved with several outreach programs this semester. These include Campus Preview Weekend (CPW) and Teach for Spark. Past outreach events include participation in the Freshman Orientation Activities Midway, Teach for Splash, and

participation in the Students for the Exploration and Development of Space (SEDS) Project Expo. CASTOR also brings a variety of MIT students into the project through the Undergraduate Research Opportunities Program.

Teach for Spark!

In March, 2010, CASTOR participated in Spark - a program geared toward reaching out to middle and high school students. During several sessions on the weekend, CASTOR members engaged students by holding a workshop on how to "Build a Satellite." CASTOR mentors coached the young scientists on how to build satellites out of various goodies (such as graham crackers, pretzels, marshmallows and toothpicks). Satellites had to pass thermal testing in the microwave and a load test (i.e. drop test), while staying close to a cost estimate and target mass. The class was a big success, and the students left excited about learning about space (see Figure 1.11-1).

FIGURE 1.11-1: SPARK STUDENTS WITH CHOCOLATE SATELLITE

2 CDR LEVEL DESIGN

2.1 OPERATIONS

2.1.1 SUMMARY OF OPERATIONS (J. ROBINSON)

The Concept of Operations (CONOPS) details the functions and timelines of the CASTOR Satellite and supporting ground systems during all phases of the mission. The CONOPS:

- Establishes a structure for CASTOR mission operations.
- Aids spacecraft design by detailing the events that occur during each mission phase and during failure scenarios.
- Supports the development of ground operations and support systems.

CASTOR operations are divided into six phases, described below:

- Pre-Launch – Flight Model (FM) interaction prior to launch
- Launch – Liftoff until lightband separation from LV/ESPA Interface
- On-Orbit Deployment – Communications acquisitions, de-tumble, deployment of solar arrays, and sun-pointing attitude.
- Commissioning – Subsystem health verification and DCFT start-up and initial operations
- Normal Operations – On-orbit maneuvers and DCFT operating
- Decommissioning – De-orbit and re-entry procedures

These phases are described in the following section. The CASTOR CONOPS document further describes the CONOPS details. The CONOPS document can be found in section 3.2-Operations in the fileshare.

PRE-LAUNCH PHASE

Pre-launch operations can be divided into three parts: mission integration, ground support and transportation and final checkout.

Mission Integration

The mission integration will consist of the final assembly of CASTOR prior to shipment. This phase will be led by the structures team. This will consist of all assembly and testing of the CASTOR flight model. Throughout this phase, detailed documentation must take place on component testing and observed results. This documentation will be saved for reference in case of launch support or on-orbit questions.

Ground Support and Transportation

Transportation of the satellite to the launch site, and all preparations necessary, will be managed by the systems team. The Ground Support Equipment (GSE) will be made up of the shipping container, mobile ground station interface (for communications testing), battery charging devices, Xenon filling device, lifting harnesses, and any tools necessary (such as a torque wrench). The transportation medium for the satellite is TBD.

Final Checkout

The operations team will manage the final checkout, that is, the final maintenance and tests of the satellite *just before* integration with the launch vehicle. This inspection will ensure that no damage occurred during transport, and prepare the satellite for integration. Actions that will occur during this inspection include filling the Xenon tank, charging the batteries, and final performance checks of the avionics, communications, power, propulsion, and ADCS/GNC subsystems. This checkout will take place in the facilities that the systems team has arranged for this purpose. As this is not being performed remotely, no communication system will need to be implemented. Twelve hours are budgeted for these checkouts, in order to provide enough time to fix any problems that arise. Following successful completion of these checkouts, the satellite will be turned over to the launch vehicle integration team; the operations team will not participate in integration, but will be available to answer questions if necessary. Integration is estimated to take 5-8 days (TBR).

Following integration, a visual check will take place (with an estimated duration of 6 hours), to ensure that nothing was damaged during integration. This check is *only* a visual check, and will not require any communication with the satellite itself. It is only to ensure that the satellite has sustained no physical damage during integration. Considerable margin has been built into this check, to provide enough time to identify any damage and to decide on the best course of action to take (since the satellite will already be attached to the ESPA ring and the launch vehicle). After this visual check and any necessary repairs, the satellite will wait for the launch date. Since this wait may be indefinite, the batteries will be re-charged approximately every 11 (TBR) days. (Nickel cadmium batteries lose their charge after about 11 (TBR) days, even if they are not in use; if the launch wait-time is longer than this, they will need to be recharged.) If batteries must be launched with minimal charge (as understood by current UNP guidelines), the batteries will be drained prior to launch. If batteries are allowed to be charged, the batteries will be charged one final time a few hours before launch. The final determination of battery charge will depend on the understanding with the launch vehicle provider. The expected scenario (and worse case) is that of launching with fully drained batteries.

The following is a list of future work that needs to be completed at the time of this documents writing:

- Transportation Procedures
    - Ground support equipment
- Xenon Tank Filling Procedures
- Battery Charging Procedures
- Final FM Integration and Handling Procedures
    - Inspection and Structural Verification (Torque Check) Procedures
    - Satellite Arming Procedures

LAUNCH PHASE

Launch operations will be managed by the launch vehicle provider and the primary payload team. Members of the team will be present for launch, in case of problems with the satellite, but otherwise will perform no operations until the satellite's release from the ESPA ring.

ON-ORBIT DEPLOYMENT PHASE

The requirement of the deployment phase is to safely deploy the solar arrays so that the CASTOR mission is not negatively affected. The objective of the deployment sequence is to ensure proper analysis of the satellite. Health is first checked upon contact with the satellite, and then the software will run diagnostic tests, followed by extensive testing of the ADCS system. The ideal state prior to deploying the solar arrays is a fully controlled satellite with sun-pointing capabilities. Under these circumstances, the satellite will remain in the same operation state but have an altered physical state.

Deployment to First Contact

Upon release from the ESPA ring, the on-orbit deployment phase will begin. A signal will be sent from the ESPA ring to TBD, notifying TBD that the release is complete. Both the nature and the destination of the signal are unknown at this time. Upon separation, the satellite will turn on and start up the initial housekeeping task, where the satellite is in an idle mode, charging batteries and waiting for a signal from the ground. Additionally, in this task will power up the modems when the batteries reach 22 V (TBR). Basic health sensors as described below will be powered at this time as well. No data will be collected and all non-essential components will be turned off to ensure that the satellite can survive indefinitely in this mode. The first communications with the ground will be initiated by operators at the MITControlCenter through the HETE Ground Station.

For the first series of contacts, operators will check the critical health data and telemetry data to ensure that the satellite is functioning properly. Critical health data includes solar panel, battery, and load voltages and currents, as well as attitude sensors and temperature sensors. The satellite clock will be updated via ground commands on the first contact The GPS will not be turned on initially. The satellite will send real-time data at a requested data rate of all voltage, current, temperature, and attitude sensors on the bus as shown in Table 2.1-1.

TABLE 2.1-1. INITIAL REAL-TIME HEALTH TELEMETRY

Subsystem	TLM Description
EPS	Battery Voltage, Battery Current, Solar Array Current (x4), Solar Array Voltage (x4), PDU Voltage (x2), PDU Current (x2)

Thermal	Temperature of Battery (x?), PDU (x?), Avionics Box (x?), Solar Array (x4), others?
ADCS	Magnetometer Voltage (x3), Gyro rates (x3), Accelerometer (x3), Sun Sensor? (x?)
Comm	n/a
GNC	n/a
Others	TBD

TABLE 2.1-2: TLM DESCRIPTION

The largest uncertainty in this phase is the consistency of the communications signal. If the ground passes are frequently interrupted, the command to deploy the solar arrays might come prior to the desired pointing of the satellite. The analysis of this possibility and the probability of communications problems are ongoing, and will affect the final operation plans.

Software Checkout

After checking critical health data and setting the clock, operators will perform checks on the more complex software pre-loaded to ensure that no software was corrupted during launch and start-up. If any software fixes are needed or any software needs to be loaded, it will be done at this time. The software will be checked and uploaded in order of necessity. That is, the higher-level tasks such as the scheduler or DCFT operations task will not be loaded until needed. The first software tasks to be loaded are the file management system and the satellite's executable task.

The executable task and file management system will allow operators to collect data between ground station contacts (store and forward technique). This is especially important, as the communications with the satellite will be intermittent until stabilization and deployment of solar arrays. A test of comparing collected data and real-time data will ensure that the file system is properly writing data and the timing in the software is correct. Critical health will be collected continuously at 15 sec sampling (TBR) from this point forward if there is sufficient coverage time to transmit it.

ADCS/GNC Checkout

Next, operators will checkout the ADCS and GNC instruments necessary to de-tumble. This is currently assumed to be done manually by operators and engineers looking at ground telemetry, however, the test may be written into the software.

ADCS and GNC De-tumble Checkout and De-tumble:

- GPS cold-start (update computer time if within proper threshold)
- Check that gyroscopes are operational, then calibrate

- Turn on magnetometers and recalibrate if necessary
- Checkout torque coils
- Checkout reaction wheels
- Fire torque coils or reaction wheels (TBR as to which exactly), using the readings from gyroscopes and magnetometers to de-tumble

Upon de-tumbling the ADCS software will be tested to see if the satellite can point its +Z-axis towards the sun and track the sun. This will ensure that post-deployment, the ADCS system can track the sun. Following this test and when the attitude rates are within limits (TBR), ground operators will command the panels to deploy. During deployment and for 10 min (TBR) after deployment, no attitude actuators will be active to ensure that there is no interference with deployment dynamics. After the 10-minute timeout, the satellite will point in a sun-tracking mode (TBR, depends on comm.). The command will be sent on the first of subsequent orbital passes, so that the command can be verified on the next pass.

Following solar panel deployment, the ADCS system will point the +Z-axis towards the sun so that the solar panels are generating the maximum power.

ADCS GNC Solar Panel Pointing Checkout and Pointing:

- Check readings from gyroscopes, magnetometers, and sun sensor to know where to point the solar panels
- Turn on reaction wheels
- Monitor sun sensor and MPPT output to confirm pointing
- Use reaction wheels rotate body until solar panels are pointed at the sun
- Check battery charging

The satellite will communicate with the ground again after the pointing of the solar panels. When the satellite tracks the sun and the batteries are fully charged, the spacecraft will enter the commissioning phase.

COMMISSIONING PHASE

The objective of the commissioning phase is to fully qualify the satellite prior to normal operations. To move to normal operations, two major tasks must occur: verification of bus health and DCFT qualification and calibration. The phase begins with fully charged batteries, a de-tumbled, sun-tracking spacecraft, and deployed solar panels. Then the detailed subsystem checkout process begins.

ADCS Subsystem

The ADCS system checks should be mostly complete by this point. However, additional tests may take place to completely verify that all components match their expected modeled behaviors, whereas in the deployment phase, the emphasis was on overall

vehicle health and general attitude pointing. The verification steps for the ADCS system are TBD and will be determined by the ADCS team.

GNC Subsystem

The CASTOR GNC system will be verified by ensuring that the hardware and software systems interact together in the predicted manner. This will be done in the following steps:

- GPS comparison to Two Line Element sets (TLEs)
- GPS satellite time update
    - GPS comparison to Two Line Element sets (TLEs)
- Orbital propagator verification
    - Downlink predicted state and compare to ground station propagator
        - Propagator validation for requirements by comparing to error to GPS
    - GPS updates propagator epoch every 24 hours (TLE)
- Check desired pointing for maneuver at different orbital positions
- Verify software interaction with operations task

Power Subsystem

The power subsystem check will determine if each of the solar panels is providing the expected amount of power at the expected efficiency, and if each of the power lines are working. Like the ADCS/GNC check, much of this has happened previously, however emphasis will be towards matching the data with the expected behavior and model of the satellite.

Thermal Subsystem

The temperature sensors will be providing readings throughout commissioning. The primary thermal subsystem verification will occur by ensuring that no components reach temperatures hotter or colder than their operational constraints, with and without DCFT operations. Additionally, the thermal subsystem can be fully verified by comparing the temperature sensors to the predicted models. This will allow either the model to be updated or sensors to be identified as faulty.

Propulsion Subsystem

The propulsion system has two major tasks during commissioning: DCFT power-up and initial operations. The propulsion system needs the camera system (avionics), the power system, and the attitude system to be functional prior to execution. Additionally, software safety checks must be in place to limit the power system and the timing of the DCFT thrusting operations.

<u>DCFT Power-Up</u>

Initial start-up of the DCFT requires the following steps:

1. Bake out (~3 hours)
2. Condition cathode:
    a. Supply 2A at 3.3 V for 90 min: 6.6 W (TBR)
    b. 4A at 7.9 V for 90 minutes: 31.6 W (TBR)
    c. 6 A at 12.8 V for 60 minutes: 76.8 W (TBR)
3. Then 0.36A at 200V of actual thrusting for 15 minutes: 72 W (TBR)
    a. Thrust in velocity direction
4. Take images of plume every 1-2 minutes (TBR)
5. Turn off anode flow and turn on cathode heater/keeper (TBR)

The batteries' capacity has been selected to ensure that this start-up will not be interrupted by eclipse. However, the high power activities will be scheduled to occur during the sunlit portion of the orbit to minimize the discharge on the batteries.

DCFT Initial Operations

The goal of the initial operations is to calibrate the DCFT while also meeting the minimum success criteria of the mission. These minimum success criteria are to operate the DCFT and demonstrate a change in the orbit with the DCFT. The source of commands for operating the DCFT (ground-based, scheduled, or autonomous) is TBR. The orbital change will be a semimajor axis increase. This will be accomplished by operating the DCFT while within 15 degrees (TBR) of the thrust axis. The verification of the maneuver will be GPS (primary) as well as TLE (secondary). A significant maneuver is defined as a 100-meter increase in the semi-major axis, which should occur after ~15 min of thrusting. The first operations of the DCFT should be able to accomplish this task, however if the pointing is off or the first firing does not go as planned, the orbit change may not be complete.

Upon meeting the minimum mission criteria, the emphasis will be placed on calibration of the DCFT. The procedures for the calibration are TBD from the propulsion team. In general, it will involve testing different flow rates to see the power draw from the DCFT. A final flow rate will be selected for normal operations. Additionally, the camera's imaging capability of the plume will also be determined, and the final camera configuration (bits per pixel and image resolution) will be determined prior to normal operations.

Commissioning Phase Exit Criteria

The commissioning phase will end and the normal operations phase will begin when the minimum success criteria have been met and all subsystems are functioning properly to allow for autonomous operations. As stated, the minimum success criteria are to

successfully operate the DCFT and thereby demonstrate a change in orbit with the DCFT. The successful operation proof will be completed using the on-board camera and power telemetry data. The orbital change will be measured by the onboard GPS or ground-based sensors.

Additional steps that may need to be completed prior to normal operations are autonomy tests with software. These would include ensuring that the autonomous scheduling and DCFT operation commands are executed as intended. Tests will include setting the maximum allowable time between contacts to fire the DCFT very low to demonstrate that the software will automatically shutoff if this time elapses.

The complete details of these software tests, their implementation on the flatsat (or qualifications model), and the implementation on the flight model will be outlined in the CONOPS and the operational procedures. Normal operations will begin when the satellite is merely being observed for the entirety of its mission and it operates in a predetermined manner.

NORMAL OPERATIONS PHASE

The purpose of the normal operations phase is to fulfill the mission objectives of CASTOR. The basic operations in this phase will be to fire the DCFT whenever safely possible (being constrained by power, lifetime, Xenon, and thermal survivability considerations), and to return payload and health data to the ground station for analysis. A basic orbit will go as follows:

- Recharge batteries at the start of the sun period by pointing solar panels to sun
- When batteries are sufficiently charged and desired thrust and power producing angles line up, operate the DCFT (assuming other factors are within limits)
- Take picture of DCFT every firing cycle
- Turn off the DCFT when power available decreases below threshold or any other factors are out of limit
- Orient solar panels towards the sun and further charge batteries
- Coast uncontrolled in eclipse to save power (TBR, potential predictive maneuver)
- Send pictures, DCFT data, and health data to ground station when overhead

Safety constraints will be programmed into the software to ensure that the DCFT does not fire after three days (TBR) without contact from the ground station to ensure that the satellite does not maneuver away from its predicted location. Additionally, thermal, power, ADCS, and GNC tasks will monitor the health of the satellite and alert the operations task if any component problems occur or observed parameters are out of the operational range, resulting in a recommendation to enter a safe operations mode. These modes have not entirely been determined; however, they will be described prior to CDR and tested on the flatsat and other software modeling tools such as SpecTRM.

The basic orbital changes that are currently planned in the normal operations phase of the mission are simple semimajor axis (radius) increases and decreases. This will be accomplished by thrusting directly with or against the velocity vector. Alternative options are plane changes (either inclination or ascending node changes); however, these are not as useful for the engine characterization and require more complicated pointing, so they are currently not in the design. An additional orbit that may be tested near the end of the mission is a low perigee drag-reduction orbit, in which the satellite will burn specifically near perigee or apogee to keep the energy of the orbit high enough to prevent re-entry, as the final operations mode is decommissioning via atmospheric re-entry.

The satellite will operate within a band of altitudes from 400 km (perigee) and 700 km (apogee). These altitudes were selected to ensure that drag effects are minimal and to ensure that the satellite does not progress too far into the radiation environment. These numbers are TBR and will likely change on-orbit due to operational optimization of groundstation coverage and the thrusting environment.

The normal operations phase will end when any of the following conditions are met:

- The fuel mass is approaching the de-orbit limit of 1kg (TBR)
- The orbit is lower than the DCFT can compensate for drag and will re-enter soon
- Critical components have failed or degraded enough to warrant decommissioning the satellite

DECOMMISSIONING PHASE

The decommissioning phase of the mission encompasses the end of life of the spacecraft. A NASA (UARS) decommission plan specifies the following five operations during this phase in order to minimizing risk to other spacecraft:

- Limit the on-orbit lifetime of the spacecraft by lowering the orbit by firing thruster with remaining fuel.
- Minimize the potential for generating orbital debris due to explosion or collision via venting remaining on-board fuel.
- Remove the ability of the spacecraft to act as an RF source by disabling, to the extent possible, the modem.
- Cease active attitude control of the spacecraft by disabling actuator control functions
- Leave the spacecraft in an inert/powerless state by disabling/severing solar power distribution functions.

Decommission Plan for Upper Atmospheric Research Satellite (UARS), 2002. Section 2.0

The NASA Handbook on Orbital Debris Mitigation specifies three acceptable options for decommissioning in LEO:

- Atmospheric Entry
- Maneuvering to a storage orbit (an orbit >2000 km)
- Direct retrieval

NASA requires that the probability of success for the chosen mission decommissioning option be greater than 90%.

The first option, atmospheric entry, is a common decommissioning technique, which has been selected for this mission. The second option is not feasible because it is unlikely that it would succeed. As there are no feasible means of directly retrieving the spacecraft, the third option is eliminated.

However, with an electric propulsion system the ability to make a controlled entry into the atmosphere is limited. This is because in lower orbits the force of atmospheric drag becomes much greater than the engine thrust. Controlling the thrust vector and attitude becomes increasingly energy-expensive as the orbit decreases until the spacecraft can no longer overcome the drag forces and the re-entry becomes uncontrolled.

This means that atmospheric re-entry must be uncontrolled. NASA specifies that uncontrolled re-entry is acceptable if it can be proven that the probability of human injury is less than 0.0001.

Event Number	Duration	Description
F1	0-52 days	Lower orbit using remaining fuel
F2	as needed	Dispose of remaining fuel (thrusting or venting)
F3	< 1 minute	Disable solar arrays (sever connection to PPT)
F4	1 minute	Disable ACS/GNC to cease active control
F5	< 1 minute	Shut down communications (modems)
F6	1 minute	Shut down computer

TABLE 2.1-3: DECOMMISSIONING TIMELINE

The CONOPS also describes safe modes, failure cases, and the data processing plan. Please reference section 3.2 in the fileshare for those details.

2.1.2 GROUND STATION INTERFACE (N. ESSILFIE-CONDUAH)

The CASTOR satellite needs to be controlled through established reliable communication connections. This ensures the ability to attain data or control it whenever necessary. The

MIT ground station thus plays a role in meeting this requirement. To accomplish this goal of sending commands and requesting data from the satellite the MIT Ground Station will be established. Essentially, it will be a control center at MIT, which will make use of the MIT Ground Station GUI to send commands. A trained controller will operate this. The operator will send commands/files to the HETE ground station in Cayenne, which will be in contact with the satellite during transmission periods. The transmission cycle would start after the commissioning phase. An example of the transmission cycle can be seen when a command is sent requesting sensor data. This command would be selected and packetized in the GUI application, which would send the packet to the HETE ground station over a TCP/IP connection. The HETE ground station would then transmit this command to the satellite. The satellite after successful or unsuccessful completion of the command would report to the HETE ground station. This response would then be forwarded to the MIT ground station control center over the TCP/IP connection for analyses.

The control center would contain two to three computer terminals. Due to reliability, widespread use, and price, these computer terminals will be the standard Athena machines. While these will have the same hardware as Athena machines, they will not be running Athena software and we hope them to be dedicated computers. Based on the different requirements for each computer, the simulation computer will be running Windows and the command and data processing computers will be running Linux. Each computer in the control center will need internet access to connect to the HETE Cayenne ground station and each other. Uninterruptable power will be necessary to ensure that if the satellite sends down data, there is a computer ready to receive it, this is particularly important during the on-orbit deployment and commissioning phases when progress is mediated by commands from the ground.

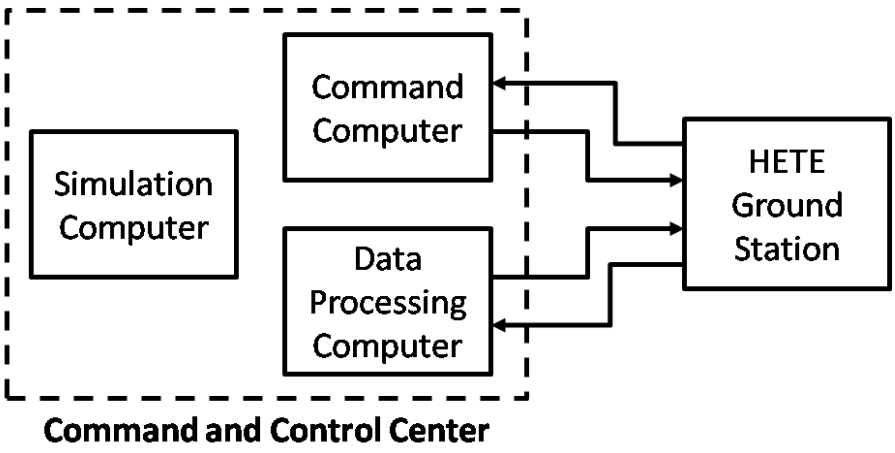

FIGURE 2.1-1: GROUND SYSTEM LAYOUT

The above diagram shows the modularization of the task, but the command and data processing computers are intended to be one machine.

In addition, the command and data processing computers will also be designed to interface with the simulation computer for ease in data transfer.

The MIT Ground Station through the command computer will run a GUI, written in java, providing a readily understandable interface for commands to be sent to the satellite and for received data to be viewed. This is the Ground Station Interface.

The look and feel of the GUI can be seen in Figure 2 below.

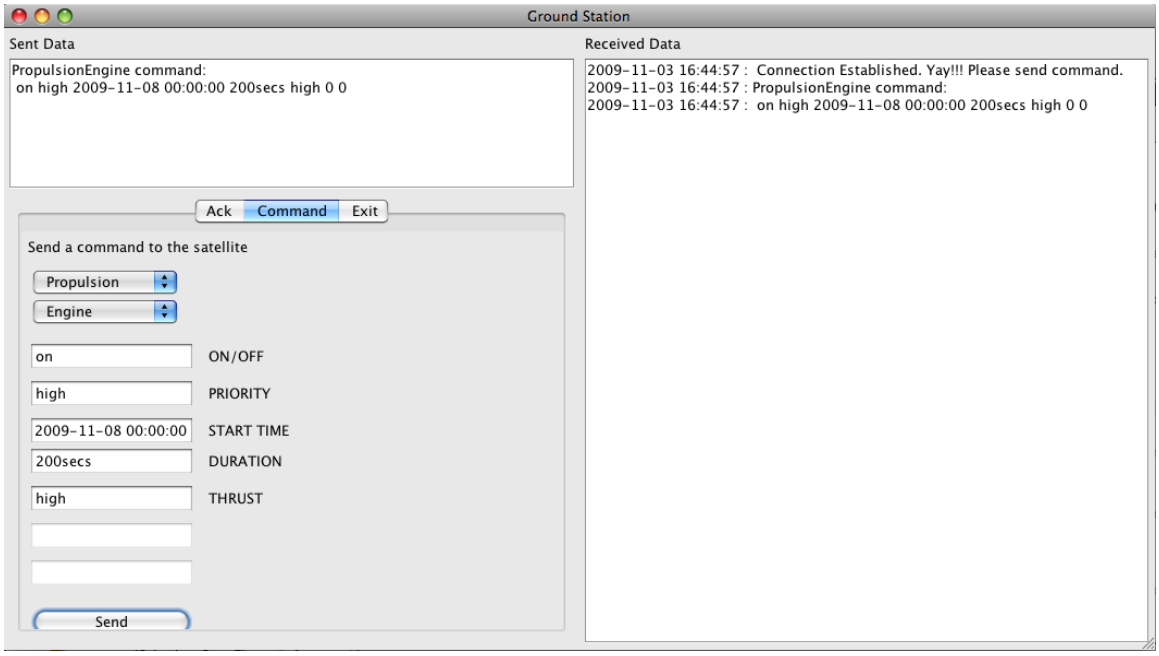

FIGURE 2.1-2: GROUND STATION GUI

To meet the requirements of the satellite, commands were established based upon the needs of each subteam. This structure was then used to govern the navigation of the commands though the GUI

Commands sent to the satellite will be chosen in a graphical interface. The operator will select from the command lists below the commands that he or she wishes to send. One special command for example will be the decommissioning command. Any of these commands will be sent to the HETE ground station and then processed by the satellite once received on-orbit.

Each individual subteam determined the structure of their commands as follows.

TABLE 2.1-4: ACS/GNC COMMAND LIST

ACS/GNC	ON/OFF	PRIORITY	START TIME	DURATION	TORQUE	AXIS	ID		
SIZE	*1 bit*	*2 bits*	*3 bytes*	*3 bytes*	*8 bytes*	*24 bytes*	*1 byte*		*Total (bits)*
GPS	X	X	X	X					*51*
MAGNETOMETER	X	X	X	X					*51*
GYROS	X	X	X	X					*51*
THRUSTER		X	X	X	X	X			*306*
THRUSTER	X	X	X	X			X		*59*
DETUMBLE MODE	X	X	X						*27*
DETUMBLE + POINT MODE	X	X	X						*27*
SUN SENSOR	X	X	X	X					*51*
RXN WHEEL	X	X	X	X	X				*115*
CALIBRATE GYROS	X	X	X						*27*
CHECKOUT A MODE	X	X	X						*27*
CHECKOUT B MODE	X	X	X						*27*
COMMISSION	X	X							*3*

TABLE 2.1-5: STRUCTURES/THERMAL COMMAND LIST

STRUCTURES/THERMAL	PRIORITY	TIME START		
SIZE	*2 bits*	*3 bytes*		*Total (bits)*
DEPLOY SOLAR PANELS	X	X		*26*

TABLE 2.1-6: PROPULSION COMMAND LIST

PROPULSION	ON/OFF (1 bit)	PRIORITY (2 bits)	TIME START (24 bits)	DURATION (24 bits)	THRUST (8 bytes)		
SIZE	*1 bit*	*2 bits*	*3 bytes*	*3 bytes*	*8 bytes*		*Total (bits)*
CHECKOUT	X	X	X				*27*
ENGINE	X	X	X	X	X		*115*
VENT FUEL	X	X	X	X			*51*

TABLE 2.1-7: AVIONICS COMMAND LIST

AVIONICS	ON/OFF	PRIORITY	TIME START	NORMAL (Y/N)	COLLECTION RATE	DESIRED DATA LIST		
SIZE	*1 bit*	*2 bits*	*3 bytes*	*1 bit*	*4 bytes*	*1 byte*		*Total (bits)*
SOFTWARE UPDATE		X	X					*26*
REBOOT		X	X					*26*
RELOAD MEMORY		X	X					*26*
COMPUTER	X	X	X					*27*
DATA COLLECTION				X	X	X		*41*

TABLE 2.1-8: COMMUNICATIONS COMMAND LIST

COMMUNICATIONS	PRIORITY	TIME START		
SIZE	*2 bits*	*3 bytes*		*Total (bits)*
SEND HOUSEKEEPING PACKET	X	X		*26*
SEND EMERGENCY DATA PACKET	X	X		*26*

TABLE 2.1-9: OPERATIONS COMMAND LIST

OPERATIONS	**PRIORITY**	**TIME START**	**MANEUVER SELECTION**		
SIZE	*2 bits*	*3 bytes*	*1 byte*		*Total (bits)*
BEGIN COMMISSIONING	X	X			*26*
BEGIN NORMAL OPERATIONS	X	X			*26*
BEGIN DECOMMISSIONING	X	X			*26*
GO-AHEAD	X	X			*26*
INITIATE NEW MANEUVER	X	X	X		*34*

The command lists above (compiled with help from Emily Grosse and Ginny Quaney) have the component or command which will be sent on the left column and the content of that command on the top row. For example, a command to the ACS Reaction Wheel will contain the following data: On/Off, Priority, Start Time, Duration, and Torque information. Some of these commands will be used in the course of nominal satellite operations and some will be used only if a problem is observed. For example, the operations commands and the ACS/GNC checkout mode commands will be used even if there are no problems on the spacecraft, but the Avionics software update or reboot commands should not have to be used unless a problem is detected.

The command lists will see a revision. The result of the revision may result in the restructuring of the command list and thus the GUI. However, it will go to satisfy requirements of data, scheduling, frequency of use and complexity of commands pertaining to the satellite as specified by each subsystem.

To help this, a Command Document will be produced to thoroughly document the needed structure of commands to operate CASTOR as needed.

2.1.3 SOFTWARE PLAN (J. ROBINSON)

The following software plan contains segments from the Software Operations Document, which is named CASTOR_SW.doc and can be found in section 3.2 of the fileshare.

Figure 2.1-3 shows the software architecture from the 83x design, which was also presented at the PDR. The avionics section has a slightly different diagram, and the complete software architecture still needs to be finalized.

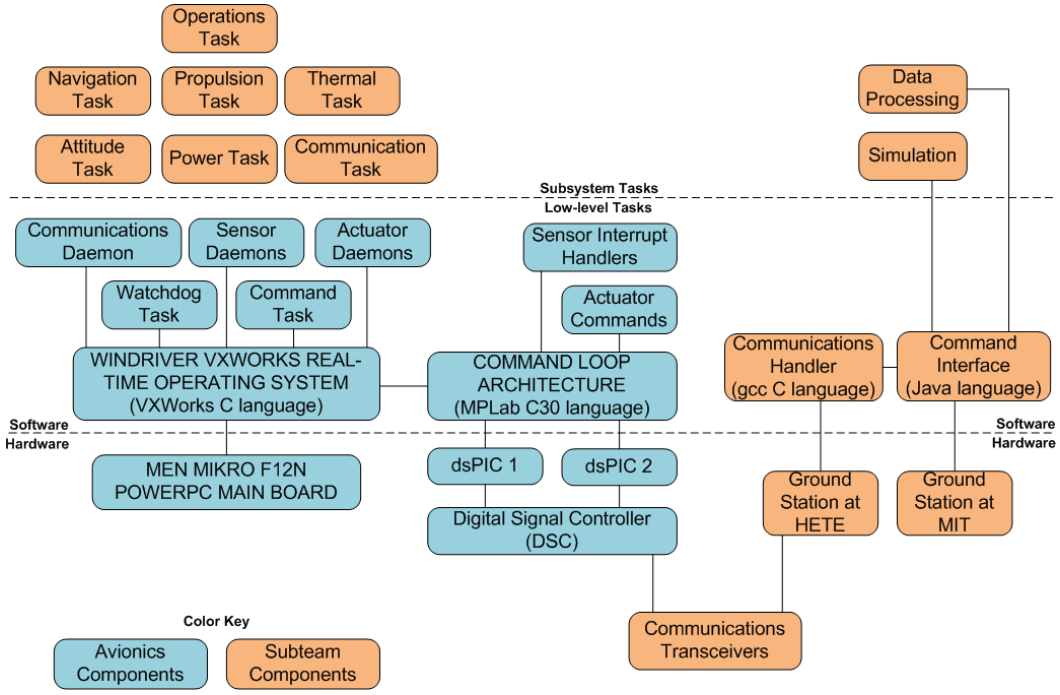

FIGURE 2.1-3: SOFTWARE ARCHITECTURE AT PDR

The tasks on the top left (operations, navigation, propulsion, thermal, attitude, power, and communications) will work together in managing CASTOR as well as ensuring needed data is transmitted. The following are the requirements for these software tasks. Further work will be done to analyze the structure of each task and the functions that will take place in each.

2.1.3.1 OPERATIONS TASK

The operations software task has the following requirements:

OT-1 The CASTOR operations software shall control the transition of CASTOR operation modes between power generating, DCFT operating, eclipse, and communicating functions.

OT-2 The operations software shall be reprogrammable and allow for software upgrades and fixes without any effect on the core CASTOR systems health.

OT-3 The operations software shall collect and monitor subsystem hardware and processes to include creating telemetry files, command files, and safely responding to any off-nominal hardware case.

OT-4 The operations software shall track DCFT system performance, to include tracking firing time, Xenon fuel consumption, operating state, and power parameters.

These task requirements may be over specified for the operations task. Requirement OT-3 will most likely be managed by a separate data collection and storage task, and requirement OT-4 may be split into the propulsion and power tasks.

The current design for the operations task is to have a two-part system: the operations survival software (OP-S) and the operations execution software (OP-X). This is similar to the FalconSAT-3 approach, and allows for the basic functionality and critical health to be taken care of in a stand-alone task (OP-S), which does not require the functionality of any high level subsystem tasks (such as pointing or DCFT operations). At separation or after any major system resets, the OP-S software will initiate the first communications and verify the state of the critical components. The CONOPS will describe the software upload steps as they are finalized..

An additional requirement may exist in the operations task that the engine cannot fire after a specified period without hearing from the ground station. This is a safety mechanism that still needs to be determined.

2.1.3.2 NAVIGATION TASK

The navigation software task requirements are as follows:

NT-1 The navigation software shall provide the position and velocity vectors of the satellite, the sun position vector, and the ground station position vector.

NT-2 The navigation task shall determine the desired pointing orientation for each maneuver, when queried by the operations task.

NT-3 The navigation software shall compare GPS data, ground tracking information (TLEs) and an on-board orbital propagator prior to sending any commands to CASTOR, and must update the epoch conditions for the propagator so that the propagator alone can predict communications intervals for one week without DCFT operations.

The navigation software needs to provide the orbital state data for attitude, communications, and propulsion purposes. The NT-2 requirement alludes to the possibility that different maneuvers can be programmed for CASTOR. Currently, only a semimajor axis change (orbital radius or altitude) is planned, however this software task would allow for upgrades if additional maneuvers are planned. Whether the scheduling will occur on-board CASTOR verses from the ground station is not finalized. The final requirement NT-3 describes how the propagators must be able to predict communications intervals for one week in the presence of no thrust. This is important to ensure that if the satellite needs to be pointed to the ground during normal operations, that the propagator knows when the ground station will be in view. One week without DCFT operations should be sufficient to uplink TLEs to update the satellite's new state.

2.1.3.3 THERMAL TASK

The thermal software task requirements are outlined below. Further work will be done to detail the design to meet these requirements.

TT-1 The thermal software shall monitor temperatures of components and identify any components that are out of desired operational range.

TT-2 The thermal task shall inform the operations software if the thermal conditions of critical components are outside the accepted range.

These requirements illustrate the need for much more defined software requirements preceding the algorithm of the task. There are many types of ways to inform the operations software, so a detailed plan must be agreed upon between the thermal team and operations team to ensure that the satellite will survive in all operational cases. The thermal sensor files will be created in either the operations task or the data collection and storage task. The thermal team will be responsible for providing the thermal task algorithm, as well as testing the final software product.

2.1.3.4 ADCS TASK

AT-1 The ADCS software shall determine the attitude of the spacecraft with respect to the inertial and orbital reference frames at any time.

AT-2 The ADCS software shall point the satellite in the desired direction to detumble body rates, generate power, point the thrust vector, or communicate with the ground.

AT-3 The ADCS task shall have the capability of collecting sensor data, calculated data, and actuator data and send the data back to the ground.

The ADCS task interacts with the operations and navigation tasks to ensure that the satellite is pointed where it is supposed to be. The attitude determination algorithms and processing (Kalman filters) will take place in this task. AT-1 and AT-2 are the general requirements that the attitude system needs to meet for CASTOR. No error values are associated with these software tasks; however, the amount of error will factor into the decision to operate the DCFT. AT-3 is the interface between the ground analysis tools and the satellite data packaging. The ADCS team will determine what scope AT-3 entails and how much detail they will want to be collected.

2.1.3.5 ADDITIONAL TASKS

The EPS, Communications, and Propulsion system tasks still need to be analyzed and the requirements written. Additionally, the high-level communication task may or may not actually be placed in the satellite software architecture, as most communications functions are inherent in the baseline software.

2.1.4 FLATSAT OPERATIONS AND TESTING (K. ANDERSON)

The CASTOR satellite must undergo extensive testing to create mission assurance. Mission assurance is defined as the general system engineering, quality, and management principles towards the goal of achieving mission success, and, toward this goal, provides confidence in its achievement. Mission success is defined as the achievement of a system to singularly or in combination meet not only specified performance requirements, but also expectations of the users and operators in terms of safety, operability, suitability, and supportability. Mission assurance focuses on the detailed engineering of the acquired system, and, toward this objective, uses independent technical assessments as a cornerstone throughout the entire concept and requirement definition, design, development, production, test, deployment, and operation phases.

There are three key reasons why a test should be performed. These reasons and the rationale behind them are listed below.

1 Functionality verification
   1.1 Evaluate that the as-built system (including interfaces) satisfies the requirements and specification baseline.
   1.2 Identify issues with the proposed test, integration, and verification plans and procedures
2 Reduce Risk
   2.1 Evaluate appropriateness and risk of verification by any method other than testing.
   2.2 Evaluate risks associated with deviations from environmental testing standards (e.g., MIL-STD 1540) and other applicable standards or best practices.
   2.3 Evaluate the fidelity to the "test like you fly" (TLYF) and "test what you fly" philosophies, especially at the system and higher levels of integration, and identify risks associated with deviations from these philosophies. This includes implications to accurate modeling and simulation.
3 Unfamiliar Area
   3.1 Evaluate analysis, simulation, inspection, and test results to determine readiness to proceed to subsequent test or program activities.

All testing will follow begin at the component level, progress through the subsystem level, and finish at the assembly level. There may be additional tests between the three major levels, but as a minimum, all aspects of the design will be tested in this order for the reasons listed above.

2.1.5 GNC DESIGN (D. DELATTE)

The GNC design is currently proposed to consist of two major navigational aides: a GPS receiver and an on-board orbital propagator. Neither of these has been analyzed fully this semester, although the current GPS receiver picked is the same from the previous class

(SGR-05). The on-board orbital propagator will utilize the SGP4 propagation technique, which propagates Two Line Elements (TLEs) forward in time. The TLEs would be uploaded from the ground station. The nominal operations include using the GPS as the primary navigation tool and having the on-board propagator as a backup as well as look-ahead for scheduling.

2.1.6 INTEGRATED MODELING (J. ROBINSON)

A CASTOR systems model is being developed to predict the expected state and behavior of the CASTOR system. At the end of this development process, an integrated model will exist that can serve two purposes:

- Predict the expected states and maneuvers of CASTOR
- Compare actual behavior with expected behavior
- Track DCFT performance/fulfillment of mission objectives
- Aid design decisions and different operational mode analysis

The first purpose of predicting the expected CASTOR behavior will be important to ensure that once on-orbit, the CASTOR operations team has full control over the vehicle and can provide any interested parties with the future predicted state of CASTOR. The CASTOR vehicle does not have a large amount of thrust capabilities, so even with large amount of prediction errors, the CASTOR state can be controlled, given the assumption that the satellite does not maneuver autonomously if it does not hear from the ground station. The second purpose of the integrated model will be to feed in the CASTOR commands to the simulation and show how the systems are interacting with each other. After calibration in the initial stages of commissioning and early normal operations, this tool will allow operators to see any divergence from the expected behavior, and thus enable operators to identify future problems or failures before they intensify.

This integrated model will be used to characterize and track the DCFT‘s performance with time to fulfill its mission objectives. The total firing time of the engine and the realized total delta-V are the main outputs of the mission, but the integrated model will allow vehicle errors (pointing or navigation) to be incorporated to get a better representation of the DCFT‘s performance.

2.2 ACS DESIGN (D. DELATTE)

The role of the Attitude Determination and Control System (ACS) is to determine and control the orientation of the spacecraft. The current sensor architecture consists of a space-qualified GPS system to determine position, a set of four space qualified sun sensors, a three-axis inertial measurement unit (IMU), and a magnetometer to determine attitude. The actuator architecture consists of three orthogonal, space-qualified reaction wheels to control about each of the three axes and three orthogonal torque coils to de-saturate the reaction wheels and provide redundant control authority. This version of this

spacecraft is designed to operate in low earth orbit (LEO), as opposed to the previous version, which was designed to operate from geosynchronous orbit (GEO) out to the moon. Therefore, torque coils can be used for desaturation in place of the nitrogen thruster system. The concept of operations and the external torque environment is a driving factor in the design of the spacecraft ACS architecture. The spacecraft will experience disturbance torques from the strong engine magnet, aerodynamic drag, solar pressure, and the gravity gradient due to its proximity to the earth. Moreover, the satellite must be able to deal with the challenges imposed by eclipse, during which attitude estimation would be limited to the magnetometer and IMU, power is constrained, and the control sequence will be limited. Finally, operation in low earth orbit (LEO) allows use of GPS for position and velocity determination.

The design of the spacecraft ACS system must meet several requirements. First, the spacecraft must orient the main engine to point in the direction specified by the desired orbit, parallel to the velocity direction. The primary goal of the main engine is to show a change in velocity. Therefore, the main engine must be oriented either in line with or opposite the velocity vector. Any inaccuracy in this pointing will result in a decrement of directional thrust efficiency and thus a loss in delta V. The thrust requirement is to achieve 97% time-averaged directional thrust efficiency. Secondly, the spacecraft must orient the solar panels in the direction of the sun, so that the sun's rays strike normal to the frontal area of the deployed solar panels. During the engine's operational phase, the solar panels can only be turned toward the direction of the sun by changing the attitude of the satellite about the x-axis. During the battery-charging phase, the solar panels will be aligned normal to the sun. As with the engine, an inaccuracy in this pointing will result in a loss of power generation. The power generation pointing requirement is to maintain 97% efficiency in solar energy generation due to pointing, which is an angle error of 14º. Finally, the spacecraft must be controlled for its designed mission length of twelve months.

To maintain these efficiencies, the instantaneous orientation of the spacecraft must be known in order to actuate the spacecraft to the reference orientation. Based on common ADCS performance from SMAD, the ratio needed between actuation accuracy and estimation accuracy is five to one. Since the overall pointing actuation requirement is set at five degrees, it was determined that the appropriate attitude estimation accuracy is one degree in each axis. To accomplish this task, a sensor suite of four sun sensors and one magnetometer is selected for the design. The IMU is needed to integrate rates to determine attitude during periods of unavailable sensor readings. The need to reliably use a magnetometer places a requirement on position accuracy. The magnetometer requires knowledge of position to determine the true magnetic field vector in order to compare the vector of the magnetometer reading with the local magnetic field from the International Geomagnetic Reference Field (IRGF) model vector and thus obtain attitude vector equivalence. The position requirement is derived from an analysis of how an error in position determination creates an error in attitude estimation. A position estimation error when the spacecraft is along the equator will have the largest impact on the attitude error. The magnetic field has the highest gradient with respect to latitude around the equator,

while changes in longitude have little effect. As latitude increases, the gradient with respect to latitude direction decreases. The analysis done compares the direction of the modeled magnetic field vector at one point on the equator with the direction of the modeled magnetic field vector with some latitude error. The angle between the two vectors obtained by a dot product gives the attitude error. The attitude error is assumed to be a linear function of error in latitude, which makes use of the linearization of the sine function for small angles. If the attitude error from the magnetometer is constrained to 0.1 degrees, there is a reference input error of 166 arc seconds (0.05 degrees). Given the assumption that the earth's magnetic field has been perfectly modeled, converting to units of distance gives 5.7 km of allowable position error in the north-south direction to maintain an attitude estimate to 0.1 degrees. Selecting 0.1 degrees leaves margin for both fluctuations in the earth magnetic field and lack of accuracy of magnetometer output.

This causes error in aligning the engine with the velocity vector. If the spacecraft estimates its position with some error, the reference thrust vector input to the ACS system will be sub-optimal: the latitude or longitude error will be equal to the error in reference input. Therefore, the 166 arc second (0.05 degrees) reference input error mentioned earlier will lead to an acceptable additional 0.05 degrees in attitude error.

The ACS control torque magnitudes are sized so that the satellite is capable of completing required state changes over each orbit. In addition, the solar panels must re-acquire the sun quickly (time << period in sunlight) after re-entering sunlight. The requirement on update frequency was based on the stability of the designed control system (detail in 2.3.5). The ACS torque requirement is based on a worst case disturbance torque build-up over two orbits and the capability for re-orientation within 10 minutes. The following is the full set of ADCS requirements:

1. ACS
    1.1. ACS shall estimate and control the attitude of the spacecraft body to point the thrust vector such that 97% of the thrust is in the commanded direction.
    1.2. ACS shall estimate the attitude of the spacecraft body to 1 degree of its true attitude in all 3 axes.
    1.3. ACS shall control spacecraft attitude to 5° of a reference input in all 3 axes.
    1.4. ACS shall be able to control the spacecraft attitude through a dynamics range of 360° in all 3 axes.
    1.5. ACS shall be able to perform a 180º slew on the spacecraft body within 10 min.
    1.6. ACS shall perform a spacecraft attitude estimate and control at a rate of 1 Hz.
    1.7. ACS shall be able to reduce angular rates to a manageable magnitude during initial deployment and departure from eclipse.
    1.8. ACS shall be able to apply a torque of 0.033 N-m during de-tumble.
2. Longevity

2.1. All ACS components shall survive launch loads.
2.2. All ACS components shall function for 12 months of spacecraft operation.

2.2.1 BUDGET (D. DELATTE)

Attitude determination and control functionality is critical in order to communicate with and operate the spacecraft. In order to design a lean, yet reliable determination and control system, several architectures fitting in weight restraints of the University Nanosatellite Program (UNP) were considered, and the system detailed in the sections below was selected for its reliability, constructability, and low relative cost.

Component	Units	Total Power (W)		Total Mass (kg)	Total Cost ($)
		Nominal Power	Peak Power		
Sun Sensor	4	0.1	0.3	0.136	48000
Magnetometer	1	0.0024	0.003	0.022	480
Reaction Wheel	3	1.5	21	0.675	90000
Torque Coil	3	3	6	0.75	750
IMU	1	0.165	0.285	0.02	620
GPS Unit	1	0.5	0.8	0.02	23010
GPS Antenna	1			0.012	
Magnet	1			0.25	2000
Total		5.2674	28.388	1.885	164860

TABLE 2.2.1-1: ACS/GNC COMPONENT BUDGET

2.2.2 DESIGN CAPTURE (D. DELATTE)

The goal of the ACS system was to optimize the system's mass and dollar cost parameters while fulfilling requirements. The ACS system is designed to have a large amount of redundancy to mitigate risk and work closely with a number of other subsystems. The requirements are driven by the needs of the payload, the DCFT. The torque coils de-saturate the reaction wheels and could be used to turn the satellite if needed (albeit much more slowly). The following points were considered: magnitudes and time-domain profiles of external disturbance torques, typical range of inclinations within which the spacecraft will operate, characteristic rotational speeds, and vehicle moments of inertia. The following paragraphs expand on various aspects of the design for the torque disturbances, vehicle inertias, and controller design.

By simulation of the torque disturbances over a typical orbit and the attitude maneuvers of the orbit, the reaction wheel max torque is set to 60 mNm, which is enough to correct for instantaneous and time-averaged disturbance torques as well as slewing.

The design of the spacecraft has assumed orbits inclined between 0 and +60 degrees relative to the earth's equatorial plane. The controller design shall be robust to inclination variation by being able to handle the worst-case disturbance torques (magnetic) and the worst-case sunlight to eclipse ratios (ecliptic, 50%) throughout this inclination range. The controller uses consumable actuation in the form of reaction wheels storing angular momentum for torque control. When one of the reaction wheels reaches a speed near saturation, magnetic torque coils will turn on to provide an external torque on the satellite and remove the stored momentum in the reaction wheel. The cycle of attitude control with reaction wheels and de-saturation with torque coils is a sustainable process under the current concept of operations.

Vehicle inertias, as provided in the structures section indicate that the spacecraft, with no actuation over the cycle of one orbit would change attitude arbitrarily over the characteristic period of approximately 90 minutes. From the start of sunlight entry, the reaction wheels are able to orient and control the spacecraft over a period of approximately 10 minutes. This period may be shortened if limited or full control is implemented during eclipse.

2.2.3 HARDWARE AND ARCHITECTURE (S. VEGA)

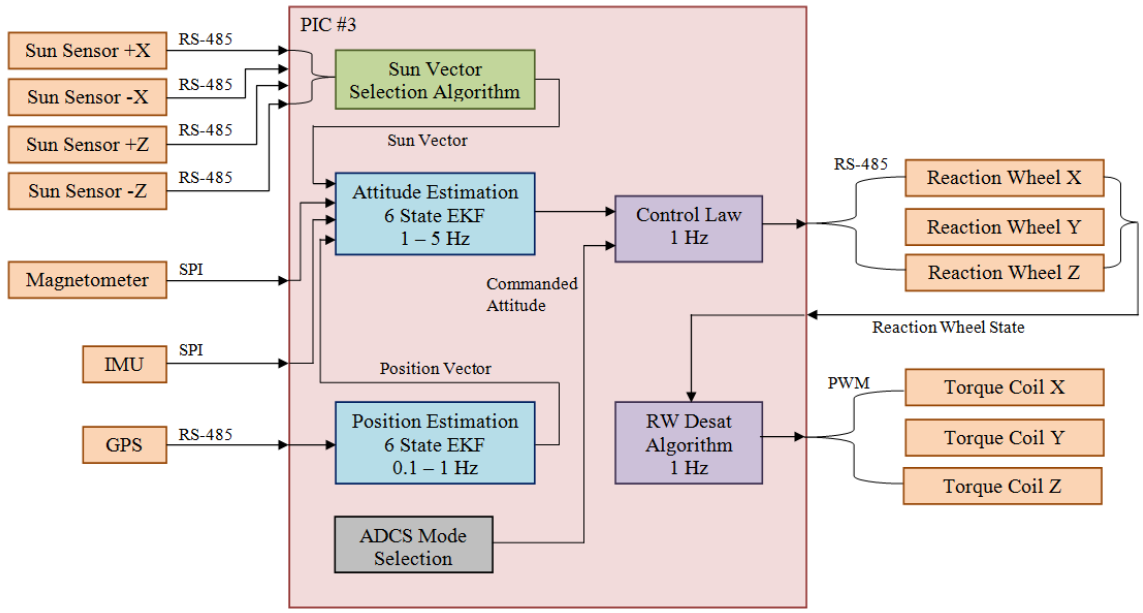

FIGURE 2.2-1: HARDWARE AND SOFTWARE SCHEMATIC

As can be seen in the above figure, the CASTOR ADCS hardware selection can be divided into two parts: sensors (left side) and actuators (right side). The sensors consist of a space-rated GPS receiver, one three-axis magnetometer, four two-axis sun sensors, and a three-axis IMU for short term angular rate and acceleration measurements. Detailed specifications for each of these instruments, including operational parameters, mounting instructions, data and power needs can be found in the appendices. The magnetometer, along with the sun sensor, provides the primary reference for attitude determination. The GPS unit provides precision position and linear velocity information. The position information is used to determine the expected local magnetic field of the Earth from an on-board look-up table and uses this to determine attitude information from the magnetometer. The sun sensors provide the missing information not available from the magnetometers. The IMU is used to determine angular rate information during the initial de-tumble and during slews. Some amount of linear acceleration information can also be determined if this is caused due to gas leaks in the main engine pressure lines. The IMU can be used to determine linear acceleration due to the main engine, but it is not the primary purpose of the IMU.

The actuators consist of three 0.12 Nms momentum storage capable reaction wheels with a continuous torque greater than 5 mNm. These reaction wheels have been chosen to provide enough momentum storage capability to offset the disturbances from external torques and maintain attitude control during slew maneuvers over one orbit without de-saturation. Three torque coils with a maximum dipole of 3 Am^2 are used to de-saturate the reaction wheels. Given a nominal orbital position of the satellite, the torque coils can fully de-saturate the reaction wheels in approximately 30 minutes.

Each sensor and actuator is chosen to comply with or exceed one of the requirements listed in the section above. This relationship between the requirements and the hardware components is provided below. The numbering scheme is the same as that used for the requirements section above.

1. ACS
    1.1. Results from the control law simulation which includes all sensors and actuators and accounts for signal noise as well as realistic estimators and filters show that the engine thrust pointing is correct for over 97.5% on average.
    1.2. Estimator error with manufacturer specified noise and error levels for magnetometer is 0.6°. The sun sensors must be characterized to determine estimator error.
    1.3. Simulation shows that control within 5˚ of reference value can be achieved in operation.
    1.4. ACS reaction wheels provide rotational movement about all 3 axes for 360˚; redundancy is achieved by using the torque coils for attitude control.
    1.5. ACS is able to provide full range state change in 10 minutes based on

calculated actuator forces and torques and spacecraft mass and inertia properties obtained from the CAD model created by the structures team.

1.6. Attitude estimate at a rate of 1 Hz is performed by the estimator. Attitude sensors update at frequencies at or higher than 5 Hz each. The GPS information is updated at 5 Hz.

1.7. ACS torque coils able to de-tumble initially since they can apply external torque on the satellite. De-tumble on eclipse exit is performed by the reaction wheels.

1.8. ACS able to provide torque of 0.01 Nm if required.

2. Longevity

2.1. Non-space-rated components have specified loading thresholds in relevant directions less than launch loads specified by ESPA.

2.2. All ACS components have specified lifecycle times exceeding requirements.

SUN SENSOR DATA

The CASTOR satellite will have four sun sensors, which will detect the position of the sun. For this project, we are using the SS-411's ±70º field of view. The abilities of different varieties of sun sensors to have the accuracy and specifications greatly impacted the decision process. The SS-411 Two-Axis Digital Sun Sensor by Sinclair Interplanetary has 0.03 kg of mass, and uses .0750-Watts max power. This component is space rated.

The price of each sun sensor has increased to $12,000. Having four sun sensors reduces the number of blind spots on the satellite, but it is currently uncertain whether the budget will allow for the unexpected increase in necessary funding.

The sun sensor's task is to determine the vector to the sun. Each SS-411 will return a three- component vector (from the satellite to the sun), which will tell the control law how to turn the satellite in order for the solar panels to be orthogonal to the sunlight. Having four sun sensors will give greater coverage of the satellite and allow the position to be determined quickly. Should one or more (but not all) sun sensors fail, the reaction wheels could be used to rotate the satellite until the sun's position is detected. This would be less efficient, but it is a viable back up plan. If all sun sensors fail, the GPS alone can provide the sun vector (the position in latitude/ longitude/ altitude provided by GPS can be used to determine when the satellite enters or exits eclipse) or the reaction wheels could be used to turn the satellite so that the solar panels could get some time in view of the sun. This would not be an efficient use of power and is extremely unlikely, but this backup would keep the mission from failing.

Although the sun sensors cannot be purchased until after this spring semester (thus delaying testing), an engineering model should be acquired with the correct connectors in order to demonstrate the placement and links of the sun sensor.

Part Name: SS-411 Two-Axis Digital Sun Sensor

Manufacturer: Sinclair Interplanetary

Contact: (647) 286-3761 voice, (775) 860-5428 fax, dns@sinclairinterplanetary.com

Accuracy	±0.1° over ±70° Field-of-View
Earth Albedo Error	Rejected by internal digital processor
Bandwidth	5 vector solutions / second
Command / Telemetry	UART, SPI, I2C or CAN
Mechanical	34 mm x 32 mm x 21 mm, 34 g mass
Outer Surfaces	Low emissivity gold, scratch-proof sapphire
Supply Voltage	4.0 to 50.0 V
Supply Current	5.0 mA avg, 15.0 mA peak
Temperature	-25°C to +70°C operating
Space Heritage	14 Sensors on-orbit on 4 LEO missions

TABLE 2.2-2: SUN SENSOR CHARACTERISTICS

INERTIAL MEASUREMENT UNIT DATA

The IMU chosen for CASTOR is the ADIS16365 by Analog Devices. The IMU's component success will be determined according to whether it meets the required specifications necessary for the CASTOR satellite and whether it correctly interfaces with the other components. From resources allotment, the IMU must draw max 0.1650 Watts and have a mass under 0.02 kg. The selected part complies with these requirements.

The rate sensor will be tested using the SPI with a 32-bit Windows operating system. Prior analysis has indicated that the communication works, but the accuracy needs to be determined. A rate table will be used to determine the static rate and this value will be compared to the output of the IMU. In an ideal situation, this component would be tested on the air bearing, but it is currently uncertain exactly when that will be completed. In the meantime, the rate table is an excellent option.

Part Name: ADIS16365

Manufacturer: Analog Devices, Contact: (781) 329-4700,

(781) 461-3113 fax, www.analog.com

	Characteristic	***Value***
Performance	Measurement Range	±10 g
	Resolution	14-bit
	Bandwidth	350 Hz
Physical Envelope	Mass	TBD
Thermal	Operating Temperature Range	−40°C to +85°C
Power	Operation	5 V ± 0.25 V
	Normal Mode at 25° C	33 mA
	Fast Mode at 25° C	57 mA
	Sleep Mode at 25° C	500 µA

TABLE 2.2-3: MEMS IMU RATE SENSOR

MAGNETOMETER DATA

The Micro-Mag3 3-axis magnetometer takes a 3-axis vector reading of Earth's local magnetic field which will be compared to the International Geomagnetic Reference Field (IRGF) model vector in order to determine attitude. Accurate attitude estimation is necessary to be able to actuate the satellite from its current orientation to the reference orientation.

The ACS magnetometer group has successfully connected the Micro-Mag3 magnetometer via the PNI communication board and collected data from the magnetometer using the CommBoard Studio graphical user interface (GUI), thereby completing acceptance testing. The measurements from the magnetometer have also been correlated to the corresponding magnetic field measurements. The correlation is as follows: (measurement + offset) * scale= field strength

where the offset=-15 and the scale=-0.00025. This information is not provided by the manufacturer.

Component testing will aim to prove that the magnetometer is capable of meeting accuracy requirements. The ACS requirement for attitude determination is within 1˚ of accuracy in each axis. To determine this capability, the magnetometer will be tested in a magnetic field created by a Helmholtz coil, so that the 1-axis magnetic field vector is known. When placed between the coils, the reading from the magnetometer should then confirm the known magnetic field, showing a vector component of the field in one axis. ACS will also be able to rotate the magnetometer to specified angles to confirm the correct vector component measurements in each axis, testing how accurately the magnetometer estimates the known magnetic field vector. This test will inform ACS as to what accuracy the magnetometer is capable of predicting the magnetic field's location.

Once this test is completed, the next stage of testing will be to test the component on the air bearing test bed, using the SPHERES satellite to give a true attitude reading to compare to the reading from the magnetometer. A larger Helmholtz coil is also being constructed around the air bearing, such that a similar test to the tabletop Helmholtz coil test can be run on the air bearing with greater degrees of freedom available to position the magnetometer. ACS will create an estimation process for the magnetometer readings to attain this accuracy.

Part Name: MicroMag3 (Part # 12349)

Manufacturer: PNI Corporation

Contact: 707-566-2266 phone, email: sales@pni.corp, web: www.pnicorp.com

	Characteristic	***Value***
Performance	Large Field Measurement Range	±1100 μT
	High Resolution Field Measurement	0.015μT
	Fast Sample rate	Up to 2000 Hz
Physical Envelope	Mass	10 g (estimate)
Thermal	Operating Temperature Range	-20° to 70° C
Power	Operation	3V
	Max DC Supply Voltage (V_{DD})	5.25 VDC
	Max Input Pin Voltage	V_{DD} + 0.3 VDC
	Max Input Pin Current	10.0 mA at 25°C

TABLE 2.2-4: MAGNETOMETER CHARACTERISTICS

GPS UNIT DATA

The Surrey Satellite Technology Ltd SGR-05U Space GPS Receiver is capable of providing standard GPS time in addition to position and velocity readings that can infer orbit determination.

The component is however extremely expensive and thus is yet to be purchased. However the GPS compent has great deal of flight heritage and requires testing briefly to utilize it.

Part Name: SSTL SGR-05U

Manufacturer: Surrey Satellite Technology Ltd

Contact: +44(0)1438 803803 phone, +44(0)1438 803804 fax,

email: info@sstl.co.uk, web: www.sstl.co.uk

	Characteristic	***Value***
Performance	Time (UTC)	1 μs
	Position	10 m
	Velocity	0.15 ms^{-1}
	Dynamic Capability	8 kms^{-1}, 2g
Physical Envelope	Mass	20 g
Thermal	Operating Temperature Range	0° to 50° C
Power	Operation	0.5-0.8 W @ 5 V
Environmental	Vibration (acceptance level)	15 g rms

Table 2.2-5: Space GPS

TORQUE COIL DATA

When in orbit, the 3 torque coils will act as momentum dumpers to desaturate the 3 reaction wheels. In operation of the satellite, angular momentum will stored up in the reaction wheels. When the angular momentum of the satellite as well as the speed of rotation of the reaction wheels verges on the maximum desired value, it is said to be saturated. It is at this point that the torque coils are needed to provide an external torque that desaturates the reaction wheels by dumping the angular momentum stored up onto the earth by torquing against the earths magnetic field. The torque coils are required to provide this function within one orbit. Desaturation of the satellite should only occur when

The torque coils are being built in house and are sized to be able to desaturate the reaction wheels within approximately one orbit. Based on the reaction wheel momentum storage capability, the torque coils should have a magnetic dipole of approximately 3 Am^2. The coils will be built in house using 32 gauge copper magnet wire. There will be three torque coils placed on the satellite and each of these coils must be located orthogonal to each other in order to provide sufficient torque capability. Two of the coils will be placed along the perimeter of the frames on the sides and the third coil will be placed on the top frame, as shown in Figure 2.2.32: Torque coil layout (top) and Figure 2.2.33: torque coil layout (side). The following description gives the details of the coils that will be placed along the structure. The magnetic dipole of a wire coil is given by the equation: u = A*i*n where:

u = magnetic dipole (Am^2) A = enclosed area (m^2)

i = current (A) n = number of turns of wire

The outside frames have rectangular shapes allowing the torque coil design to have rectangular geometries of sides roughly measuring at 30 by 43cm on the sides and 43 by 43 cm on the top. The coil will be lined along the inside face of the frames.

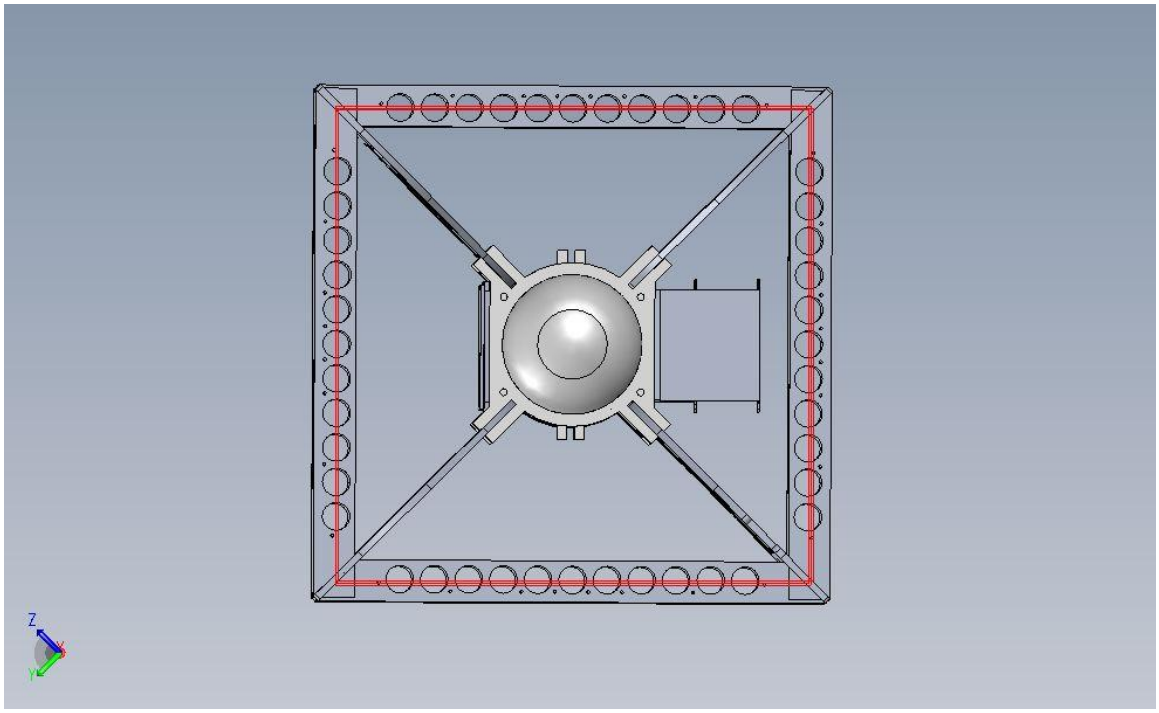

FIGURE 2.2.3-2: TORQUE COIL LAYOUT (TOP)

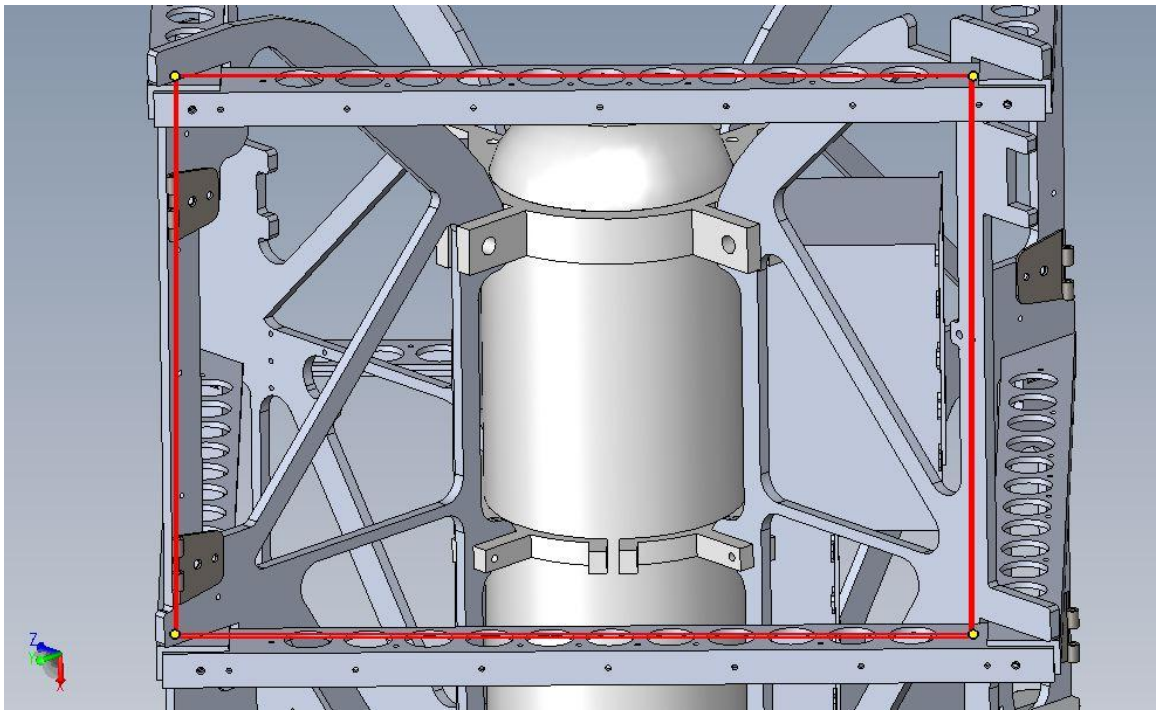

FIGURE 2.2.3-3: TORQUE COIL LAYOUT (SIDE)

The torque coils on the side provide desaturation along the y and z axis. After optimization calculations the desired specifications have an enclosed area of 0.129 m^2. In order to minimize power use and stay within the limitations of 32 gauge copper wire chosen, the current has been chosen to be 0.05 A. This leaves the number of turns to be 466. This gives a total length of 680.4m of coil in each case and a power rating of 1.57 W. In order to mount the coil, the use of straps will be used initially. If this is not sufficient for vibration testing a more permanent attachment such as hooks may be used. The straps/hooks will be spaced in a manner to increase the fundamental frequency of the coils so that they will withstand the launch environment.

The torque coil on the top side makes available a larger area of 0.1849 m^2 for use, thus the parameters are different from the other two. Staying with the 32 gauge wire and keeping in mind the same power limitations as before a current of 0.05A will be in use. This provides the number of turns as 325. Giving a total length of about 558 m and a power rating of 1.917 W.

The torque coils will be controlled using an H bridge, which allows the input power to be reversed based on a control voltage placed on the H bridge. The torque coils will need to provide a dipole in both directions depending on the momentum vector of the satellite and reaction wheels. The avionics processor can switch inputs into the H bridge in order to switch the direction of the current flowing through the coil, and therefore switch the dipole provided. The avionics processor can also provide a pulse width modulated signal to the H bridge so that the current flowing through the coil is a percentage of the maximum current. Therefore, the coils can be powered at various levels depending on the amount of torque they need to provide.

The H bridge currently being used as a pinout diagram shown below. This H bridge is a dual model and can be used to operate two torque coils. The entire specifications sheet for this device can be found at:
http://search.digikey.com/scripts/DkSearch/dksus.dll?Detail&name=NJM2670D2%23-ND

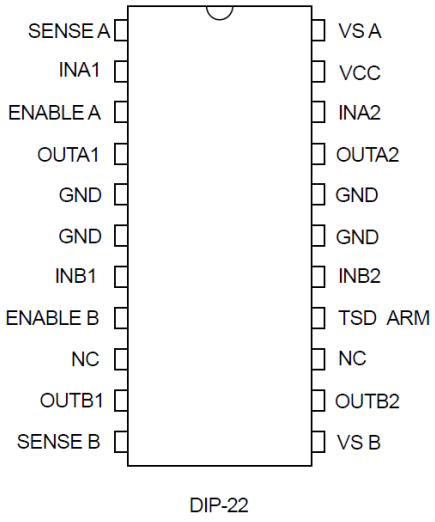

FIGURE 2.2.3-4: TORQUE COIL PINOUT

The torque coils will also have a current sensor providing current feedback to the processor. The current sensor is not intended to be used for active feedback control since high precision of the magnetic dipole is not necessary. However, a current feedback option on the sensor would allow the avionics processor to know the coil is on and operational.

The resistance of a 3 Am^2 coil with the dimensions given above is approximately 366 Ohms. The maximum power required by each coil is approximately 2 W. When in desaturation mode, all three coils could be on and all three could be providing 3 Am^2 of dipole. In this worst case scenario, the coils could require 6 W of power. However, this case is unlikely. On average, the coils will be on for approximately 15 minutes per orbit with a nominal power use of 1.5 W.

REACTION WHEEL DATA

The reaction wheel model used on the satellite will be the Sinclair Interplanetary RW-0.060-28 model which provides a momentum storage capability of 0.12 Nms and weighs 0.225 kg per wheel. The specifications for the Sinclair Interplanetary reaction wheel are given below.

Part Name: RW-0.060-28
Manufacturer: Sinclair Interplanetary
Contact: 647-286-3761 voice, 775-860-5428fax
HYPERLINK dns@sinclairinterplanetary.com

Nominal Momentum	60 mNm-sec @ 6500 RPM
Nominal Torque	> 5 mNm @ 28 V
Control Mode	Speed or Torque, built-in control CPU
Command / Telemetry	UART, I^2C/SMBus, SPI, RS-485, CAN
Mechanical	75 mm x 65 mm x 38 mm, 225 g mass
Supply Voltage	7.5 V to 35 V nominal (50 V max)
Supply Power	7.0 W at full torque, full speed 0.5 W @ 5000 RPM steady-state 0.2 W @ 2000 RPM steady-state
Environment	-40ºC to +70ºC operating temperature >12 g_{RMS} Vibration, >15 krad total-dose
Reliability	Diamond coated hybrid ball bearings Redundant motor windings
Heritage	Flight units delivered for 2 satellites. Fabrication for 3 more satellites ongoing

TABLE 2.2-6: REACTION WHEEL CHARACTERISTICS

CANCELLING MAGNET

ADCS will be incorporating a cancelling magnet to counteract the permanent magnetic dipole of the engine.

•Neodymium – 50% stronger magnetic field than SmCo

Theoretical System Dipole: 0.00552 Am^2

2.2.4 HARDWARE OPERATIONS DETAILS (N. CONDUAH)

It is important to have low power use during eclipse because the battery mass required over the length of the mission has to increase with greater required power. The ACS team has developed a power cycling system in conjunction with the power team such that sufficient knowledge of the state can be maintained at all time while reducing power consumption, especially during eclipse.

A number of the components, such as the IMU, magnetometer, and GPS, can be run in faster or slower modes. We expect slow changes in our angular rates, and the GPS maximum velocity range (8 km/s) is within that of the maximum projected velocity of the

satellite, such that the amount of information provided in a slow mode will be sufficient for orbit propagation and the slower settings can be used for normal operations. During specific events, such as the commissioning phases of the hardware, it would be useful to have the higher data rates. In emergency states from other systems that result in low available power, the components have sleep or standby modes.

For our reference orbit of 90 minutes, the sunlight period is 54 minutes, and the eclipse period is 36 minutes. In eclipse, little power is available to the subsystem to maintain the attitude of the vehicle. The sun sensor is not available, for lack of sunlight. The largest power draw, the GPS, requires up to 10 minutes to turn on from a cold start, which is prohibitive when the eclipse time/ sunlight time ratio is high. A warm start from standby, on the other hand, takes an initialization of position and can take only 90 seconds to start. However, if the GPS fails to issue data within 10 minutes, then a cold start reset is completed.

As can be seen in the figure below, to avoid the need for a cold start, the GPS will be put on standby at the start of eclipse for 7 minutes, then give it a warm start command (90 s) and operate for 30 seconds, long enough to get a Position/Velocity/Time solution. This solution will be stored in the orbit propagator and the GPS will be put on standby again. A 36-minute eclipse period gives four of these 9-minute cycles. The final cycle will have a standby time of less than 7 minutes such that the GPS can remain on for more information during any maneuvers performed while exiting eclipse. The precise time for this maneuver is yet to be determined, but will be less than 5 minutes, for a final 9-minute cycle of 6 minutes of standby, 90 seconds of startup, 30 seconds to acquire a position, and 1.5 minutes of additional information gathering before eclipse exit.

The magnetometer and IMU will remain active during eclipse. The IMU will not be able to be re-initialized fully, as the magnetometer reading will be depending on a position propagation to determine attitude. However, the drift rate of 4.2 °/√hr (where the √ refers to a root-mean-square value) is small enough that over the 36 minute eclipse, the unit can be relied upon to give control inputs if necessary.

The reaction wheels operate with steady-state power of 0.2 W each at 2000 RPM and 0.5 W at 5000 RPM. The reaction wheels are capable of a maximum power rating of 7 W at 5000 RPM when maximum torque and speed are called, however this is not a state we desired, since power will be kept low as stated. Since the orbit buildup of non-cyclic torques during each eclipse cycle is small and this momentum will need to be dumped at some point, the team has chosen to desaturate the wheel to 1000 RPM using torque coils once it reaches 4000 RPM steady-state. This allows the reaction wheel to maintain a large amount of control authority but keeps the required power during eclipse at low levels. Thus the reaction wheels will be on during eclipse to avoid resultant undesired torques on the satellite from slowing down.

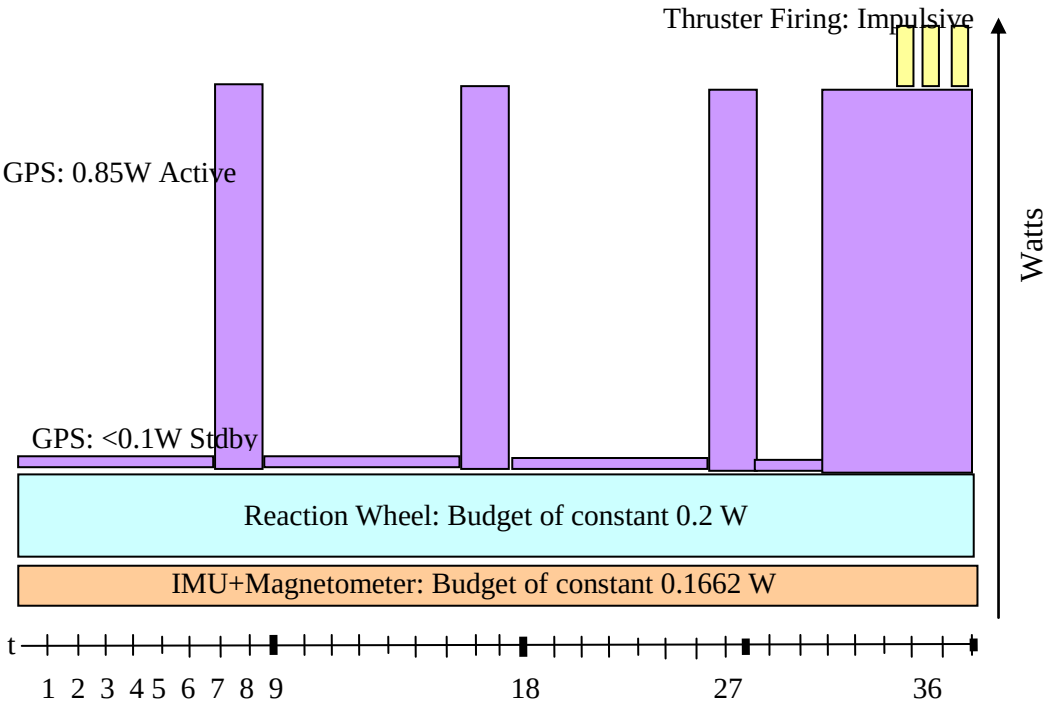

FIGURE 2.2.4-1: POWER USE IN ECLIPSE

The power team is currently budgeting power for the ACS team during eclipse for the cycling of the GPS, which will require up to 0.85W when on and a non-zero number of Watts during standby but is estimated to be less than 0.1 W, as well as 0.2 W of constant power to the reaction wheel (this allows a time-averaged margin of control authority for torquing maneuvers as the reaction wheel nears a steady-state of 2000 RPM, but has not yet surpassed it), a combined 0.1662 W for the IMU and magnetometer at constant, normal-speed operation.

Total W-hrs budgeted during eclipse is 3.28 W-hrs before efficiencies are factored in, which comes to 4 W-hr including inefficiencies.

TABLE 2.2.4-1: POWER USAGE FOR SENSORS (SS = SUN SENSOR, MAG = MAGNETOMETER)

Sun/Eclipse, State	Components	Power
Sun, Nominal Power	SS (active) + IMU (normal) + Mag (nominal) + GPS	1.0912 W
Sun, Min Power	SS (idle) +IMU (fast) +Mag (sleep) +GPS	1.1612 W
Eclipse, w/GPS, Nom Power	IMU (normal) +Mag (nominal) +GPS	1.0162 W
Eclipse, w/GPS, Min Power	IMU (idle) +Mag (sleep) +GPS	0.8573 W

Eclipse, w/o GPS, Nom Power	IMU (normal) + Mag (nominal)	0.1662 W
Eclipse, w/o GPS, Min Power	IMU (idle) + Mag (sleep)	0.0253 W

TABLE 2.2.4-2: POWER USAGE, ACTUATORS

Component	Power
Reaction Wheel	0.2 W @ 2000RPM (maintaining wattage); 0.5 W @ 5000 RPM(maintaining wattage); max torque @ 7 W; expected average speed of 5000 RPM at 0.5 W (maintaining wattage)
Torque Coil	2.0 W @ 3 Am^2; max dipole

As shown in **Error! Reference source not found.**, the data rates and frequencies for different components are listed below. The GPS, being utilized on the normal setting (i.e quiet not verbose mode) provides a position, velocity, and time solution every 10 seconds. Utilizing an orbit propagation program within software, this will be sufficient for position information and the lower-power setting can therefore be used.

The IMU and magnetometer will both run at 5 Hz gain sufficient sampling and accuracy. Both these sensors are capable of sensing beyond 100 Hz for additional accuracy; however, running them slightly slower reduces the data and processing loads. The sun sensor is run at 5 Hz as a default.

The reaction wheels are run at 1 Hz and the torque coils require pulse with modulation at a rate sufficiently lower than the number of dipole divisions. The avionics processor provides capability of 2^{16} levels of fidelity in width size. As such it is possible for ADCS to continuously command dipole levels between -3 and 3 Am^2.

TABLE 2.2.4-3: DATA RATES AND FREQUENCIES

Component	Data Rate	Command or Sensing Rate
GPS	19.2 kbps	0.1 Hz
IMU	8.4 kbps	100 Hz
Magnetometer	2.4 kbps	100 Hz
Sun Sensor	57.6 kbps	5 Hz

Reaction Wheels	57.6 kbps	1 Hz
Torque Coils	1 kbps	100 Hz

2.2.5 ATTITUDE CONTOL LAW (C. DEVIVERO)

A fully parametric simulation of the three dimensional attitude and position dynamics of the vehicle has been developed and is in the process of final debugging. This simulation is intended for use as an assessment tool for developing attitude control algorithms for the CASTOR satellite in a simulation environment which accurately represents the environment of space, including all sources of external torque and force.

CONTROLLER DESIGN

This section details the control algorithms which will be implemented in three dimensions, including descriptions of how they are reduced to two dimensional problems and how the two dimensional control laws are extended back to three dimensions. For most aspects of attitude control, desired torques will be computed, and mixing functions used to set actuator states to produce approximately the desired torque. These mixing functions are not discussed in detail here.

The overall design of the attitude control algorithms is driven by a desire for control law robustness to variation in the physical parameters of the system and the external environment, as well as efficient performance, and the ability to point the solar arrays toward the sun using only the minimum attitude information required to do so.

For the purposes of the following discussion, a diagram indicating some of the geometric CASTOR parameters and the definition of the body frame axes used by the simulation is included in Figure 2.2.5-1: CASTOR BODY FRAME AXIS.

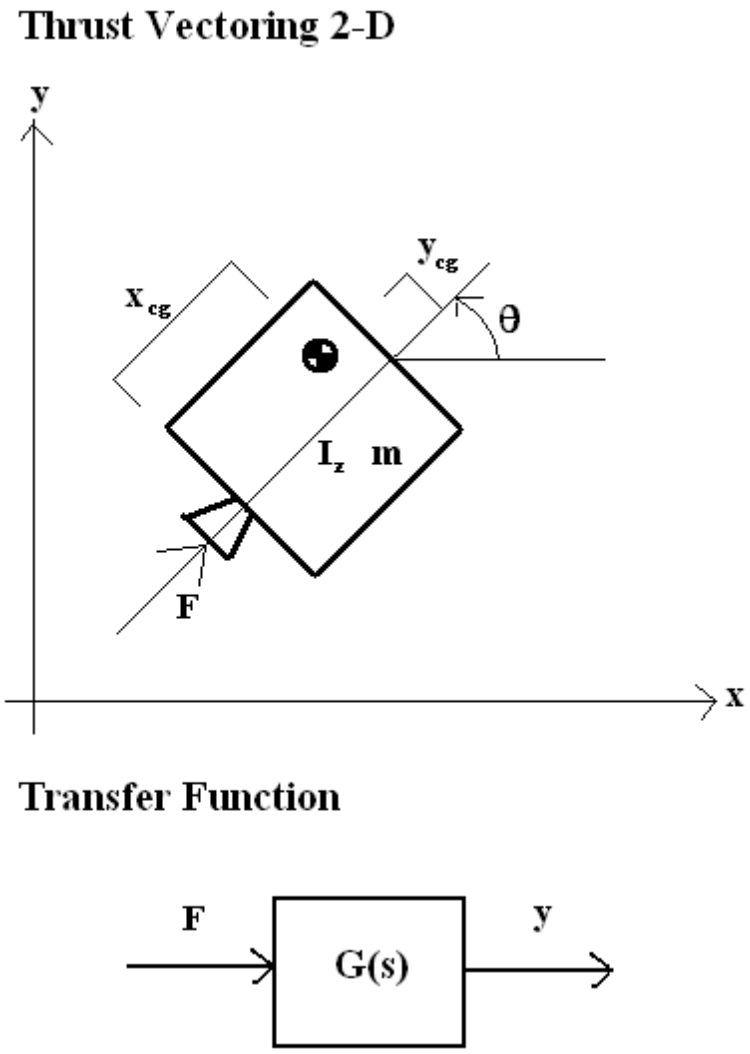

FIGURE 2.2.5-1: CASTOR BODY FRAME AXIS

SIMULATION RESULTS

Determining the value of the engine's magnetic dipole moment is required in order to accurately model the effects of the space environment on the satellite. Readings of the local magnetic field have been taken for several positions with respect to the engine in the off state, and the results indicate a relatively strong effect on the magnetic field measured by the engine.

TABLE 2.2.5-1: NON-THRUSTING MAGNETIC FIELD

Location Relative to Engine	Magnetic Field Reading (x y z)* (Gauss)

0.6m x, along thrust axis	-0.191997	-1.150754	37.8
0.4m x, along thrust axis	-0.247530	-0.335008	37.3
0.2m x, along thrust axis	-0.716794	-0.224456	39.2
0.1m x, along thrust axis	-10.394747	-0.572864	36.3
0.4m x, 0.1m toward cathode	0.042921	-0.144054	38.5
0.4m x, 0.1m away from cathode	-0.382171	-0.495812	35.8

The following steps were taken to determine the dipole moment of the engine in the off state:

1. Calibrate magnetometer and place it in a fixed location far (over 2 m) from the main engine.
2. Record several magnetometer readings, and average them to determine the baseline magnetic field direction.
3. Place the main engine at various locations relative to the magnetometer, recording magnetic field readings for each location.
4. Using the corrected value of the magnetic field readings at various locations relative to the engine, apply a regression using the point dipole equation to estimate the dipole moment of the engine.

After performing the test described above, the main engine dipole is determined to be approximately 20.4 A-m^2. Tests must be performed for the engine in the on state, and the estimated values of the engine magnetic dipole moment incorporated into the parametric simulation, and accounted for in the design of control and estimation algorithms.

An initial simulation has been performed, and its results shown in Figure 2.2-2 and Figure 2.2-3. This simulation models the three dimensional attitude dynamics of the satellite with environmental disturbances and plots the external torques and forces on the vehicle as a function of time as it progresses through several circular orbits at four hundred kilometers of altitude and twenty six degrees of inclination, with fixed attitude and reference tracking attitude respectively. The decomposition of net torques by source indicates that the external torque on the vehicle is dominated by magnetic dipole-dipole interaction, and the net external force is dominated by aerodynamic drag. Due to the large magnetic dipole of the engine and its strong interaction with the earth's magnetic field, a permanent magnet will be placed on the satellite to counteract the magnetic dipole of the main engine.

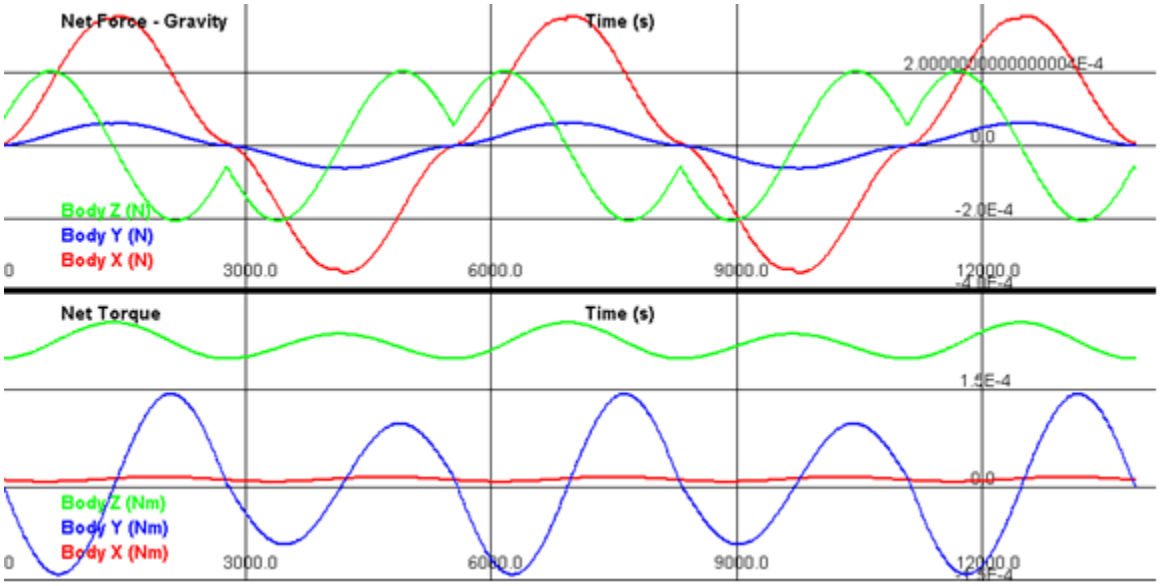

FIGURE 2.2-2: NET EXTERNAL DISTURBANCES (FIXED ATTITUDE)

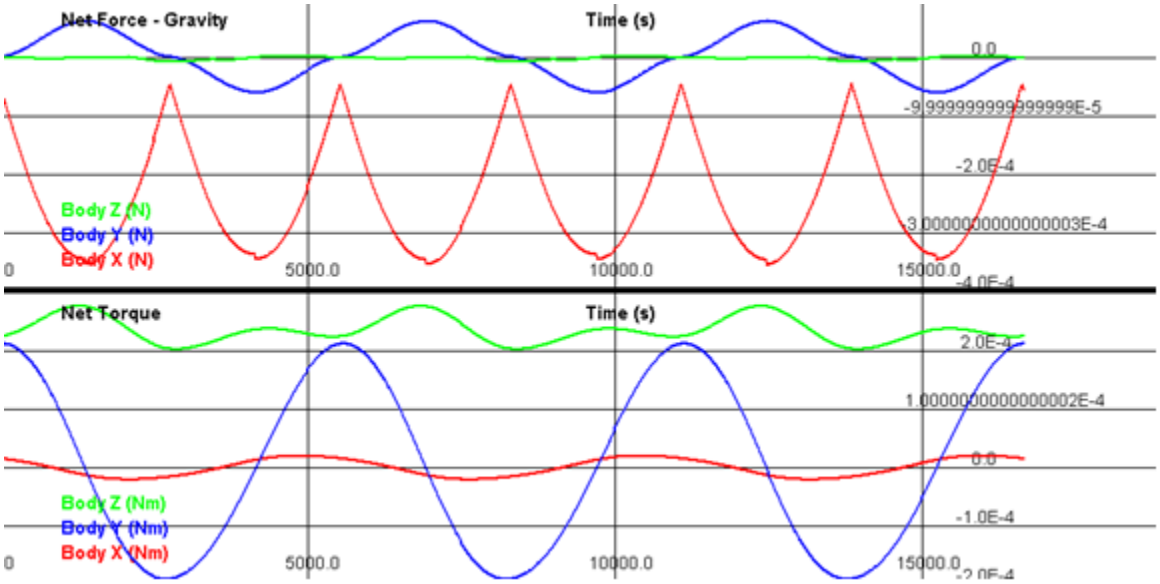

FIGURE 2.2-3: NET EXTERNAL DISTURBANCES (REFERENCE ATTITUDE)

The physics implemented to simulate various aspects of the space environment are not detailed in this document. However, the parameters from which this simulation was based on have since changed. Most importantly, the planned orbital altitude is 550km, with an inclination of 45 degrees. A new simulation is currently under development, and will take into account the addition of the cancelling magnet to reduce the effect of earth's magnetic field on the dynamics of the satellite. The new simulation will also demonstrate the performance of the current ACS design, i.e. its ability to control the satellite attitude to meet mission requirements.

ATTITUDE CONTROL ALGORITHMS

For the purposes of the control algorithm that will operate the satellite, the state of the satellite shall be defined in terms of its position and attitude:

$$\bar{x} = \left[x\ y\ z\ v_x\ v_y\ v_z\ \theta_x\ \theta_y\ \theta_z\ \omega_x\ \omega_y\ \omega_z\right]^T$$

This state includes the full position and velocity of the CASTOR, its attitude as described by three Euler angles, and its rotational rates.

A state space model defined by,

$$\frac{d\bar{x}}{dt} = A\bar{x} + B\bar{u} \quad (1)$$

$$\bar{y} = C\bar{x} + D\bar{u} \quad (2)$$

can be used to linearize the dynamics of the satellite and the sensor/actuator suite for CASTOR. This state space model will be used in simulations as an aid to designing the control law algorithm, and will also be used for orbit propagation to estimate satellite position and attitude during operations. Attitude control will be performed primarily by the reaction wheels. Torque coils will be used for detumbling, rate damping, and desaturation of the reaction wheels if they exceed acceptable rate limits.

Over the course of each orbit, the attitude control requirements will change, and the reference attitude to be tracked by the satellite will be determined in various ways. Additionally, sensor suite capability will be reduced during eclipse because the sun sensors cannot be used. This gives rise to three distinct modes of operation and two different means of determining reference attitude.

Mode 1 - Full attitude control mode

This mode provides full attitude tracking for any reference attitude, and is suitable for all situations in which full attitude control is required, including periods of engine firing and battery recharge. Sensor input shall be taken from the magnetometer, sun sensor, IMU, and GPS. The reaction wheels shall be used to actuate the satellite. The reference attitude is derived from one of the following two conditions:

1. Pointing of the engine along the velocity vector, to maximize thruster efficiency.
2. Pointing of the solar panels towards the sun to maximize solar array power output during the battery recharge phase.

Mode 2 - Eclipse mode

This mode disables attitude control (i.e. the reaction wheels), and shall receive sensor input from the magnetometer, IMU, and GPS. During this mode, accurate attitude tracking is not essential, and disabling control of the reaction wheels conserves power.

Mode 3 - Desaturation mode

This mode is similar to Mode 1, as it will provide for full attitude tracking, but will use the torque coils to exert an external torque on the satellite, with the purpose of desaturating the reaction wheels. Sensor input shall be taken from the sun sensor, IMU, and GPS. Note that the magnetometer cannot be used since the torque coils will skew the measurement readings.

For full attitude tracking, the control law can be formulated as follows:

Defining,

Three coordinate systems: E – Fixed to the earth. B – Fixed to the body of the satellite. R – Fixed to the body of the reference attitude.

$T_{EB}\ T_{ER}\ T_{BR}$ Matrix transformations from E to B, E to R and B to R respectively.

$v_E\ v_B\ v_R$ Representation of a vector in each coordinate system.

$s\ m$ Unit vectors pointing from the satellite to the sun, and in the direction of the local magnetic field respectively.

The sensor suite acquires a magnetic field vector in B, and the magnetic field vector in E can be determined according to the satellite's orbital position (acquired from the GPS). Applying matrix transformations to these two vectors, the coordinate system B relative to E can be determined, yielding the satellite's attitude relative to E. The same process can be applied to the sun vector acquired from the sun sensor (s_B), and the known sun vector in E (s_E) as inferred by the orbital position of the satellite, in order to derive the satellite's attitude as well. The two attitude determinations are passed through an Extended Kalman Filter to arrive at a single attitude determination. The control law then takes as input the satellite's attitude and the reference attitude to yield rotations necessary to bring the satellite's attitude to the reference attitude.

Dynamic output feedback control will be used to command angular acceleration, and knowledge of the vehicle's moment of inertia will be used to mix these commands to a three dimensional torque to be applied by the reaction wheels. Assuming a simple model of the satellite dynamics given by,

$$\sum \tau = I\ddot{\theta} \tag{3}$$

where the sum of torques is given by the torque produced by the reaction wheel, τ_R,

$$\sum \tau = -\tau_R = -I_R\dot{\Omega}_R \tag{4}$$

a state-space model can be formed following equations 1 and 2:

$$\bar{x} = \begin{bmatrix}\theta \\ \dot{\theta}\end{bmatrix},\ \ y = \theta,\ \ u = \dot{\Omega}_R$$

$$\begin{bmatrix}\dot{\theta}\\ \ddot{\theta}\end{bmatrix} = \begin{bmatrix}0 & 1\\ 0 & 0\end{bmatrix}\begin{bmatrix}\theta\\ \dot{\theta}\end{bmatrix} + \begin{bmatrix}0\\ -\frac{I_R}{I}\end{bmatrix}\dot{\Omega}_R$$

$$\theta = [1 \quad 0]\begin{bmatrix}\theta\\ \dot{\theta}\end{bmatrix} + [0]\dot{\Omega}_R$$

Using a Dynamic Output Feedback controller yields the following closed-loop dynamics:

$$\begin{bmatrix}\dot{x}\\ \dot{x}_c\end{bmatrix} = \begin{bmatrix}A & -BC_c\\ B_cC & A_c\end{bmatrix}\begin{bmatrix}x\\ x_c\end{bmatrix} + \begin{bmatrix}BN\\ BN\end{bmatrix}r \tag{5}$$

$$\theta = [C \quad 0]\begin{bmatrix}x\\ x_c\end{bmatrix} \tag{6}$$

where x_c is the estimated state; A_c, B_c, and C_c correspond to the compensator's dynamics; r is the reference state, and becomes the new input to the system; N is a scaling factor applied to the reference input.

$$A_c = A - BK - LC,\ B_c = L,\ C_c = K,\ N = \left(-[C \quad 0]\begin{bmatrix}A & -BC_c\\ B_cC & A_c\end{bmatrix}^{-1}\begin{bmatrix}B\\ B\end{bmatrix}\right)^{-1}$$

There are two degrees of freedom with this compensator, which are the regulator gain, K, and the estimator gain, L. The regulator gain can be found by implementing a Linear Quadratic Regulator which optimizes the choice of K, given a more understandable set of specifications. The gain K is found by minimizing the equation:

$$J = \int_0^\infty [x^T Q x + u^T R u]dt \tag{7}$$

The details of optimizing this equation are not represented, since there is a Matlab function that produces the gain K, given the plant dynamics, Q, and R. The matrices Q and R are chosen according to a set of rules of thumb:

$$Q = \begin{bmatrix}\frac{\alpha_1^2}{\theta_{max}^2} & 0\\ 0 & \frac{\alpha_2^2}{\dot{\theta}_{max}^2}\end{bmatrix},\ R = \rho\frac{1}{\dot{\Omega}_{max}^2}$$

where θ_{max} and $\dot{\theta}_{max}$ are the maximum desired output of these signals, α_1 and α_2 are relative weights assigned to each signal, $\dot{\Omega}_{max}$ is the maximum desired input of this signal, and ρ is a relative weight between input and output. The sum of α_1^2 and α_2^2 must equal 1. The LQR then produces a set of regulator poles in the final closed-loop system.

The estimator gain L is selected based on the rule of thumb of making the estimator poles about twice as fast as the regulator poles, i.e. the real component of the estimator poles is twice that of the regulator poles. The details of deriving L are not presented, since there is a Matlab function that produces the gain L, given the plant dynamics and the desired estimator pole locations.

The closed-loop dynamics given by equations 5 and 6 yield the control law equation:

$$u = -C_c x_c + Nr \tag{8}$$

Using the procedure outlined above, equation 8 becomes:

$$\dot{\Omega} = -K \begin{bmatrix} \theta_{est} \\ \dot{\theta}_{est} \end{bmatrix} + N\theta_{ref} \tag{9}$$

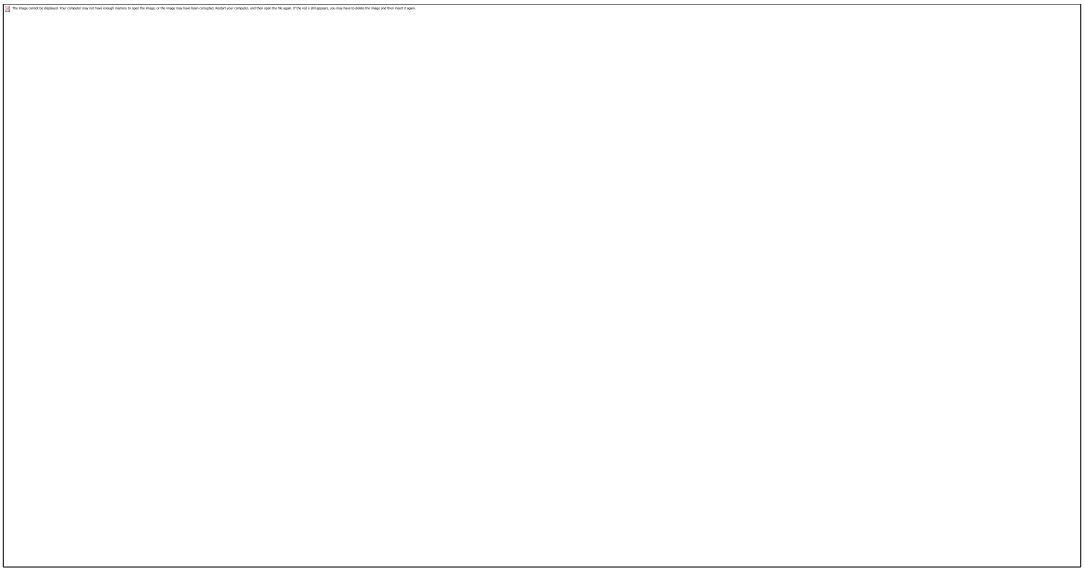

FIGURE 4: REACTION WHEEL CONTROL LAW

Figure 4 shows a block diagram of the control algorithm used to actuate the reaction wheels, as given by equation 9. The control law is applied to each of the three reaction wheels, in terms of the Euler angle that corresponds to the reaction wheel. The reference angle, θ_{ref}, may be determined by the sun sensor, or the estimated velocity vector. The estimated angle, θ_{est}, is determined by the sensor suite. The angular rate, ω (equivalent to $\dot{\theta}$ in eq. 9), is determined by the IMU, and the resulting torque command, τ_R, is sent to the reaction wheels. The gains k_p and k_d correspond to the elements of matrix K; $K = [k_p \quad k_d]$. The gain N is a scaling factor applied to the reference input, as described previously.

Applying this control torque will cause the vehicle to stably converge to the reference attitude using the shortest angle of rotation possible. If the inertia matrix is not a multiple of the identity matrix however, this will be a sub-optimal path in terms of energy use.

ATTITUDE CONTROL SOFTWARE

The general structure of the software will consist of an Extended Kalman Filter for estimation, acquiring full attitude measurements with a relatively low frequency (5Hz), execute control law functions which run at a yet lower frequency (1Hz), and compute the required control torques which serve as the input to mixing functions. The mixing functions will translate these higher level control commands into specific actuation

commands for the various actuators. Auxiliary matrix math, vector math, and mixing functions will be called whenever required by the core estimation and actuation threads. A full description of these auxiliary libraries and mixing functions is TBR.

Table 2-2 describes the ACS Application Programming Interface (API), a preliminary list of basic avionics software functions that must be implemented in order to interface with the ACS hardware components.

TABLE 2-2: ACS API

Component	**Function**	**Signal Direction (w.r.t. Avionics)**	**Return Type**	**Units**	**Description**
IMU	Get_Acc_Vector()	Input	float*	meters/second^2	Returns a pointer to an array of 3 floats, where the first element is the x-component of acceleration, second element is y-component, and third element is the z-component.
	Get_Rate_Vector()	Input	float*	radians/second	Returns a pointer to an array of 3 floats, where the first element is the angular velocity about the x-axis, second element about the y-axis, and third element about the z-axis.
Magnetometer	Get_Mag_Vector()	Input	float*	microtesla	Returns a pointer to an array of 3 floats, where the first element is the x-component of the magnetic field, second element is y-component, and third element is the z-component.
Sun Sensor	Get_Sun_Vector(int id, int* fit, int* geometry)	Input	float*	N/A	Takes as input one integer and two integer pointers, where id is the sun sensor to query (0, 1, 2, or 3). The function sets the value of fit to the queried sun sensor's Fit Quality, and geometry to the sun sensor's Geometry Quality. Returns a pointer to an array of 3 floats, where the first element is the x-component of the vector to the sun, second element is y-component, and third element is the z-component.

GPS	Get_Position_Vector()	Input	float*	meters	Returns a pointer to an array of 3 floats, where the first element is the x-component of the position (in WGS-84 XYZ Cartesian coordinates), second element is y-component, and third element is the z-component.
	Get_Velocity_Vector()	Input	float*	meters/second	Returns a pointer to an array of 3 floats, where the first element is the x-component of the velocity (in WGS-84 XYZ Cartesian coordinates), second element is y-component, and third element is the z-component.
Reaction Wheel	Get_Wheel_Torque(int id)	Input	float	Newton-meters	Takes as input one integer, where id is the reaction wheel to query (0, 1, or 2). The function returns the amount of torque being generated by the queried wheel.
	Get_Wheel_Speed(int id)	Input	float	radians/second	Takes as input one integer, where id is the reaction wheel to query (0, 1, or 2). The function returns the angular velocity of the queried wheel.
	Set_Wheel_Torque(int id, float torque)	Output	void	Newton-meters	Takes as input one integer and one floating point value, where id is the reaction wheel to command (0, 1, or 2), and torque is the amount of torque the specified reaction wheel should be commanded to generate.
Torque Coil	Set_Coil_Torque(int id, float torque)	Output	void	Newton-meters	Takes as input one integer and one floating point value, where id is the torque coil to command (0, 1, or 2), and torque is the amount of torque the specified coil should be commanded to generate.

The continuous-time control law given by equation 9 can be discretized to be implemented on a micro-controller. Equation 9 can be expanded to:

$$\dot{\Omega} = -k_p\theta - k_d\dot{\theta} + N\theta_{ref} \quad (10)$$

The commanded acceleration is substituted with a discrete-time equivalent,

$$\dot{\Omega} = \frac{\Omega_{i+1} - \Omega_i}{\Delta t_i}$$

where Ω_{i+1} is the speed of the reaction wheel to be commanded in the current time-step, Ω_i is the current speed of the reaction wheel, and Δt_i is the difference in time between the last time-step and the current time-step. The gains k_p, k_d, and N are given by the control law algorithm, θ is the best estimate of the satellite's attitude, $\dot{\theta}$ is the angular rate given by the IMU, and θ_{ref} is the desired attitude reference angle. Equation 11 is the resulting equation that can be implemented on the micro-controller.

$$\Omega_{i+1} = \left(-k_p\theta - k_d\dot{\theta} + N\theta_{ref}\right)\Delta t_i + \Omega_i \quad (11)$$

2.3 AVIONICS

2.3.1 REQUIREMENTS (L. DE LA GARZA)

The avionics system is the primary interface between: ADCS, Thermal, Power, Propulsion, Structures, Communications, and Operations. The avionics subsystem is composed of two primary aspects: hardware and software. The hardware provides the physical connections and logic circuits necessary for connecting to sensors and actuating devices. The software provides the logic for ensuring that the sensor data is acted upon properly. The requirements for the avionics subsystem are:

- Provide all necessary interfaces between subsystems
- Accommodate all required onboard data processing

The full design requirements can be found in 5.1 below.

Avionics and Software shall:

1. Provide the necessary data interfaces to support all subsystems

- Poll sensor data at a frequency of at least 4 Hz

- Run the propulsion system's engine firing logic twice per orbit as well as continually monitor the propulsion system

- Integrate with ACS subsystem to execute estimation and control

- Kalman Filter

- Periodic control law

- GPS data

- SPG4 propagator
- Interface with the communications subsystem to send and receive data.
- Provide the interface for power subsystem
- Interface with the imaging subsystem
    - One image per orbit without overriding the data for 2 weeks
    - Provide the computing power and data storage capacity necessary

Be fault tolerant and able to recover from SEU failure

- Detect SEU faults by checksums of the memory and storage
- Recover from an SEU fault <1 minute from the time of detection

2. Retain programming and state when unpowered
3. Permit software updates

2.3.2 OVERVIEW (S. GOMEZ)

The avionics hardware consists of three dsPIC33F microcontrollers mounted on a custom avionics board and a 1GB NAND Flash module. These dsPICs provide the computational power necessary for all operations to occur during flight as shown in the Computing Budget in Section 2.3.3 . The usage of three microcontrollers adds a level of robustness and redundancy to the overall avionics system. The three microcontrollers have the ability to reprogram one another in flight to recover from operational hazards such as Single Event Upsets (SEUs). In addition to the ability to reprogram the satellites the PIC shall be responsible ensuring the proper resources are allocated across all the PICs to ensure that no single PIC failure will cause the entire system to stop functioning.

The most computationally intense portion of the flight operations will be the Attitude Determination and Control System's (ACDS) state estimation and control algorithms. Previous tests have shown that a single dsPIC is more than capable of running the Kalman Filter code at the required accuracy. The third microcontroller will, almost exclusively, handle the ADCS's Kalman Filter for attitude estimation and control propagator. The first two dsPICs will handle more general flight operations. PICs one and two shall run identical software and will handle sensor reading, communications, and engine operations. In the event of a failure in PIC 3 the remaining two PICs will be able to run a reduced accuracy version of the control system.

The avionics system will also be responsible for the handling of all data onboard the satellite. The avionics board provides the hardware interface between the microprocessors, the NAND flash, and the various sensors aboard. The dsPICs will process all of the data coming in from these sensors and transmit or store the data on the flash module when necessary. The data stored in the flash memory will later be

accessible to the Communications subsystem for downlink to the ground. The overall hardware architecture of the avionics hardware system is present in Figure 2.3-1.

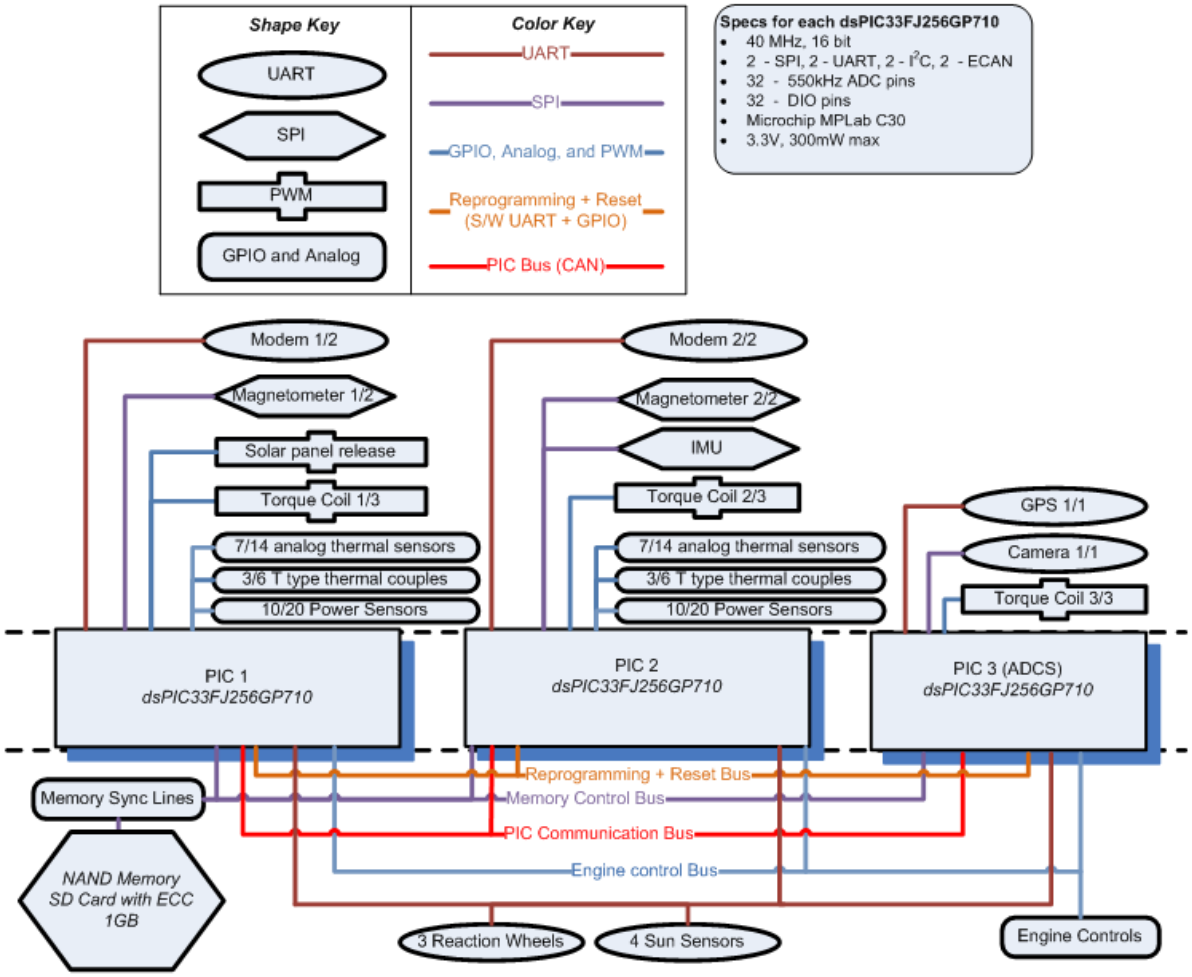

FIGURE 2.3-1: AVIONICS HARDWARE SCHEMATIC

The Avionics software system requires a hard real time operating system (RTOS) to manage system operations and schedule required tasks in order to meet operational deadlines. Avionics will be deploying the ThreadX RTOS to handle scheduling of the multiple threads necessary for CASTOR to operate. Individual threads will be responsible for different tasks that are required to run concurrently. The RTOS will schedule these threads to run periodically with deadline constraints while handling hardware interrupts. The general software task are listed below.

Operations Task	Task: provides overarching logic and control of system
--Regular Operations	Thread: basic structure of tasks and priorities for normal operations
--Commissioning	Thread: basic structure for how the satellite will begin life

Control Task	Task: runs attitude control law
Propagator	Task: estimates current orbital position and attitude
--Attitude	Thread: estimates the satellite's current attitude
--Position	Thread: estimates the satellite's current position
Power Management	Task: manages the distribution of power throughout the system
Communications Task	Task: manages communication between the satellite and the ground station
Sensor Recording	Task: records sensor data
Imaging Task	Task: takes pictures of the thruster's plume
Operate Actuators	Interrupt: operates control actuators
--SP RM	Thread: logic for solar panel release mechanism
--Torque Coil	Thread: logic for operating torque coils
--Reaction Wheel	Thread: logic for operating the reaction wheels
Threshold Interrupt	Interrupt: ensures sensor measurements are not over threshold values
Sensor Measurement	Interrupt: reads sensor values
--Thermal Sensors	Thread: logic for reading thermal couples and thermal sensors
--Power Sensors	Thread: logic for reading voltage and current sensors
--GPS	Thread: logic for reading GPS unit
--IMU	Thread: logic for reading IMU gyros
--Magnetometer	Thread: logic for reading magnetometer values
--Sun Sensor	Thread: logic for reading sun sensor data
TX Data	Interrupt: processes incoming data
RX Data	Interrupt: packetizes and sends data to ground station

TABLE 2.3-1: TASK BREAKDOWN

Additionally, the Avionics software system will provide a common software interface for other subsystems to communicate effectively with their hardware components. Avionics has defined an API for accessing various sensor data.

2.3.3 COMPUTING BUDGET (S. GOMEZ)

Establishing an accurate model of the utilization of avionics resources is a crucial part of ensuring that the avionics hardware can handle all of the necessary operations for CASTOR's flight. An in-depth analysis has been performed to estimate, and where possible measure, CPU, Memory, and Bus utilization under different operational conditions. The system has been designed so that avionics resources are capable of handling the worst case scenario events.

Start Up and Self Test

The Start Up and Self Test scenarios will not be commonly reoccurring scenarios during CASTOR's flight. Regardless, these scenarios must be accounted for and shown to be within the realm of feasibility for the designed flight hardware.

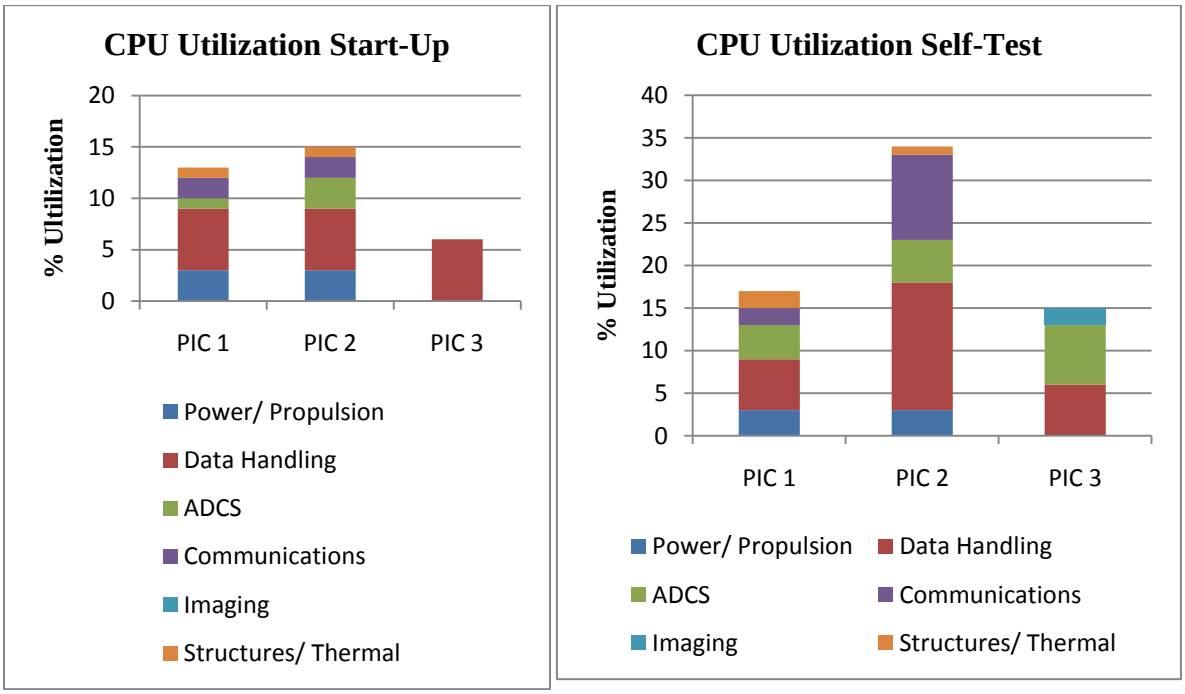

FIGURE 2.3-2: CPU UTILIZATION

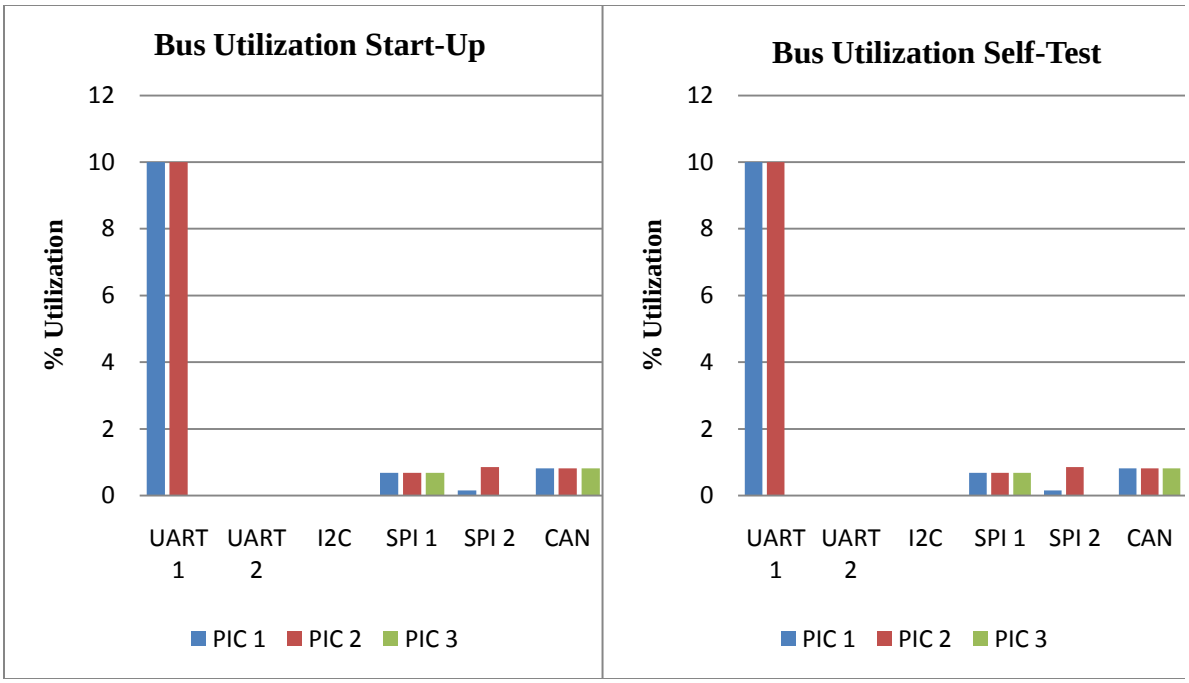

FIGURE 2.3-3: BUS UTILIZATION

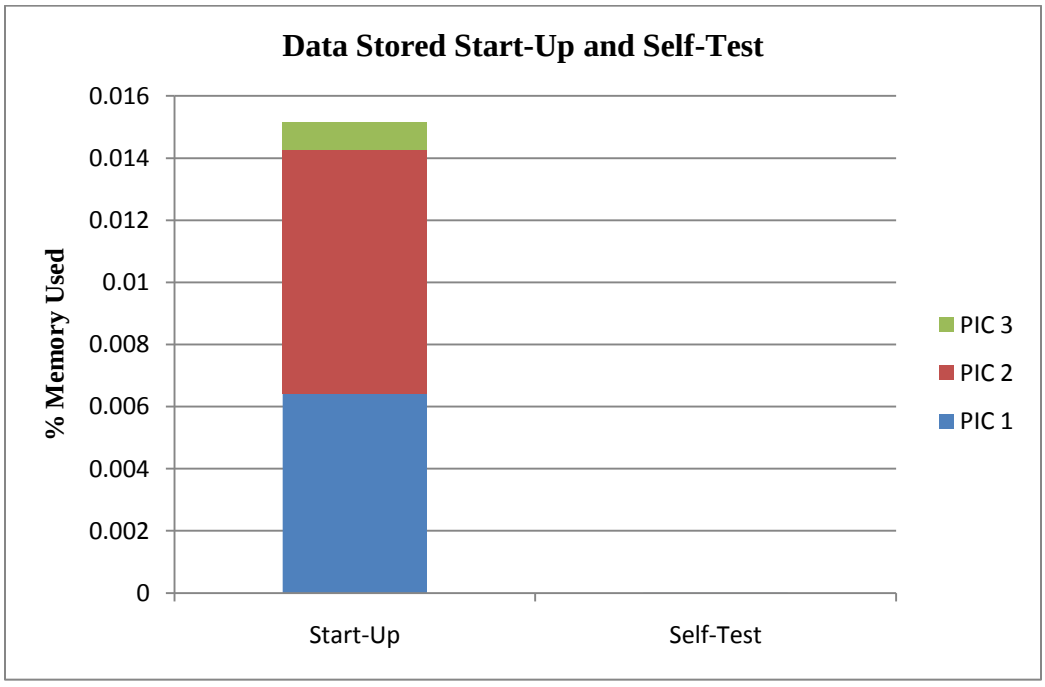

FIGURE 2.3-4: MEMORY UTILIZATION

The figures above show that the avionics hardware can easily handle the computational and data load put forward during satellite start-up and self-test. The CPU utilization peaks at 34% on PIC 2, Bus Utilization peak at only 10% on UART 1 for PICs 1 and 2, and data storage is minimal. Less than 0.016% of memory at start-up and several orders of magnitude lower during a satellite self-test (not visible in Figure 2.3-4).

Regular Operations (Sun and Eclipse)

The regular operations states will be the most common states for CASTOR to remain in. There are two phases of regular operation. In the Sun phase CASTOR is in orbital day, the satellite is able to use its deployed solar panels to provide power across the satellite and store energy in CASTOR's batteries. In contrast the Eclipse operations will take place during orbital night. The power available is only what was stored in the batteries during previous orbital days. This places a much tighter constraint on the power that can be utilized by the satellite. This puts less of a constraint on CPU, Bus, and Memory Utilization because all operations are power limited.

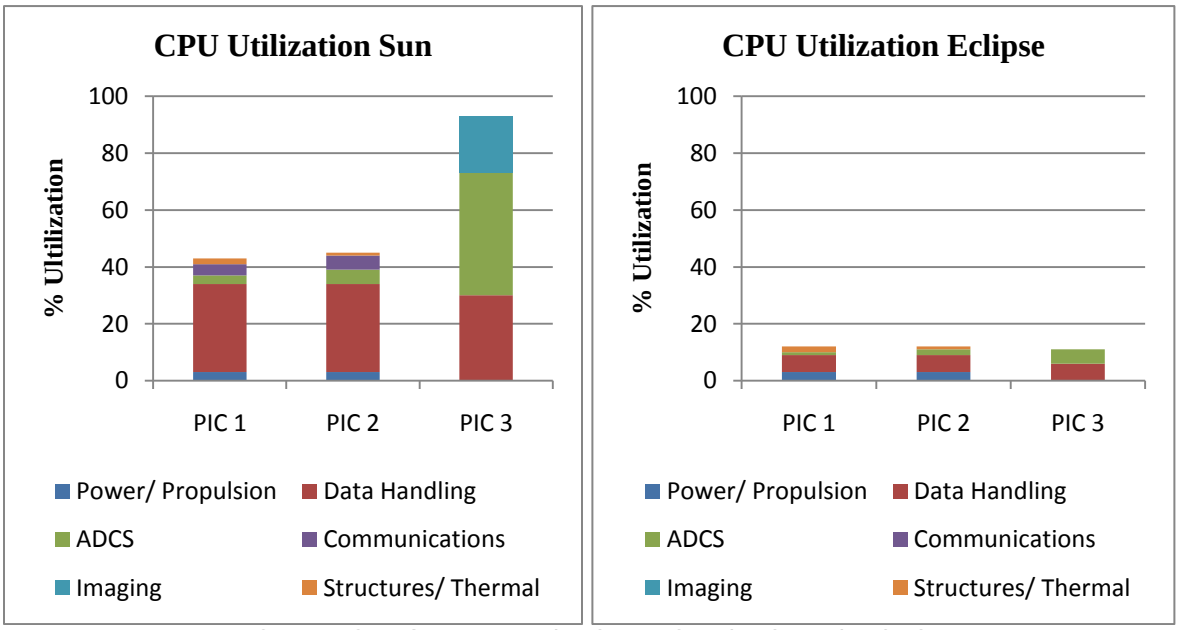

FIGURE 2.3-5: CPU UTILIZATION REGULAR OPERATIONS

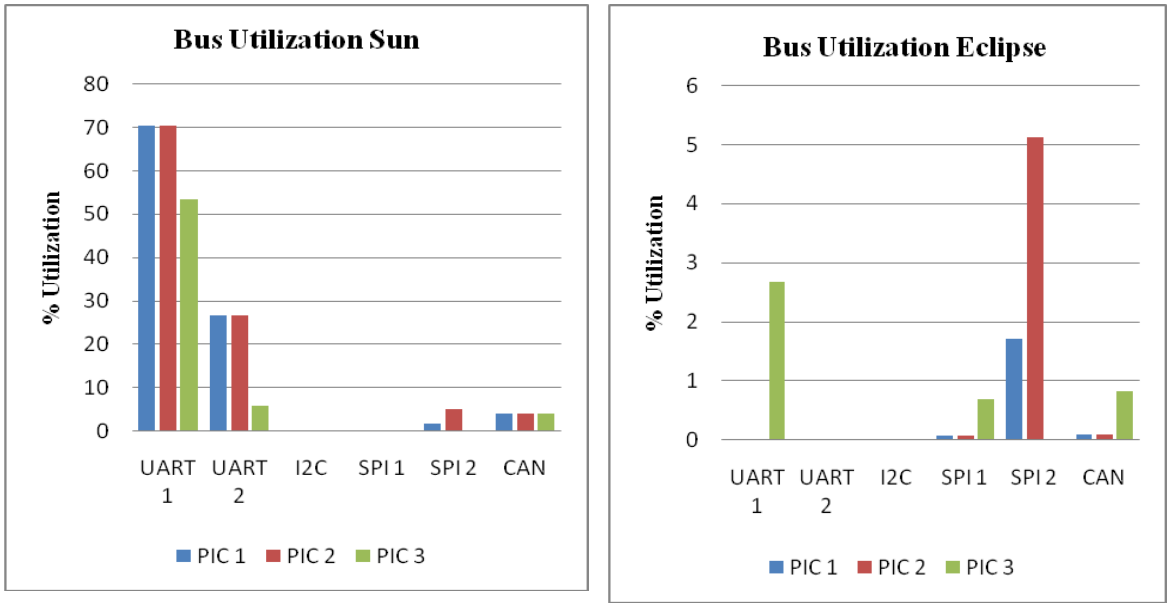

FIGURE 2.3-6: BUS UTILIZATION REGULAR OPERATIONS

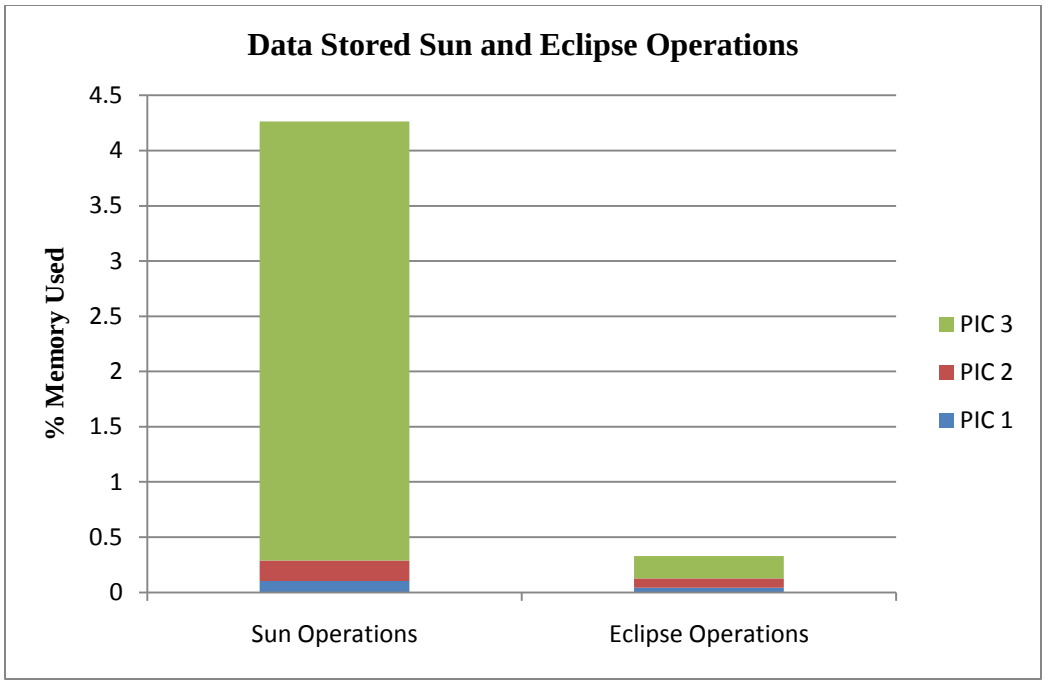

FIGURE 2.3-7: MEMORY UTILIZATION REGULAR OPERATIONS

Under normal operations all resources necessary by the satellite are available during all planned operational procedures during flight. Memory usage is minimal in all cases and Bus utilization is well within bounds. CPU usage during orbital day increases to an estimated 93%, still within the capabilities of the system, however the margin for error might be too small.

Worst Case Operations

A worst case scenario computing budget has be created to ensure that CASTOR will have the resources available to endure any event possible during flight. The worst case scenario occurs when one PIC undergoes an SEU and must be reprogrammed by the remaining PICs while those PICs are still undergoing normal operations. Estimates for resource utilization are given in the figures below. The load on each PIC is calculated with the assumption that one other PIC has failed in some way. All three PICs would not have these loads at the same time even in this worst case scenario.

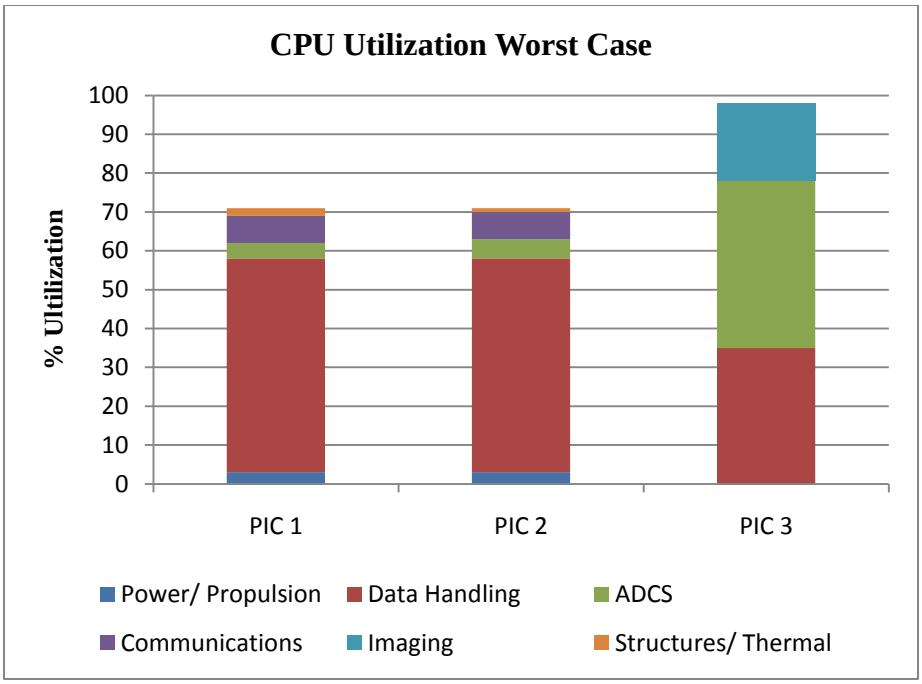

FIGURE 2.3-8: CPU UTILIZATION WORST CASE

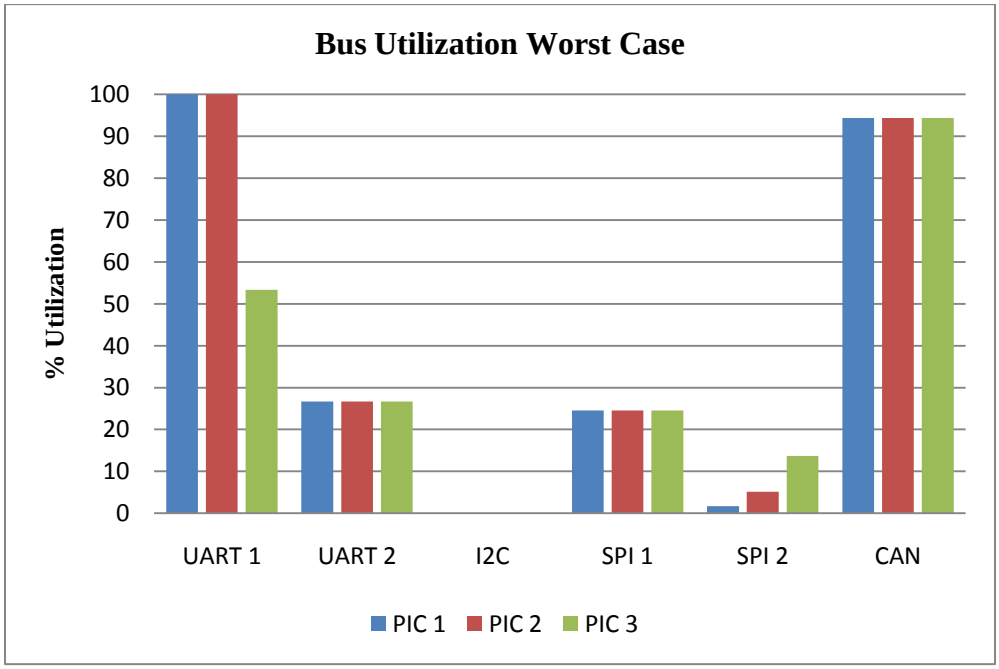

FIGURE 2.3-9: BUS UTILIZATION WORST CASE

FIGURE 2.3-10: MEMORY UTILIZATION WORST CASE

In the worst case scenario CPU utilization is near 100% in PIC 3 and the UART 1 Buses are completely saturated on PICs 1 and 2. However, all the loads put on the avionics resources are within the range of feasibility for the system. The saturation of the UART buses represents communications using the full capabilities of the data bus, and does not imply a lack of resources. The CPU utilization on PIC 3 is estimated at 98% during this worst case scenario, leaving little margin for error. However, this could be reduced by performing imaging tasks at a lower frequency or moving some responsibilities to the other functioning PIC until the final PIC is back up and running.

2.3.4 RISKS & MITIGATION STRATEGIES (J. NASH)

The following list enumerates the various risks the avionics system shall be designed to mitigate, along with the mitigation strategies that are being followed by the CASTOR avionics team. A summary of the information is found in Table 2.3-2.

- PIC hardware failure
    - If the PIC fails to respond with a given timeout interval, it will be considered failed
    - Radiation hardened components were not chosen due to their cost, so space and solar radiation is a potential cause of failure in Low Earth Orbit (LEO)
    - Mitigation strategies:
        - Perform the following steps in order until successful recovery
            1. Hardware watchdog reset

2. CAN bus watchdog reset by other PIC
3. Reprogramming (ICSP)
4. Disabling (reprogram other PICs to fulfill functions)

- Severity: 4. If one PIC fails, the mission will be delayed, but due to hardware redundancy, the failure of one PIC does not jeopardize the ability to complete the mission
- Likelihood: 1. In LEO, the avionics system will not be heavily bombarded by radiation so it is unlikely that a transistor will be struck in such a manner that it suffers a destructive single event latchup (SEL), single event gate rupture (SEGR), or single event burnout (SEB).

- PIC Single Event Upset (SEU)
  - Ions/Radiation causes a transistor to flip state
  - Mitigation strategy:
    - Use memory with hardware ECC and scan (read all memory sectors) periodically
      - On failure of ECC, mark file as invalid and log error for the next download session
    - Scan PIC internal memory to compute ECC internally
      - On failure, return to bootloader mode and reprogram sector from backup copy
  - Severity: 2. An SEU is a temporary condition (no hardware damage) so the processor or memory bank can be reset quickly. The other, redundant PIC connections can take over control in the meantime.
  - Likelihood: 4. In LEO, it is highly probably that a number of SEU's will occur over the duration of the mission

- Inter-PIC communications failure
  - CAN bus stops working, drops packets, or corrupts data temporarily or permanently to one or all PICs.
  - Could be due to a software or hardware problem
  - Mitigation strategy:
    - RS-485 bus might be usable for inter-pic communications
      - Would require a software update
      - Would reduce the frequency the avionics system could the Sun Sensors and control the Reaction Wheels
    - Memory bank is an alternative communication device.
      - Already used as a full storage location for commands before processing by any chip
      - Would require a software update for full use
      - Difficult to synchronize access to a communications file
      - Slow to push messages
    - Active acknowledgement of packet reception (for detection)
    - Reset of non-responsive PIC
    - Replacement code upload with a revised implementation of communication protocol and/or hardware interface layer

    - Severity: 3. Without the ability for the PIC's to communicate, the effectiveness of the redundant system would be significantly reduced
    - Likelihood: 1. Significant testing before launch should catch any software bug. Wires are laid out as traces on PCB and are not prone to mechanical disconnection during launch. The only potential threat is micrometeorites, which we do not expect the satellite to hit and, in the event that the satellite does encounter one, will hopefully be stopped by the aluminum structure or enclosure.
- RTOS Software deadlock (or livelock)
    - Multiple threads become stuck in a race condition waiting for a resource.
    - Four Conditions for Deadlock (taken from Concurrency3 lecture in 16.35 by Nicholas Roy, February 23rd, 2010)
        - Mutual exclusion condition
            - each resource assigned to 1 process or is available
        - 2. Hold and wait condition
            - process holding resources can request additional resources
        - 3. No preemption condition
            - previously granted resources cannot forcibly taken away
        - 4. Circular wait condition
            - must be a circular chain of 2 or more processes
            - each is waiting for resource held by next member of the chain
    - Mitigation strategy:
        - Eliminate one of the four conditions for deadlock from the system [the preferential order for eliminating problems is: 1. address mutual exclusion (spool everything – simplest solution, never an issue) 2. address circular wait condition (order resources numerically) 3. address hold and wait condition (request all resource initially and simultaneously) 4. address no preemption condition (take resources away – generally not feasible)]
        - Reset task or entire system if a task or the system becomes nonresponsive to watchdog messages
    - Severity: 3. If the system or a task becomes nonresponsive it may miss events and cause the entire satellite to become lost or fail to execute tasks correctly. Deadlocks (and livelocks) are very difficult to debug and fix since there are no simple tests to detect them and are often impossible to reproduce the same way twice
    - Likelihood: 4. Deadlocks can slip into the most innocent code and there is no simple way test for their existence of to eliminate them
- Wires or connectors break or separate
    - A broken connection means that one or more components will become inaccessible to the avionics system control
    - Could be due to the vibrations during launch, a bad solder joint, or a partially damaged wire (nicked during stripping or placement)
    - Mitigation strategy:

        - Use many low pin-count connector with locking clips or screws instead of large connectors or plain wires
        - Separate redundant components onto unrelated connectors
        - Visually inspect and electrically test all joints during and after board assembly before releasing to launch
        - Choose strong connectors and plan the wiring harness to eliminate tight corners and sharp bends
        - Use care in construction of the final board and wiring harness
    - Severity: 4. One or more components will be completely disabled.
    - Likelihood: 1. With proper care and thought, the final design and construction should be free from unnecessary risks
- Memory overflow
    - If too many picture are taken between comm. passes or the system is unable to fully relay the picture and telemetry data at each comm. pass, the memory will eventually reach capacity and "overflow"
    - Overflow could also occur if the filesystem is leaking file sectors through improper space management or a processor reset occurring during writing
    - Mitigation strategy:
        - Purchase a memory card well in excess of the calculated maximum (since it is the inexpensive and the same weight and volume)
        - Lower the rate of pictures when the memory usage level reaches a high-water mark. Also, the thruster should not be firing and thus few pictures will be needed if the satellite has missed several consecutive communications passes
        - (critical stage, must be initiated by ground command) Reset the memory entirely to restart with a fresh and clean file-system
        - Deletion over overwrite of less critical data when possible or necessary
    - Severity: 1. The full data stored in memory has a high degree of redundancy and is not essential to the mission. Much of the data should be reconstruct-able by extrapolation of remaining data
    - Likelihood: 2. The memory is considerably oversized for the expected amount of data and comm. passes are both sufficiently frequent and high bandwidth to permit a full download of the captured data even if several passes are missed or a portion of a comm. pass is missed
- Avionics processes an invalid, corrupted, or incorrect command
    - A command gets misinterpreted or a wrong command gets processed by the avionics system due to either a communications error, a storage error, an execution error, a code error, or a user error.
    - Mitigation strategy:
        - Require multiple confirmations of critical-type commands (such as decommissioning / fire-code, mode change, and engine firing – see Ops and Comm. sections)
        - Include redundant information in transmissions and command encoding to detect errors. Confirm upon receipt and again before execution of action

        - Log details of the failure
        - Restart or disable the offending process or request a retransmission of the invalid command packet
    - Severity: 2. The severity depends upon the type of command, but typically will be transient and thus have only a small effect on the system
    - Likelihood: 2. The confirmation and redundancy safeguards will catch most errors before they are executed
- Other environmental damage
    - Thermal, vibration, impact, or radiation conditions exceed the operating tolerances of the design
    - Mitigation strategy:
        - Select components with military specifications for a wide temperature range and work with Thermal Team to develop procedures and coatings to keep components within the desired temperature range
        - Process the board according to AFRL's Procedures for Conformal Coating of Printed Circuit Boards (available from http://www.universitynanosat.net/NS6/?q=Documents/NS6)
        - Subject the avionics design to vibe testing before and after system integration
        - Simulate errors due to radiation and expose the board to high energy particles at the MIT nuclear reactor to verify detection and recovery
        - Enclose the entire avionics system in a Aluminum enclosure
    - Severity: 4. Without the avionics board, the mission will fail.
    - Likelihood: 1. The UNP user's manual and extensive simulation and testing greatly reduce the likelihood of environmental damage occurring.

TABLE 2.3-2: SUMMARY OF AVIONICS RISKS

Component Failure Mode	Severity	Likelihood	Risk Level
PIC hardware failure; PIC fails to respond	4	1	MED
PIC SEU; Ions/Radiation causes a transistor to flip	2	4	MED
Inter-PIC communications failure; Software/Hardware implementation error	3	1	low
RTOS Software Deadlock; ThreadX software implementation error	3	4	HIGH!
Wire separation; Wiring harness breaks; Solder connections fail	4	1	MED
Memory corruption; Data stored in memory becomes unreliable	1	2	low
Memory overflow; Data not correctly offloaded when appropriate	1	2	low

Invalid command processed; Incorrect software implementation	2	2	low
Environmental damage to avionics equipment; Heat/Vibration reach beyond controllable levels	4	1	MED

2.3.5 DSC BOARD (J. NASH)

The system layout was designed in coordination with the ADCS and Power team leads to determine which interfaces are critical and which could be considered redundant. The connections were then spread out across the dsPICs in an attempt to balance the interface load between PIC1 and PIC2 and to minimize disruption due to the partial or total failure of a single microcontroller. Pins were chosen to place as many connections to a given device on a single port as possible, and then to duplicate that choice across all PICs.

Avionics chose to go with 3 PICs rather than a single, more powerful processor because it offers redundancy in case of a SEU or other failure. The PICs also provide a large number of I/O pins. The current design makes use of about three quarters of the total available pins. Approximately 130 pins will be connected external to the avionics box for signals, power, and ground connections to other subteam's components.

Analog inputs were allocated evenly across PIC1 and PIC2 so that the ADC converter could be disabled on the ADCS PIC 3 to reduce overhead when executing the Kalman Filter. Small, 200 ohm resistors are placed on each of the thermal IC's, voltage measurement, and current measurement input lines to guard against electrical shorts from damaging the microprocessor.

Each microprocessor can access the onboard 1GB NAND memory through a shared SPI bus that is connected to SPI 2 on each dsPIC. Exclusive access to this bus is enforced by a bus arbitrator chip (P/N 74F786) and tri-state octal buffers (P/N SN74AHC373DW). This combination helps to ensure data will not easily be accidentally corrupted during access due to multiple, simultaneous attempts. A discrete Secure Digital (SD) card was chosen for extra memory make debugging easier. Since the card is removable, and a common standard, it can be read, verified and written with most computers. An SD card adaptor has been chosen for the PCB; however, a SD card selection has not been finalized. Our requirements state that our memory must have sufficient capacity to store telemetry, log, housekeeping, task, command/schedule, and imaging data. However, since there are very few cards produced with a capacity less than 1GB and costs are quite low (< $25), this requirement does not pose an issue. The sum of the requirements specify collecting only a fraction of that amount of data between communications passes, but the additional space will give us extra margin for storing data so that data will not be overwritten even in the occurrence of missing multiple communications passes. As there is no difference in size or mass for the additional space and only a minor cost difference, there is no disadvantage to over-sizing the memory.

Our requirements state that the selected memory must be fault tolerant and long-lasting. This is derived from the requirements for reliable storage of system data -- such as

pictures, telemetry, commands, and logs -- which are important for the mission, so consideration was only taken of memory modules that came with documentation (few manufacturers make this readily available) and specified that the memory had a built-in error correction code (ECC) which transparently detects and corrects the random bit flips that are likely to occur due to radiation. Transcend Information, Inc, Apacer Technology, Inc., and SanDisk all seem to have some form of hardware ECC.

Each PIC is provided the ability to reprogram any of the other PICs in hardware through their run-time-serial-programming interface (RTSP). Note that they always have the ability to reprogram themselves though the In-circuit-self-programming API (ICSP). Since each PIC has three inputs for data connection, each PIC is connected to a set of programming pins on each of the other PICs and one set external to the board for connecting to the ICD2. Since there is only one reset input pin, the three reset connections are joined together using a three input AND gate (P/N CD74HC4075M) with each of the inputs held at logic high using a pull-up resistor when not actively being driven low. This ensures that the PICs do not reset except when specifically being programmed.

One of the magnetometers, the IMU, and the GPS are located in the avionics box and connected directly to the board. The board contains the footprint connectors for the magnetometer and IMU since these components have already been acquired. Because the GPS is too expensive to purchase early, the connections to the GPS does not need to be included on the design until a later revision of the board. For connecting the components that are external to the box, latching low-profile socket connectors with strain relief (AVX Series 8290) have been selected. The 10-pin version of this connector allows a one-to-one mapping to the 9-pin (plus shell) d-sub connectors that may provide the interface between the avionics board and components that are external to the avionics box. If necessary, in a later revision, the pin counts of each connector can be revised upwards to reduce the number of connectors required. Since ADCS has many more components than can be connected to separate ports, even across all of the PICs, avionics requested that other subteams select devices that can communicate over SPI or RS-485 and then multiple devices were multiplexed onto SPI 1 and UART 2 on each PIC.

Because the operation of the Propulsion system and is critical to a successful mission, and it depends upon working control over a Power system, all power controls from the avionics system are duplicated between PIC1 and PIC 2. Then they are combined using an OR gate (P/N 74AC11032D) with pull-down resistors on the inputs. The net result is that either PIC is able to turn on the power components. If one PIC becomes stuck with a component in the on state, the other PIC can force that PIC's reset line high to turn off the component. The analog trim for the heater on the PPU is controlled in a similar way using two DAC chips (P/N MCP4821) with their outputs summed using an Op-Amp (P/N MCP619-I/SL) and then divided by 3 to make the maximum output voltage be 1.1V, which is less than the point at which the converters would break, 1.23V. These components were chosen because they are manufactured by the same company that makes the dsPIC, Microchip, and their output was within our specifications.

The camera that was selected communicates over UART, however all 6 UART ports across the 3 microcontrollers are already occupied by other important devices. The

decision was made to multiplex the camera on the SPI port of the ADCS PIC 3 using a standard SPI-to-UART converter chip (P/N MAX3100). Since the camera is used relatively infrequently and is not time-critical, this conversion is not expected to overload this PIC with data that would hinder its performance in its primary task of executing the Kalman filter state estimation and feedback control tasks.

Thermocouples attach to an isothermal interface on the exterior of the avionics box that also provides 2 reference thermistors. Exactly half of these devices are read out on each of PIC1 and PIC2. The circuitry for translating the voltage difference of the thermocouple to absolute voltages is part of the avionics board. This circuit multiplies the difference by 100 and then biases the result by 1.2V so that positive temperature differences (as referenced against the thermocouple) measure as voltages above 1.2V and vice versa. Refer to Microchip document AN844 copyright 2002 for more details, noting that we believe the circuit diagram we used as a reference for our circuit design, marked Figure 3: Simplified Digital Circuit, to be in error.

All three of the dsPICs can communicate with each other over a CAN bus. An additional connection to the CAN bus is provided on the lightband connector for the purposes of reprogramming and debugging the hardware after launch vehicle integration prior to launch. The CAN bus is a logical choice for this communication as it provides a robust and communication protocol for packetizing and transmitting data between multiple host microprocessors. It was electrically designed for use in the noisy environment of a car due to its use of differential signaling and it handles collisions automatically through the use of identifier priority levels. Since the last design document, Microchip has begun selling a new revision of the silicon for the dsPIC that we are using (now dsPIC33FJ256GP710A) that is supposed to have corrected the flaws that corrupted prior attempts to use the full capabilities of the CAN bus. Tests to confirm will be started when the coding work moves from focusing on a single dsPIC to developing the code that controls the interactions between the dsPICs. The largest remaining block of pins on each dsPIC is connected to an array of LEDs. There are 4 LEDs on PIC 1, 2 LEDs on PIC 2, and 5 LEDs on ADCS PIC 3. There are also LEDs to indicate the presence of +3.3V and +5V power to the board. On the final construction of the PCB for flight, these components will simply be left off of the board to save power.

The avionics board layout is designed to fit exactly into the space currently allocated by the structures team. The maximum allowable size is 4" by 7". The final revision of the board will have more layers for the purpose of thermal conduction, but otherwise the current board contains all of the flight components and fits in the space allocated.. These external connectors will be a combination of 9-pin or 25-pin, d-sub or micro d-sub connectors. Refer to section **Error! Reference source not found.** for the wiring harness diagram. Please also refer to the avionics sections of the Manufacturing and Integration plans. The tall items on the board layout are designed so that on one side of the board, the PDU, Magnetometer 1, and IMU will fit side-by-side for the best use of volume. On the opposite side (facing outwards on the satellite) the two modems are placed side-by-side and made to be in thermal contact with the interior of the avionics box wall to remove heat from them. Thermal paste will be applied to the modems on the surface in contact with wall of the avionics box to increase the rate of heat transfer and prevent when

communicating. Please refer to Structure's layout for the positions of the remaining components that have some connection to the avionics microcontrollers.

The remaining, shorter components are laid out on the board in the remaining space between the tall components using two general principles. One, related components are located physical close to each other and, if possible, placed in a marked rectangle, for easier assembly and to reduce the amounts of long distance wiring on the board. Two, similar resistors are lined up in banks of identical values to speed up the hand assembly process while reducing errors in the selection and placement of these component.

The thermocouple circuit is placed to one side of the board that requires less wiring to provide better noise characteristics. Tests will be performed to verify that the stability of their measurements are within bounds and are not affected by the power flow to the modems or other signal currents. If this criterion cannot be met with the current configuration, other options for isolating the thermocouple inputs fromsignal noise (until they have been amplified) will have to be considered.

The filtering capacitors on the 3.3V line are placed directly over the input line to ensure the incoming signal is sufficiently free of noise that may disrupt a component such as the PICs. Similarly, the crystal resonators and accompanying capacitors are placed near the pin they connect to, in order to improve signal quality. These components are also routed by hand before running the auto-router to ensure they are connected correctly to the correct pin and not another random nearby source that looks electrically equivalent, but would not provide the same signaling characteristics.

Once the components are placed in an efficient manner, the auto router tool in Altium is able to create the board. Many of the features on the board have been selected to exactly meet the minimum tolerances specified by our preferred manufacturer, Advanced Circuits (www.4pcb.com), for standard 4-layer boards. This manufacturer is very responsive to requests by email and phone, they provide an affordable student discount on small orders, and have already produced other printed circuit boards for the MIT Satellite Team Avionics, Communications, and Power subteams. The avionics board is composed of two internal power planes of 3.3V and ground, and two exterior signal planes. The final board will be composed of more layers to allow for the printing of two thermally conductive layers connected to ground and more signal layers, if necessary, to compress the board's footprint. Several of the components on the board require a maximum clearance distance of 7mil between traces, which still leaves a small margin on the manufacturer's minimum of 6mil. Using standard online lookup tables for trace width a trace width of 8mil is sufficient for most components on the board. Because space is a vacuum, the temperature specifications for an internal plane trace are used (the external numbers assume convection cooling), giving a maximum current of 0.3 amps at this thickness. Thus, only the modem power supply lines and structure's linear actuator power feed will require thicker traces. Using the same calculator, it can be found that a trace width of 12 mil is sufficient to handle the currents driving the linear actuator and 45 mil traces are sufficient to handle the currents for the modem. These traces were routed by hand before running the auto-route function.

The current avionics board is composed of 2 signal layers on the top and bottom and 2 power planes in the middle connected to 3.3V and Ground. This will allow us to alter traces during testing if something does not work properly. After we gain confidence through experience with the board layout, the board will be designed and manufactured to include more internal layers, possible internal signal layers and thermal (ground) planes. The board layout can be compressed further at that stage to better fit within the satellite structure limits. Additionally, internal signal layers will allow the placement of thermal pads beneath any component that consumes a noticeable amount of power. The list of such components definitely includes all of the dsPICs and the oscillators. Thermal team's help will be needed to determine which other components require the extra cooling help of a thermal pad.

2.3.6 WIRING HARNESS (S. GOMEZ)

CASTOR's wiring harness is a crucial part of the structural and avionics design of the satellite. Now that all of the components on the satellite have been chosen and the avionics board design has been completed the plans for navigating wires across the satellite can be completed.

Some of the sensors (i.e. IMU and Magnetometer) are being housed within the Avionics box as well as the communications Modems. This greatly simplifies the wiring that must travel across the span of the satellite. However, there are still several major components that exist on all corners of the structure. The wiring plan will consist of several locations for wiring harnesses to be strategically placed around the satellite to organize and guide the wires to and from the avionics box, battery box, and other components.

Major considerations for the wiring harness are included below.

Component Name	Number of Components	Number of Avionics Connections
Temperature Sensors	14	2 10pin connectors
Thermo Couples	6	2 10pin connectors
Reaction Wheels	3	1 10pin connector
Sun Sensors	4	4 10pin connectors
Camera	1	1 16pin connector
Linear Actuator	1	2 4pin connections
Antennae Cables	1	1 Cable
Battery Box	1	(PDU Power) 40pin + (PDU Data) 16pin + (PPU) 20pin

TABLE 2.3-3: MAJOR CONSIDERATIONS FOR THE WIRING HARNESS

Current Plan for the wiring harness:

Large bundles of wires will travel from bottom, middle, and top of avionics box.

Bundle from bottom will split toward two reaction wheels at the base of the structure, toward nearby sun sensor, and thermal sensors at the base of the tank.

Bundle emanating from center of avionics box will connect to thermal sensors on the tank clamps and fins. This bundle will then split to extend to thermocouples located on solar arrays and battery box and reaction wheel above.

Top bundle will split and connect to the suns sensors nearest to it. It will also wrap around to thermal sensors/thermocouples near cathode and anode and continue to the camera box and final sun sensor.

These wire paths must have several connection points along their routes to adequately secure the bundles of wires as they approach their destinations. The locations of these harnesses are the core of the wiring plan throughout the satellite.

UPDATE: The wiring harness was built over summer 2010. However, nobody from that time frame is around to describe it in more detail for this section.

2.3.7 REALTIME OPERATING SYSTEM API (B. KROESE)

A satellite must run semi-autonomously throughout it s operational life using real-time operating systems to control the organization and data of the system. Naturally there are many different processes which must occur concurrently controlling items such as sensors, data manipulation, and packet transmission. Satellites handle this concurrency through a multithreading system assigning different tasks to individual threads. Keeping these considerations in mind, ThreadX by Express Logic was chosen as the real time operating system for the CASTOR embedded system. This C based software kernel manages a system of tasks controlling the satellite's its internal processes while also interacting with sensors and data transmission.

The avionics hardware centers on the three 16-bit dsPIC33F microcontrollers. Each of these components runs a separate copy of the operating system code while controlling sensors and computational aspects of the satellite. Repetition allows the system to check and recover from single even upsets. Figure 2.3.7-1 shows the different operations which are defined and regulated by the microcontrollers. The main purpose of the ThreadX technology is to manage how these tasks are executed using interrupts from each of the components to move between different processes.

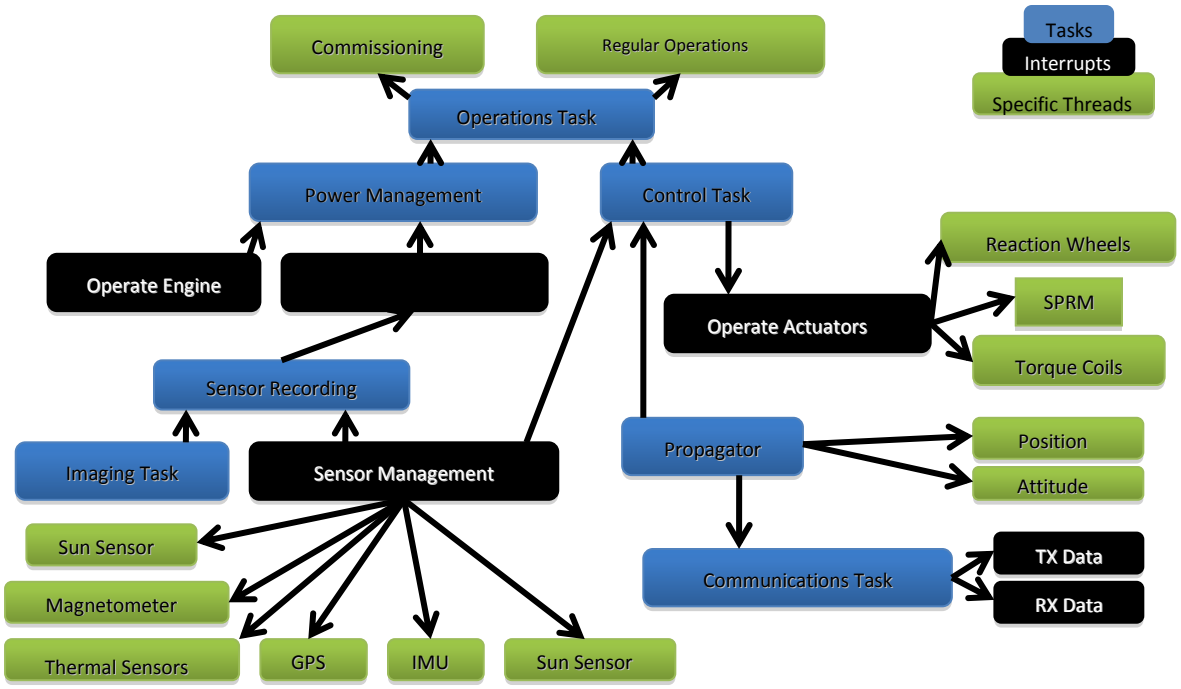

FIGURE 2.3-11: OPERATING SYSTEM STRUCTURE

The satellite's lifespan can be grouped into two different sections: the initial start up and then the steady state or regular operations. Both are defined within the real time operating system. ThreadX simplifies this process through its issued library. The user specifies the different processes and threads then calls the ThreadX software to initialize all of these processes. The following Figure 2.3.7-2 shows the commissioning process. The user calls tx_kernel_enter within its main function to turn control to the ThreadX software. This in turns calls the tx_application_define which initializes all processes in the microcontrollers. The real time operating system then enters its steady state where is remains throughout the rest of its lifespan.

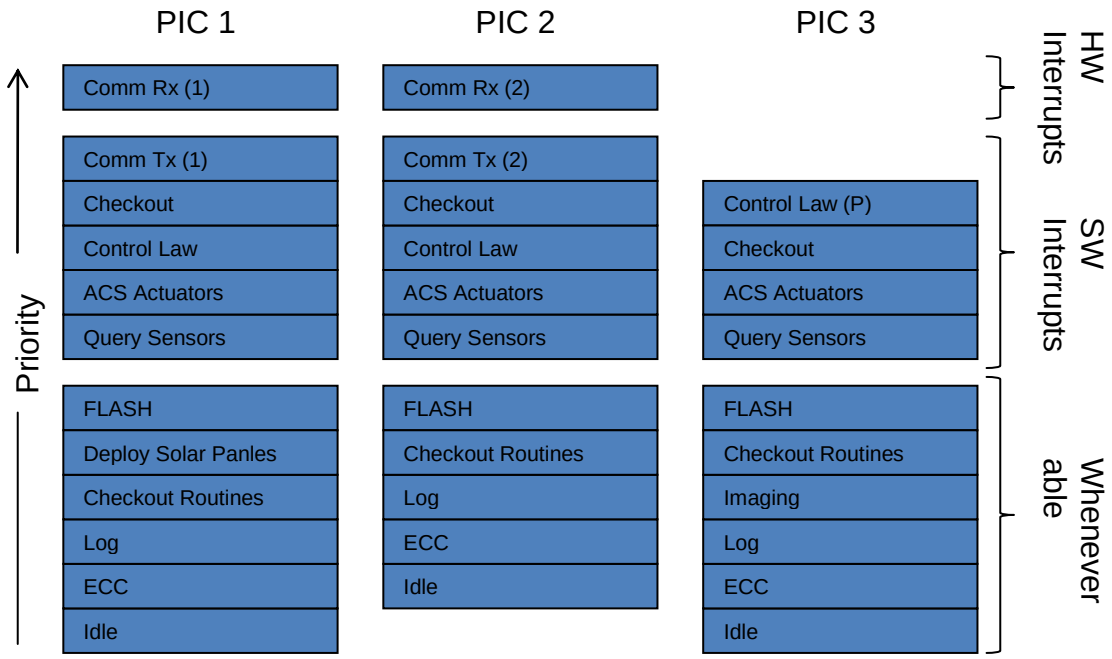

FIGURE 2.3-12: PIC BREAKDOWN

One of the most important features of the ThreadX software, aside from its ability to distribute control to each parallel process, is its ability to prioritize each of these tasks and integrate them. Since the satellite must perform many simultaneous operations it is constantly receiving requests or interrupts from multiple components. ThreadX requires the assignment of priorities to each thread and interrupts to ensure that the most important tasks are executed before other others. Execution priority levels between 1 and 1023 are available. Figure2.3-13 shows the priority hierarchy of CASTOR's interrupts and how they will be handled.

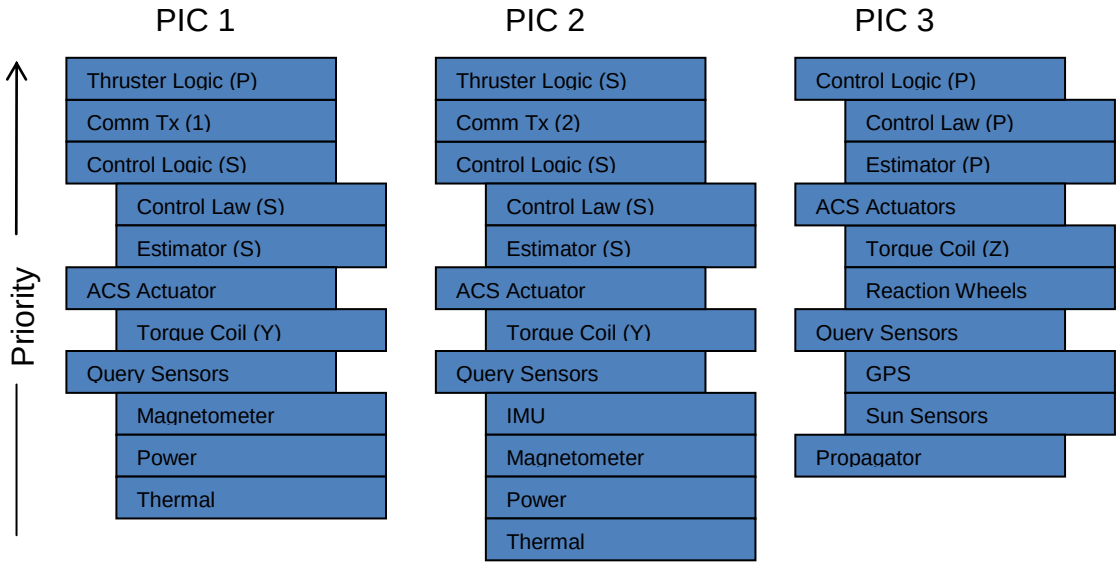

FIGURE 2.3-13: PRIORITY HIERARCHY

A thread should consist of the following elements:

- A header that defines or described the following
  - Resources invoked by the task (timers, ports, devices, memory, etc.)
  - Priority level of the task (in relative terms and the absolute number)
  - Communication structs (if passing data back to the ground)
  - Description of data logging formats and rates
- Local variables
- Any initialization code that must be run immediately on startup
- Command and/or timer interrupt-driven processing loop
- Hardware-interrupt signal processing (the amount of code here should be kept to an absolute minimum, with the majority of the processing done in the normal processing loop)
- Resource locks (these should be kept to an absolute minimum, and avoided where possible by using a unique thread for each device to prevent access conflicts, but they will certainly be necessary for the shared SPI bus)

The full list of tasks necessary for satellite operation, which need to each be converted to a thread on the respective dsPIC, are outlined below for reference (grouped roughly in terms of input-only, input/output, output-only tasks)

A. On dsPIC 1
   1. Thermal (-sensors and -couples)
   2. Power sensors
   3. Magnetometer
   4. Watchdogs
   5. Modem
   6. Memory
   7. CAN
   8. Debugging LEDs
   9. Torque Coil
   10. Linear Actuator
   11. Power converter activation signals
       i. Also controls propulsion system
       ii. Includes DAC

B. On dsPIC 2
   1. Thermal (-sensors and -couples)
   2. Power sensors
   3. Magnetometer
   4. IMU
   5. Watchdogs
   6. Modem
   7. Memory
   8. CAN
   9. Debugging LEDs
   10. Torque Coil
   11. Power converter activation signals
       i. Also controls propulsion system
       ii. Includes DAC

C. On dsPIC 3
   1. Control Loop
   2. Kalman Filter
   3. GPS
   4. Sun Sensors
   5. Reaction Wheels
   6. Camera
   7. Watchdogs
   8. Memory
   9. CAN
   10. Debugging LEDs
   11. Torque Coils

The system will also need to keep track of certain elements of global data that are necessary across many threads. These variables will be propagated to the other dsPICs across the CAN bus. This will allow every dsPIC simple and transparent access when any thread requires their values. The list of variables that this applies to is provided below. Other variables are local to their thread and should not be accessed by another thread. They may be made accessible to another thread via the message passing and notification architecture that ThreadX provides, or by explicitly extending the enumerated list. These structures should all be defined in the header file "main.h".

- Analog voltage readings (the raw, unconverted values)
- Whether or not the satellite is in the sun (0=Eclipse)
- Whether or not the satellite is in a safe state to fire the thruster, broken out by possible failure parameter (0=NOT OK to fire)
- Magnetometer readings
- IMU Readings
- Attitude and position state data
- Time bias (synchronized between the PICs infrequently and on startup)

2.3.8 SD CARD API EXAMPLE

Access to the SD Card is buffered in local flash memory on each dsPIC to facilitate easy and fast access. Because access to the SD memory is shared across all 3 dsPICs processors, the hardware design includes a request access bus enable that blocks access to the memory until the dsPIC requests, and is granted, access. To ensure that threads do not stall whenever they need to write to the flash, data for writing is first buffered into the internal flash memory on the dsPIC, and written to the SD Card when it becomes available. It is necessary to buffer using the flash memory first since there is not enough space in the data ram to provide a buffer of sufficient size given the need to be executing a number of threads and other routines (there is 28KB). There is 256KB of flash memory, less than half of which is needed for the actual program, so the remainder can be used as buffer.

We have chosen to implement a first-in-first-out (FIFO) circular buffer structure for the SD write buffer. New data is added to the tail and old data is read from the head. Writing to flash provides an interesting challenge since data must be written in 128 byte chunks ("a row"), but it must be erased before it can be written. Unfortunately, it can only be erased in 1024 byte chunks ("a page"). Thus, items can only be added to the buffer if there is a sufficient gap to the next item. Additionally, before starting on a new page, the entire page must first be erased.

We chose to have data written to the buffer in 128 bytes chunks. Because of the restrictions listed above, we needed to choose a multiple of 128 and a factor of 1024. The choice of 128 bytes is expected to make the most efficient use of flash space since that figure is greater than the expected value for the number of characters that will need to be written in a typical step to one file. This size includes both a header of 34 bytes and 98 bytes for data. The header contains the information on the number of byte values in this array, the sequence number of the write, the offset at which to write the values, and 30 characters for specifying the file name, including its

path. The offset can be a number from 0 to 0xFFFE (inclusive) and will result in the data being written at that location in the file. Alternatively, an offset of 0xFFFF can be specified which will result in an append operation. If both the offset is 0 and the number of characters is 0, the file will instead be deleted.

Reading the data is much more straightforward than writing since any chunk can be read independently. To enable recovery and error detection, after reading the data block, the first row is set to zero. Thus, by scanning the first integer of each block, the program can determine the state of that block. When erased, the memory is set to all 1's (0xFFFF). When writing, bits can be flipped from 1 to 0, but not vice-versa. Thus all 0's (0x0000) is used as a flag that the chunk has been filled and read, but not yet erased. If (when) the dsPIC is reset, it can scan through the space allocated to the circular buffer and read these flags to locate the contiguous space that contains real data, or determine that the buffer was previously empty.

The ADC module continuously measures the voltages on the analog input pins, but these values are only read out on a periodic timer interval (currently specified as 0.2 Hz by the Power and Thermal teams). The Magnetometer and IMU values are also read their values at a periodic rate. (Other sensors will be read periodically as well, but these are already known to be working and a full list can be found in the previous section of the design document, with the details on each given in their respective sections by subteam). Upon reading of these sensors, the values are immediately stored in a global buffer and synchronized across the 3 dsPICs using the CAN bus. Saving them into a local RAM buffer enables simple and rapid access to any of these values by any process on any dsPIC. Since the CAN bus operates at 500kbps, it should have plenty of excess capacity to handle this slow rate of update. Making the data continuously updated and available in memory also eliminates the need for request/response packets, and the overhead associated with generating and processing them. The full list of variables that this currently applies to can be found in the previous section of the design document.

2.3.9 SOFTWARE INTERFACES/ DEVICE API (L. DE LA GARZA)

See the Interface Control Documents for specific functions controlling particular hardware, as well as pinout diagrams and specifications.

In general, control of hardware involves five categories:

1. Initialization or setup

In this kind of operation, the first interaction with the device is established. In this operation, the pins on the dsPICs associated with the device are configured correctly (tristate, high/low, clock settings, etc.). Additionally, if there are any initial commands that must be sent to the device, such as a Configuration operation, those might be covered here. The convention is for this function to contain "Init" or "init" somewhere in the name, and to have no arguments.

2. Wait/idle

Certain devices can be set to operate in low-power modes, maintaining their configured settings. The magnetometer, for example, is capable of entering sleep mode for an indefinite amount of

time; when awoken it is capable of immediately taking readings, without having the dsPICs need to reset any hardware settings of the magnetometer. The convention for this function is to contain “idle”, “sleep”, or “wait” within the name, and possibly possess arguments.

3. Read/Write

Sensors and storage are capable of sending data to or receiving data from the dsPICs. These functions must be called after proper initialization and configuration operations. The names, arguments, and return types of these functions, by necessity, have no strict conventions.

4. Operate/execute

These kinds of operations carry out the necessary activities to ensure the success of the mission – actuating the torque coils, controlling the power switches, taking pictures with the camera, sending data to the modems, and so on. The names, arguments, and return types of these functions, by necessity, have no strict conventions, but usually it is a good idea to have the name of the component performing the action within the function name.

5. Configuration

In this operation, operating settings of the device are set. Examples of this operation include setting camera resolution or oscillator speed in the magnetometer. This kind of operation should happen occasionally, as determined by mission logic or commands sent from the ground.

2.3.10 SOFTWARE STATUS (L. DE LA GARZA)

As of 16 April 2010, operating code of the PAC and Groundstation is incomplete. The current status of the code is expanded in Table 2.3-4. All items needs to be green (preferably dark green) before launch, where green is used to indicate a functional segment of code. Other colors were chosen to give an intuitive understanding of the current work focus on the components and their importance. The comments then go into further detail on the status and/or function name to provide helpful information from the last person to work on the functionality implementation.

Function	Status	Comments
Ability to reprogram (lab)	Done	ICD2 commercial PIC re-programmer was made functional for our design by 83x class.
Ability to reprogram (other PIC)	Incomplete	
ADC	Done	May need to check/revise timing of samples. In RTOS, this sample collection may be done in a thread instead of an interrupt.
CAN	Mostly	Receive is working, buffered. Transmit has many issues (incorrect packet ordering, no buffer, busy-wait stall, loss of

	working	packet SID's) which are most likely related to hardware errata number 10 for dsPIC33FJXXXGPX06/X08/X10 family of processors.
UART	Working	Buffered bidirectional for both U1 and U2
SPI	Working	Bidirectional flow that triggers off of the DRDY pin
External memory	Unwritten	Have selected SD memory; unimplemented
Watchdogs	On hold	Needs to include monitors on: code integrity, code not in lockup, code not in error condition, other PIC responding (over CAN), configure ThreadX
PIC Flash	Incomplete	Simulation of code storage works; error correction unimplemented
SEU logic	Unwritten	Error detection/correction unimplemented
RTSP (Run time serial programming)	Partially working	83x class demonstrated a direct RTSP reprogramming over serial. Much of the code for a buffered write is in place, but untested and configuration registers are probably wrong. Possibly want to convert to RTSP2 for faster reprogramming times.
ICSP (In-circuit self programming)	On hold	Requires separate bootloader code architecture, in parallel with the main DSC code, which can be written into low memory and then dropped into to reprogram the rest of the PIC's memory.
Linear Actuators	Mostly working	Code executes correctly, behavior of linear actuators is far from ideal (low precision, unstable positioning for small distances, large power draw to hold large distances (beyond physical maximum)
Thermal Sensors	Working	Tested the measurement of several thermal sensors and received acceptable (and stable) voltage measurements.
Thermocouples	Unwritten	
Torque Coil	Mostly working	Code tested to operate torque coils. Creates a scalable bidirectional magnetic field. Needs integration into PAC.
Magnetometer	Working	Code tested and verified for collecting three axis magnetometer data.
Voltage Sensors	Mostly	Code written to sample ADC data for value of voltage dividers for the actual voltage at the DC/DC converter. Code

	working	is awaiting formal test session
Current Sensors	Mostly working	Code written to sample current sensors at DC/DC converters. Code is awaiting formal test session.
Power MOSFETs	Untested	Implemented; proper pin registers have not been set.
Communications - transmission	Incomplete	Receives, validates, and acknowledges packets correctly. Need to incorporate lookup table with task registration after integrating RTOS). Complete command interpretation must be fleshed out. Limited validation of packets can be improved. CRC revision needs completion. New segmentation protocol unimplemented.
Communications - groundstation	Incomplete	Receives, validates, and acknowledges packets correctly. CRC revision needs completion. New segmentation protocol unimplemented. Full packet vocabulary must be fleshed out. Image transmission to MIT must be implemented. Code upload must be implemented.
Communications– MIT groundstation	Incomplete	Full packet vocabulary must be fleshed out. Image reception must be implemented. Code upload must be implemented.
IMU	Incomplete	Code for reading the accelerometer and gyroscope data from the IMU has been written. This code is awaiting a test session for verification.
Reaction Wheels	Unwritten	
GPS	Unwritten	
Sun Sensors	Unwritten	
Camera	Untested	Camera code from the manufacturer has been converted to work with dsPIC. Awaiting flash memory to perform test of operability.
Time	On hold	Tracking current time using GPS
ThreadX / RTOS	Untested	Source code acquired; thread management not configured
Message passing	Untested	Not evaluated/configured.
RPC (remote procedure call)	Untested	Not evaluated/configured.
Ops code	Incomplete	Full set of mission procedure unimplemented.

Ops code-comissioning logic	Unwritten	
Ops code – power management logic	Unwritten	
Ops code – thermal management logic	Unwritten	
Ops code – engine logic	Unwritten	
Ops code – command log	Unwritten	Command list, telemetry, file system
Xenon Feed System logic	Unwritten	
ADCS Control Logic	On hold	Waiting for ADCS development : propagator, estimator, EKF, control law

TABLE 2.3-4: STATUS OF CODE

2.4 COMMUNICATIONS

2.4.1 REQUIREMENTS (S. PARRA)

Below is the updated requirements verification matrix for the CASTOR communication subsystem.. A green status indicates that the requirement has been fully met by the communication subsystem. A yellow status indicates that the requirement has been met, but not fully verified, and further testing is needed to ensure verification. A red status indicates that the requirement has not been met. Most requirements have been met; however further testing still needs to be done to verify requirements. Multiple services also still need implementation such as packet retransmission, queuing, and command interpretations.

Requirement	Details	Status
1	The communications system shall provide the ability to transmit and receive data	

1.1	The communications subsystem shall provide the ability to transmit telemetry and picture packets from the satellite to the ground station.
1.1.1	The communications subsystem shall be equipped with at least one antenna and one modem on the satellite.
1.2	The communications subsystem shall provide the ability for the ground station to receive telemetry and picture packets from the satellite.
1.2.1	The communications subsystem shall be equipped with a dish and a modem at the ground station.
1.3	The communications subsystem shall provide the ability to transmit commands from the ground station to the satellite.
1.3.1	The communications subsystem shall be equipped with a dish and a modem at the ground station.
1.4	The communications subsystem shall provide the ability for the satellite to receive commands from the ground station.
1.4.1	The communications subsystem shall be equipped with at least one antenna and one modem on the satellite.
2	The communications system shall be able to establish a robust and periodic link
2.1	The communications subsystem shall recognize correct packets from incorrect packets and be able to request retransmission if the packet is faulty.
2.1.1	The link layer protocol, from the modem, shall be able to recognize correct packets from incorrect packets and be able to request retransmission if the packet is faulty.
2.1.2	The upper layer protocol, from the software on the satellite and ground station, shall be able to recognize correct packets from incorrect packets and be able to request retransmission if the packet is faulty.
2.2	The satellite shall be able to receive a set-up ack from the ground station and start a communications link
2.2.1	The modem shall be able to wake up from sleeping mode when commanded to so as to start a communications link.
2.3	The communications subsystem shall be able to store packets to prevent overflow.
2.3.1	The communications protocol shall be able to set up packet queues on the satellite and the ground station.
2.4	The communications subsystem shall be able to identify lossy packets and out of order packets.
2.4.1	The communications protocol shall be able to identify lossy packets and out of order packets.
3	The communications subsystem shall be able to support a bandwidth and data rate necessary to transmit all telemetry (67bps) and pictures (2 per orbit 640*480 pixels).

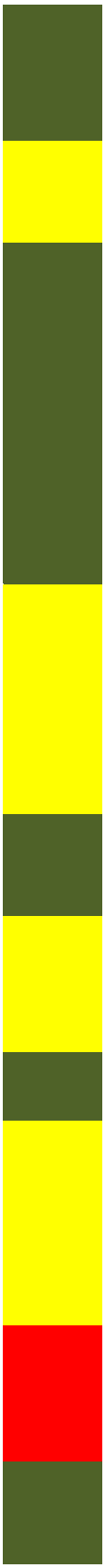

3.1	The communications subsystem shall transmit at 115.2 kbps
3.2	The communications subsystem shall have a bandwidth of 2.4GHz
4	The communications subsystem shall be fully redundant
4.1	The communications subsystem shall be equipped with 2 antennas
4.2	The communications subsystem shall be equipped with 2 modems
5	The communications subsystem shall be able to encrypt data packets

TABLE 2.4-1: COMMUNICATIONS REQUIREMENTS

2.4.2 OVERVIEW (S. PARRA)

The subsystem consists of two redundant communication mechanisms. The first mechanism consists of two antennas connected to one of the modems via a splitter. This modem is then connected to one of the dsPICs on the PCB. The second consists of a single antenna connected to the other modem which is connected to another dsPIC. When the avionics board wants to send a message to the ground station, it first selects an antenna to communicate with (using an algorithm developed by the ACS subsystem which takes into account distance, attitude, etc… and chooses the best antenna to use for communication). Then the flight computer sends packets to the modem which send the packet to the ground station. At the ground station, the signal is received using a 3 meter dish and then the packet will be forwarded to the MIT station via TCP/IP where the packet will be fully decoded. Communication in the other direction works the same way. Below is a diagram that displays the CASTOR to MIT ground station communication.

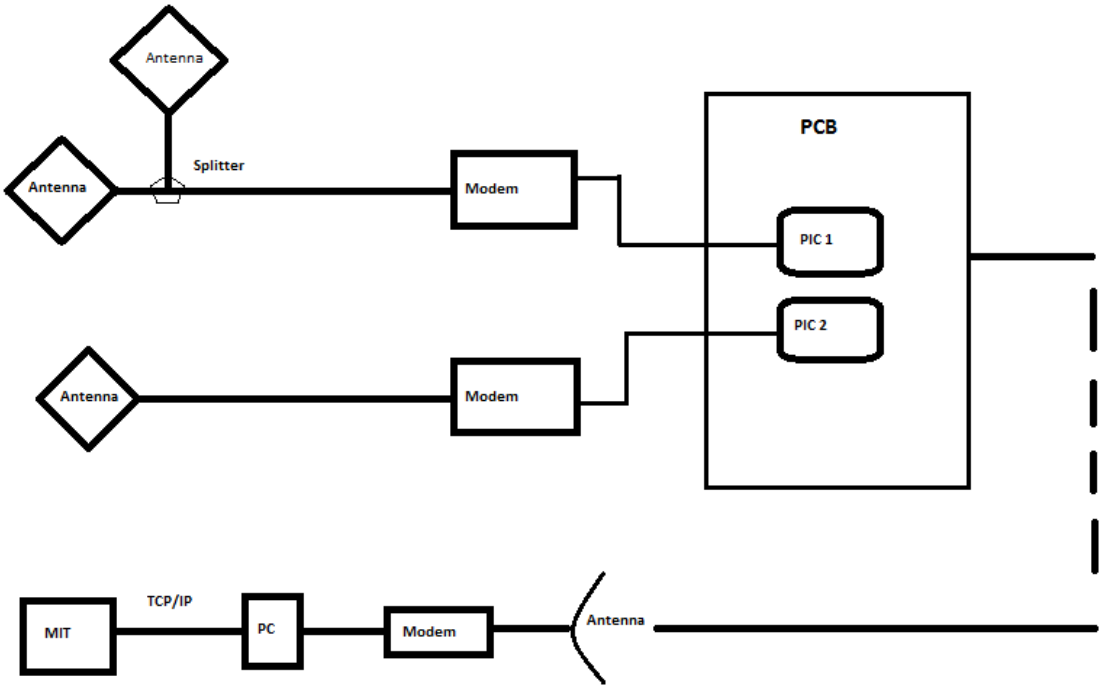

FIGURE 36: OVERVIEW OF CASTOR COMMUNICATION LINK

In addition, the antennas will be located on various parts of the CASTOR body. The figure below depicts the exact positions of these antennas, represented by the yellow on green squares.

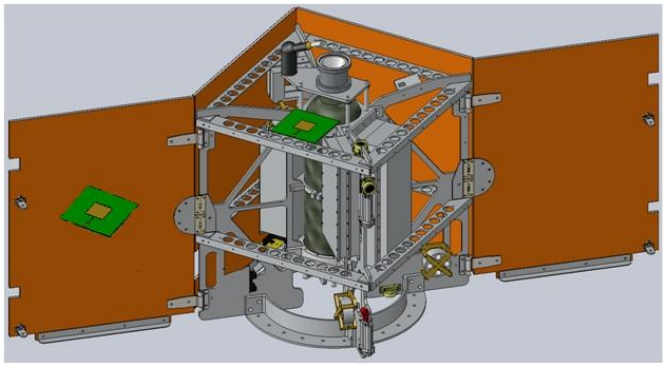

2.4.3 BUDGET (S. PARRA)

The estimation of the cost of the communication subsystem has been done breaking the system into a satellite component, and into a ground station component. The first is related to the communication hardware elements that will be placed on the satellite. The former is related to the hardware elements of the ground station plus the cost of upgrading the station in a way to make it suitable for CASTOR mission.

Component	Part number	Company	Quantity	Price per unit	Total price
Antennas	Custom	Custom	3	$33	$99
Straight PCB	R330-074	RCA Solutions	3	$3.30	$9.90

Jack					
Modems	MHX2420	Microhard Systems Inc. Building 17, 2135-32 Ave NE Calgary, Alberta T2E 6Z3	2	$800	$1600
MCX(M) to SMA(F)- 9 inch cable	202309SFB9	RCA Solutions	2	$13.28	$26.56
SMA(M) to SMA(M)- 40 inch cable	307303SFC40	RCA Solutions	2	$24.53	$49.06
SMA(M) to SMA(M)- 50 inch cable	307303SFC50	RCA Solutions	1	$27.80	$27.80
SMA(M) to SMA(M)- 13 inch cable	307303SFC13	RCA Solutions	1	$15.71	$15.71
Power Splitter	ZAPD-4-S+	Mini-Circuits	1	$64.95	$64.95
TOTAL					**$1892.98**

TABLE 2.4-2: SATELLITE COMM BUDGET

Component	**Part number**	**Company**	**Quantity**	**Price per unit**	**Total price**
Antenna (2.3m dish)	---	Already available in Kwajalein	1	N/A	N/A
Modem	MHX2420	Microhard Systems Inc. Building 17, 2135-32 Ave NE Calgary, Alberta T2E 6Z3	1	800$	800$
Cable	N-female to pigtail cable	L-com Global Connectivity HyperLink Wireless Division 1201 Clint Moore Road Boca Raton, FL 33487, USA	1	25$	25$
Ground station computer	--	Already available in Cayenne	1	N/A	N/A
Operation computers at MIT	Generic computer	Not defined	3	~2k$	6k$
Personnel at MIT	--	Done by MIT students	3 people	N/A	N/A
TOTAL					**$6825**

TABLE 2.4-3: GROUND STATION COMM BUDGET

2.4.4 LINK BUDGET AND DATA RATE ANALYSIS (M. MUNOZ)

The final link budget according UNP reviewers suggestions, and under the assumption of using the 3m antenna is shown below:

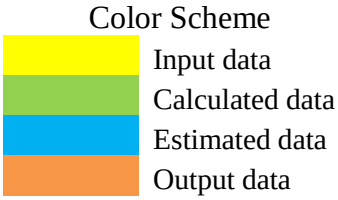

Link budget at 115200bps	Downlink (6 dB)	Uplink (35.3 dB)
R (Data rate in bps)	115200.00	115200.00
P (Tx Power in dBW)	0.00	0.00
Gt (Tx Antenna Gain in dB)	6.00	35.30
Gr (Rx Antenna Gain in dB)	35.30	6.00
B (Rx Noise BW in Hz)	83500000.00	83500000.00
Eb/N0 required (dB)	12.80	12.80
f (Desired Tx Frequency in MHz)	2442.00	2442.00
θaos (Earth Centric Angle @ AOS in rad)	0.45	0.45
h (Circular Orbit Altitude in km)	700.00	700.00
Te (Earth noise in K)	290.00	290.00
Gk (Boltzmann's const in dB)	228.60	228.60
Lion (Ionospheric Loss in dB)	-1.00	-1.00
Latmo (H20 & O2 Losses in dB)	-0.30	-0.30
Lrain	-0.20	-0.20
Pointing Loss transmitter (dB)	-2.00	-0.14
Pointing Loss receiver (dB)	-0.14	-2.00
Demodulator Loss (dB)	-1.40	-1.40
Tgal (Galactic noise temp in K)	50.00	50.00
Tant (Total Antenna Noise in K)	340.00	340.00

Treceiver(k)	290.00	290.00
Splitter Loss (dB)	-3.00	-3.00
Ll (Line Loss in dB)	-0.77	-0.77
Raos (Dist to SAT @ AOS in km)	3067.48	3067.48
Rmin (Dist to SAT @ Zenith in km)	700.00	700.00
Ls-max (Free Space Loss @ AOS in dB)	-169.94	-169.94
Ls-min (Free Space Loss @ Zenith in dB)	-157.11	-157.11
Ts (Total System Noise Temp in dBK)	-27.99	-27.99
Lr (Data Rate Loss in dBHz)	-50.61	-50.61
Eb/No-aos (Bit Energy to Noise Spec Density @ AOS in dB)	16.62	16.62
Eb/No-min (Bit Energy to NoiseSD @ Zenith in dB)	29.45	29.45
C/No-aos (Carrier to NoiseSD @ AOS in dB)	67.23	67.23
C/No-min (Carrier to NoiseSD @ Zenith in dB)	80.07	80.07
C/N-aos (Carrier to Noise at Rx @ AOS in dB)	-11.98	-11.98
C/N-min (Carrier to Noise at Rx @ Zenith in dB)	0.85	0.85
System Margin -aos(dB)	**3.82**	**3.82**
System Margin -min(dB)	**16.65**	**16.65**

TABLE 2.4-4: LINK BUDGET

Both the downlink and the uplink have the same energy bit to noise ratio (Eb/No**)** and the same system margin. This is because the communication system uses of the same type of modems and data rate on both the satellite and ground station. It is therefore a communication system with a symmetric link.

Data Rate Analysis

In order to define the amount of images that the communication system is able to transmit a data rate analysis was developed. The analysis helped determine the amount of pictures that could be transmitted using a data rate of 115.2 Kbps. This analysis required the graphing of the amount of data gathered by the satellite per time, and the amount of data downloaded per time when the satellite was in view of the ground station. The analysis also required that different amounts of pictures be taken in a 24 hour period to test the capabilities of the communications system. As of now, the propulsion team would like to take a picture every time the engine fires. Therefore, in consultation with the propulsion team, the communications team has set the picture resolution to be within 70-300 kpixels in order to be able to take a large amount of pictures per day. In order to meet this requirement it is necessary to calculate the total amount of data collected by the satellite per day and the total amount of data that can be downloaded from the satellite per day. So using the equation:

$$Total amount download able data - total amount of data accumulated = data left \ for \ pictures$$

One can determine how many downloadable bits are left for pictures. The *total amount of downloadable data* is calculated by multiplying the download rate (115.2 kbps) by the total amount of communication time. It was determined by the operations team that the total amount of satellite subsystem health data and telemetry rate of upload would be 67 bps; if the packet header data is included the total data rate is 71 bps. Therefore, the *total amount of data accumulated* is calculated by multiplying 71 bps by 86400 sec (total seconds in a day). Table 2.4-5shows the amount of data left for pictures when satellite is at a 45 degree inclination (comm. Time= 3045 sec) and when it is at a 90 degree inclination (comm. time= 870 sec).

Data available per day (45 degree inclination)	
Comm. time= 3045 sec	
Download Rate (kbps)	Amount of data left (Mbits)
115.2	344.665
Data available per day (90 degree inclination)	
Comm. time= 870 sec	
Download Rate (kbps)	Amount of data left (Mbits)
115.2	94.105

TABLE 2.4-5: DATA AVAILABLE

TABLE 2.4-6 AND

Table 2.4-7show the different picture resolutions the camera that will be mounted on the satellite has. Using the camera resolution, the amount of bits plus its packet header of a picture can be calculated. This information, along with the download rates and the communication time can be used to calculate how many pictures per day can be taken at the different camera resolutions. The resolutions highlighted in yellow correspond to those resolutions that match the 10-200 kpixel requirement of the propulsion team. The amounts of pictures that can be taken represent ideal numbers, therefore the rows and columns in green show a 40 percent loss in the number of pictures that can be taken. The 40 percent was chosen by the communications team and it represents the losses of pictures to due loss of satellite communication, incorrect data transmission, etc.

	Pictures per day (45 degree inclination) comm. time: 3045 sec						Assuming 40% loss	
			Download Rate (kbps)					
	pixels	Kbits	19.2	115.2	19.2	115.2	19.2	115.2
Res. Type	Pic. size	Kbits/(Pic. + Header)	# of pictures/day		# of pictures/orbit		# of pictures/day	
VGA	307200	783.168	66	440	4	27	39	264
CIF	101376	258.445	202	1333	12	83	121	799
SIF	76800	195.792	267	1760	16	110	160	1056
QCIF	38720	98.711	530	3491	33	218	318	2094
160*128	20480	52.211	1002	6601	62	412	601	3960
80*64	5120	13.052	4010	26407	250	1650	2406	15844

TABLE 2.4-6: PICS PER DAY (45 DEGREE INCLINATION)

	Pictures per day (90 degree inclination)		comm. time: 870 sec				Assuming 40% loss	
			Download Rate (kbps)					
	pixels	kbits	19.2	115.2	19.2	115.2	19.2	115.2
Res. Type	Pic. size	kbits/(Pic. + Header)	# of pictures/day		# of pictures/orbit		# of pictures/day	
VGA	307200	783.168	13	120	0	7	7	72
CIF	101376	258.445	40	364	2	22	24	218
SIF	76800	195.792	54	480	3	30	32	288
QCIF	38720	98.711	107	953	6	59	64	571
160*128	20480	52.211	202	1802	12	112	121	1081
80*64	5120	13.052	811	7210	50	450	486	4326

TABLE 2.4-7 PICS PER DAY (90 DEGREE INCLINATION)

2.4.5 HARDWARE (M. MUNOZ)

The selection of the antennas has been revisited with respect to the design proposed in the 16.83 class. Our past choice of antennas was the Hyperlink Technologies 8 dBi and 11dBi 2.4 GHz patch antennas. These antennas, designed for wireless internet broadcast, were designed with a hemispherical radiation pattern. However we were unsure whether these antennas could withstand the forces they would experience during the launching phase of the operation because of their flimsy construction. We decided to design and manufacture our own antennas.

The type of antenna we decided to design is a microstrip patch antenna. This type of antenna is a narrow bandwidth, wide-beam antenna fabricated by bonding the antenna copper element to an insulating dielectric substrate with a continuous metal layer bonded to the opposite side of the substrate which forms a ground plane. Our microstrip patch antenna would be edge fed and Figure 2.4-2 shows a basic drawing of an edge fed patch antenna.

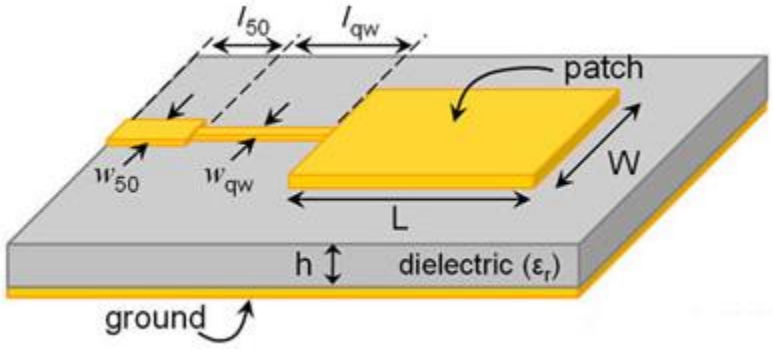

FIGURE 2.4-2 MICROSTRIP PATCH ANTENNA

The necessary measurements to make an antenna with a center frequency of 2.442 GHz can be found through derived equations.

THE EQUATIONS USED TO GET THE REQUIRED DIMENSIONS FOR THE RADIATING COPPER ELEMENT ARE SHOWN IN

Figure 2.4-3. Look at Figure 2.4-2 for variable reference.

PATCH GOVERNING EQUATIONS

$$CONSTANTS$$
$$center\ frequency\ f_c = 2442$$
$$\lambda = 0.1228\ m$$
$$speed\ of\ light\ c = 3.00 \times 10^8\ m/s$$
$$dielectric\ constant\ \varepsilon_r \approx 4.2$$
$$f_{max} = 24835\ MHz$$
$$h = 1.57 \times 10^{-3} m$$

WIDTH $(\boldsymbol{w})$

$$w = \frac{c}{2f_c}\left(\frac{\varepsilon_r + 1}{2}\right)^{-\frac{1}{2}} \times \left(\frac{1000mm}{1m}\right)$$

LENGTH $(\boldsymbol{L})$

$$L = \frac{c}{2f_r\sqrt{\varepsilon_e}} - 2\Delta l$$

EFFECTIVE DIELECTRIC CONSTANT $(\boldsymbol{\varepsilon_e})$

$$\varepsilon_e = \frac{\varepsilon_r + 1}{2} + \frac{\varepsilon_r - 1}{2}\left(1 + \frac{12h}{w}\right)^{-\frac{1}{2}}$$

LINE EXTENSION $(\Delta \boldsymbol{l})$

$$\frac{\Delta l}{h} = \frac{0.412(\varepsilon_e + 0.3)\left(\frac{w}{h} + 0.264\right)}{(\varepsilon_e - 0.258)\left(\frac{w}{h} + 0.8\right)}$$

INPUT IMPEDANCE OF PATCH $(\boldsymbol{z_a})$

$$z_a = 90\left(\frac{\varepsilon_r^2}{\varepsilon_r - 1}\right)\left(\frac{L}{w}\right)^2$$

FIGURE 2.4-3 PATCH ANTENNA EQUATIONS

In addition to the radiating copper element, the feeding microstrip and the quarter wave transformer also needed to be designed. Figure 2.4-4 shows the equations used to calculate the dimensions of the microstrip and quarter wave transformer so that there is matching impedance across all the antenna elements.

MICROSTRIP GOVERNING EQUATIONS

MICROSTRIP IMPEDANCE (Z_0)

$$Z_o = \begin{cases} \frac{\eta_0}{2\pi\sqrt{\epsilon_e}} \ln\left(\frac{8h}{W'} + 0.25\frac{W'}{h}\right), & \frac{W}{h} \leq 1 \\ \frac{\eta_0}{\sqrt{\epsilon_e}}\left[\frac{W'}{h} + 1.393 + 0.667\ln\left(\frac{W'}{h} + 1.444\right)\right]^{-1} & \frac{W}{h} \geq 1 \end{cases}$$

$$\eta_0 = 120\pi \; ohms$$

WIDTH OF MICROSTRIP (w_{qw}, $\mathbf{W_{50}}$)

$$\frac{W'}{h} = \frac{W}{h} + \frac{1.25}{\pi}\frac{t}{h}\left(1 + \ln\left(\frac{4\pi W}{t}\right)\right), \qquad \frac{W}{h} \leq \frac{1}{2\pi}$$

$$\frac{W'}{h} = \frac{W}{h} + \frac{1.25}{\pi}\frac{t}{h}\left(1 + \ln\left(\frac{2h}{t}\right)\right), \qquad \frac{W}{h} \geq \frac{1}{2\pi}$$

$$\epsilon_e = \frac{\epsilon_r + 1}{2} + \frac{(\epsilon_r - 1)}{2}F\left(\frac{W}{h}\right) - \frac{\epsilon_r - 1}{4.6}\frac{t/h}{\sqrt{W/h}}$$

$$F\left(\frac{W}{h}\right) = \begin{cases} \left(1 + \frac{12h}{W}\right)^{-\frac{1}{2}} + 0.04\left(1 - \frac{W}{h}\right)^2, & \frac{W}{h} \leq 1 \\ \left(1 + \frac{12h}{W}\right)^{-\frac{1}{2}}, & \frac{W}{h} \geq 1 \end{cases}$$

FIGURE 2.4-4 MICROSTRIP/QUARTER WAVE EQUATIONS

Table 2.4-8 shows the calculated dimensions for the antenna.

TABLE 2.4-8 ANTENNA DIMENSIONS

Patch	**Microstrip line**	**Quarter-wave transformer**
Length (mm): 29.6094	Length (mm): 15.0	Length (mm): 15.0
Width (mm): 38.0942	Width (mm): 1.0934	Width (mm): 1.9554
Char. impedance (ohms): 85.6764	Char. Impedance (ohms): 85.6742	Adapter impedance (ohms): 65.4501
Efficiency: 61.72%		Impedance (ohms): 65.451

The CASTOR Communications system will therefore consist of three of these custom made antennas. One will be located on the interior of the left hand side deployable solar panel. Another antenna will be located on the top of the satellite. The third antenna will be located on the bottom of the satellite opposite to the top antenna.

Modem

Our choice of communications band has been based on flight heritage and costs. Since the high cost of a Space Qualified Modem was prohibitive, we chose the MHX2420 S-band transceiver mainly due to the flight experience on Cubesat missions. This modem has the advantages of low power consumption, including a very low power sleep mode, low cost, and broad thermal tolerances. In its base configuration, this modem also performs frequency hopping in order to maintain a better link under terrestrial conditions; the issue related to this specific modem characteristic will be discussed in a separate section of this document.

MHX2420 Parameters of Interest	
Thermal Tolerance	-40 degrees C - +85 degrees C
Input Power	4.0 – 5.5 VDC
Output Power	100mW – 1W
Maximum Throughput	230.4 kbps
Dimensions	89 mm x 53.4 mm x 17.8 mm
Weight	55 grams

TABLE 2.4-9: MHX2420 PARAMETERS OF INTEREST

The power characteristics of a test MHX2420 modem have been measured in the lab and are shown in figure 2.4-15.

Operational State	**Measured Power Draw (W)**
Command mode (no TX or RX)	1.62
Data transfer mode, sleep	0 (power draw too small to measure)
Data transfer mode, unconnected idle	2.13
Data transfer mode, connected idle	2.16
Data transfer mode, connected data transfer	2.85 – 4.22
Data transfer mode, slave waking from sleep	1.59

TABLE 2.4-10: MEASURED POWER DRAWS

The command mode of the MHX2420 allows the computer access to the modem's configuration registers, suspending all modem transmission and reception in the meantime. The modem can be configured to enter command mode automatically on startup or can be put into command mode manually by entering a sequence of three plus signs ("+++").

Data transfer mode is the normal operating mode of the modem. In the chosen network topology, point-to-point, one modem operates as "master" and one as "slave". The modem onboard the spacecraft will be designated the "slave", since only slaves can enter the very low power sleep mode. The last mode in the table, waking from sleep, indicates the power drawn when a slave modem wakes up and checks for data in order to decide whether or not to go back to sleep.

When data is being transferred between the two modems, one modem will occasionally buffer incoming data, resulting in power spikes during the transfer. The maximum measured peak was 4.22 W, a reasonable value given the required 1 W of RF power and the 33% average efficiency of amplifiers in the 2.4 GHz range.

Connections and placements

The modems will connect directly to the dsPIC over two RS232 connections. All connections outgoing from the modem are at TTL voltage levels, hence a voltage conversion between the modem and the RS232 is necessary. These connections have a maximum transfer rate of 115.2 kbps, the tightest restriction on our maximum communications link rate. The top and bottom antennas will connect to a splitter over coaxial cable with SMA connectors. The splitter will connect to one of the modems through its own coaxial cable with an MCX connector terminating the modem end and an SMA connector terminating the antenna. The Antenna on the solar panel will connect directly to the 2nd modem over coaxial cable with an MCX connector terminating the modem end and an SMA connector terminating the antenna.

Both modems will be housed in the avionics stack with the following pins connected. Red indicates PWR/GND connections, green indicates data transfer, and blue indicates control to UART1. All connections outgoing from the modem are at TTL voltage levels. These connections have a maximum transfer rate of 115.2 kbps, the tightest restriction on our maximum communications link rate.

Both modems will be housed in the avionics stack with the following pins connected. Red indicates PWR/GND connections, green indicates data transfer, and blue indicates control

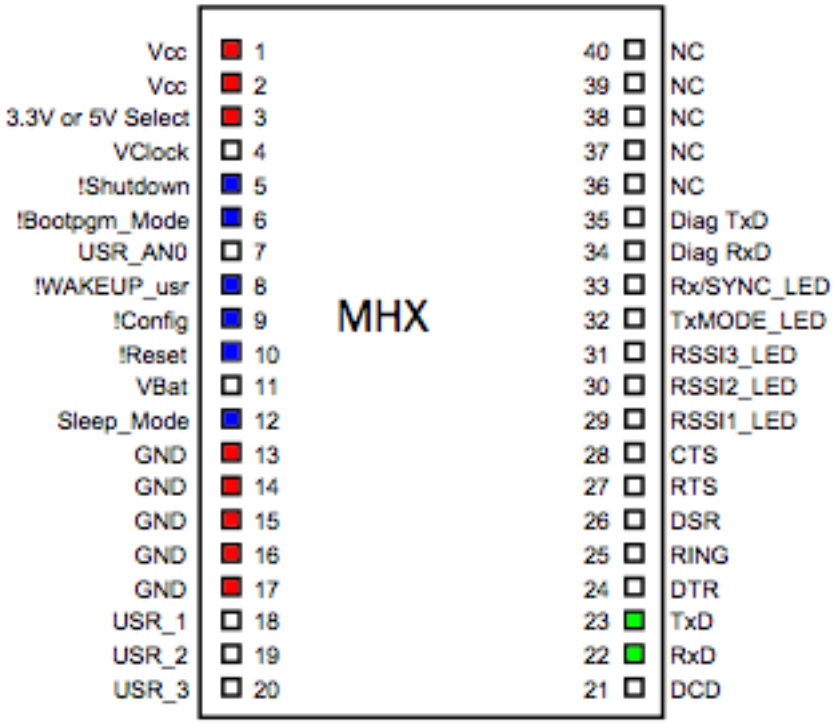

FIGURE 2.4-5: MHX2420 CONNECTED PIN DIAGRAM

The pins perform the following functions:

Pin Mnemonic	**Function**
Vcc	Provides power
Voltage Select	Selects whether modem will talk on 3.3V or 5V
!Shutdown	Active low input shuts down modem
!Bootpgm_Mode	Active low input downloads firmware to modem
!WAKEUP_usr	Active low input wakes up modem
!Config	Active low input on startup puts modem into known default serial configuration (9600 baud, 8/N/1, no flow control)
!Reset	Active low input resets modem
Sleep_Mode	Output pin, active high indicates modem is in sleep mode

GND	Ground
RxD	OUTPUT pin. Sends data received over wireless link to computer
TxD	INPUT pin. Receives data from computer to be transmitted over wireless link

TABLE 2.4-11: PIN FUNCTIONS

The two antennas, as previously indicated, will be bolted to the long edges of the radiator fins in order to provide signal coverage around as much of the spacecraft as possible.

2.4.6 SOFTWARE AND PROTOCOL (S. PARRA)

The CASTOR software protocol follows the standard 7 layer OSI model for communication systems. For the communication system, we will focus on the bottom 4 layers of the OSI model, namely the physical, data link, routing, and transport layers.

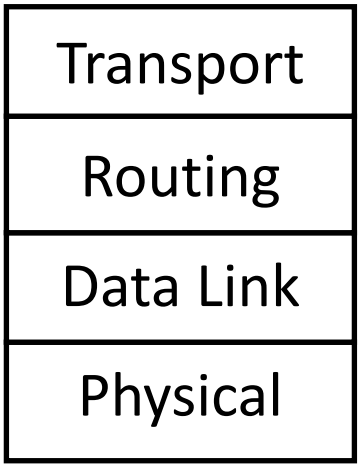

FIGURE 41: PROTOCOL STACK

Physical/Data Link/Routing Layer

The physical and data link layer of the CASTOR communication protocol are not implemented by the team at MIT. These layers are implemented through the transceiver purchased. They use the 802.11g standard at a frequency of 2.4GHz. Other standard features include packet retransmission, FEC Coding (Hamming/Reed Solomon) and a differential binary phase shift keying (DBPSK) modulation scheme. For data encryption, the modems selected come with an added feature that allows data to be encrypted at the data link layer. The type of encryption that this modem supports is 128-AES.The constraint on packet size (255 bytes) comes from this layer due to its implementation as well as our chosen data rate. Since CASTOR is only communicating with the ground station via point to point link, the routing layer does not need to be implemented.

Link Layer Error Detection

The selected modem provides guidelines as to what additions it makes to a packet on the link layer before it is transmitted. In short, the modem allows 255 bytes of data maximum to be included in one packet. The modem them adds its own preamble and CRC to this body of data to form a packet, although it does not specify the format or size of this additional information.

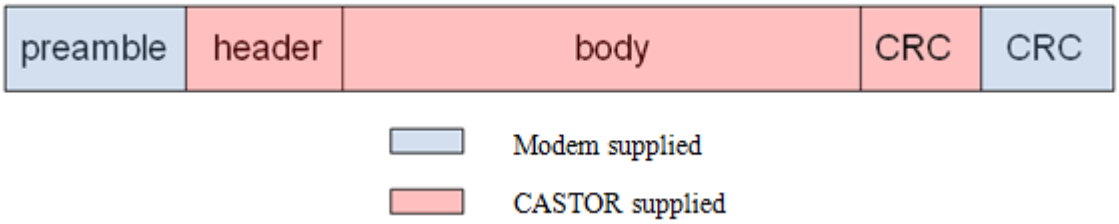

FIGURE 7: MODEM PACKET STRUCTURE

The link layer is transparent to upper layers. Therefore with this modem the operation defined by the protocol can be carried out without having to incorporate how to explicitly deal with the additions. The modem can also request to have a packet resent based on the link layer CRC. If a packet fails this first CRC, the modem will automatically request the packet before it ever gets to the user-defined CRC. The user can however limit the number of retransmissions that are allowed.

Transport Layer

The bulk of the transportation protocol comes from the transport layer. This is fully implemented by the MIT team. Below are specifics of the transport layer.

Initializing and Terminating Communication

The ground station will communicate with CASTOR whenever CASTOR is within range of communication. Refer back to 2.4.4 for specifics and analysis of this time window. The ground station will continually send a set up packet and CASTOR will receive this packet as a start of communication i.e. the ground station will always initiate communication. Once CASTOR receives the set-up packet, it will respond with a series of set-up packets as the modem requires four packets in succession to determine which antenna is better positioned to receive transmissions. Once CASTOR has decided which antenna to use, it will begin the communication session.

A communication session between CASTOR and the ground station can consist of a sequence of commands, down linked images, and down linked telemetry. Any combinations of these are acceptable. At the end of communication, the ground station shall send CASTOR an end packet and with an ack reception, terminate communication. The figure below shows this sequence, with details on automatic retransmission.

COMMAND SCENARIO

Ground Station *Satellite*

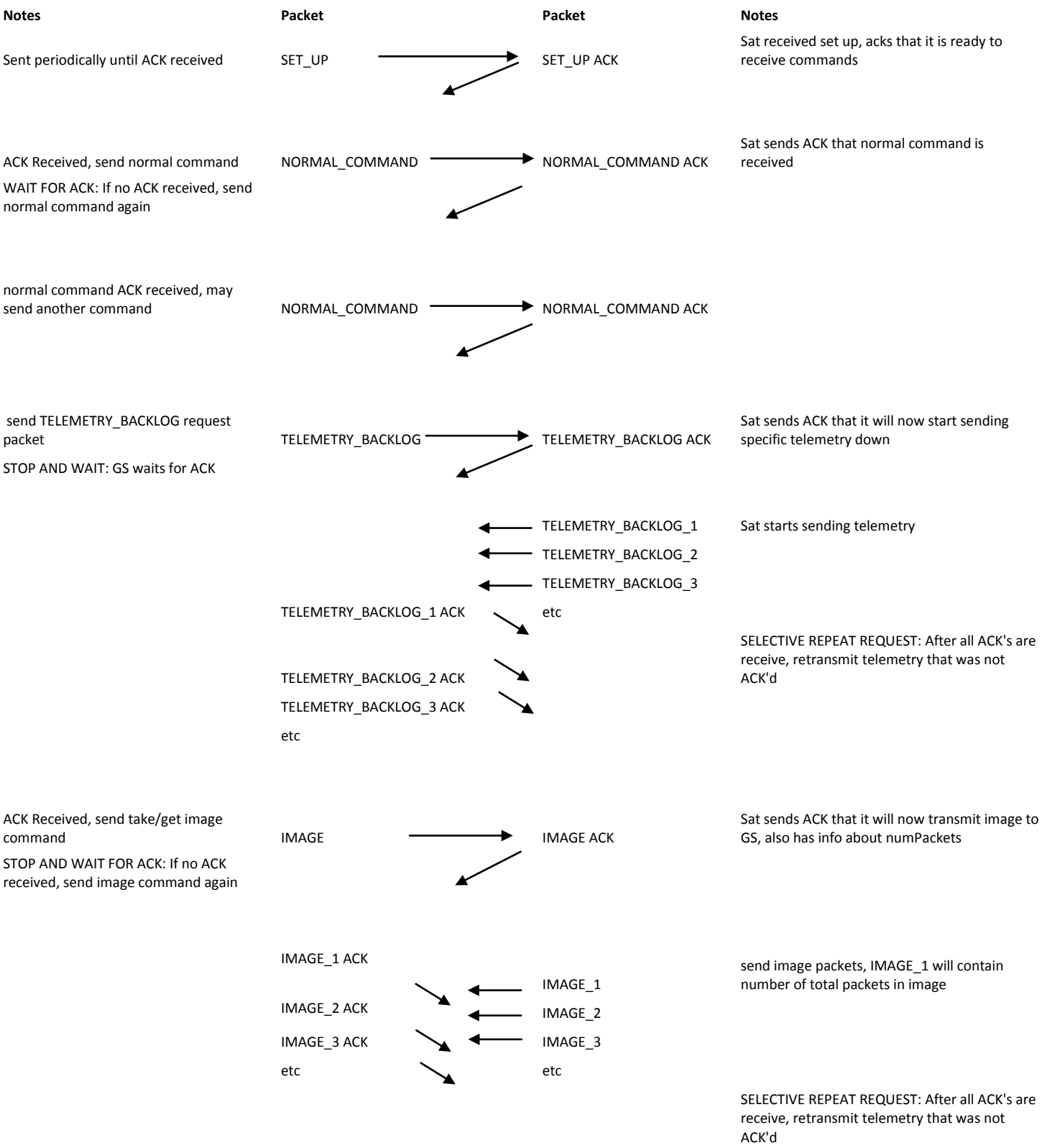
Notes
Packet
Packet
Notes
Sent periodically until ACK received
SET_UP
SET_UP ACK
Sat received set up, acks that it is ready to receive commands
ACK Received, send normal command
WAIT FOR ACK: If no ACK received, send normal command again
NORMAL_COMMAND
NORMAL_COMMAND ACK
Sat sends ACK that normal command is received
normal command ACK received, may send another command
NORMAL_COMMAND
NORMAL_COMMAND ACK
send TELEMETRY_BACKLOG request packet
STOP AND WAIT: GS waits for ACK
TELEMETRY_BACKLOG
TELEMETRY_BACKLOG ACK
Sat sends ACK that it will now start sending specific telemetry down
TELEMETRY_BACKLOG_1
TELEMETRY_BACKLOG_2
TELEMETRY_BACKLOG_3
etc
Sat starts sending telemetry
TELEMETRY_BACKLOG_1 ACK
TELEMETRY_BACKLOG_2 ACK
TELEMETRY_BACKLOG_3 ACK
etc
SELECTIVE REPEAT REQUEST: After all ACK's are receive, retransmit telemetry that was not ACK'd
ACK Received, send take/get image command
STOP AND WAIT FOR ACK: If no ACK received, send image command again
IMAGE
IMAGE ACK
Sat sends ACK that it will now transmit image to GS, also has info about numPackets
IMAGE_1 ACK
IMAGE_2 ACK
IMAGE_3 ACK
etc
IMAGE_1
IMAGE_2
IMAGE_3
etc
send image packets, IMAGE_1 will contain number of total packets in image
SELECTIVE REPEAT REQUEST: After all ACK's are receive, retransmit telemetry that was not ACK'd

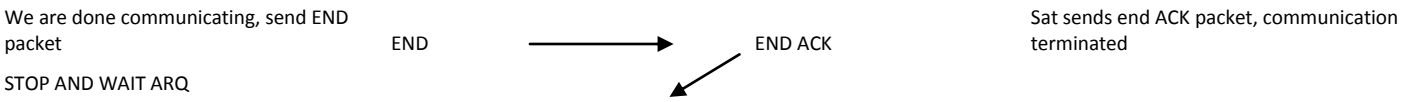

FIGURE 8: EXAMPLE OF A TELEMETRY COMM LINK

Packet Definition

CASTOR and the ground station can have at most 31 different packet types. This number comes from the header definition (specified later) which indicates a 5 bit memory allocation for packet type. As of now, there have been 11 specified packet types, specified below.

Type of Packet	Description
None	Generic packet
Empty	Generic packet
Set up	Initiating communication
Normal Command	Various commands that the ground station can send CASTOR
Critical Command	Time critical commands yet to be specified
Telemetry Backlog	Used for down linking .csv files that contain telemetry logs
Telemetry Current	Sending current telemetry readings
Image	Sending images to ground
Code 1 2	Sending new code to PICs 1 and 2
Code 3	Sending new code to PIC 3
Debug Text	Used for debugging software

TABLE 2.4-12: PACKET TYPES WITH DESCRIPTIONS

The type of packet will contain information based on what command shall be executed on CASTOR. On top of this, the normal command packet type has specific command type designators: TYPE_ACTUATE, TYPE_GETADC, TYPE_PICDIRECT, TYPE_GET_MAGVALUE, TYPE_GET_IMU, TYPE_ACTIVATE_TORQUE_COILS, TYPE_GET_PICTURE, TYPE_READ_MEMORY, TYPE_GET_TIME, TYPE_SET_TIME, TYPE_HEATER, and TYPE_TELEMETRY_BACKLOG. These type designators specify their respective commands in CASTOR software.

Every packet consists of a 12 byte header, 2 bytes of start and end flags, a variable amount of user data, and 1 byte of error detection. Each of the fields is discussed in further detail in the following sections.

Header

The header for every packet consists of 12 bytes of identification information. The breakdown of the header is summarized below.

Field	Packet Origin	Ack Nack	Needs Ack	Packet Type	Packet Data Length
Bits	1	1	1	5	8
Description	0-CASTOR 1-HETE	0-ack 1-nack	0-no 1-yes	00000-None 00001-Empty 00010-Set up 00011-Normal Command 00100-Critical 00101-Command 00110-Tel. Backlog 00111-Tel. Current 01000-Image 01001-Code 1 2 01010-Code 3 01011-Debug Text	Bytes in user data

TABLE 2.4-13: PACKET HEADERS

ID	Time Sent	Packet Count	CRC
8	32	24	8
Packet ID	Time data collected	Absolute count of transmits	Error Detection

TABLE 2.4-14: HEADER DEFINITION

The Packet Type field identifies the packet as one of the 11 types of packets. Packets can then be specified as a type of acknowledgement packet via the ackNack field. The Needs Ack field is used for packets that must be acknowledged by the receiver to proceed with communication. The

3 byte count field is a late addition that can be used for a variety of applications, specified by the user. Other fields of the packet header are self explanatory.

User Data

The functional packets vary in user data content, which is summarized in Table 2.4.6-3.

Functional Packet	Content	Size
Set-up	Source antenna	1 byte
Set-up (empty)	Source antenna	1 byte
Set-up (normal command)	Source antenna, command code*, normal command	varies
Set-up (critical command)	Source antenna, command code*, critical command	varies
Telemetry (empty)	none	N/A
Telemetry (backlog)	State and System Health data**	225 bytes
Telemetry (backlog cutoff)	State and System Health data**	225 bytes
Telemetry (current)	State and System Health data**	225 bytes
Command (empty)	none	N/A
Command (normal command)	Command code*, normal command	varies
Command (critical command)	Command code*, critical command	varies

TABLE 2.4-15: FUNCTION PACKET CONFIGURATION

* Command code is a 1 byte identifier, see command reference list in Operations Section
**State and System Health data defined by Orbits and Operations

The Set-up packet simply indicates from which antenna the packet originated. This information will be useful in determining CASTOR's orientation and the functionality of the two communication systems. The Set-up packets also contain information for CASTOR on which antenna's packet did the ground station hear and respond to. These packets however, as well and the Command packets) can contain commands from the ground station. Each command is associated with an identification code. All the identification codes are known to CASTOR and allow it to know the size, content, and organization of the following command. A normal command packet can contain up to 25 normal code and command pairs. A critical command packet however can only contain one critical code and command. This restriction is necessary because of the additional steps required to execute a critical command. Three of the Telemetry packets contain the Sate and System Health data as defined by the Orbits and Operations team. For backlog telemetry reports, this data will have been collected twice a minute while out the ground station's range. For the current telemetry, the data will be collected when a command to do so is received. The backlog cutoff Telemetry packet indicates that it is the last packet in the packets to be sent, although not the last packet in the backlog Telemetry. Empty telemetry packets are used only as a nack. The command packets function just as the Set-up packets do, without the source antenna information.

ARQ Protocol

The CASTOR Satellite communication protocol must be able to detect faulty packets and automatically request that new packets be sent. Therefore, the communication protocol will support an ARQ (automatic repeat request) protocol based on what type of packet is being sent. A Stop and Wait ARQ shall be used when sending any type of normal command and a Selective Repeat ARQ shall be used for backlogged telemetry and image packets.

In a Stop and Wait ARQ for commands, the ground station sends a normal command to the satellite and waits to receive an ACK (acknowledgement) packet back from the satellite before issuing another command. In the event that an ACK packet is not received, the ground station shall automatically resend the command packet after a timeout window, *S*, which must be equal to or greater than the total transit time of the packet and ACK plus any time for processing. A Stop and Wait ARQ is the best choice for normal commands because the ground station must issue commands one at a time (each command is also only one packet) to CASTOR with confirmation that CASTOR has received that command.

A Selective Repeat ARQ works well for CASTOR when sending multiple packets to the ground station. In Selective Repeat, the transmitter (the satellite) sends all packets in a row. The receiver (the ground station) sends an ACK packet back to the transmitter for each packet they receive. After all packets have been sent, the transmitter selectively and automatically resends all packets that it has not received an ACK for. This works well for backlogged telemetry and images because the satellite is sending hundreds of packets. It is far more time efficient to implement a selective repeat and automatically retransmit only those packets that have not been ACK'd.

Error Detection

The Cyclic Redundancy Check, or CRC, is a hash code designed to detect unexpected changes in a packet body. It is 8 bits long and generated using a communications engineering industry standard polynomial equal to $X^8 + X^5 + X^4 + X^0$ or, written in binary, 10011001. To generate the CRC, the data stream is shifted 8 bits to the left, creating 8 zeros at the end of the data stream. The data is then divided by the polynomial. In binary, this division is equivalent to the bitwise XOR operation. At the end, the remainder, which will be 8 bits long, is the CRC.

Due to data packet structure, after the CRC is generated, it will be placed at the end of the header. The received data must be verified by using the CRC. On the receiving end, the communication protocol will receive a packet, generate the CRC in the same manner, and check to see that the CRC that was just generated matches the CRC associated with the packet. If it matches, then the data packet does not contain errors. If not, then the data is corrupted and the packet must be retransmitted.

Type of Packet	Error	Detection	Response
Set-Up	lost	Time Out	Send again
	corrupt	Fails CRC	Nack, send again

TABLE 2.4-16: SET-UP PACKET ERROR

Type of Packet	Error	Detection	Response
Set-Up (empty)	lost	Receive Set-Up again	Send again
	corrupt	Fails CRC	Nack, send again
Set-Up (normal command)	lost	Receive Set-Up again	Send again
	corrupt	Fails CRC	Nack, send again
Set-Up (critical command 1)	lost	Receive Set-Up again	Send again
	corrupt	Fails CRC	Nack, send again
Set-Up (critical command 2)	lost	No further packets after current telemetry	Send again after timeout
	corrupt	Fails CRC	Nack, send again

TABLE 2.4-17: SET-UP (GROUND STATION) ERRORS

Type of Packet	Error	Detection	Response
Telemetry (empty)	lost	No further packets received	Send again after timeout
	corrupt	Fails CRC	Nack, send again
Telemetry (backlog*)	lost	Skip in count, cutoff comes before 20 packets	Ignore if 90% received, resend chunk otherwise
	corrupt	Fails CRC	Nack, send again
Telemetry (cutoff backlog)	lost	No further packets received	Send again after timeout
	corrupt	Fails CRC	Nack, send again
Telemetry (current)	lost	No further packets received	Send again after timeout
	corrupt	Fails CRC	Nack, send again

TABLE 2.4-18: TELEMETRY PACKET ERROR

* Continue & exit designators addressed by sequence flag header field

Type of Packet	Error	Detection	Response
Command (empty)	lost	No further packets received	Send again after timeout
	corrupt	Fails CRC	Nack, send again
Command (normal command*)	lost	No further packets received	Send again after timeout
	corrupt	Fails CRC	Nack, send again
Command (critical command 1*)	lost	No further packets received	Send again after timeout
	corrupt	Fails CRC	Nack, send again
Command (critical command 2*)	lost	No further packets after current telemetry	Send again after timeout
	corrupt	Fails CRC	Nack, send again

TABLE 2.4-19: COMMAND PACKET ERRORS

* Continue & exit designators addressed by sequence flag header field

Encryption

Based on UNP recommendations, it has become necessary to add encryption to data communication. To remedy this CASTOR will be equipped with modems that support simple AES-128 encryption built in. The encryption will happen at the data link layer so no software implementation needs to be done to support the encryption.

2.4.7 GROUND STATION (M. MUNOZ)

The HETE (High Energy Transient Explorer) network was constructed by a university consortium led by MIT's Kavli Institute in order to communicate with the HETE satellite in Earth orbit. However, since the HETE satellite went silent in 2007, the network has not been carrying traffic. We have negotiated with the Kavli Institute for use of this network.

The HETE network consists of three ground stations located in Cayenne, Singapore, and Kwajalein. Since our system requires a frequency allocation license from the FCC (refer to section 2.4.8 for more information on licensing), we will only be able to use the Kwajalein station. The Kwajalein ground station is equipped with a 1.8m dish, an MHX2420 modem, and a computer.

The scheme of the ground station is showed in Figure 2.4-9:

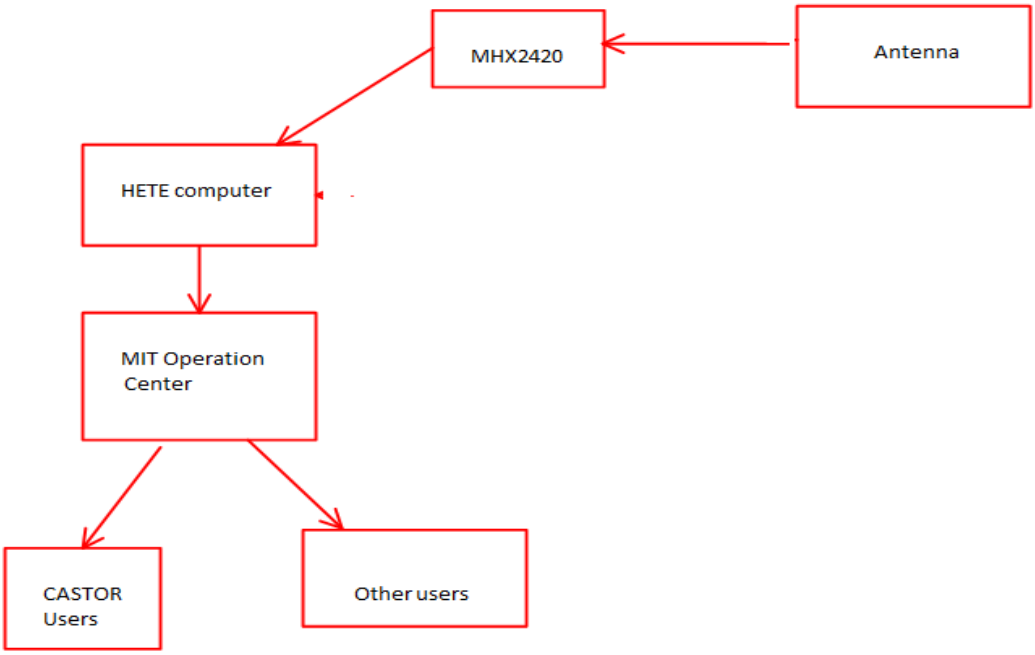

FIGURE 2.4-9: GROUND STATION BLOCK DIAGRAM

The 1.8m dish is old; hence some work will be required to upgrade the whole system. We will need to test the functionality of the dish, to connect it with our modem, and to upgrade the pointing and tracking system. The estimation of the cost for these upgrades is still to be defined, as well as when these upgrades will be implemented.

In case we are unable to obtain a license from the FCC or if something were to go wrong with the Kwajalein station, the CASTOR team is currently looking to alternative ground stations as backup solutions.

One backup solution being considered is using the GENSO ground stations. GENSO is a worldwide network of ground stations which can interact via a software standard and therefore dramatically increase the level of access to orbital satellites which in turn increases the return from educational space missions and the opportunities for sending commands to the spacecraft and receiving telemetry from it.

2.4.8 LICENSING (M. MUNOZ)

In order to be able to communicate successfully under FCC regulations, the communication system of the CASTOR satellite needs a license that will allow us to transmit and receive data at the system frequency of 2.442 GHz.

The types of licenses we had could have chosen from for CASTOR are from the following:

-experimental licenses: easy to be obtained, maximum amount of communication time of two years. The system does not have to cause interference, and it has to be able to be turned off if it is requested;

-amateur licenses: they have fewer constraints in the power and in the interference. The process is longer, but this type of license guarantees the allocation of a band as primary user. Also in this case, the system has to be designed in a way to be easily turned off, if requested.

Given the possibility of using the communication channel as primary users, the Amateur Radio License option seems to be the most appealing. Unfortunately, the fact that the flight modems are equipped with FHSS and a standard data encryption code makes it difficult for us to apply for this license. In addition to the data encryption the modems will have, they are also equipped with FHSS which is a form of spread spectrum technique that can be seen also as a sort of encryption and this is against the scope of amateur radio services. It is maybe possible to obtain a waiver, but to be sure to obtain a license the team decided to apply for an experimental license.

The application for the experimental license was submitted on Oct. 07, 2010. This is our third attempt at obtaining a license from the FCC and unlike the second time where the provided coordinates located the Kwajalein ground station in the middle of the ocean, we were able to provide all the correct information to complete the application process. Currently we are in dialogue with the FCC in order to provide them some more details that they have requested relating to the ground station. If no more issues arise, we should have an approved license in about 4 weeks.

2.4.9 FHSS (M. MUNOZ)

The issue of FHSS (Frequency Hopping Spread Spectrum technique) is emerged during the UNP PDR, where the reviewers have expressed some concerns about the FHSS scheme currently implemented in our modem. An analysis has been conducted to decide:

- If CASTOR should use the FHSS or not.
- What are the conditions for the correct functioning of the FHSS for space application?

The final decision concerning FHSS is that CASTOR will keep the modems equipped with FHSS and that it will use a data rate of 115.2kbps in order to have the modems operating correctly.

The final decision has been taken on the base of different parameters:

1) Flight heritage: the current modems equipped with FHSS have already been used in Cubesat missions successfully (example: MAST mission). Additionally, we don`t have any data about the same type of modems without the FHSS. Hence, nobody can guarantee that the elimination of the FHSS in this type of modem will affect it in a way that it will not be able to operate correctly in space. There is no apparent reason for which this can happen, but we simply don`t have any flight heritage of MHX2420 without FHSS to be able to confirm that this system will work.
2) Expert opinions: in order to deal with FHSS issue two communication experts at MIT have been contacted: Muriel Medard and Vincent Chan. They both have suggested to keep the modems with FHSS since:
    - FHSS is a good way to counteract interferences that are strong in the 2.4GHz band;
    - FHSS is already implemented in the modems ,hence the elimination of the FHSS will bring the modem to work in a suboptimal condition with poor results in terms of communication;
    - Using long hopping intervals the problem of mismatch due to propagation delay will be considerably reduced;
    - Using a communication rate high enough with respect to the Doppler shift, the frequency shifting problem will be considerably reduced.
3) UNP other teams: four of the eleven UNP teams are equipped with our same modems. Hence, they have been contacted to understand how they are dealing with this issue. The result is that they don`t have at the moment solved this issue. They are thinking about this, but probably they will keep the modems as they are.
4) Microhard experts: Microhard engineers have been contacted to analyze the possibility of changing the settings of the modems. The result is that they can eliminate the FHSS, but there is no guarantee about the behavior of the system. According to their experience, they know that modems equipped with FHSS are currently working in space. These transmitters are working fine if they are used at a data rate greater than 115.2kbps. This is due to the Doppler shift and to the fact that the receiver needs to have a band large enough to identify the shifting of the signal in order to detect it correctly.

In conclusion, the analysis has determined that the final configuration for the CASTOR modems will be:

1) MODEMS equipped with FHSS;
2) DATA RATE of 115.2kbps;
3) HOPPING INTERVAL of 150ms (maximum available).

2.4.10 RISK ANALYSIS (S. PARRA)

Risk is a serious concern to the CASTOR Communication Subsystem. The communication system must function at all times due to the sensitivity of the data stream. One huge risk

mitigation factor that we have implemented is full modem/antenna redundancy. Our risk matrix is below with analysis on a risk level associated with each risk mitigation factor.

Risk Description	Mitigation	Severity	Likelihood	Risk Level
If the new patch antenna configuration is used, before deployment there will only be one operational antenna on the outside hence there will be no redundancy. Still can communicate, but less oppurtunity to communicate	A possible solution is to put a 6dBi antenna on the outside however this would require a switch between the 2 antennas. A 3dB loss would be incurred but the link budget would remain fine.	3	0	low
System is set up to switch between antennas depending on which one provides a better communications link.	There is no way to overcome the failure of the switching mechanism, however it is safer than having no switch and no second antenna to solve the previous risk	3	3	MED
There could be interference on the communications subsystem due to other components of the satellite.	An EMI test will be performed to model and characterize the interference due to other components.	unknown	1	unknown
Plastic cover of antenna might be damaged in space which could make the antenna inside perform sub optimally.	Testing will be done at MIT Lincoln Lab on the antennas without their plastic covers to analyze their performance	1	1	low
Plastic cover of antenna might be damaged in space which could make the antenna inside perform sub optimally.	Testing will be done at MIT Lincoln Lab on the antennas without their plastic covers to analyze their performance	1	1	low
A connection between antenna, modem, or a PIC could fail.	Need to verify that the different connections between antennas, modems, and PICs are all strong and in a position where the connection cannot be lost.	3	1	low
Modem could be short-circuited.	Need to ensure that the board where the modem will be placed on is properly designed to avoid such possibilities.	3	2	MED
Both Modems could be short-circuited.	careful manufacturing & testing	4	2	MED

TABLE 2.4-20: COMM RISK ANALYSIS

2.4.11 MULTI-ANTENNA SWITCHING ALGORITHM (M. MUNOZ)

The satellite is equipped with three antennas as a mitigation strategy for antenna failure and as a means to communicate with the ground station at a larger range of attitude orientations than is available for a single antenna. Furthermore, the communication system will include an algorithm for switching between antennas while the satellite is in the deployed and controlled state. Even

though the final location of the antennas has been chosen, the algorithm to determine which antenna should be used to communicate with the ground station can be updated with antenna locations on the satellite body with little effect on the algorithm process.

The switching process is a function of the satellite attitude, the location of the ground station, and the location of the antennas on the satellite. At each time step of the switching algorithm, the direction cosine matrix relating the body axis of the satellite to the inertial reference frame is used to rotate the position of each antenna from the satellite's body axis to the Earth centered reference frame. Each of these vectors is then added to the vector from the ground station to the center of the satellite. The two resulting sums are the vectors from the ground station to each of the antennas. The magnitude of each of these vectors can be compared to determine which antenna is closed to the ground station, and therefore is not blocked by the body of the satellite. The below figure depicts the algorithm process.

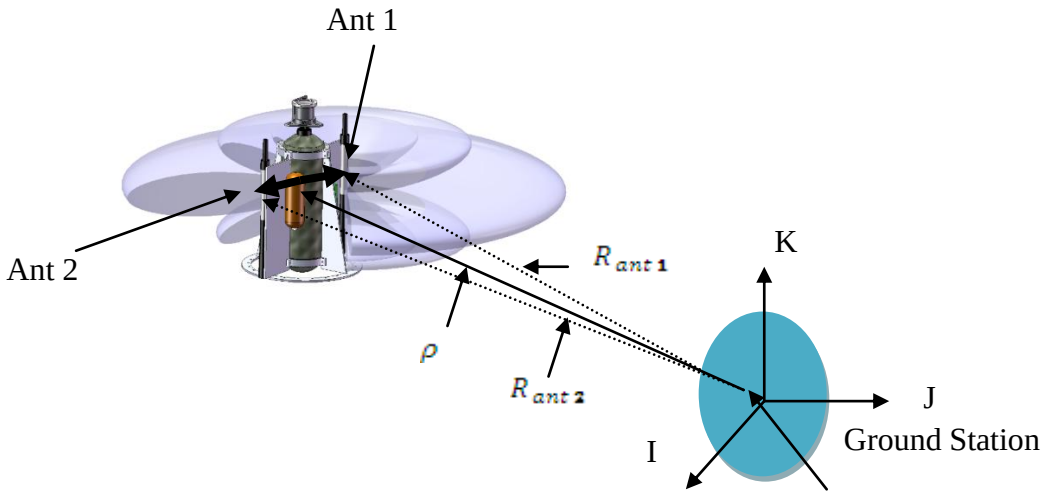

FIGURE 2.4-10: ANTENNA SWITCHING PROCESS

The vector ρ is the vector from the ground station to the satellite in the inertial frame. It is calculated by subtracting the position vector of the ground station from the position vector of the satellite in the inertial frame. The vector from Ant 1 and Ant 2 is rotated into the inertial frame using the direction cosine matrix, which is updated by the ADCS system at each cycle in the ADCS control period. The switching control period will be at a lower frequency than the ADCS control period, so an up to date direction cosine matrix will always be available. The sum of the vector ρ and the Ant 1 and Ant 2 vectors gives the vectors $R_{ant\,1}$ and $R_{ant\,2}$ respectively. Whichever of these vectors has a lesser magnitude will correspond to the antenna unobstructed by the body of the satellite, in this example Ant 1.

This algorithm must be combined with orbital propagation information provided by the GNC system in order to determine when the Earth is not obstructing the view of the ground station by the antennas. This information can be found by transforming the vector from the ground station to the satellite (represented above by ρ) into an azimuth, elevation, and range as seen from the

ground station reference frame using a known series of transformation rotations. If the elevation is above an acceptable range (usually 10 degrees) the satellite is within line of sight of the ground station and can communicate using the antenna that is unobstructed by the body of the satellite.

The algorithm is fairly robust to angular rates on the satellite body. According to Matlab simulation of the attitude of the satellite with applied control and disturbance torques, the antenna switching algorithm could have a frequency as low as 0.1 Hz or one cycle per ten seconds and will calculate approximately 95% of the antenna switches required to maximize communication opportunities. Furthermore, the algorithm is robust to position error because the same position vector is added to both antenna vectors in order to calculate the distance between each antenna and the ground station. If the position vector has error, it will be the same for both calculations.

When the satellite is in a tumbling state, the algorithm will be turned off and instead all modems/antennas will be turned on and allowed to transmit. The purpose of this is to provide better coverage during the period when the satellite's orientation can't be controlled. The communications team believes that during tumbling mode, the switching algorithm will not be able to effectively change between antennas especially if the satellite has a high rotation rate. Consultation with the power team is still necessary at this point in order to determine if they can provide us the necessary power (about 8 watts) to have both modems 3 antennas working at the same time.

Lastly, when the satellite is in the stowed configuration, the algorithm will also be turned off and only the top and bottom patch antennas will be functioning. This is because the solar panels when in the stowed configuration block the interior patch antenna and dramatically reduce its ability to transmit and receive data and commands.

2.4.12 COMMUNICATION TESTING (M. MUNOZ, S. PARRA)

FlatSat Testing

The purpose of the FlatSat test is threefold. First of all, we want to test system hardware by simulating a complete packet transmission from the ground station to the satellite. This includes modems, avionics hardware, antennas, and PCB/proto-board setups. Secondly, we want to ensure that the communication protocol and software is functioning as expected. This also includes hardware/software integration. Lastly, this test is helpful for new communications subsystem members to get familiar with the CASTOR communication subsystem, the FlatSat testing environment, and the communication subsystem hardware and software layout.

The simulated ground station/satellite setup shall be as closely related to that described in the Communication Subsystem Overview (2.4.2) as possible. For FlatSat testing, we will demonstrate the capability to communicate a command packet to the satellite and visibly view the command being interpreted by watching a linear actuator physically move. The MIT ground station GUI has capabilities to initiate communication. The user specifies FlatSat/Actuator test and inputs 2 arguments. Input 1 describes which actuator to use, in this specific case, the

command is for the Linear Actuator, so a 1 is inputted. Input 2 describes the percentage extension the user was the actuator to move. For power and reliability reasons, this number should be an element of (0,100) exclusive.

The successful demonstration of the test shows that the communication system is integrated with avionics and that our hardware and software is correctly functioning. Below are further scheduled tests and their status.

Type of Test	Description	Status
Linear Actuator	Show that the ground station can send a linear actuator command to CASTOR	Code complete, test verified
CRC	Show that the CRC is fully implemented and properly functioning	Code complete, test verified
Magnetometer Sensing	Show that we can correctly read data from the magnetometer	Code complete, test verified
Temperature Sensor	Show that we can accurately read temperature data	Code complete, test verified
Camera Imaging	Show that the camera is fully integrated and CASTOR is able to send camera images to the Ground Station.	Code complete, test verified
Automatic Repeat Requests	Show that functionality exists for losing packets for files requiring segmentation	Code complete, test verified

ARQ Protocol Testing

Overall Goal and Objective: To demonstrate functionality of the ARQ protocol for image retransmission. Based on requirements, the communication protocol must be able to automatically detect packet errors and be able to automatically request new packets be sent. The automatic repeat request for images and telemetry shall work by using the ground station to detect failed packets and automatically send a single packet to the satellite requesting failed packets be resent.

Setup: The test shall occur at the avionics and communications bench in the SSL using the flatsat format. After complete implementation of software support, we shall simulate an image command followed by downlink of that image. The ground station shall then purposefully lose some packets which will then result in a check list for failed packets to populate on the ground station. Once the entire image has been downlinked to ground, the ground station shall then automatically send a request for those specific packets to be resent back to ground.

Expected Results: Since we are specifying what specific packets will be lost, we expect the retransmit list to be populated with the exact packets specified on the ground station. We then expect this message to be received on the satellite followed by an acknowledgement back to

ground, as all commands to the satellite shall be acknowledged by the satellite. After this, the satellite should read the image specified by an image id off the SD card and retransmit lost packets back to the ground station.

Actual Results: Screen shot below of flatsat testing

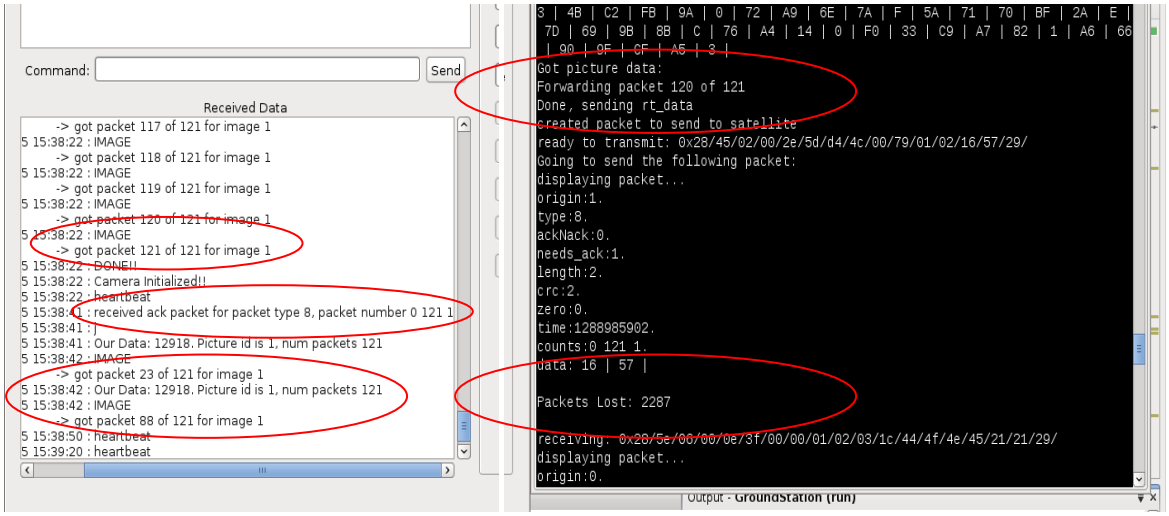

FIGURE 11: FLATSAT TESTING SCREENSHOT

The GUI above depicts ground station operations. The left side of the figure shows this ground station GUI while the right figure shows the “under the hood” operations of the ground station, displaying technical data such as hexadecimal packet interpretations and any print statements made through the C code. We can see that this test was successful by analyzing the packet flow from the screen.

On the right, we notice that the ground station has finished receiving packet data, and will now send retransmission data to the satellite (top red circle). Further below, the packet has been sent to the satellite with the requested information, and we notice that the data sent contains two packets, packet number 22 and packet number 87. It is important to note that these two numbers show incremental values based on C arrays, meaning that the first packet is labeled packet 0. When actual data is being sent back to the ground station, these numbers become incremented by one to show that packet numbers begin with packet 1, as shown on the ground station GUI.

The GUI shows packets being sent to the ground station from the satellite. We see that the ground station received all packets from the satellite. Then, the retransmit data is automatically sent and we receive an acknowledgement packet showing that that retransmit data command has been received. The satellite now sends the image packets again corresponding to the correct image id and the correct packet numbers.

The test shows that we have successfully sent an automatic repeat request to the satellite, and the satellite has resent the specified packets without any prompt from the user.

Antenna Testing

In order to determine how well the custom patch antenna will perform on the satellite, it is necessary to test their functionality. The communication team wrote a comprehensive test plan that seeks to determine the gain and radiation pattern of the patch antenna. This test will consist of three different test scenarios. The first test will consist of testing the patch antenna isolated from the satellite structure. The 2nd test will consist of the patch antenna installed on the interior of one of the deployable solar panels. The other test scenario will consist of the patch antenna located near the thruster and in the same axial direction as the thruster. The last two tests are geared towards determining the effects the satellite structure has on antenna performance. The first test will be done on Nov. 23rd at the MIT Lincoln Lab. The test will be performed in the tapered chamber found at the lab. First the antenna under test (AUT) is set on some sort of rotator at the "box" end of the chamber. The transmit signal is launched from the tip of the "cone" end, and is basically guided to the AUT by the wedge absorber lining the cone. The AUT receives the transmitted signal. Any energy "splattered" off the mechanical portions of the test setup (non-receiving portions of antenna, the mount, the pedestal, etc.) is attenuated by the pyramidal absorber lining the box end. The signal received by the AUT is converted to a frequency through a mixer, and the level is recorded by the receiver. This will be done for every 1 degree angle for which the antenna was rotated for a total of 360 degrees. Furthermore, the test will run for 10 frequencies between 2.4 and 2.5 GHz. The Frequency step will be .01 GHz.

In addition, the 8dBi patch antennas that were previously going to be used in the design will also be tested. They recently underwent vibration testing so we want to verify that their gain and radiation pattern were unaffected by the vibration tests. If these antennas still function adequately we will consider them as a viable alternative in case the custom antennas do not work.

Splitter Testing

The Power splitter is connected to the modem and to two of the custom antennas. Its purpose is to split the transmission power into two parts, one part for each antenna. We need to test the splitter to make sure that it is functioning correctly. We plan on testing the splitter by connecting it to a vector network analyzer and measuring the S-parameters of the splitter. The port connected to the modem is called port 1 and the other ports connected to antenna 1 and 2 are called port2 and 3 respectively. In order to determine that the splitter is functioning correctly, the S11 measurement should be a large negative decibel value. Ports 2 and 3 should see a 3 dB loss when signal is passed through them. In other words, the S12 and S13 parameters should see a 3 dB power loss from the input signal. Any deviation from the expected measurements described above signifies the splitter is not functioning.

2.4.13 CONCLUSION AND FUTURE WORK (S. PARRA)

The current CASTOR Communication Subsystem nearly meets all requirements as outlined in 2.4.1. We have successfully demonstrated the capability of data transmission from the ground station to the satellite through the FlatSat testing environment in the SSL. However, more work still needs to be done with regards to specific packet transmissions, command interpretation, and satellite telemetry. The timeframe for these tasks varies from the end of the fall term to the end of the spring term. On the hardware side, further antenna design and testing needs to be done. Licensing is near completion and needs to be finalized. Furthermore, along with software implementation, hardware integration, and testing, work needs to be done on finalizing ground station operations.

2.5 PROPULSION

2.5.1 INTRODUCTION (J. PARHAM)

For the mechanical design section, the hardware, testing, and technical analysis for the propulsion system will be detailed. Additionally, mission operations and their requirements for the propulsion system will be covered. It includes a general overview of the system and details on thruster efficiency testing, operational procedure. It also follows up with future work and analysis to be completed as pertains to the NASA Xenon gas feed system and the plumbing system of the Castor satellite that will be finalized and tested in the coming months.

2.5.2 OVERVIEW (K. LOEBNER)

The propulsion system onboard CASTOR will use electric propulsion to propel the small satellite. The system consists of the xenon propellant feed system, associated plumbing and pressure vessel, and the Diverging Cusped Field Thruster (DCFT). Using the DCFT as its primary propulsion system, CASTOR must operate throughout the mission lifetime of 1500 hours. Hence, the propulsion system must likewise be operable for the same amount of time so that on-orbit performance, efficiency, and degradation of the DCFT can be measured and compared to thrusters of similar technologies and power levels. Those metrics will be measured on-orbit by tracking the state of the spacecraft and thruster during the mission. Data on the orbital path of CASTOR after repeated firings will allow performance and efficiency to be determined, and the rate of degradation will be measured using the change in those metrics. The duties of the Propulsion team are to design a system to properly deliver xenon to the thruster, to determine the operating point for the DCFT that will permit optimal performance while ensuring maximally efficient use of xenon propellant, as well as perform all integration tests necessary to ensure all components perform as expected in their final configurations.

TABLE 2.5-1: PROPULSION BUDGET

Component	Mass	Nominal Power	Cost
DCFT	1.20 kg	88 W	$3500
Xenon Tank	2.95 kg	N/A	$836
Cathode	1.10 kg	(Included in DCFT)	$6000
Plumbing	5.064 kg	1 W	$1498
Xenon Gas (Fuel)	5.90 kg	N/A	$29,500
Total	16.214 kg	101 W	$41,334

2.5.3 RELEVENT SYSTEM REQUIREMENTS

1. The propulsion system shall be able to operate for 1500 hours as stated in mission requirements
2. The thruster/cathode system shall be fully insulated electrically from the rest of the system
3. The thruster/cathode system shall be far enough from other systems so they are not damaged by the thruster. (this requires that the plume emitted by the thruster does not contact any surface. The plume shape will be determined through testing.)

2.5.4 DIVERGING CUSPED FIELD THRUSTER

ANALYSIS

The thruster used on the CASTOR satellite is the Diverging Cusped Field Thruster. The thruster is based on a design by D. Courtney. It was built in-house and requires a minimum of 40W to provide approximately 5mN of thrust to the satellite when operating. The engine functions using the principle of electrostatic ion propulsion, in which an electrically charged plasma is accelerated by an electromagnetic field. The plasma in this case is made from Xenon ions, and the electric potential is created across the anode and cathode while a cusped magnetic field is created by a set of three permanent magnets in the thruster cone. Xenon is ionized in the cathode, and the resulting free electrons flow towards the anode and are caught in the magnetic field. Neutral Xenon atoms are pumped from the anode and then ionized by the trapped electrons, and the resulting Xenon ions are accelerated by the electric field out of the thruster cone, producing thrust. The thruster itself consists of two main components: the BHC-1500 hollow cathode and the thruster cone, which contains the anode.

While in sunlight, the DCFT will be provided 88 W to produce an expected thrust of 5.3 mN at an I_{sp} of about 700s and an efficiency of 25%. These numbers are tentative and will be solidified after efficiency testing and analysis has been performed. During eclipse, Xenon flow to the anode and cathode will be shut off. The power to the anode will be turned off as well, and to prevent the need for cathode reconditioning when re-entering the sunlight period, 36 W will be supplied to the engine's heater to keep the cathode hot and allow for a rapid restart upon reentering sunlight.

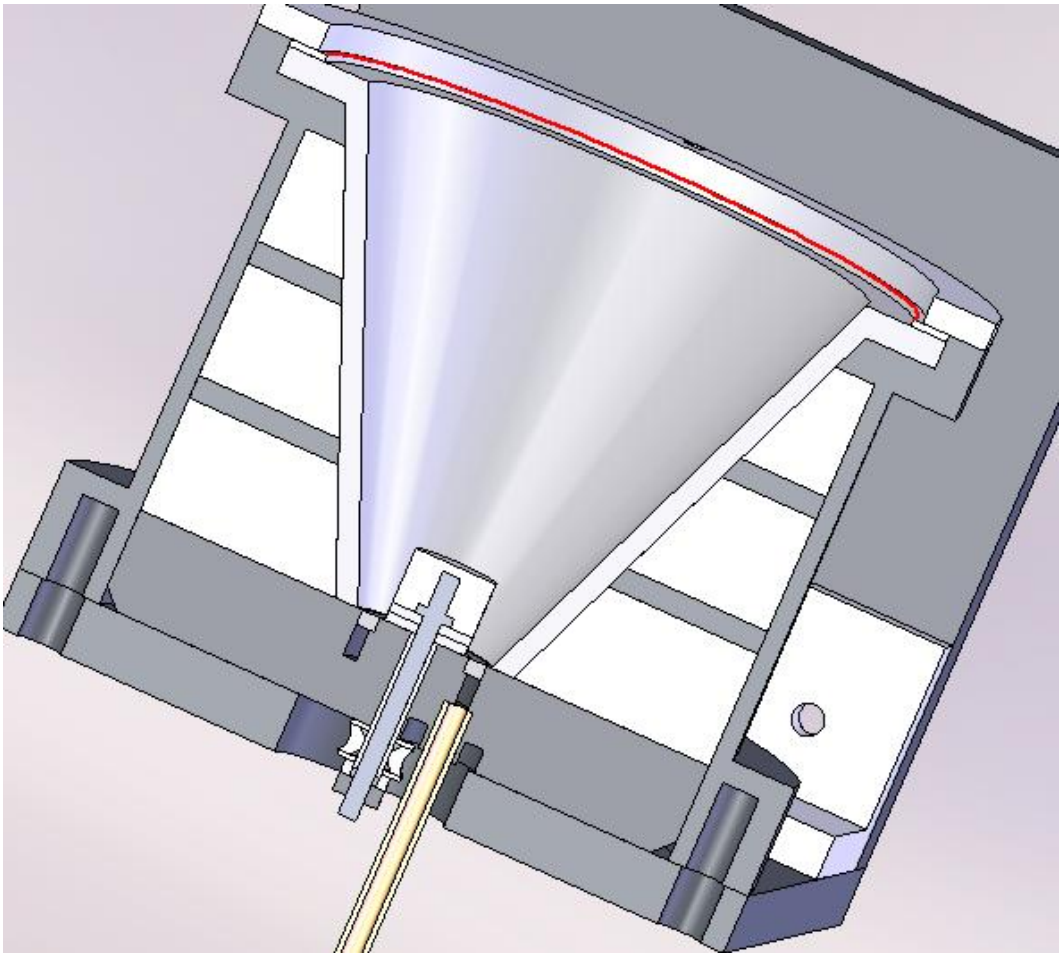

FIGURE 2.5-1: SOLIDWORKS DESIGN OF THRUSTER

Rocket Propulsion Elements, 7th Edition (Sutton and Biblarz, Chapter 19) contains the necessary equations to determine the properties of the thruster based on our chosen ΔV. Relevant equations for electric propulsion are:

$$\frac{m_f}{m_o} = e^{-\Delta\frac{v}{c}} \qquad \text{Eq. 1}$$

$$c = I_{sp} g \qquad \text{Eq. 2}$$

$$\frac{m_p}{m_o} = \frac{(m_o - m_f)}{m_o} \qquad \text{Eq. 3}$$

$$P = \frac{I_{sp} T g}{2 * \eta} \qquad \text{Eq. 4}$$

$$F = ma \qquad \text{Eq. 5}$$

$$\Delta v = at \qquad \text{Eq. 6}$$

Where Δv is the difference in velocity of the two circular orbits and gives the change in velocity necessary for an electric propulsion spiral transfer orbit.

m_f is the final mass of the system

m_o is the initial mass of the system

m_p is the mass of the propellant

c is the effective exhaust velocity

P is the power required

I_{sp} is the specific impulse of the thruster

T is the thrust produced

g is the gravitational constant for the earth

η is the propulsive efficiency

1500 hours of firing time will achieve an approximate velocity change of 1000m/s and will require 5.9kg of 99.999% purity Xenon to fuel the thruster.

2.5.5 TESTING

Operational testing, as well as preliminary integrated power system testing, has been performed on the thruster. Both tests were successful and provided valuable information about the operation of the engine. Future testing will focus on the characterization of the engine using a thrust balance. Engine performance will be measured for the power ranges of 40-300W and the flow rate ranges of 4-12 standard cubic centimeters per minute. The thrust balance will measure the thrust, from which the I_{sp} and efficiency can be determined. Plots graphing efficiency, I_{sp}, thrust, power, and flow rate against each other will be created from this testing, and the results will determine the maximum efficiency of the DCFT.

THRUST BALANCE CALIBRATION

Prior to performing the DCFT efficiency testing, the thrust balance must be calibrated. Calibration is required to form a relationship between the output of the thrust balance and the actual thrust produced. The thrust balance uses voice coils placed at the bottom stand of the thrust balance to measure the amount of thrust produced by the engine. When the DCFT produces thrust, the voice coils produce an opposite and equal force, keeping the thrust balance in equilibrium. The voltage required to produce the requisite restoring force is measured using a specially designed LabView program, and then converted into a force using the data obtained during calibration. This resultant force is the thrust value.

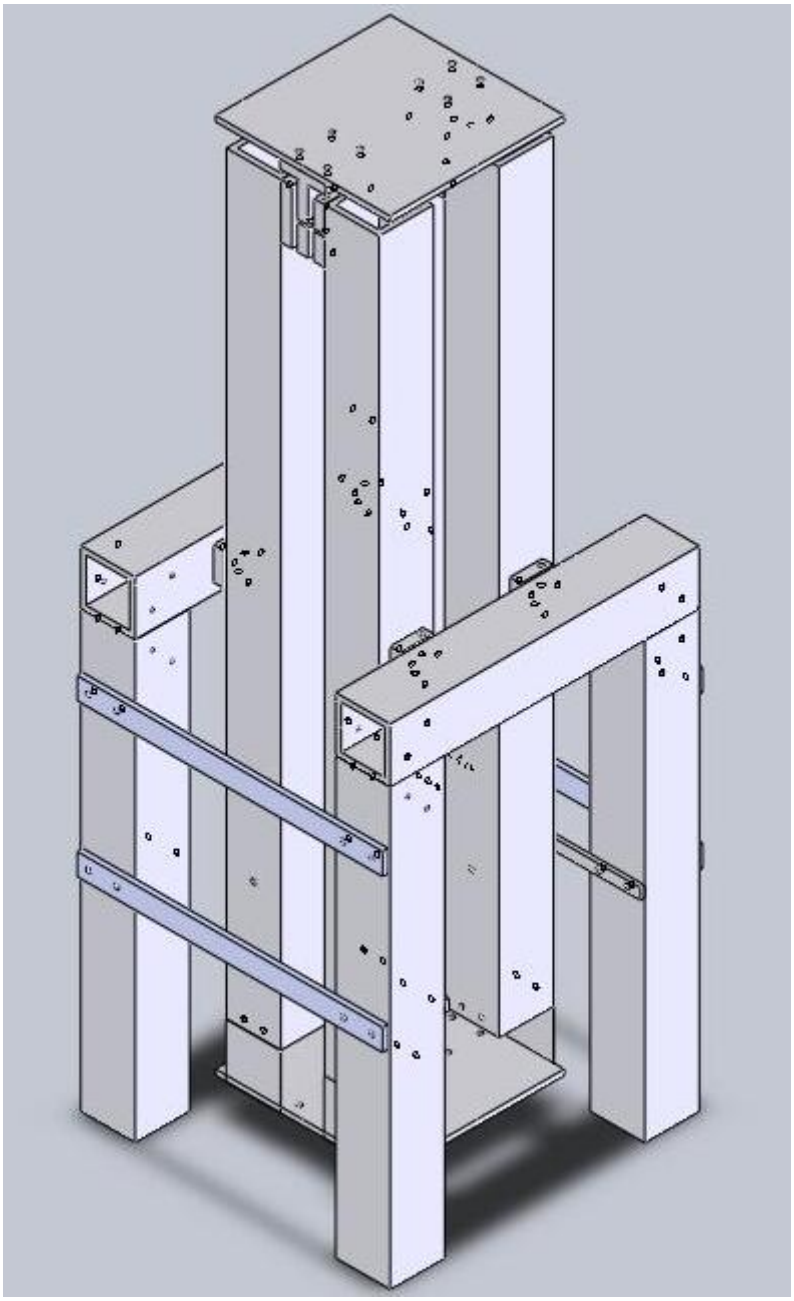

FIGURE 2.5-2: THRUST BALANCE

DCFT EFFICIENCY TESTING PROCEDURE

Cathode Conditioning

The DCFT's cathode must be conditioned to cleanse the engine of any debris or contamination prior to firing.

1. Connect PPU to power supply

2. Connect PPU to anode and cathode of engine
3. Turn on power supply
4. Turn cathode heater on to 2A @ 2V for 90 min (4W) with PPU
5. Increase heater amperage to 4A @ 4V for 90 min (16W) with PPU
6. Increase heater amperage to 6A @ 6V for 60 min (36W) with PPU
7. Increase heater amperage to 6.5V @ 7V for 30 min (45.5W) with PPU
8. Turn on keeper with PPU

DCFT Efficiency Testing Procedure

1. Perform cathode conditioning
2. Ignite thruster
3. Set Xenon flow rate
4. Incrementally adjust power between 40 and 300W, taking thrust measurements at each increment
5. Increment flow rate
6. Perform another power sweep between 40 and 300W, once again taking thrust measurements at each increment
7. Repeat process until all flow rates between 4 and 12 sccm have been tested

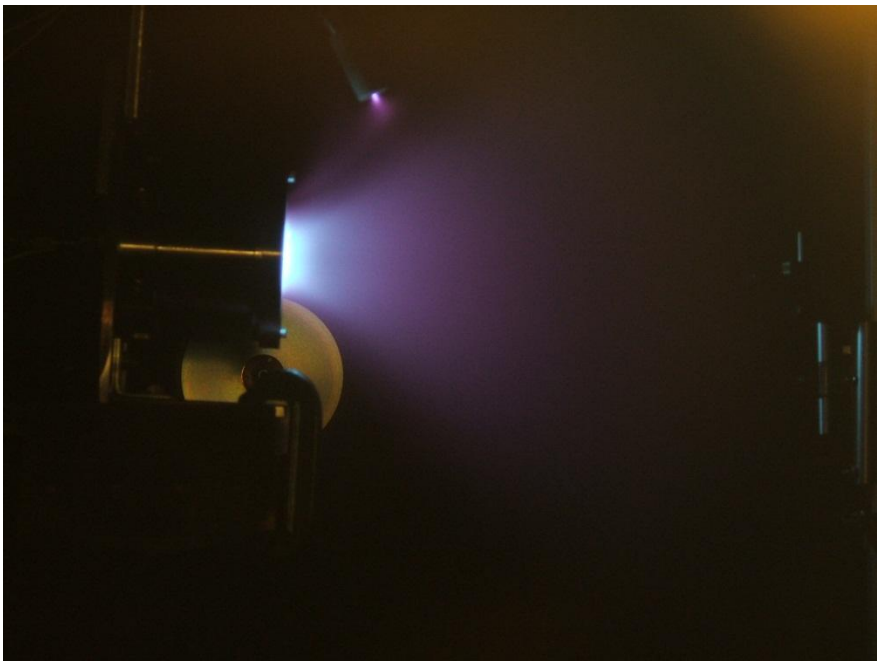

FIGURE 2.5-3: ENGINE TESTING

After data at each power level and each flow rate has been collected, analysis will begin. Analysis will be done using a spreadsheet specifically designed to calculate the efficiency of the thruster at different power levels and different flow rates given the data output by the data collection software written using LabView. The important values on the spreadsheet include the power, flow rate, and thrust, and by inserting different values for power and flow rate, we can determine an efficiency level. The main equation is:

$$\eta = \frac{F^2}{2P\dot{m}}$$

η is efficiency

F is thrust

P is power

$\dot{m}$ is fuel mass flow

Using the force produced by the thruster (calculated using the thrust balance), the power put into the thruster, and the fuel mass flow rate set, the efficiency of the DCFT can be determined. Because sets of data at different combinations of power levels and fuel mass flow rates, a plot of efficiency at various levels can be plotted, and the maximum efficiency of the thruster can be determined.

2.5.6 CATHODE

ANALYSIS

The cathode used for the thruster is the BHC-1500 Hollow Cathode, manufactured by Busek. This is the same cathode that has been used during testing. This cathode has also been flown in space and has proven its functionality on orbit. The cathode costs approximately $6000 and will be purchased as a single unit. It will be mounted to the thruster mounting plate at a distance from the thruster to be determined from characterization testing. There is little risk with the use of this cathode as it will be purchased off the shelf and has been proven to operate with the DCFT.

RISKS

There are significant risks if the cathode is improperly used. The cathode is a fragile piece of equipment and can be easily contaminated if conditioned or operated incorrectly. It is imperative that the operation procedures detailed in Section 1.1.10.4 are followed without deviation.

2.5.7 TANK, XENON, AND PLUMBING SYSTEM (K. CHOU)

RELEVANT SYSTEM REQUIREMENTS

1. The plumbing system shall safely transfer Xenon gas from the tank to the thruster.
2. There shall be a procedure for cleaning the plumbing system prior to launch so that there is no contamination with the Xenon.
3. The plumbing system shall have safety valves to prevent a pressure build-up capable of bursting the system

PLUMBING SYSTEM DESIGN, ANALYSIS, AND COST

The plumbing system will transfer Xenon gas from the tank to the anode and cathode while CASTOR is in the sunlight portion of its mission. A schematic of the plumbing system is shown below in Figure 2.5-4. The system consists of the tank, a pressure regulator, and multiple safety valves to ensure proper operation.

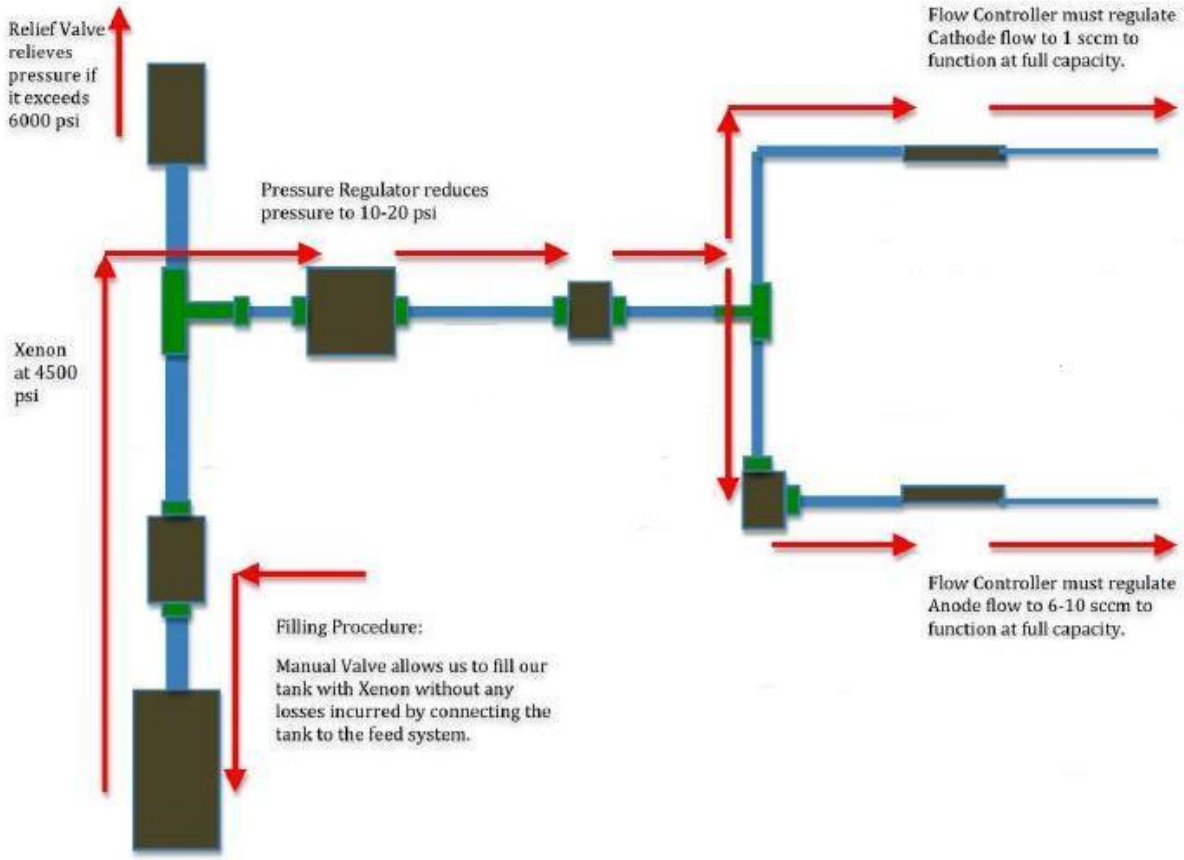

FIGURE 2.5-4: PLUMBING SYSTEM CONFIGURATION

A fill valve (not pictured) will be used to fill the tank with Xenon. Prior to launch, it will also be used to decontaminate the plumbing system of any air by flushing air out of the system with a cheap, nonreactive gas, such as Argon. The plumbing system components on the low-pressure side and to the left of the solenoid valves will be decontaminated during the heating process necessary for cathode conditioning. The Xenon on the high-pressure side will be at 1800psi. A pressure relief valve set at 6000psi is also located on the high-pressure side and will be used to bleed out excess pressure to prevent the tank or plumbing system from bursting. Once the system's pressure is within operable conditions, the relief valve will reseal so that Xenon is not drained into space unnecessarily. The GO pressure regulator will reduce the pressure to about 15psi, the operational pressure on the low-pressure side, and the flow controller will reduce the flow to the proper flow rate for the cathode and anode. The cathode's flow rate will be one standard cubic centimeter per minute (sccm). We are currently looking into decreasing the flow rate to the cathode, which would increase the DCFT's efficiency, as can be seen by the equation:

$$\eta = \frac{F^2}{2P\dot{m}}$$

η is efficiency

F is thrust

P is power

$\dot{m}$ is fuel mass flow

The flow rate to the anode is expected to be in the range of 4 sccm to 12 sccm, based on previous testing. The piping for the plumbing system will be 1/8" and 1/4" stainless steel tubing. The estimated cost and mass of the plumbing system are $1833.34 and 4.51kg respectively. Table 2.5-2 breaks down the plumbing system into its individual components, including the tank

TABLE 2.5-2: PLUMBING SYSTEM COMPONENT LIST

PART	COMPANY	PRODUCT	MASS [kg]	COST [USD]
Tank	Luxfor	L45J	2.95	350
Stainless Tube	McMaster	SS316 Tube	0.1	23.84
Pressure Regulator	GO Regulator	CPR-1	0.5	280
Solenoid Valves	ASCO	AL1124LOS	0.038	50
Relief Valve	Swagelok	SS-4R3A	0.216	144.50
Flow Control	Omega	FMA3204ST	0.2	935
Manuel Valve	McMaster	7833K95	0.51	50

TANK AND TANK ADAPTER

The cylindrical tank will hold 5.2kg of Xenon to achieve mission requirements, although it is capable of holding up to 7.7kg. The tank costs $350, has a mass of 2.95kg, and has dimensions of 46.8cm in length and 13.9cm in diameter. The cost of Xenon is $5000 per kilogram, and the company from whom we purchase the Xenon will also perform the tank filling procedure.

The current plumbing system connection to the tank consists of two individual pieces: a mating adapter and a tubing connector. To create a simpler and more reliable configuration, a solid part was deemed necessary.

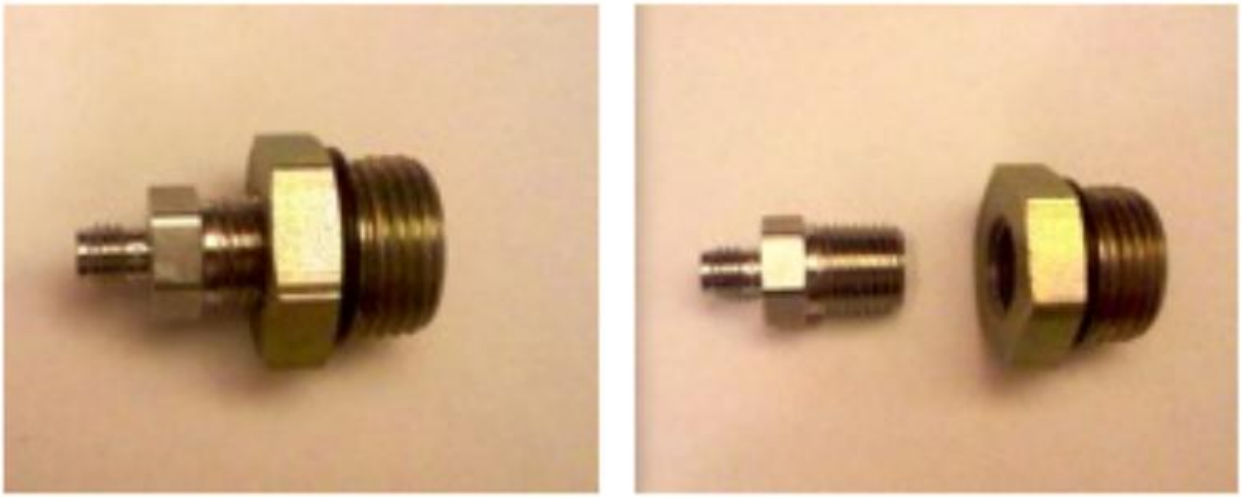

FIGURE 2.5-4: PREVIOUS TANK CONNECTOR ASSEMBLY

The initial design (see Figure 2.5-4) was built from off-the-shelf Swagelok connectors. The main piece was a stainless steel 1/16” duct that threaded into a 1/4" fitting, which funneled gas from the tank to the tubing system. The second piece was an adapter that fit the 1/2" tank opening to the main piece. These two pieces tightened together, protruding 1 1/4" from the mouth of the tank, and expelled gas axially.

The profile of the assembly was constrained by the way the tubing could connect the flow between the tank and piping because the tubing had to be routed so that the flow could exit normally to the plane of the assembly orifice. Another problem with the initial design was that there was an extra seal, or point of failure, between the two pieces.

To remedy the problems presented, the pieces were merged into one part, preserving the functionality of the original assembly. As seen in Figure 2.5-5, the projection of the tank adapter is now less than one inch, and the tubing is redirected at a 90º from the axial direction. The new design introduces the ability to turn the flow off sooner without any bent tubing or adapters. A feature that carried over to the new design includes the hexagonal molds for ease of tightening. Also, the small diffuser at the exit of the tank adapter prevents instabilities from forming in a sudden expansion to the tubing size.

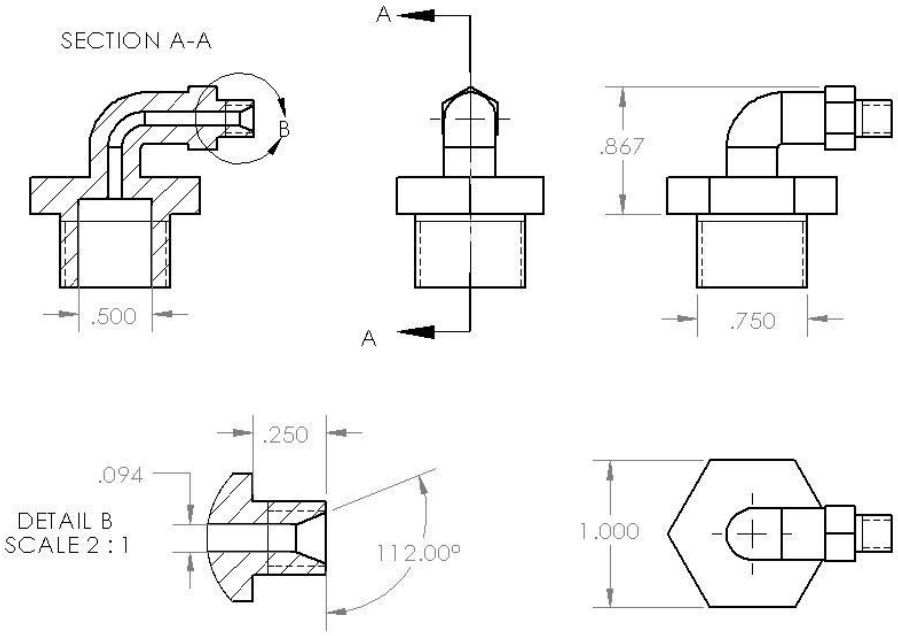

FIGURE 2.5-5: CUSTOM TANK ADAPTER

2.5.8 OPERATIONAL PROCEDURE (T. HERY)

THRUSTER OPERATING POINT

The thruster depends on several variables to determine its thrust, efficiency, and I_{sp}. From these characteristics, the amount of Xenon required, flight time, and power required from the solar panels and batteries can be calculated. Although many of the thruster's characteristics, such as thrust for a specific power input, have not been tested in the vacuum chamber yet, the following is the Propulsion team's best estimate of the engine operating point.

The driving factor in determining the thruster operating point is available power. According to UNP requirements, the volume of the satellite is limited to a 50 x 50 x 60 cm box, which limits the size of the solar arrays. With the current design, the satellite will have 0.278 m^2 of solar cell area, which can generate up to 165 W of power. After including inefficiencies in the EPS system, 100 W will be delivered to the PPU, which powers the cathode keeper and the anode.

SUNLIGHT

The operation of the DCFT during eclipse will provide thrust to the CASTOR satellite. It is expected that 10 W will be provided to the PPU during sunlight, which will deliver 88 W to the thruster to produce an expected 6.1 mN of thrust at an I_{sp} of about 920 s and an efficiency of 27%. These numbers are based on previous performed tests and are expected to improve with thruster optimization. Due to the solar panels being fixed on the body, there will be some times during sunlight when the engine will not be able to fire. This will be considered part of eclipse operations.

ECLIPSE

During eclipse (and the non-firing portions of sunlight) the Xenon flow to the anode and cathode will be shut off. The power to the anode will be shut off and the cathode will go into a heating state using the heater. The keeper will be shut off and 36 W will be delivered to the heater so that the cathode remains hot and is ready for a quick start the next time the satellite enters sunlight.

ALTERNATIVE OPERATING POINTS

The motivation for keeping the engine hot during eclipse derives from engine fatigue. Both the anode and cathode have parts that will degrade with time, and the degradation is accelerated by the voltage and current spikes associated with starts and stops, as well as heat cycling associated with cooling and reheating the thruster cone and cathode. To keep the cathode hot, the heater will be run on battery power during eclipse.

The current design uses 36 W during eclipse to keep the cathode hot. There is a possibility that the keeper can be left on instead of the heater during eclipse which requires only 12 W as opposed to 36 W. There is also the possibility of using the heater at a lower power. Both of these options will be investigated during the thruster efficiency testing.

These two alternative points for eclipse operation first need to be tested before they are considered viable options. Using the keeper during eclipse requires using Xenon which reduces the overall mission I_{sp} or requires additional Xenon mass. The lower power heater operation may damage the cathode due to thermal cycling. Requiring less power during eclipse is considered a priority and will be tested as soon as possible.

NORMAL THRUSTING CYCLE

This process describes the steps taken in the lab to start the thruster from a cold initial sate. By heating the thruster during eclipse, the first two heating steps are not needed in a typical orbit.

1. Turn heater on to 3.5 A @ 3.5 V for 15 min (12.25 W).
2. Increase heater current to 7.0 A @ 7 V for 15 min (49 W).
3. Turn cathode keeper on. The converter should automatically go to 0.5 A @ 24 V (12 W).
4. After 5 min, reduce the current to the cathode heater to 0 A in 30-second steps of 2A.
5. Then turn anode converter on. The voltage should go straight to 200 V @ 0.5-1 A (120 W).
6. Keep the cathode keeper and anode converter on, and the thruster should provide thrust.
7. To shut down, turn cathode keeper and anode converter off.

CATHODE CONDITIONING

Cathode conditioning is a one-time event that must take place right after launch, to cleanse the cathode of any debris or contamination.

1. Turn cathode heater on to 2 A @ 2 V for 90 min (4 W).
2. Increase heater amperage to 4 A @ 4 V for 90 min (16 W).
3. Increase heater amperage to 6 A @ 6 V for 60 min (36 W).
4. Increase heater amperage to 6.5 A @ 7 V for 30 min (45.5 W).

Note: All cathode heater voltages are based on experimental results.

LEO requires a special conditioning procedure because the orbital period is only 90 minutes, with a typical eclipse of around 36 minutes. To complete the cathode conditioning in LEO, power from the solar panels will heat the cathode while in sunlight and stored power from the batteries will heat the cathode in eclipse. This way, the conditioning will not be interrupted by eclipse.

PLUMBING OPERATION

DECONTAMINATION

The main risks associated with the plumbing system are inadequate decontamination and procedures before launch and leaking during the mission. Decontamination will occur before the filling of the tank from the high pressure side to the solenoid valves and will occur on orbit for the low pressure side after the solenoid valves. Decontamination requires creating a vacuum from the tank to the solenoid valves (while the first is closed and the second opened) and then pumping Xenon into the system until the desired fuel mass is reached. Once on orbit, both solenoid valves will be opened and 1 sccm of Xenon will flow through the system for 30 minutes before the conditioning procedure begins.

NORMAL OPERATION

During normal operation, the majority of the plumbing system components are mechanically set and do not require inputs to operate. The exceptions are the solenoid valves and flow controllers. The 1st solenoid valve will remain closed from launch until decontamination and will remain open during the sunlight portions of the mission and closed during the eclipse portions. The second solenoid valve will remain open until decontamination. It will close during decontamination and conditioning and then will remain open for the remainder of the mission. The flow controllers will operate only when the thruster is firing (as well as conditioning for the cathode flow controller). They will be shut off during eclipse.

2.6 POWER

2.6.1 OVERVIEW (M. HABIB)

The Power System is responsible for producing and storing power for the CASTOR bus and DCFT. An array consisting of four solar panels will capture solar energy and using a Maximum Power Point Tracker (MPPT) a maximum power of 165.1W will be produced in the sunlight. 20 Nickel Cadmium (NiCd) batteries will be responsible for storing energy on the spacecraft to be used for powering the satellite during all eclipse. Voltage converters will be used to convert the voltage from the bus voltage to specific voltages required by components.

Nickel Cadmium Batteries

CASTOR will use 20 Nickel Cadmium (NiCd) [1] battery cells connected in series. The batteries are required to power all the necessary sub-systems for CASTOR as well as the Cathode keeper during eclipse. The NiCd battery cells are rated for 4.5Ah with a nominal voltage of 1.2V. 20 cells are used to create a bus voltage of 24V for the satellite. This leads to a total battery mass of 2.64kg.

Battery Box

In compliance with UNP-6 guidelines, the battery cells are contained in an aluminum box [2] in a 7-6-7 egg crate configuration. The battery box is necessary to protect the battery cells, contain

any electrolyte leakage (if it occurs in flight which is highly unlikely), and regulate the temperature of the battery cells both by insulating them and providing a radioactive surface.

MPPT

A Maximum Power Point Tracker (MPPT) [3] is used to maximize the amount of power absorbed by the solar cells and to distribute the power to both the battery and the satellite loads. The MPPT used by CASTOR is the SunSaver MPPT designed by Morningstar Corporation. The output voltage of the MPPT is 24V. Battery charging is not controlled or regulated by the MPPT; that functionality is left to a separate battery charging circuit incorporated between the MPPT and the battery.

Battery Charging Circuit (D. Ainge)

The battery charging circuitry is responsible for safely charging and discharging the batteries. To do this, the circuit must provide the batteries with a constant current and sufficient voltage. Based on the expected depth of discharge during normal operations, the CASTOR charging circuit must provide 2A and 30V to the cells. Unlike terrestrial chargers, the onboard charging circuit must be extremely efficient to avoid unacceptable power loses. After researching both analog and integrated ways to accomplish this, the power team decided on an analog circuit because of its extremely low power consumption. The platform circuit chosen is shown below.

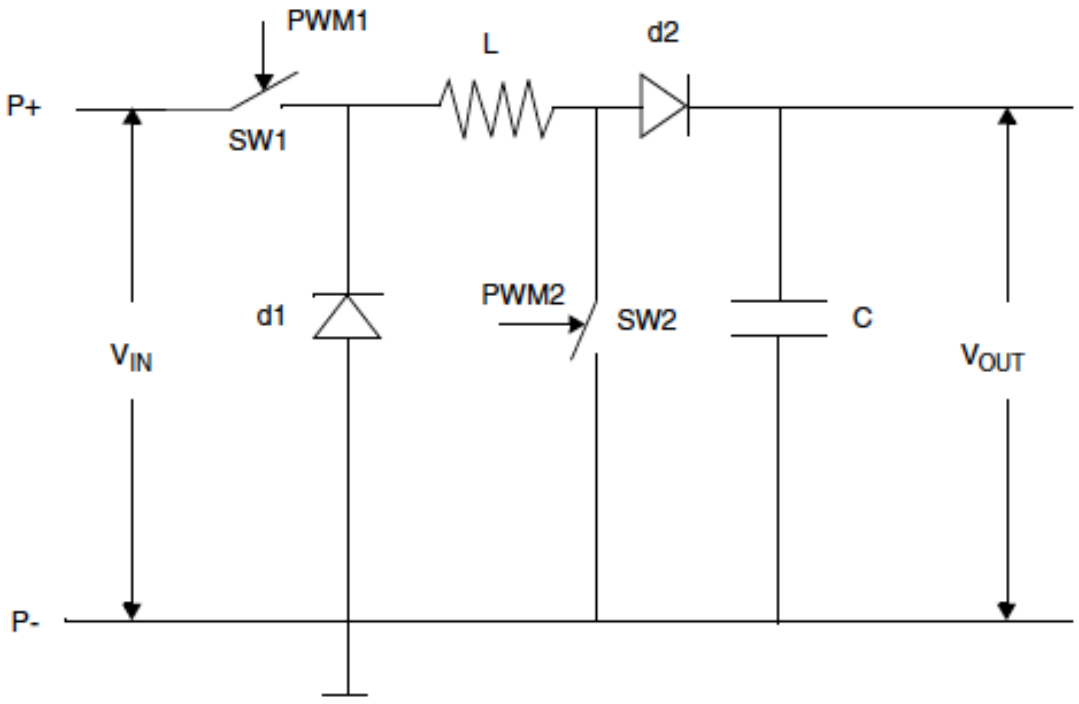

FIGURE 2.6-1: SCHEMATIC OF BATTERY CHARGING CIRCUIT

This circuit has two main functions: providing constant current to the NiCd battery cells and automatically shutting off current flow at full charge. Current regulation is accomplished by

using a transistor (Q3) in parallel with a resistor (R8). The transistor sets a constant voltage (specified by the part) across the resistor which in turn sets the current according to I=V/R. Using a MOSFET at Q2 allows higher current to flow to the batteries – with a 0.3 Ω resistor as shown the current is 2A.

The automatic shut-off function is accomplished using two capacitors, C1 and C3. When the NiCd cells reach full charge their internal potential drops by approximately 20mV. The potential of C3 reflects the potential of the battery at all times, however the potential of C1 lags that of C3 because of the circuit's time constant. This means that C1 serves as a reference potential – when its value is greater than that of C3 the voltage in the battery must be falling. This will cause that the output of the operational amplifier to go high, shutting of transistor Q1 and therefore the entire charging circuit.

The circuit as shown in Figure 2.6-1 has been assembled on a prototyping board using off-the-shelf components; now we will test the circuit to prove current stability under a variety of operating conditions. The second stage of the circuit design will involve both determining the exact current needed by the batteries and accounting for inherent power losses --- allowing us to tailor the design to the CASTOR power system. With this complete, we will have the circuit printed on PCB, order any necessary additional circuit components, and assemble the board.

Plans for Integrated Circuitry

Only after the analog charging circuit has been completed will we begin to explore the possibility of using imbedded circuitry to handle charging logic. This will ensure that should hiccups arise from the use of the micro-controller we will have a comparable and functional charging circuit.

The analog circuitry uses a hard switch to turn charging on and relies on the Q1 transistor to shut charging off. After a shut-off the switch must be reset and re-triggered to again begin charging. As chip logic (provided by the avionics subsystem) will dictate when charging begins, it is natural to also use chip logic to sense a full charge and terminate the charging cycle. By using a dedicated micro-controller on the charging circuit we would also be able to take over the responsibility of stimulating charging and would rely only on a trigger from avionics.

Inhibits (D. Odhiambo)

CASTOR will utilize a Lightband separation switch to check for separation between the launch vehicle and the CASTOR satellite. Immediately after separation, power from the solar panels is able to flow into the batteries but not the rest of the electrical components. Only after separation is confirmed is the solar panel power allowed into the electrical components. This confirmation will be by use of a comparator operating between the 24V from the solar panel and 12V.

Here the 12V input is an arbitrary design choice (a voltage value halfway between 0V and 24V), where other values greater than 12V but less than 24V can be proven to work just as well, that compensates for the lack of internal hysteresis when using an OpAmp in open loop configuration as a voltage comparator.

There is no guarantee that the entire solar array will be illuminated at separation, and as such no

guarantee of a constant 24V output at the time of separation. Therefore designing the inhibit system to exhibit electrical hysteresis is necessary as this provides a dead band where voltage comparable to 24V is let through to supply the comparator.

The 12V is supplied by a voltage regulator that operates at 24V. The comparator takes in the two voltage inputs and sets its output value to the higher of the two (24V). Aft of the comparator are a series of DPDT relay switches used to connect the solar panel voltage to the rest of the satellite electrical components. To avoid the need for voltage amplification DPDT relay switches with a pick-up voltage rating of 24V will be sourced.
NB: An additional [DPDT relay switches] is used to switch off the inhibits logic circuit in order to conserve power once separation has been confirmed.

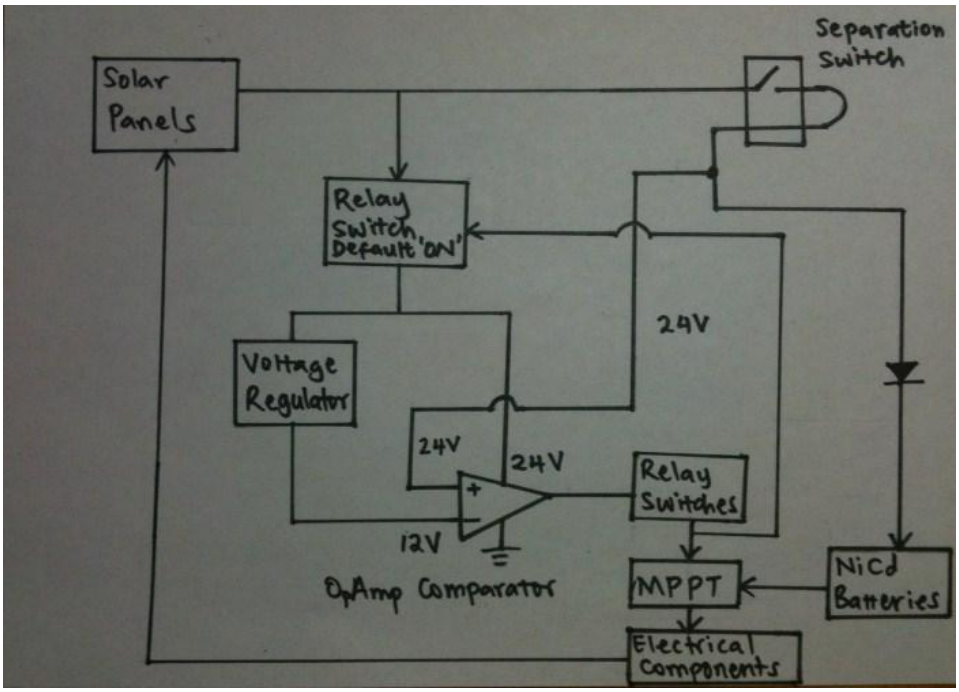

FIGURE 2.6-2: POWER ARCHITECTURE SHOWING INHIBIT CIRCUIT COMPONENTS

PPU

The function of the Power Propulsion Unit is to distribute the power drawn from the system power bus (from the MPPT) to the various components that comprise the propulsion system, namely: the cathode heater, the cathode keeper and the anode. The PPU board has three power converters: a 24V to 15V converter to power the cathode heater, a 24V to 36V converter to power the keeper and a 24V to 200V to power the anode and the xenon feed system.

PDU

The Power Distribution Unit (PDU) is intended to supply power to structure, thermal, communication, avionics and ADCS expect the reaction wheels and the magnetic torque coil. It must supply proper voltage and current levels to the spacecraft electronics and be fully controllable by the avionics computer.

2.6.2 OVERVIEW OF THE PPU REDESIGN (D. ODHIAMBO)

RELEVANT SYSTEM REQUIREMENTS

- Provide $150W_{nominal}$ to DCFT while operating
- $130W_{nominal}$ to the DCFT Anode
- Provide $15W_{nominal}$ to the DCFT while not operating

SUMMARY OF CURRENT PPU DESIGN

The function of the Power Propulsion Unit is to distribute the power drawn from the system power bus (from the MPPT) to the various components that comprise the propulsion system, namely: the Cathode Heater, the Cathode Keeper and the Anode. The PPU board has two power converters: one steps down the bus voltage supplied by the MPPT from 24V to 15V for the Cathode Heater, while the other steps up the voltage from 24V to 300V for the Anode.

It was decided that the 24V to 36V converter was obsolete. The keeper no longer requires 36V and can operate at 24V optimally. All of the components on the PPU board, in particular the BuckPuck, could also work at 24V instead of 36V. The removal of this converter decreases the complexity of the system, while also significantly increasing efficiency.

A summary of the voltage breakdowns is shown in Table 2.6-1:

TABLE 2.6-1: VOLTAGE REQUIREMENTS FOR PROPULSION SYSTEM

Propulsion Component	**Voltage Requirement**	**Current Requirement**
Cathode Heater	15V	
Cathode Keeper	24V	0.5A
Anode	300V	
Solenoid Valve conditioning (for 36 ms)	24V	

The diagram in Figure 2.6-3 further details the wiring for the PPU. The red and black lines represent +/- power lines, while the blue lines represent data/command lines between the converters and the avionics computer. The anode converter's voltage has been set at 200V.

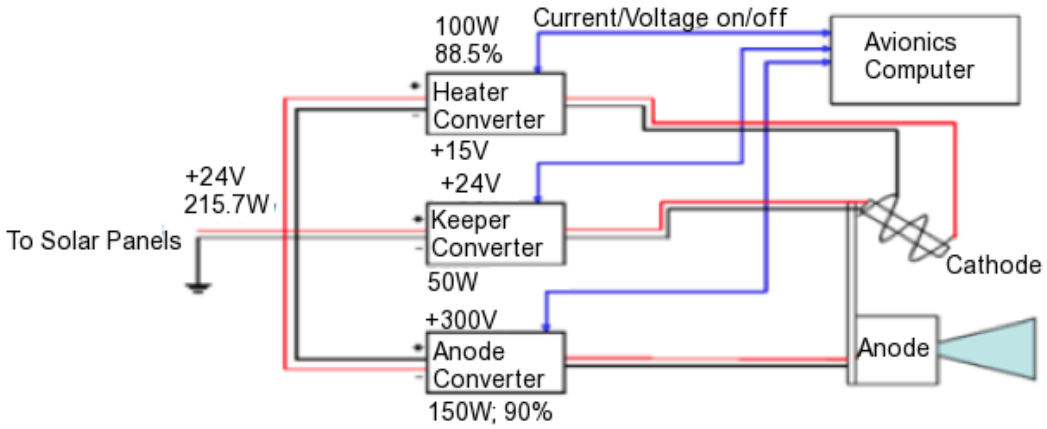

FIGURE 2.6-3: PPU ARCHITECTURE SHOWING PROPULSION COMPONENTS AND MAX CAPABILITIES OF THE POWER CONVERTERS IN USE

Anode Converter

- Outputs 300V
- Delivers 150W maximum to the anode
- Requires an on/off switch, to be controlled by the avionics computer
- Tie switch between on/off pin and –Vin (ground) pin, as seen below
- 90% Efficiency (typ.) = 15W max heat generated

Pin #	Single	Dual
2,3	- INPUT	- INPUT
4,5	+ INPUT	+ INPUT
6	ON/OFF	ON/OFF
7	CASE	CASE
8	N/C	OUTPUT 2 +
10	N/C	OUTPUT 2 -
12	OUTPUT 1 +	OUTPUT 1 +
14	OUTPUT 1 -	OUTPUT 1 -

FIGURE 2.6-4: ANODE CONVERTER (LEFT) AND PIN WIRING DIAGRAM (RIGHT)

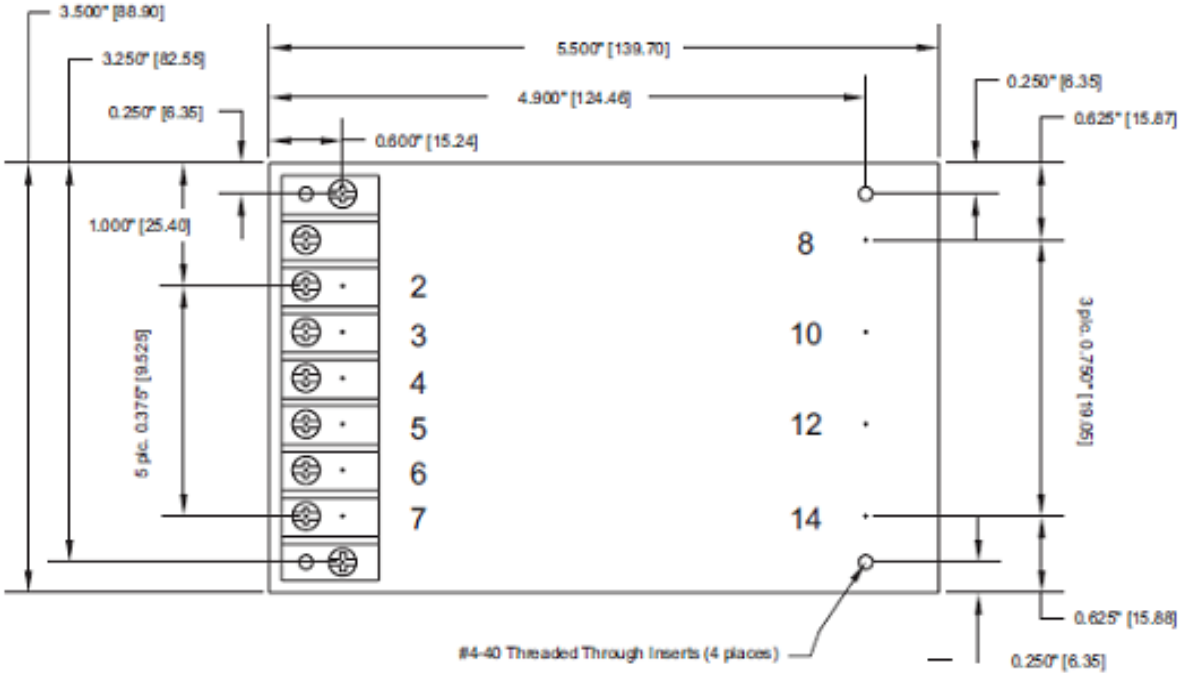

FIGURE 2.6-5: ANODE CONVERTER PIN SCHEMATIC

Cathode Heater Converter

- Outputs 15V, 100W
- Requires on/off switch, controlled by the avionics computer
- Requires a 0.5-1.5V analog control signal, supplied through a DAC to the control pin
- 88.5% at 50W and 89% Efficiency at 100W = 12.5W or 11W max heat generated respectively

Shown actual size:
2.28 x 1.45 x 0.5 in
57,9 x 36,8 x 12,7 mm

FIGURE 2.6-6: CATHODE HEATER CONVERTE

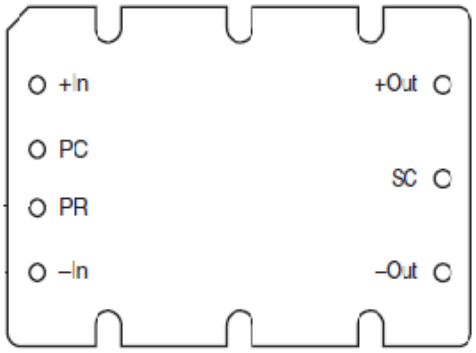

FIGURE 2.6-7: CATHODE HEATER CONVERTER WITH CORRESPONDING PIN-WIRING DIAGRAM (RESPECTIVELY)

Various MOSFET-controlled switches, capacitors and resistors are mounted to the PPU printed circuit board in addition to the power converters, for effective power delivery to the propulsion subsystem components.

Schematics of the PPU board prepared using Altium are available on fileshare under:

3-Subteams\3.8-Power\Altium \PPU\CASTOR PPU v3\

SUMMARY OF CURRENT PDU DESIGN (E. MCKINNEY)

The Power Distribution Unit (PDU) is intended to supply power to structures, thermal, communication, avionics and ADCS expect the reaction wheels and the magnetic torque coil. It must supply proper voltage and current levels to the spacecraft electronics and be fully controllable by the avionics computer. It is currently at Version 4.

Power Conversion

Two Lambda CC-E converters have performed the power conversion. One is a 5V converter rated for 15W input power limit and the other is a 3.3V converter rated for 3W input power limit. The power limit has been picked based on the maximum power calculated in the power budget, so that the converters operate in the high efficiency range. Figure 2.6-8 shows the circuit diagram for the 5V converter, Figure 2.6-9 shows the circuit diagram for the 3V converter, Figure 2.6-10 shows the result of the efficiency test performed on the 5V converter, and **Error! Reference source not found.** shows the result of the efficiency test performed on the 3.3V converter. 100pF capacitors have been placed between the -V and +V for both input and output to minimize voltage ripple.

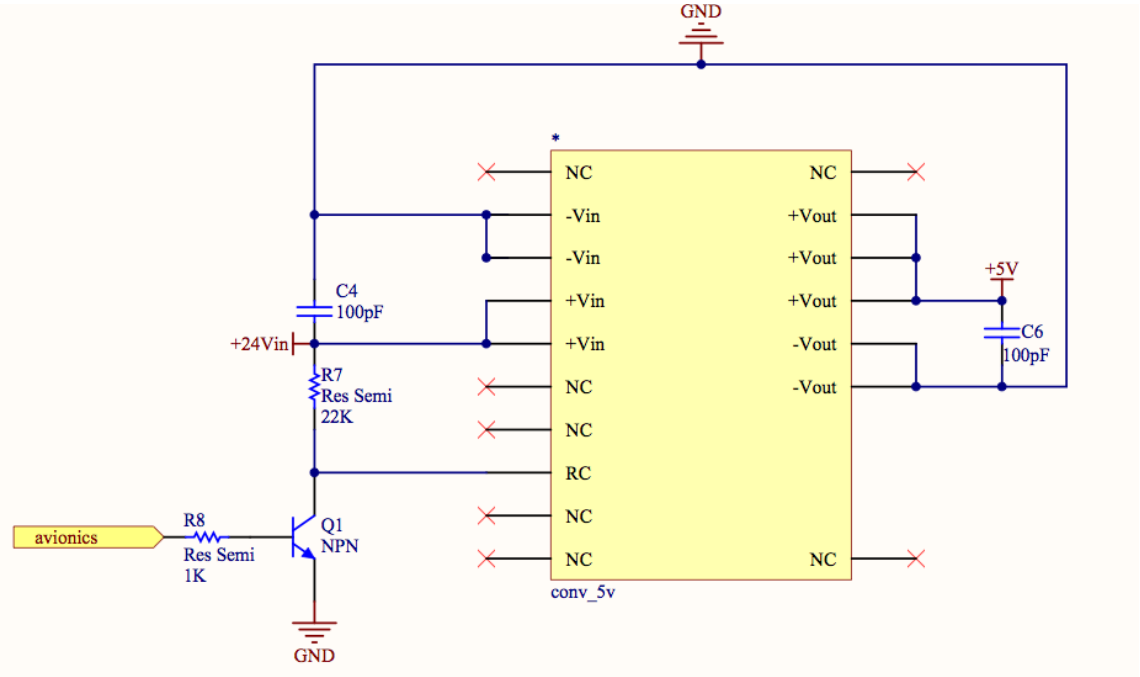

FIGURE 2.6-8: THE CIRCUIT DIAGRAM FOR THE 5V CONVERTER RATED FOR 15W POWER LIMIT

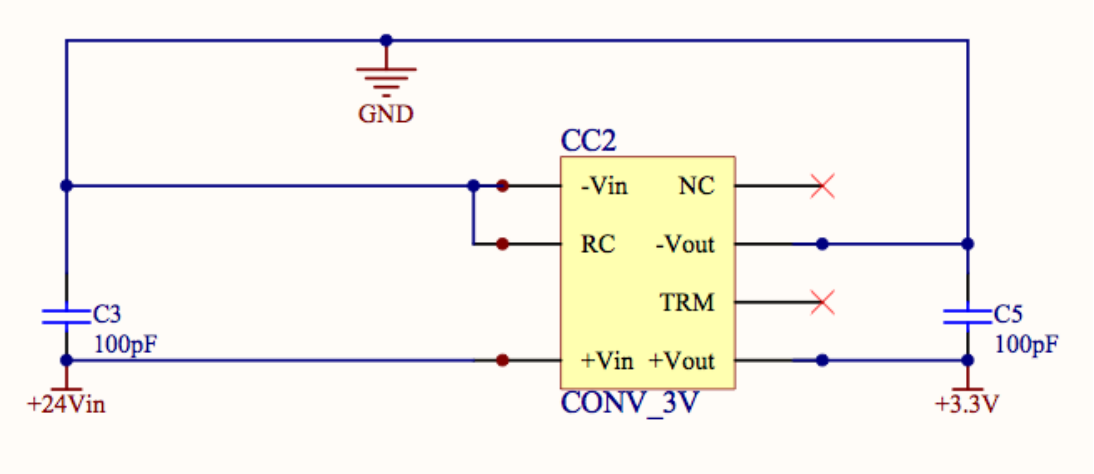

FIGURE 2.6-9: CIRCUIT DIAGRAM FOR THE 3V CONVERTER RATED FOR 3W POWER LIMIT

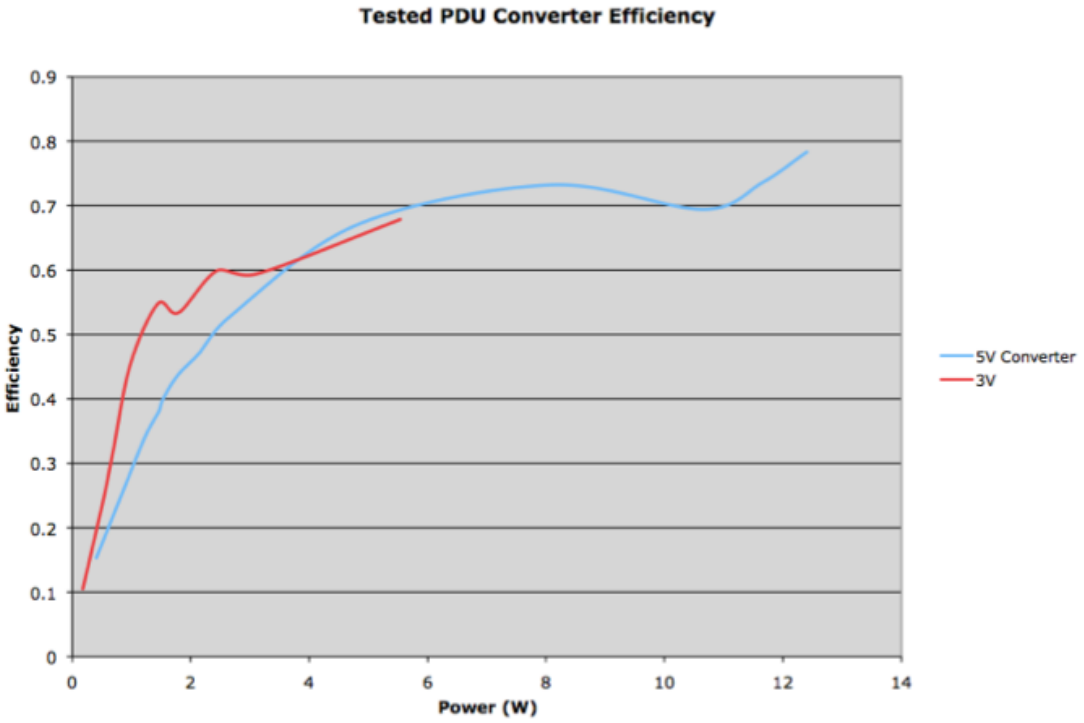

FIGURE 2.6-10: EFFICIENCY RESULTS FOR THE BOTH PDU CONVERTERS

On/off Switching

Each of the Lambda converters can be switched on and off using a MOSFET. The MOSFET are placed between +Vin pin and the RC pin. For the on mode, the RC terminal is brought low by tying it to ground, while for the off mode, the RC terminal is left open and internally brought high. For FlatSat testing, the converters have been controllable with both a MOSFET and a manual switch as shown on Figure 2.6-8 and Figure 2.6-9.

Voltage and Current Sensors

Voltage sensing has been achieved through voltage dividers that step down the output voltages of the two CC-E converters by a half making the output voltages below +3.3V, to the maximum allowable input into the avionics computer. The voltage divider should not interfere with the rest of the circuit, so 100k resistors have been picked to make the dissipated power minimal.

Current sensing has been done with an ACS712 hall-effect current sensor, which comes in a surface-mount chip package. The sensor, placed in series with the output voltage line of any converter, will generate an analog voltage signal proportional to the output current, which will then be sent to the avionics computer. From experimental data, the relationship between current and voltage signal is: Output Voltage [V] = 0.1831 [V/A]*Output Current [A] + 2.524[V], approximately 183mV/A, with a DC offset of 2.524V.

The circuit diagram of the current sensors used in the PDU is shown in Figure 2.6-11 and Figure 2.6-12. A 100pF capacitor has been placed between the filter and ground to filter out the noise. Both current sensors have been powered by a 5V power input. The 5V power input has been provided from the 24V input through a voltage adaptor. The schematic of the voltage regulator is provided in Figure 2.6-13 . Both the Isense and Vsense have been sent to a terminal where they can be read by a multimeter, the Lab View software, or the avionics board.

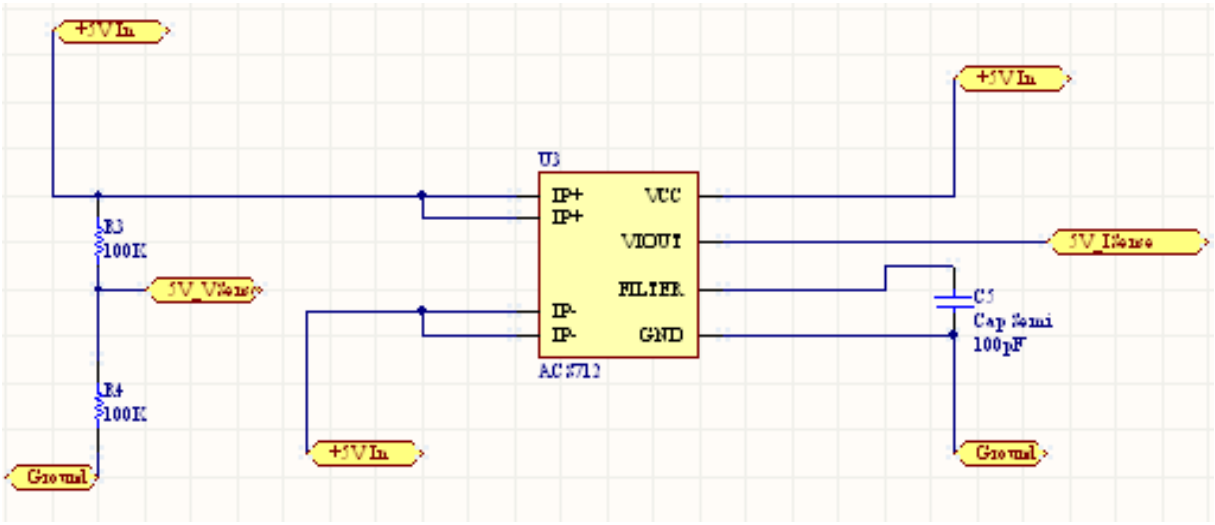

FIGURE 2.6-11: ACS712 HALL-EFFECT CURRENT SENSOR FOR THE 5V CONVERTER

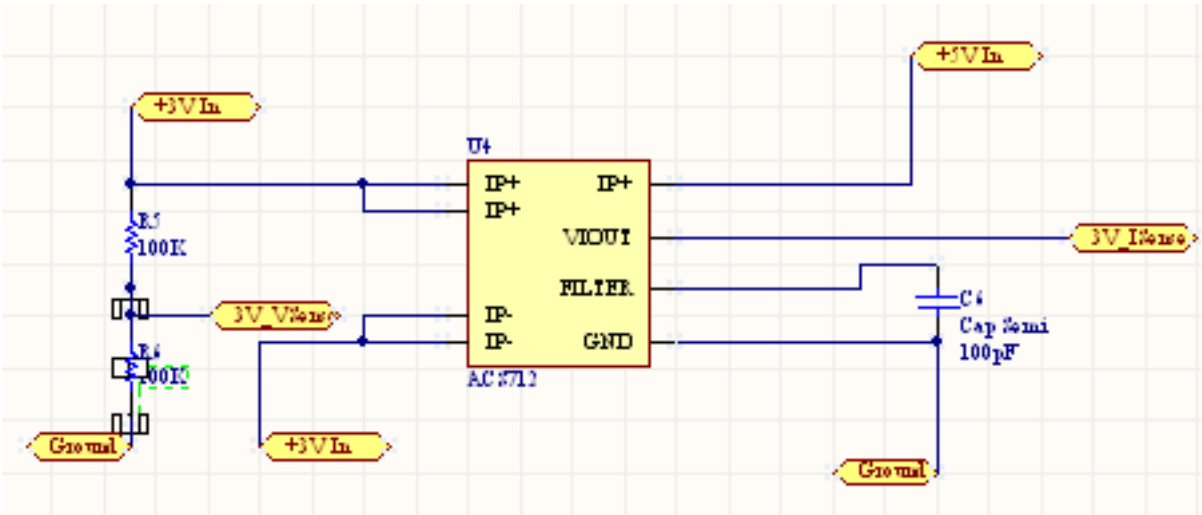

FIGURE 2.6-12: ACS712 HALL-EFFECT CURRENT SENSOR FOR THE 3.3V CONVERTER

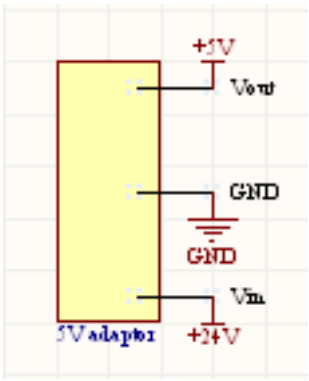

FIGURE 2.6-13:5V VOLTAGE ADAPTER

Voltage Regulator

A 3.3V voltage reference has been used to provide a 3.3V reference voltage to the avionics computer, for precision ADC. The avionics computer needs a reference voltage with a high precision; thus, the LTC6652, a low drift and low noise buffered reference voltage, has been picked. The LTC6652 has a tolerance of 0.05%, a voltage input of 5V provided from the voltage adaptor shown in Figure 2.6-13, and a voltage output of 3.3V. The circuit diagram of the 3.3V voltage reference is provided in Figure 2.6-14. A 0.1 uF capacitor bypass Vin to GND and a 10 uF capacitor bypass Vout to ground. These capacitors have been added to improve precision and the value has been picked according to the data sheet.

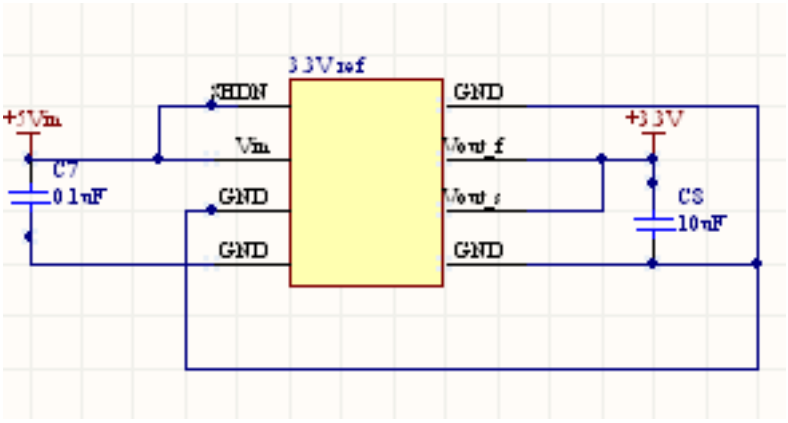

FIGURE 2.6-14: CIRCUIT DIAGRAM FOR THE 3.3V VOLTAGE REFERENCE

Connectors

7 Connectors have been used in the PDU board to achieve the following functionalities: input +24V, output +5V, output +3.3V, output a reference +3.3V to the avionics computer, sense the voltage and current for the 5V converter, sense the voltage and current for the 3.3V converter, and input commands from the avionics computer to turn on and off the 5V converter. In addition, we have two diodes to show when the converters are on and off. Figure 2.6-15 shows the schematics off all the connectors and the diodes that are in the PDU.

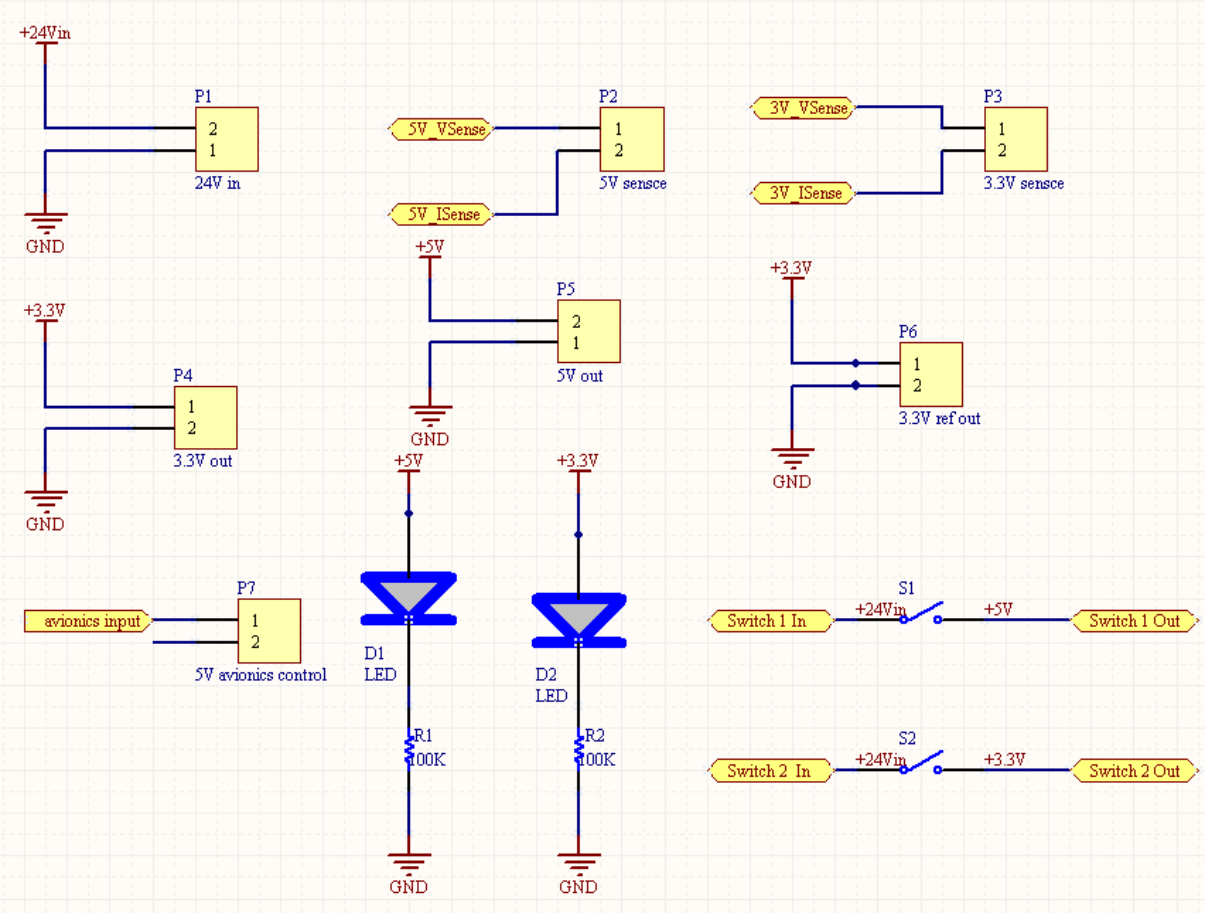

FIGURE 2.6-15: CIRCUIT DIAGRAMS FOR THE CONNECTORS AND DIODES ON THE PDU

Overall design

The current PDU designed has the properties shown in Table 2.6-2, and the PCB board layout is shown in Figure 2.6-16. On PCB layout, the green color represents ground traces and is situated on the bottom layer of the PCB, while the yellow color represents positive traces and is situated in the top layer. The board has three different ground traces based on the fact that the input and output ground of each converter needs to be isolated. The bottom yellow trace represents the input +24V, the yellow trace on the top left represents the +3.3V output, and the yellow trace on the top right represents the +5V output.

TABLE 2.6-2: PROPERTIES OF THE CURRENT PDU

Component	Digikey Number	Number of Components	Cost
The PDU board	non applicable	1	$33
3.3 V Converter	445-2474-ND	1	$11.37

Component	Digikey Number	Number of Components	Cost
5 V Converter	CC15-2405	1	$36.39
Current sensor	620-1191-1-ND	2	$3.3
3.3V ref	LTC6652AHMS8-5#PBF-ND	1	6.73
5V adaptor	LM2936MX-5.0TR-ND	1	$2.38
Heather	A98333-ND	7	$4.55
100k Resistor	P100KADCT-ND	6	$.99
MOSFET	IRFD123	1	$1.5
Switch	EG2610CT-ND	2	$14.2
100pF capacitors	399-1022-1-ND	6	$0.12
Diode	160-1579-2-ND	2	$0.8
Capacitor (0.1uF)	478-5778-1-ND	1	$0.901
capacitor (10uF)	PCC2479CT-ND	1	$0.56
Total			$121.62

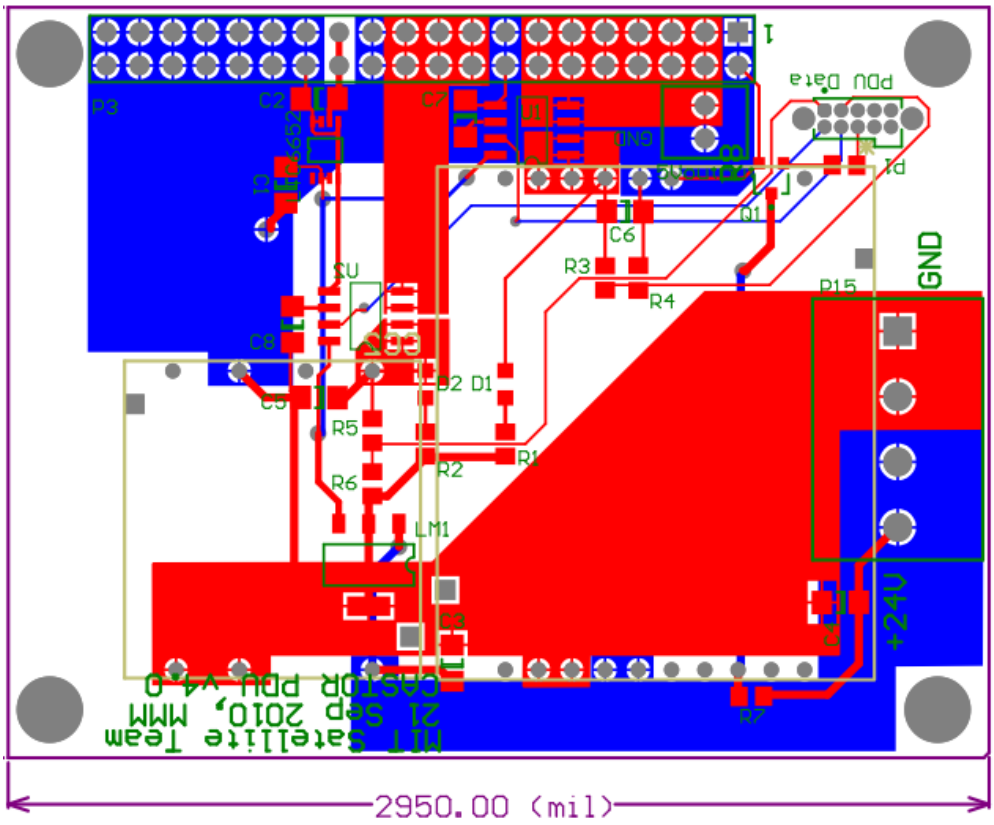

Figure 2.6-16: PCB Layout for the PDU

2.6.3 SOLAR PANELS (E. MCKINNEY)

The solar panel design uses a total of four panels arranged such that two panels are at a 90 degree angle to one another and mounted to the body of the satellite, and the others are deployable panels attached at 135 degree angles to the edges of the inner panels as shown in Figure 2.6-17. There is 1.139m^2 of total solar panel area (not all of which is covered with solar cells), consisting of six 0.586m x 0.486m panels with 96 cells each in an 8x 12 configuration, depending on whether or not the solar panel is deployable or attached. The cells are space-grade silicon cells, donated by Loral Space Systems, and are 6.91cm x 3.59cm x 0.4cm and have 16% efficiency. The cells have cover glass over their sun-facing surface, and are attached to a rigid backing using space-rated RTV adhesive. The backing is honeycomb aluminum sandwiched between two FR4 printed circuit boards (PCB), bonded using ceramic epoxy that electrically insulates them while also conducting heat from the cells to the back surface of the panels. To ensure manufacturing integrity, these backing panels need to be ordered instead of fabricated.

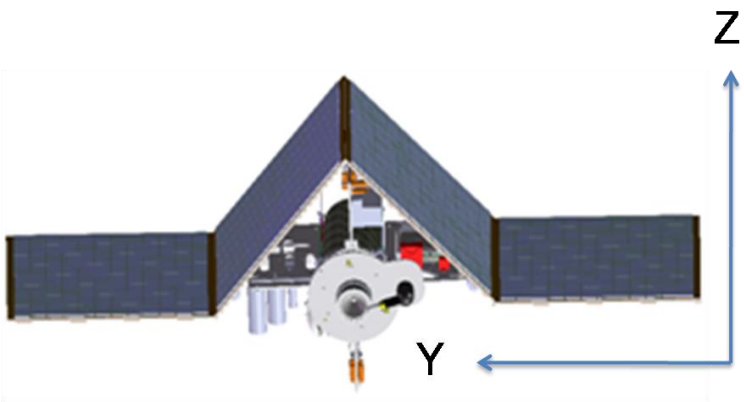

FIGURE 2.6-17: SOALR PANEL LAYOUT

RELEVANT SYSTEM REQUIREMENTS

The spacecraft shall have a wet mass under 50 kg.

Thus the backing, support structure, and coverglass for the solar panels must be no thicker than necessary to protect the cells from breaking and to electrically insulate them from conductive metal structures.

S9.5.4.11 The structure shall fit, collapse, or fold down to fit within 50cm X 50cm X 60cm in order to fit UNP specifications.

Thus the Structures Team requires that the solar cells fit on an area of 56.8cm x 46.8cm per panel so that they will have room to attach their hinges to the panel edges. Their design requires that the total panel area be 58cm x 48cm.

S7.1 The spacecraft shall contain a power subsystem capable of supplying a continuous source of electrical power to spacecraft loads during the mission life.

Each of the subsystems' equipment pieces only require power for a fraction of the total time of the cycle, and the most power intensive are summarized in Table 2.6-3. This allows both the batteries to be charged and the thruster to be fired, all within the 169.95W that the solar panels produce when in direct sunlight.

TABLE 2.6-3: POWER BUDGET SUMMARY

Subsystem - Sun Cycle	**Power Required (Watts)**
All systems - Eclipse	23.92
All systems - Sunlight	121.25
Charging batteries - sunlight	69.47

Thruster firing - sunlight	103.13

Mass and Cost Budget

Some of the purchases listed below were made through donations, and for others, minimum purchase requirements made it necessary to buy more of an item than will be used in the design.

TABLE 2.6-4: MASSES AND COSTS OF SOLAR PANEL COMPONENTS

Item	**Quantity**	**Total Cost**	**Total Mass Used (kg)**
Solar cells1	416	Free	0.874
FR4 PCB5	8 sheets, 0.58m x 0.48m	$528.00	0.65
.74 cm thick carbon fiber composite3	4 sheets, 0.58m x 0.48 m	$671.96	2.43
150 micron thick coverglass2	4 sheets, 0.565m x 0.45m	Free	0.375
500°F Duralco 128 ceramic-based epoxy4	~10% of panel mass	$129.90	0.487
NuSil CV10-2568 RTV adhesive	1 kit	$463.50	0.250
Total		**$1,793.36**	**5.066**

1. The solar cells are free, donated by Loral Space Systems.
2. The coverglass is donated by Loral's supplier, Qioptiq.
3. The carbon fiber composite with honeycomb comes from Protech Composites.
4. The ceramic epoxy comes in 8-ounce containers, and 10% of the panel mass is about 15.7 ounces, so two containers would be needed.
5. The PCB will be designed in Altium and ordered through the software.

SOLAR PANEL DIMENSIONS

The Structures Team has determined that each solar panel can be at most 0.58m x 0.48m, with 0.568m x 0.468m for the solar cells and coverglass and the rest for structural interfaces like hinges. The dimensions of the solar panels were set not by the power requirements, but by the space restrictions of the UNP. Within UNP constraints, solar cell area was maximized to maximize power, and any power beyond the vehicle's minimum functional needs will go to the thruster to increase the force from the propulsion system. Four panels of this size are sufficient because, as shown below, they can provide 169W—enough power to fire the thruster and run the other subsystems with additional watts to accommodate power usage spikes among the subsystems and to allow the thruster to operate at higher power (greater thrust) when possible.

The orientation of the solar cells on the panels was designed to maximize the number of cells that will fit and therefore maximize power output. The design will use a 96-cell arrangement with an array of 12 cells by 8 cells. Loral Space Systems has agreed to donate cells that have 6.91cm x 3.59cm faces and are 0.4cm thick. There are two ways to fit these cells onto a 0.5m x 0.62m panel: align the long side of each cell with the long side of the panel, or align the short side of each cell with the long side of the panel. Using the former method, 96 cells have been shown to fit on the panel.

The minimum allowable distance between cells is 1.5mm, both between rows and between columns. This margin provides room for the wiring between cells and lessens the danger of cells touching and either shorting out or transferring loads to each other that could cause them to shatter.

To account for wires that connect the solar panels to the rest of the satellite, holes will need to be cut in the open spaces on the panels for the wires to transfer through.

POWER OUTPUT

With 96 cells for each of the 4 panels, at 6.91cm x 3.59cm each, the total power-generating area on each panel is 0.238m^2. The maximum power generated can be calculated using the equation below.

$$P = Q_{solar} A \varepsilon_{mppt} \varepsilon_{glass} \varepsilon_{cell} \sin(\theta)$$

A = total solar cell area = 0.982m^2

Q_{solar} = the solar power constant = 1350 W/m^2

ε_{cell} = solar cell efficiency = 0.16

ε_{glass} = efficiency of transmittance of usable light through coverglass = 0.94

ε_{mppt} = efficiency of maximum power point tracker (MPPT) = 0.95

θ = the smallest angle between the light vector and the panel's surface = 90° for deployable panels, 45° for body mounted panels

P = power output from solar panels after passing through MPPT due to MPPT inefficiencies = 156W

For the standard Q_{solar} of 1350 W/m^2 and the Loral solar cell efficiency of 16%, the total panel area above gives 165W. This is the maximum power output when the deployable panels face the sun directly (θ = 90°), and the body mounted panels, by geometry face the sun at 45° which they should for most of the mission thanks to actuators from the ADCS Team.

ELECTRICAL LEADS

The leads that connect to the front of one cell will connect to the back of the next cell. The cells used for this design are rectangular and not octagonal like the cells in Figure 2.6-18, but the connections are the same, using flux and tinned tabbing wire. With this type of connection, a column of cells will typically be connected in series, but since the MPPT is designed for nominal voltages 24V-36V, and each cell provides ~0.5V based on the power analysis above, there must be 48-72 cells in each series to provide voltage within this range. With 13 cells per column and 8 columns per panel, there are two series of cells per panel, each with 4 columns. These series provide roughly 24V, which is at the lower end of the MPPT's range.

The solar cells are expected to degrade by 10% by the end of a year in space, according to the team's contact at Loral, so the voltage to the MPPT would decrease to 21.6V. It will be necessary to run the MPPT with an adjustable voltage source to see how it performs under these conditions.

In terms of wiring, tabbing wire connects the bottom of one column to the top of the next when the two columns are in series, and this next column is oriented "upside down" compared to the first column, in terms of the direction of the tabbing wire weaving from one cell to the next. The two series each have a positive and negative lead, and all the leads are on the same side of the panel. The two positive leads are connected to each other using tabbing wire, as are the negative leads, so that the panel has two leads total. These leads are on opposite sides of the panel so that the panels can be connected in parallel with their longer edges adjacent to each other. 16 AWG insulated wire connects the strings, and 12 gauge wire connects the panels to each other and to the MPPT.

Diodes at the end of each series of cells prevent backflow of current in case the voltage across that series is not sufficient to produce current in the desired direction. If a series does not produce current, the mission is still viable, but there will be approximately 23W less power output. If a solar cell shatters, its tabbing wire connections tend to stay intact (based on accidents during prototyping when cells shattered), the particular series of cells will be unable to provide power, and the satellite will lose approximately $1/8^{th}$ of its power. The mission can still continue without this power due to the power margin provided, but the frequency and duration of the thruster firing will have to be reduced.

Electrical leads, "Weaving" From the Front of one cell to the back of the next is shown in Figure 2.6-18. The directionality of this top-to-bottom connection determines the direction of current along the series. There must be enough space between cells to allow this connection.

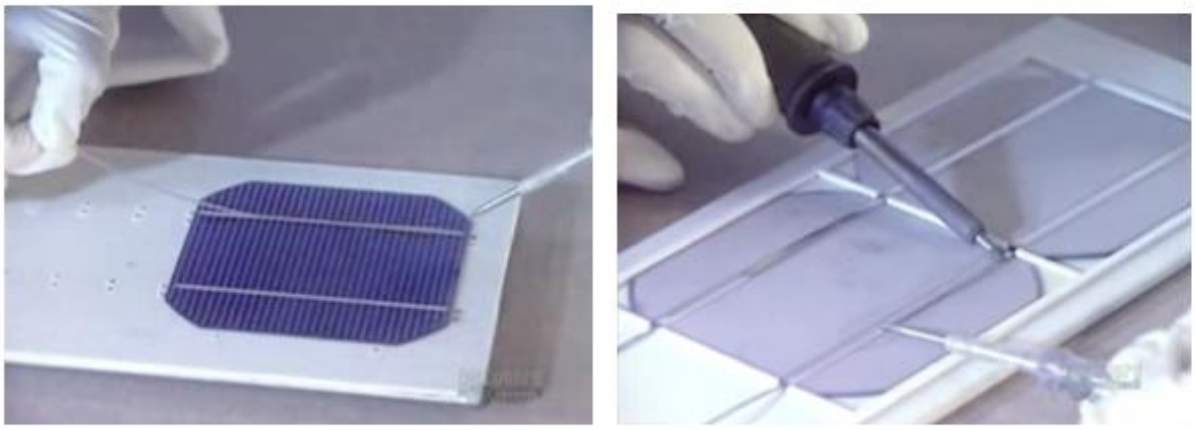

FIGURE 2.6-18: SOLAR PANEL FABRICATION

COVERGLASS

The ideal design uses as much blue/red reflector (BRR) coated glass as possible, distributed evenly among electrical series on the panels so that all series have the same voltage, and covers the remaining cells with anti-reflection (AR) coated glass. The glass Qioptiq has offered to donate is 150 micron thick CMX with BRR coating, but Qioptiq only has enough of this coverglass for 160 cells and thus more will need to be obtained. They have enough AR glass to cover all the cells in the design. JDSU has also offered to donate coverglass, 100 micron BRR CMX glass, so these covers would be lighter, but it's uncertain how many JDSU will be able to donate, so the current design the Qioptiq glass for all cells. BRR glass is more desirable because it reflects wavelengths of light that the solar cells cannot use. The energy of this light would only become heat without providing electricity, and the additional radiation would speed the cells' degradation. Other wavelengths are not reflected, and as with AR coating, this lack of reflection means more useable light hitting the cells.

For comparison, the properties of CMX glass and several other coverglass types are documented in Table 2.6-4. The glass comes in 6.923cm x 3.604cm pieces, just slightly bigger than the cells, so with 1.5mm gaps between cells, there would be 1mm and 1.37mm gaps between coverglass pieces.

Property	**CMX**	**CMG**	**CMO**	**Corning 0213**	**Corning 0214**
Density (g/cm^2)	2.605	2.554	2.536	2.6	2.5
Refractive index	1.5265	1.516	1.490	1.528 at 589nm	1.516 at 589nm
Young's Modulus (GN/m^2)	75±1.0	78.7±1.0	69±1.0	73.7	73.0

Poisson's Ratio	0.22±0.01	0.175±0.01	0.22±0.01	0.224	0.22
Thicknesses available (mm)	0.05-0.50	0.05-0.50	0.05-0.50	0.075-0.50	0.075-0.50

TABLE 2.6-4: SOLAR CELL COVERGLASS PROPERTIES

The reason to use coverglass is that power output can be increased if the glass protects the cells from infrared, ultraviolet, and particle radiation that would degrade the cells' efficiency. The glass can also decrease power output by not allowing all photons that hit the panel to reach the solar cells, but the Power Team's Loral contact explained that in practice there is a net improvement in power output. These effects on power—the glass' transmittance of light and its effectiveness at protecting the cells—have not been quantified by the manufacturers. The transmittance efficiency ε_{glass} used above is based on information from the team's contact at Loral.

The benefits of increasing the efficiency of the cells are currently being weighed by the manufacturing difficulties of installing the cover glass. Currently, the decision is to continue with the use of cover glass.

SUPPORT STRUCTURE

Since the solar cells are extremely brittle, shattering in a person's hand under minimal bending loads, the solar panels must be rigid to protect the cells from bending, especially during launch and deployment. The current design is ¼ inch (0.635cm) thick honeycomb aluminum sandwiched between two 0.020 inch carbon fiber composite sheets (0.01016 cm). This manufacturing will be outsourced.FR4 PCB with thickness of 0.005 cmwill then be epoxied to carbon fiber on either side. The sandwich structure is shown in Figure 2.6-20. With the tall, thin, hexagonal honeycombs to provide structural strength along one axis (the axis perpendicular to the panel) and the carbon fiber composite and PCB to provide strength along the other two axes, this panel is more rigid than the alternative designs, which used an aluminum plate with holes to reduce mass. The PCB simplifies the wiring of the cells and eliminates the need for Kapton tape. Enough sandwich material for one solar panel would weigh 0.38kg, compared to the 1.30kg 1/16-inch aluminum panel design in Figure 2.6-20. The solar cells are sealed against this backing under the coverglass. The PCB and honeycomb are attached to each other using thermally conductive, electrically insulating ceramic-based epoxy as shown in Figure 2.6-20. This epoxy doesn't outgas unless its max temperature of 533.15K is exceeded. The solar cells require a different adhesive to bind them to the backing, a space-rated RTV adhesive like NuSil, which is the current choice due to its lower price compared to Dow Corning at no cost to quality.

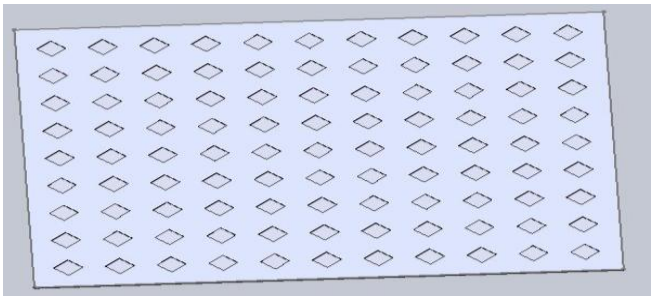

FIGURE 2.6-19: A 1/16 INCH THICK ALUMINUM DESIGN

It was rejected because it was heavier and less rigid than the honeycomb sandwich structure

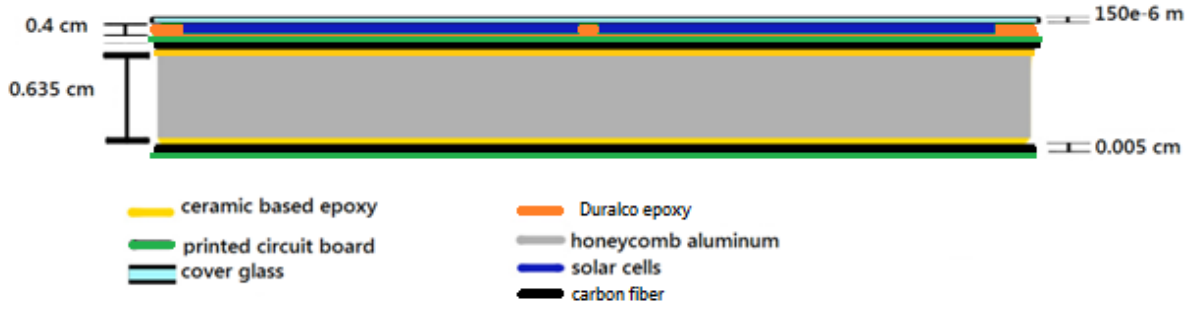

FIGURE 2.6-20: A CROSS-SECTION OF A SOLAR PANEL, NOT DRAWN TO SCALE

2.7 SCIENCE/PAYLOAD

2.7.1 OVERVIEW AND SCIENCE CASE (M. KNAPP)

CASTOR will carry a C328-7640 RBG JPEG camera to observe the DCFT plume. The camera's purpose will be to support DCFT operation and augment measurements of the thruster's performance. While some performance and efficiency metrics can be monitored by other means (delta-V, temperature, etc), the camera will provide visual feedback as well as independent data on thruster performance.

The camera will observe two main phases of DCFT operation. During cathode conditioning (before first firing), the camera will capture images of the cathode. If operating properly, the cathode tip will glow. Once the camera provides confirmation that the cathode is operating properly during cathode conditioning, the DCFT can be fired. Cathode function cannot be measured by other means, so the camera is essential for this process. The camera will also confirm that the thruster is operating properly (a plume appears) and that the plume is properly ionized (plume will be purple to blue in color). Figure 2.7-1 shows the glowing cathode and a well-ionized plume.

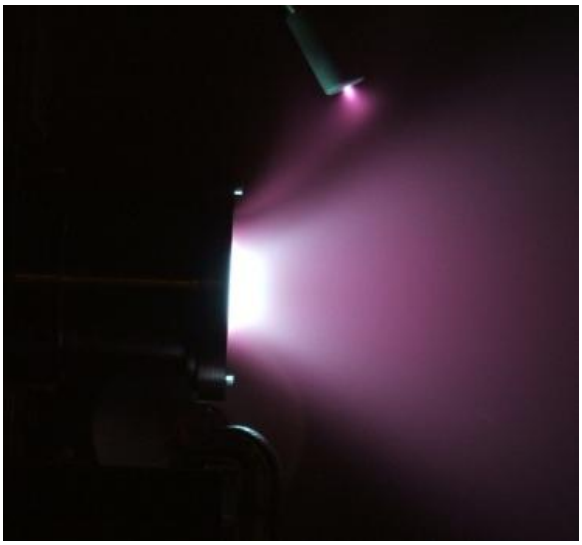

FIGURE 2.7-1 DCFT IN OPERATION

During normal satellite operations, the DCFT will fire during each period of sunlight. During each thruster firing, the camera will take images that will serve two purposes. First, they will provide visual confirmation that the thruster is operating properly. Second, the color of the thruster plume will be used to determine the engine efficiency. RGB data from the camera will be compared to data taken on the ground during testing in order to correlate the observed plume color on-orbit with known efficiencies and power levels. During vacuum chamber testing on the ground, plume images will be analyzed by binning RGB data from each pixel and correlating those histograms with the engine performance data for the same time period. In this way, RGB data is correlated with detailed performance data so that RGB data taken on orbit will provide quantitative information on thruster performance.

2.7.2 CAMERA SPECIFICATIONS (A. FIDONE)

CASTOR will be using the C328 camera system with the 7640-stylelens (Figure 1.1.2-1). This system will allow CASTOR to image the DCFT's plume. During operation, the camera will use its maximum resolution (VGA) of 640x480.

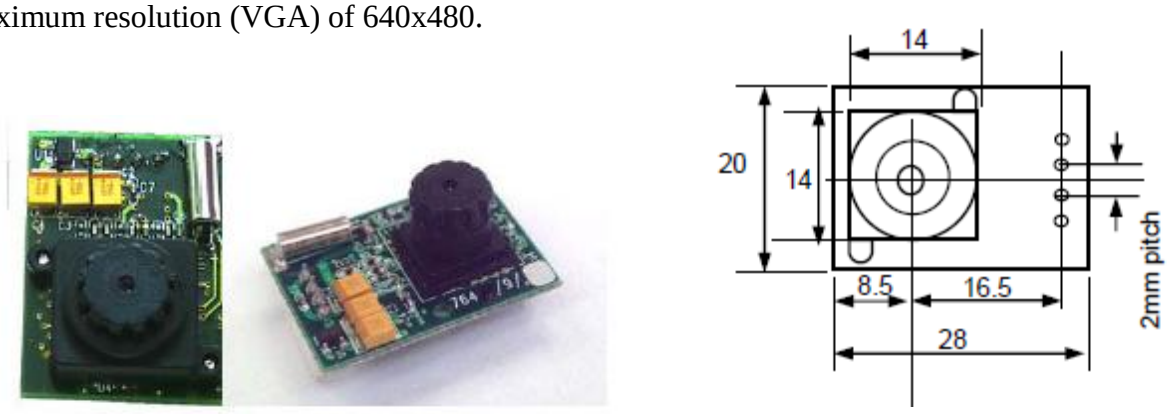

FIGURE 2.7-2 C328 7640 CAMERA BOARD WITH DIMENSIONS

As a quick reference, important values are listed in Table 1.1.2-1. However, more detailed information can be found in Tables 1.1.2-2 and 1.1.2-3.

TABLE 2.7-1: C328 KEY VALUES

Field of View	57 °
Operating Temperature Range	-20 and 60 °C
Resolution Range	CIF to VGA
Operating Voltage	3.3 V
Power Consumption	60 mA

TABLE 2.7-2: PIN DESCRIPTION WITH BOTTOM VIEW OF C328

Pin	Description
VCC	Power 3.3VDC
TxD	Data Transmit (3.3V)
RxD	Data Receive (3.3V)
GND	Power Ground

Connector specification: 2mm pitch, 4pin single row
Reference part no: Suyin 190600
Mating connector: Suyin 140600

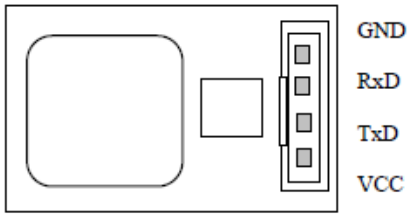

Bottom View

TABLE 2.7-3 ELECTRICAL PROPERTIES

V_{DD} = 3.3V+10%, TA = 0 to 25°C

Symbol	Parameter	Condition	Min	Typ	Max	Unit
V_{DD}	DC supply voltage		3.0	3.3	3.6	V
Io	Normal Operation Current	Operating		60		mA
Is	Suspend Current	Suspend		100		uA
V_{IH}	High level input voltage	TTL	2.0			V
V_{IL}	Low level input voltage	TTL			0.8	V

During flight, the camera will operate under the avionics specifications found in Table 1.1.2-4. The values below are calculated with the resolution of 640 x 480.

TABLE 2.7-4: DATE RATES

Total downlink intervals per orbit	3
Window of opportunity per interval	360 Seconds
Corrected window (40% loss)	216 Seconds
Downlink strength	112.5 Kilobits per second
Maximum data downlinked per interval	24,300 Kilobits
Total allocated storage for imaging	0.5 Gigabytes = 4,194,304 Kilobits
Total size of each image	240 Kilobits
Total images per interval that can be transmitted	101

The margin value for other downlink/uplink activities is 67% i.e. the C328 will use 33% of the downlink capacity per interval to downlink images.

Concept of Operations

After initial launch, the camera system will begin monitoring the cathode activation sequence. During this phase, it will capture an image every 10 minutes until the cathode is fully operational, a condition which is indicated by the cathode's spectral resolution. The cathode is expected to remain activated for the remainder of the mission.

Each time the thruster fires, the camera will capture one image every two minutes to monitor thruster functionality. The thruster is expected to remain active for 22-30 minutes, yeilding a maximum of 15 images.

The camera may also be used to take extra images To Be Determined but will amount to no more than a few images for any given interval.

Throughout each interval, the system is expected to yield approximately 33 images, which falls below the maximum capacity of 140 images. This leaves a substantial margin for other downlink activities of about 75% (of maximum downlink capability per interval).

2.7.3 MASS BUDGET (A. FIDONE)

Table 1.1.2-5 documents the mass of the camera system.

TABLE 2.7-5: MASS BUDGET

Component	Mass (g)
Camera	8
Wires	3
6061 Al Shield	26.74

2.7.4 SHIELDING (M. KNAPP)

The DCFT will create a high flux of high-energy ions in the region posterior to its position. These ions can damage components like the camera, so the camera must be shielded to ensure that it functions properly for the duration of the satellite lifetime.

It is necessary to construct an aluminum encasement for the camera to protect it from degradation and deposition caused by the ions released from the thruster. It will be made of an aluminum alloy of approximately 1.5 mm in thickness. This box will be approximately 1.25x1x0.5 in and positioned a maximum distance of 353.5 mm from the central axis of the satellite (at a corner of the CASTOR structure). It will be secured to a structural truss with two #4 screws.

The encasement will be equipped with a bi-stable (latching) shutter provided by Brandstrom Instruments (DWG No: A1037). The shutter will be controlled by electrical impulses (at a maximum of 5V), causing the 15x15mm blocker to alternate between opened and closed states. It will be constructed from black anodized aluminum and other low outgassing materials. Figure 1.1.4-1 shows a preliminary design for this shutter.

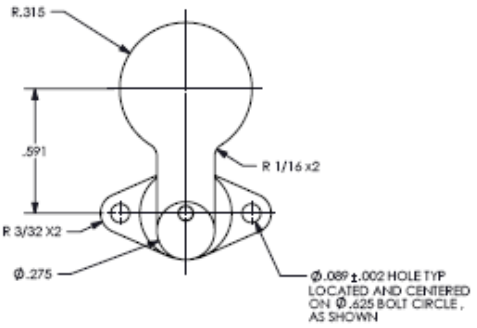

FIGURE 2.7-3: SHUTTER DIMENSIONS

2.7.5 CAMERA TESTING (M. SQUIERS)

To verify the sustainability of the camera, it is necessary to perform the following tests with the ultimate aim of simulating the mission-like conditions of a space environment: the Thruster, Thermal Vacuum, Avionics, Vibration I & II, and Integrated Camera Function Tests.

The Thruster Test will be used to assess both the functionality of the lens after exposure to the ion-saturated environment posterior to the ignited thruster and the effectiveness of shielding materials. A stand was equipped with the 7640-style lens and three separate aluminum alloys of varying masses and thicknesses (Table 1.1.5-1). The stand was then placed in a vacuum chamber approximately 30cm perpendicular from the central axis of the thruster, and the thruster was run through a flight simulation. Upon return to atmospheric conditions, the samples were removed and massed. At this time, the lens has been left in the chamber for further exposure. After the thruster is allowed to run through approximately three additional thruster cycles, the lens will be removed and massed. The lens will be used to take images that will be compared to pre-test images and evaluated based on their relative clarity.

In addition to the image clarity assessment, the effective degradation of and deposition on the lens and aluminum alloys will be evaluated based on a percent mass difference. The passing criteria of this test include: high clarity of post-exposure images and little to no degradation/deposition of the acceptable aluminum samples. If the lens cannot take clear images, a shutter must be purchased. Since the aluminum samples show minimal degradation/deposition, the lowest density aluminum with minimal thickness will be used to construct the camera encasement. (Expected completion date: May 2010)

TABLE 1.1.5-1: Mass of components

Component	**Pre-Test Mass (g)**	**Post-Test Mass (g)**
Lens	0.5720	-
Alloy 1: 20/24	39.25	39.27
Alloy 2: 50/52	52.41	52.46
Alloy 3: 60/61	57.32	57.40

The Thermal Vacuum Test is to be performed to determine the overall durability/functionality of the camera in a thermal/vacuum environment comparable to that expected in space. The camera will be equipped with five Resistive Thermal Devices (RTDs) to monitor the temperatures the camera reaches as a result of the thermal conditions in the chamber. The chamber will be brought down to a vacuum and run through a five orbit thermal cycle. Throughout this process, the camera will be programmed to take images of six mounted LED lights – two of each red, green, and blue. The passing criteria of this test include: relatively high level of functionality of the camera as monitored through visual inspection of the image capture and clarity. (Expected completion date: May 2010)

The Avionics Test is to be performed to verify the compatibility between the camera signal converter board and the CASTOR flight electronics by demonstrating the ability to capture and store images in the flight computer. The camera will be secured to the camera signal converter board that will then be connected to the flight computer. Power will be supplied to both the camera and the computer. A diagnostic routine will be initiated on the computer issuing commands to the camera to take images. The passing criteria of this test include: verification of image receipt and proper image storage. (Expected completion date: May 2010 – prior to the SHOT II test)

The Vibration Tests I & II are to be performed to verify the robustness of the camera mechanical design thus ensuring that it will comply with launch survival requirements. The camera and enclosure will be affixed to a shake table. For Test I (Broadband Dynamics), the broadband profile specified by the University Nanosatellite Program will be used as the input dynamics. Upon completion of this cycle, the unit will be removed from the shake table and visually/functionally assessed. For Test II (Shock Loading), the camera and enclosure will be re-affixed to the shake table. A shock loading will serve as the input dynamics. Upon completion of this cycle, the unit will be removed and assessed as before. In each case, no acceleration data is to be recorded. The passing criteria of both of these tests include: the complete physical integrity of the camera enclosure determined via a visual inspection and the maintained electronic functionality of the camera determined via an image capture/receipt/clarity verification. (Expected completion date: August 2010)

The Integrated Camera Function Test is to be performed to verity the integrated functionality of the camera for imaging the CASTOR thruster in flight-like conditions by demonstrating the ability of the camera subsystem to effectively monitor the cathode ignition and plume qualities. This test is comprised of two subtests: the cathode ignition test and the plume characterization test. The satellite with the camera/enclosure will be placed in a vacuum chamber that will be brought down to a vacuum. The camera will be initialized such that an image is captured every second. Cathode ignition will be initialized and a response will be measured by the camera. The passing criterion for this subtest includes: confirmation of the cathode ignition by the camera. After the cathode has been ignited, the Diverging Cusped Field Thruster (DCFT) will be run through its full range of power settings over a course of 60 minutes. Data will be collected from the camera at one image per minute. These data will be archived for analysis after the test sequence to demonstrate that the camera images can be used to characterize the thruster performance via plume color and shape. The pass criteria for this subtest includes: the ability of applying a post-test analysis of the image data to determine the thruster energy level to within 5% of the actual level given by the known DCFT setting during the test. (Expected completion date: September 2010).

2.8 STRUCTURES

2.8.1 SATELLITE OVERVIEW (E. PETERS)

Structural Requirements

The CASTOR structure configuration is driven by requirements defined by CASTOR subsystems and UNP[1]. Key requirements include:

- Provide a means of attachment for all components.
- Dimension and Mass Requirements:
  - Volume: 50cm X 50cm X 60cm.
  - Mass: < 50 kg.
- Launch Environment Requirements:
  - Factors of Safety: 2.0 for yield, 2.6 for ultimate.
  - Loading: ±20 g along X, Y, and Z principal axes.
  - Fundamental Frequency: >100 Hz in all directions.
- Center of Mass Constraints:
  - Within 40cm of interface plane.
  - Within 0.5cm of Lightband centerline (+X Axis).
- Provide sufficient surface area for solar arrays to meet power requirements.

Structure Overview

The satellite has two configurations: the Stowed Configuration and the Deployed Configuration, which will occur during launch and after launch, respectively. The primary motivation for a dual-configuration structure is CASTOR's power requirements: while the Stowed Configuration meets UNP's volume and frequency requirements and has a higher likelihood of surviving launch conditions, the Deployed Configuration provides more solar cell exposure. The two configurations are depicted in Figure 2.8-1

[1] NANOSAT 6 USER'S GUIDE. AFRL Space Vehicles Directorate. January 2009.

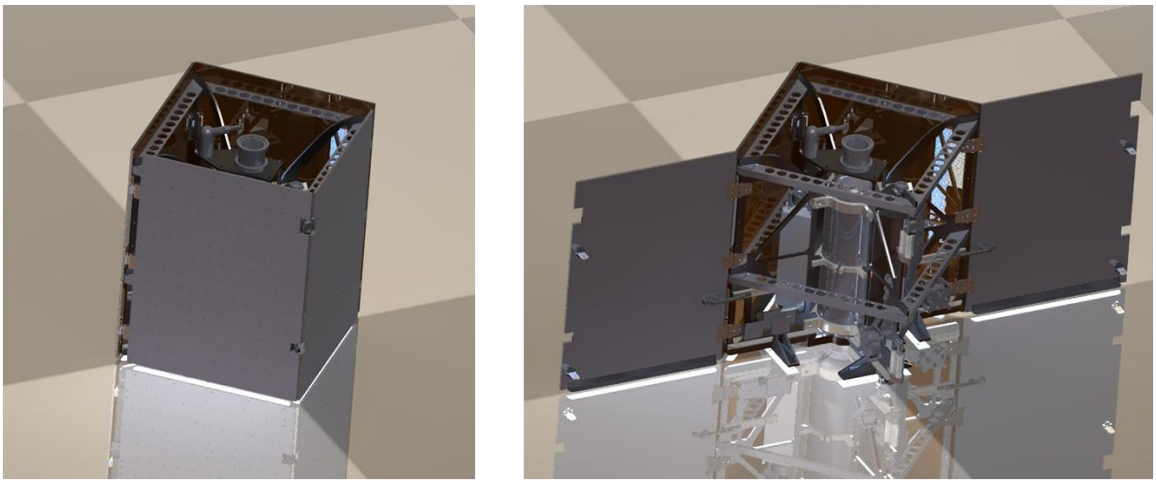

FIGURE 2.8-1: CASTOR STOWED AND DEPLOYED CONFIGURATIONS

Coordinate System

CASTOR's coordinate system, which is a right-hand coordinate system, is reflected in Figures 2.8-2 and 2.8-3 for the Stowed and Deployed Configurations, respectively. These figures employ "bottom view" perspectives; the positive X direction is into the page, while the direction of thrust is out of the page. Note that the origin of the CASTOR satellite is defined geometrically as the intersection between the satellite interface plane (Y-Z axis) of the ESPA Lightband and the central axis of the Xenon tank (X axis).

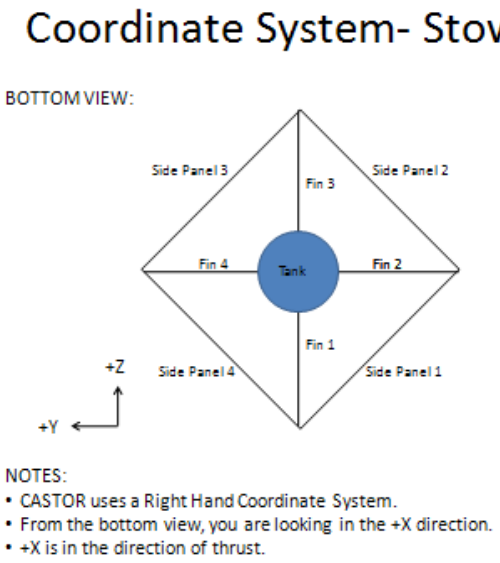

FIGURE 2.8-2: COORDINATE SYSTEM IN THE STOWED CONFIGURATION

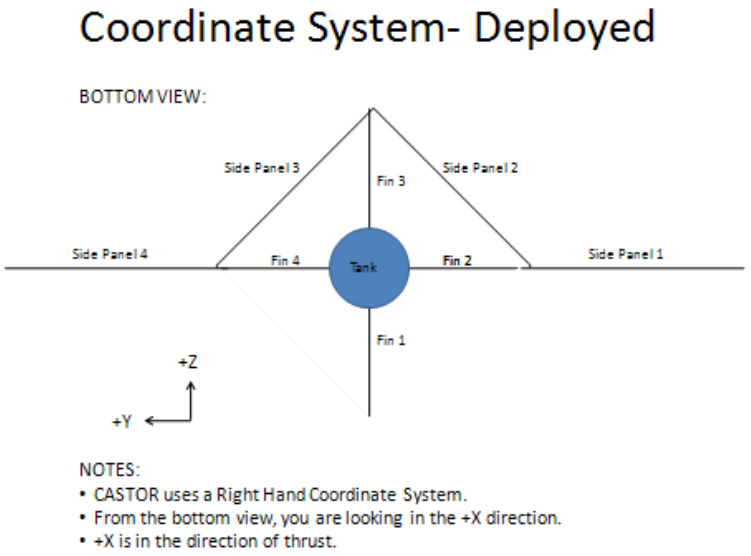

FIGURE 2.8-3: COORDINATE SYSTEM IN THE DEPLOYED CONFIGURATION

Recent Modifications

During Spring – Summer 2010, the Structures Team modified the satellite's overall structure in an effort to: (1) address CDR feedback regarding ways to reduce risk and complexity; (2) ensure that the satellite will survive launch conditions; (3) simplify integration; and (4) minimize mass while still accomplishing these goals. Specific modifications include, among others:

1) Modifying placement, interfacing, and mount design of several non-structural components based on new, higher fidelity models, and other considerations.
2) Shifting the tank section up by 10 cm, to raise the Xenon tank nozzle out of the Separation Interface Plane
3) Creating two separate avionics boxes, one each for high- and low-voltage components.
4) Revising the Bottom Tank Clamp to allow for easy installation/removal of the Xenon tank.
5) Creating a new Lightband interfacing bracket that meets structural requirements.
6) Modifying solar panels to include cut-outs for various components, and to meet a new understanding of UNP requirements.

2.8.2 CAD MODEL (E. PETERS)

CAD Overview

The objective of the Unified CAD Model (UCM) is to provide a three-dimensional simulation of the satellite, including all parts, components, and hardware. The UCM is a helpful tool for determining satellite configuration, estimating center of mass and moments of inertia, and performing mechanical and thermal analyses.

The CASTOR UCM is a SolidWorks-based assembly organized by parts and subassemblies using a six-digit drawing numbering scheme. Table 2.8-1 summarizes the satellite's dimensions, mass, and inertial properties. Note that the external dimensions in the Y and Z directions take into account the thickness of bolt heads external to the solar panels. When these are considered, the true Y and Z external dimensions still adhere to UNP volume guidelines, with approximately 3mm in margin. Furthermore, the total mass estimate comes from the Master Equipment List (MEL), which accounts for several items not included in the CAD model, namely the wiring harness. The calculated center of mass is relative to the CASTOR coordinate frame, and does not include the mass of the wiring harness. The subsequent figure depicts the CASTOR satellite in the deployed configuration.

It should be noted that the current dimensions exceed the limits imposed by UNP. The throat of the Xenon tank previously extended past the separation interface plane. The tank section was thereby raised to prevent this. A volume waiver is currently being sought.

Property	**Requirement**	**Current Estimate**
External Dimensions (x,y,z) (cm)	(60, 50, 50)	(69.61, 49.81, 49.81)
Mass (kg)	< 50	40.57 (45.86 margined)
Center of Mass (x,y,z) (cm)	(>-40, <0.5, <0.5)	(-36.763, 0.621, 0.612)
Moments of Inertia (Ix, Iy, Iz) (kg*cm^2)	N/A	Ix = (0.991, -0.053, -0.123) Iy = (0.120, 0.763, 0.635) Iz = (0.060, -0.644, 0.762)

TABLE 2.8-1: CASTOR STRUCTURAL PROPERTIES

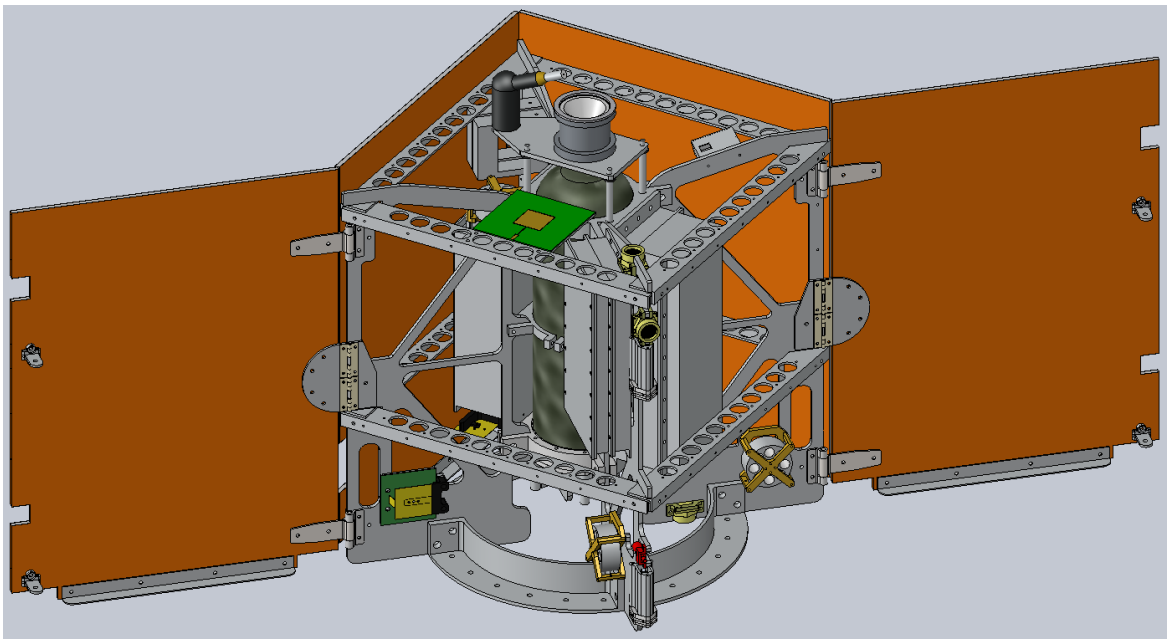

FIGURE 2.8-1: CASTOR DEPLOYED CONFIGURATION

Structure Organization: Major Sub-Assemblies

The structure of the satellite is centered symmetrically around the propellant tank in the stowed configuration. The thruster, battery, and large avionics assembly are mounted on the tank clamps. This configuration keeps the most massive components closest to satellite's strongest structures, and helps to ensure that the satellite's center of mass is nearly concentric with the X-axis. The propellant tank is cradled by three tank clamps designed to transfer loads around the tank to mitigate structural loading on the pressure vessel. The tank clamps connect to four trusses clocked at 90° increments. The trusses are further supported by eight angle braces spanning the diagonal between each exterior truss edge. Combined, the trusses and braces support the four solar panels and connect the satellite to the ESPA Lightband.

CASTOR's structure can be divided into 4 primary assemblies: the Tank Section, the Truss Section, the Solar Panel Section, and the Trans-Structure Section. This organization is used to determine part numbers and subassemblies for the UCM. These subassemblies keep the various components grouped by section and reduce the number of single components used in the master assembly.

The Tank Section is comprised of the centrally located Xenon Tank and surrounding components. Among these components are 3 tank clamps that cradle the tank, 2 tank plates fastened to those tank clamps, and the Thruster Mounting Assembly that supports the Diverging Cusped Field Thruster.

Next, the four trusses that connect to the tank clamps and components mounted to them make up the Truss Section. These trusses integrate the satellite together by interfacing with components from all three other structural sections. Moreover, the trusses serve as mounts for components from non-structure subsystems, such as reaction wheels, a patch antenna, the plumbing system,

and more. With the exception of the Small Avionics Box, the more massive components – namely the Large Avionics Box and Battery Box – are mounted to the tank clamps, to reduce the required mass of the trusses, among other reasons.

CASTOR has four solar panels: two deployable and two body-fixed. The satellite remains in a stowed configuration when the deployable solar panels are stowed during launch. It enters the deployed configuration when the deployable solar panels are released after insertion into orbit. All four solar panels are composites of aluminum face sheets and a honeycomb aluminum core. Solar cells are mounted to FR4 printed circuit board sheets, which are then fixed to the exterior face of the panels with epoxy.

Finally, the Trans-Structure Section includes both structural brackets and non-structural parts that span across several sub-assemblies. Key examples of such non-structural components include the plumbing system for the Xenon tank and the wiring harness. Among the structural brackets are: (1) Solar Panel Braces, which both provide stiffness between the trusses and prevent the formation of a drumhead mode in the center of the solar panels; (2) Lightband bracket, which interfaces between the four trusses and the ESPA mount; and (3) solar panel support braces, which further stiffen the solar panels.

2.8.3 INTERFACING (E. PETERS)

The components shall be mounted to the trusses using steel bolts; the lengths and type of bolt shall depend on the component. Tables 2.8-2 – 2.8-8 show the current bolts that are needed and a brief description of relevant information.

TABLE 2.8-2: CURRENT BOLT INFORMATION ADCS

	System	Mount To:	#	Bolt Type	Mounting Information
ADCS	Reaction Wheel	Truss	12	M3 x 3”	There are 3 wheels (one on truss #1, one on truss #4, and one on the X-face of the battery box)
	Sun Sensor	Truss	8	2-56 x ½”	4 sun sensors distributed between trusses 1, 2, and 3. 2 bolts and 1 pin per sensor.
			4	M2 alignment pins	
			8	10-24 x 1”	
	GPS Antenna	Truss 1	2	10-24 x 1”	
	Magnet Bracket	Bottom Tank Clamp	4	10-24 x 3.5”	Bolted into bottom tank clamp
	Torque Coils	Braces/Trusses	-	-	Held in place with zip ties

TABLE 2.8-3: CURRENT BOLT INFORMATION AVIONICS

	System	Mount To:	#	Bolt Type	Mounting Information
Avionics	High-voltage avionics assembly	Tank Clamps	4	1/4-20 x 5/8”	Shorter bolts for middle hole in top/bottom clamps
			2	1/4-20 x 7/16”	
	Low-voltage avionics assembly	Truss 1	4	1/4-20 x 5/8”	Shorter bolts for middle hole in top/bottom clamps
			2	1/4-20 x 7/16”	
	Wiring harness mounts	Various			

TABLE 2.8-4: CURRENT BOLT INFORMATION COMMUNICATIONS

	System	Mount To:	#	Bolt Type	Mounting Information
Comm	Patch Antenna Bracket	Various	6	10-24 x 5/8”	Face +X and –X directions; cantilevered off truss 4
	Patch Antenna	Various	12	8-32 x 5/8”	Two attached to brackets, one attached to Solar Panel 4
	Antenna Splitter	Truss 4	4	6-32 x 1”	-

TABLE 2.8-5: CURRENT BOLT INFORMATION PROPULSION

	System	Mount To:	#	Bolt Type	Mounting Information
Propulsion	Xenon Tank	Tank Clamps	-	-	No bolts into tank; cradled by clamps
	Relief Valve	Truss 3	2	10-24 x 0.75”	2 bolt holes separated by 0.75”
	Pressure Regulator	Truss 3	2	10-32 x 0.75”	2 bolt holes separated by 0.75”
	Latching Solenoid	Truss 3	2	4-40 x 0.5”	2 bolt holes separated by 0.375”
	Flow Controller	Mounting Plate	4	4-40 x 0.75”	2 flow controllers
	Flow Controller Mounting Plate	Truss 3	4	10-24 x 5/8”	Mounted to top of Truss 3
	Cathode Heater	Thruster Mounting Plate	6	4-40	-
	Cathode Keeper	Thruster Mounting Plate	3	4-40	-
	Anode	Thruster Mounting Plate	4	8-40 x 5/8”	-

TABLE 2.8-6: CURRENT BOLT INFORMATION POWER

	System	Mount To:	#	Bolt Type	Mounting Information
Power	Anode Converter	High-Voltage Avionics Box	4	4-40 x 0.75”	Mounted through bottom of box into converter
	MPPT	High-Voltage Avionics Box	4	10-24 x 5/8”	-
	Battery Box	Tank Plate	10	4-40 x 0.5”	-
	Tank Plate	Tank Clamps	4	1/4-20 x 5/8”	Smaller bolts go into middle holes of clamps
			2	1/4-20 x 7/16”	

TABLE 2.8-7: CURRENT BOLT INFORMATION LAUNCH VEHICLE

	System	Mount To:	#	Bolt Type	Mounting Information
LV	Lightband Ring	Lightband Brackets	24	1/4-28 x 1”	Mounted through bottom of ring into brackets
	Thermal Sensors	Various	-	-	20 thermal sensors, all attached via thermal adhesive

TABLE 2.8-8: CURRENT BOLT INFORMATION STRUCTURES

	System	Mount To:	#	Bolt Type	Mounting Information
LV	Tank Clamps	Trusses	8	3/8-16 x 1.5”	8-32 bolts for middle tank clamp
			4	8-32 x 1.5”	
	Solar Arrays	Trusses	26	10-24 x 0.5”	20 thermal sensors, all attached via thermal adhesive
	DMB	Truss 3	4	10-24 x 5/8”	Truss 3
	Hinge	Trusses	8	10-24 x 5/8”	Trusses 1 and 4
	HMB	Trusses	8	10-24 x 5/8”	Trusses 1 and 4
	SPB Bracket	Trusses	8	10-24 x 5/8”	2 on each truss
	SPB	SPB Brackets	16	10-24 x 3/8”	Flat-head machine screws
	Spring Hinge	Spring Hinge Plate	16	6-32 x 0.25”	Flat-head machine screws
	Spring Hinge Plate	Trusses	4	6-32 x 5/8”	Trusses 1 and 4
	SPRM	Truss 1	4	10-24 x 1”	-

2.8.4 TANK CLAMPS (E. PETERS)

Three centrally located tank clamps serve (1) to integrate the entire primary structure, and (2) to provide an interface between the xenon fuel tank and the primary structure by cradling the tank. All three clamps are concentric with the tank and the X-Axis, with the Bottom Tank Clamp located the farthest in the +X direction, the Top Tank Clamp the farthest in the –X direction, and the Middle Tank Clamp in between. The three clamps are shown integrated with other components in the Tank Section in Figure 2.8-2: Tank Section.

FIGURE 2.8-2: TANK SECTION

The tank clamps are focal components within the satellite's primary structure, as they connect most other key primary structure components together. All three clamps interface with all four trusses and both tank plates—on which the majority of CASTOR's components are mounted. In addition, the Thruster Mounting Assembly is attached to the Top Tank Clamp. The Top and Bottom Tank Clamps, which are 1" thick, are fastened to the trusses with 3/8" bolts and to the tank plates with 1/4" bolts, whereas the ½" thick Middle Tank Clamp is fastened to both the trusses and the tank plates with #8 bolts.

In order to fully constrain the Xenon tank, the Top and Bottom Tank Clamps have concave curvature to match the shape of the tank. This can be seen in Figures 2.8-6 and 2.8-7. While the Top Tank Clamp is a single piece, the Bottom Tank Clamp is a two-piece assembly that consists of the clamp and a cap. The cap contains the concave surface, and is bolted to the clamp after the tank is inserted. This allows the tank to be easily inserted or removed during the integration process. The Middle Tank Clamp has no such curvature, but rather consists of two halves that can be tightened together to increase lateral friction. Strips of low-outgassing, silicone rubber [TBR] will be included between the tank and the three clamps to allow for minute error and prevent damage to the tank's surface.

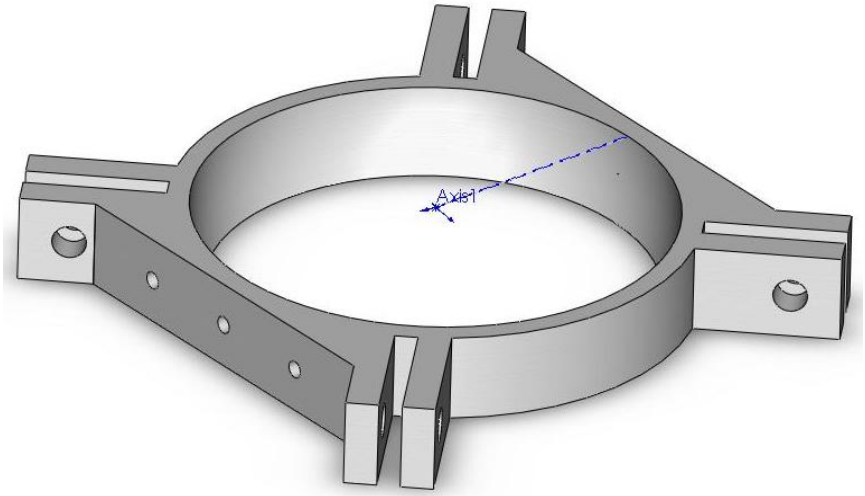

FIGURE 2.8-6: TOP TANK CLAMP

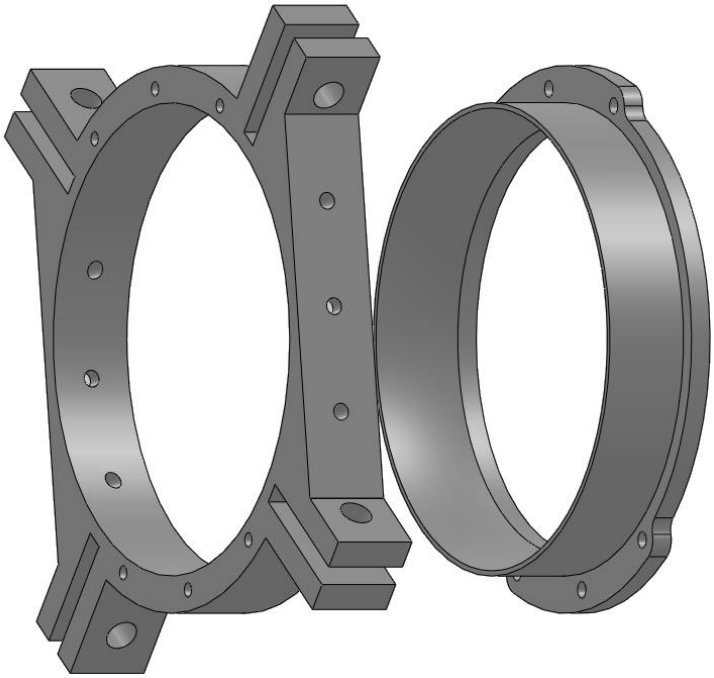

FIGURE 2.8-6: BOTTOM TANK CLAMP

2.8.5 SOLAR PANEL DEPLOYMENT (E. PETERS)

Design Overview

Two mechanisms govern solar panel deployment: the Solar Panel Release Mechanism (SPRM) and the Solar Panel Deployment Mechanism (SPDM). While the SPRMs control *when* the solar panels deploy, the SPDMs affect *how* they deploy, in addition to ensuring that the satellite maintains its Deployed Configuration once attained. To reduce the risk of premature deployment, two independent SPRMs will be employed to constrain the deploying solar panels. There are also two SPDMs, but each SPDM only interfaces with a single, whereas both SPRMs interface with both deploying solar panels.

Solar Panel Release Mechanism (SPRM)
In designing the Solar Panel Release Mechanism, the following factors were considered: (1) striving for simplicity to maximize the probability of successful solar panel deployment; (2) lowering mass and power requirements to minimize impact on the mass and power budgets; (3) incorporating a reasonable margin for error, (4) ease of manufacturing.

Each SPRM is restrained by a linear actuator. Once activated, the actuator will retract its pin, after which the two solar panel pins attached to each of the adjacent solar panels will be released. Then, with the help of the Solar Panel Deployment Mechanism, the solar panels will be able to deploy. This SPRM will constrain the deploying Solar Panels in the X, Y, and Z directions at two points. During launch, these rigid constraints serve the added purpose of stiffening the solar panels, increasing the vibration resistance.

The SPRM consists of the following components: two solar panel pins, one linear actuator and pin, and one main bracket that attaches the mechanism to the primary structure. The bracket will be made of several 1/4" and 1/8" thick aluminum extrusions for ease of fabrication. The two SPRMs are both located on the farthest point of Truss 1 in the –Z direction. The integrated SPRM is depicted in Figure 2.8-7.

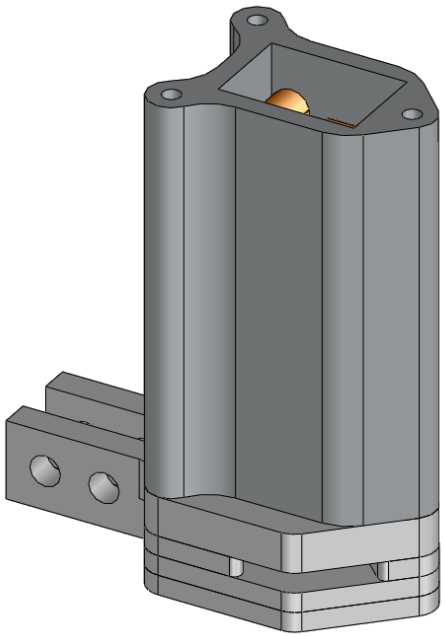

FIGURE 2.8-7: SOLAR PANEL RELEASE MECHANISM

The SPRM Bracket consists of 4 stacked aluminum plates: 2 1/8"-pieces in the middle that constrain each of the solar panel pins in the Y and Z directions, and 1/4" and 1/8" pieces on the top and bottom, respectively, that (a) constrain the solar panel pins in the X direction; (b) constrain the actuator pin in the YZ plane; and (c) attach the mechanism to the primary structure. The four extrusions are bolted together with three bolts. Manufacturing the bracket out of four pieces – as opposed to machining the bracket from a single piece – is necessary because the slots for the solar panel pins have a complex geometry and are not aligned with each other, and hence

must be machined individually. The second iteration of the SPRM is depicted below in Figure 2.8-8.

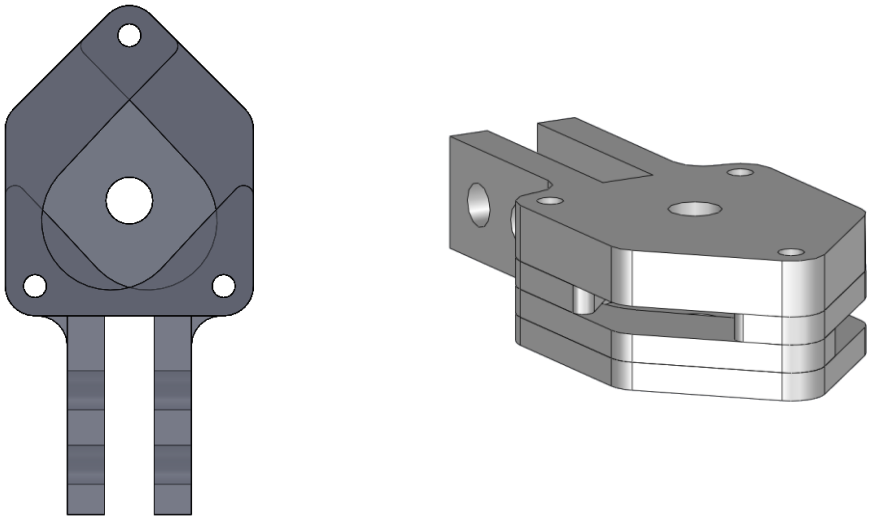

FIGURE 2.8-8: SPRM BRACKET, TOP VIEW (LEFT), ISOMETRIC VIEW (RIGHT)

The Solar Panel's path of release has a radius of curvature of 18.44", which is the distance between the SPRM and the pivots of the hinges about which the Solar Panels rotate when they deploy. The solar panel pin, therefore, has an identical curvature. As a result, due to machining considerations, the pin is uniformly shaped in one dimension. The pins attach to the solar panels bolts and corresponding inserts, which will be included to bolster the panel's structural integrity (specifically, that of its honeycomb core).

Because there will only be two SPRMs on Truss 1, each SPRM will have to be able to withstand 50N loading from each solar panel. Static analysis has shown that this part will be able to withstand 50N loading with a lowest factor of safety (FOS) of 6.44. Whether the forces of both panels were applied simultaneously or not made no difference in the results, as the lowest FOS occurs in the solar panel pins (which are independent of each other), not the solar panel bracket. These calculations assumed that the force was normal to each solar panel; any other direction would result in a higher FOS because of the larger cross-sectional axial area of the solar panel pins. All of the pieces of the SPRM bracket were approximated as one component.

Solar Panel Deployment Mechanism (SPDM)

The SPDMs serve three primary functions: (1) provide the force necessary to rotate the deploying solar panels once the SPRMs are actuated; (2) provide a physical mechanism that stops the deploying solar panels from rotating once they become co-planar with Trusses 2 and 4; and (3) provide a limitation on the deploying solar panels' movement after they are deployed. The current SPDM design and its position with respect to the primary structure is illustrated below in Figure 2.8-3.

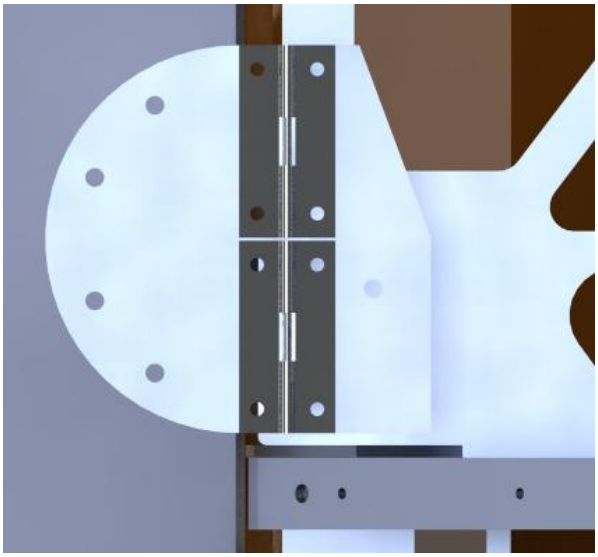

FIGURE 2.8-3: SOLAR PANEL DEPLOYMENT MECHANISM

Originally, Delrin inserts combined with strategically placed springs formed the deployment mechanism. After the SPRMs released, the springs would begin rotation, until 45 degree Delrin inserts within the deploying solar panels came in contact with the side faces of the fixed solar panels. The springs would continue to exert a force after this deployed state was reached, in order to limit further motion of the solar panels. This design was abandoned due to manufacturing problems with the deploying solar panels, mass considerations, and doubts about it functionality.

The current design uses spring-loaded hinges with a mechanical stop. The spring-loaded hinges are of a smaller plate thickness than the main hinges being used. A mounting plate is therefore required to keep the axis of rotation of the spring-loaded hinges concentric with the axis of rotation of the main hinges. The interior faces of the mounting plates were designed to contact each other once the rotation reached 180 degrees, and prevent further rotation.

It can be assumed that attitude adjustment maneuvers will impart small disturbances on the deployed solar panels. While the spring-loaded hinges provide a sufficient moment when fully-compressed to successfully deploy the panels, they do not provide a sufficient restoring moment for small (< 10 degrees) displacement from the deployed configuration. To remedy this, a locking mechanism is being considered. This mechanism will utilize tape springs mounted to both the truss and the solar panel such that the convex portion points away from the solar panel when deployed. In this orientation, movement of the panel would require buckling the springs. This mechanism is currently being prototyped.

2.8.6 SOLAR ARRAY (L. SHUMAKER)

Requirements

The solar array and accompanying structure must meet loading and frequency requirements specified by UNP. In particular, the frequency requirement—that the satellite design have a first

natural frequency of 100 Hz or more—is of concern in designing the solar array. In addition, the solar array must maximize area available for power generation (requirement of the Power team) while obeying spatial requirements from UNP and ideally use the least possible amount of the UNP mass allocation while remaining a robust and reliable structure. While the stowed design of the solar panels allows for some power generation, proper and reliable deployment of the two deployable panels remains a primary requirement for the structure since power generation is key to mission success.

Design

Current architecture of the satellite places the propellant tank in the middle of the structure, with four trusses protruding from the tank clamps in an X shape. The solar panels are attached to these trusses in their stowed positions by mounting brackets which are bolted to the fins and bolted to the edges of each solar panel. When stowed, the satellite presents four rectangular solar panels with outward-facing cells. This allows some solar collection before the panels deploy. When deployed, the edges of two of the panels (referred to as the deployable panels) release from one of the trusses and pivot to lie parallel to the trusses while remaining connected to the structure by hinges, as shown in Figure 2.8-4.

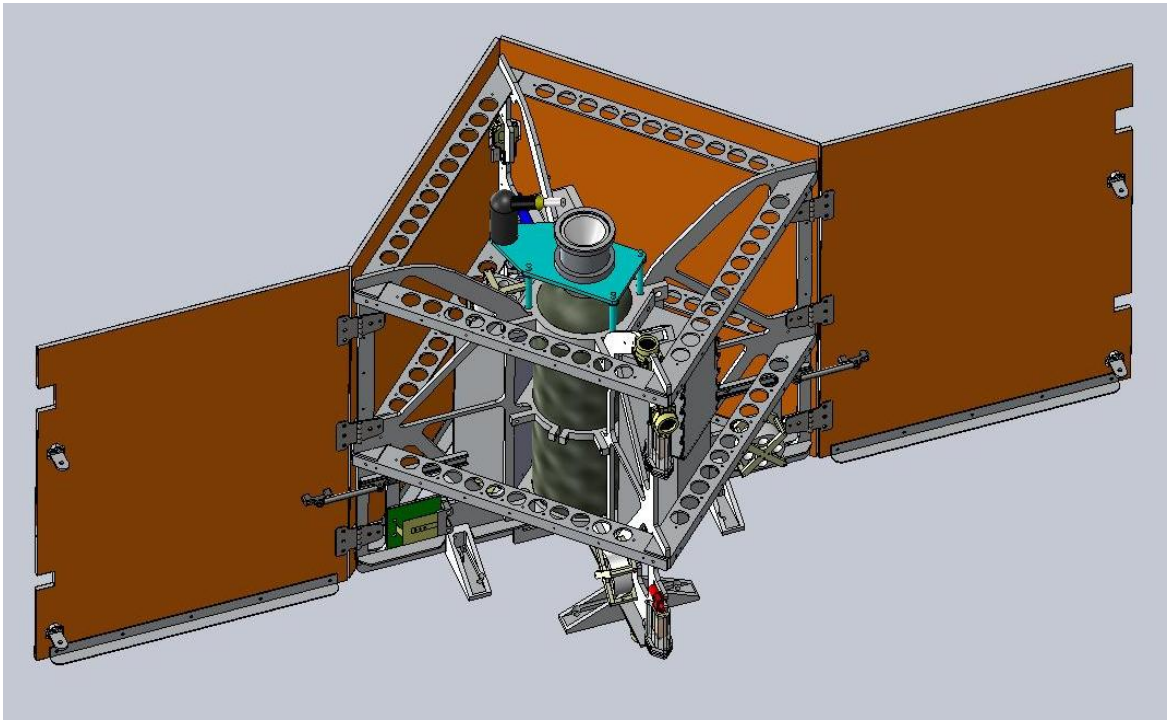

FIGURE 2.8-4: SOLAR PANELS IN DEPLOYED CONFIGURATION

To address the requirement that the satellite fit inside a 50cm x 50cm x 60cm box when in the stowed configuration (with the two deployable solar panels stowed against the trusses), each of the four solar panels must actually be narrower than 50cm by twice the thickness of a panel. Currently, the solar panels are 0.25” thick, thus the maximum panel dimensions are 60cm x 43.2

cm. These dimensions are for the FR-4 on aluminum honeycomb composite on which the solar cells will be mounted, and include all area for solar cells, wiring, and space necessary to attach solar panel mounting brackets to each panel in the array.

FR-4 on aluminum honeycomb composite has been chosen as the substrate material over either aluminum sheet on aluminum honeycomb or an carbon fiber on aluminum honeycomb because of concerns over not meeting the frequency requirement, conduction between solar cells through the face sheet material, and exceeding the UNP mass limit. The FR-4structures performed better than the carbon fiber and aluminum composite during vibration testing and thermal issues can be overcome through the use of properly specified surface treatments. The current design also offers significant mass savings over the other two options, which would have needed additional PCB layers.

Previously, both deployable solar panels included a chamfered edge that served as a stop when they deployed. This edge was the side of a Delrin tab that protrudes from underneath the face sheet as shown in

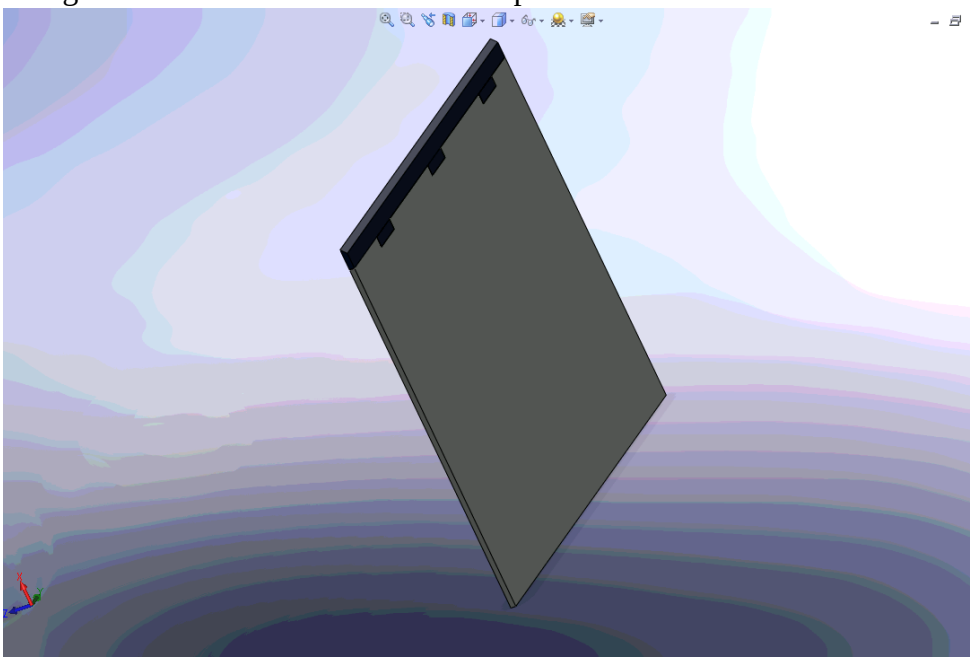

Figure 2.8-5.

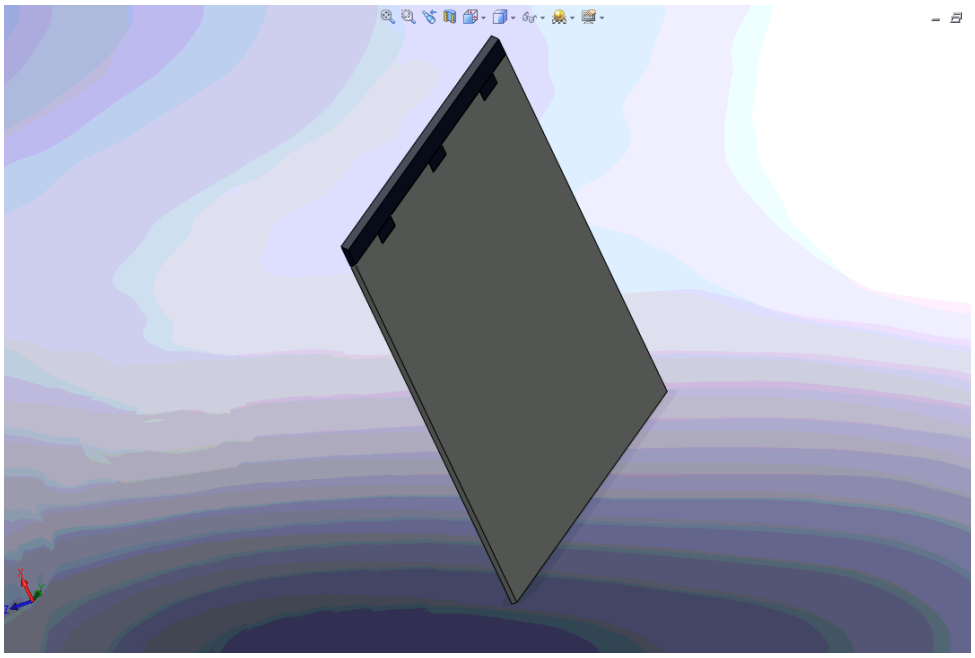

FIGURE 2.8-5. HONEYCOMB AND DELRIN LAYUP WITHIN A DEPLOYABLE PANEL

Since the inclusion of this tab introduced manufacturing problems and delaminated during vibration testing –penalizing the satellite's fundamental frequency—it is no longer included in the design. Its purpose, to ensure deployment at the proper angle, is now taken care of by the solar panel deployment mechanisms (SPDM), and thus the design still meets requirements and is simpler and more robust than previously.

Panel Connector Arrangement

Between two to four mounting brackets will be used per side of each of the body-mounted panels. Three hinge mounted brackets will be used on each deployable panel as well as two solar panel release mechanisms (SPRM). These brackets fix the panels to the trusses (in the case of the two body-mounted panels) and to the hinges and to the trusses in the stowed configuration (in the case of the two deployable panels). Each static bracket or release mechanism is attached to the panels with one bolt. Each hinge is attached to the panels with three bolts. Furthermore, one SPDM will connect each deployable panel to the trusses that support the hinges as well. Each bolt hole will contain two flanged inserts (McMaster-Carr part number 93835A340) placed end to end that will help clamp the face sheets onto the composite substrate. The vertical spacing between bolt holes is determined by the optimal placement of clamping conditions such that a panel has a first natural frequency of over 100 Hz.

Load Considerations

In order to meet the criterion that the satellite structure withstand at least 20 G loading, finite element modeling was performed for a solar panel. Each panel weighs approximately one kilogram, so under launch conditions, the panel must withstand 200 N. A plot of the stress tensor generated by Patran and Nastran (FEM software) for a carbon fiber on aluminum honeycomb

panel is replicated below in Figure 2.8-6. The white areas are where the stress is zero, and the stress ranges up to 492 Pa at the bolt holes. In the light blue areas, however, the stress is only 110 Pa.

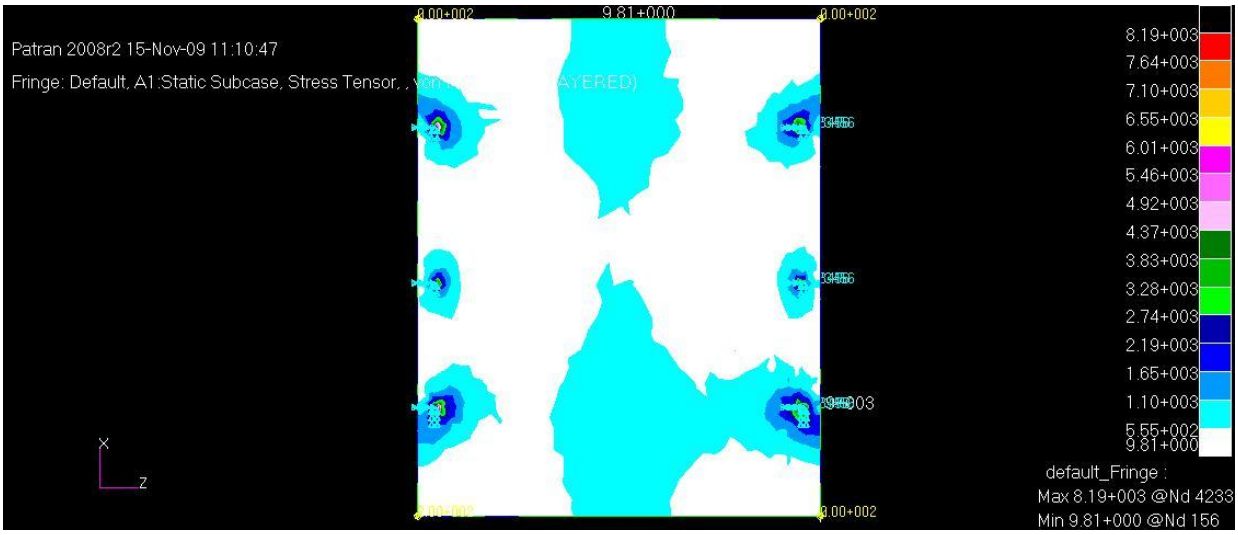

FIGURE 2.8-6: STRESS TENSOR UNDER 200N LOADING ON THE FACE OF A PANEL WITH THREE ATTACHMENTS PER SIDE

The yield strength of carbon fiber sheet ranges from 289 MPa upwards[2] and the 2% yield stress of aluminum honeycomb is 190 MPa [3]. Clearly, the composite panel structure will be able to withstand the requisite loads. Stress is concentrated at the connection points between the panel and mounting brackets, so the bolts will be appropriately sized to transfer loads safely from the panels to the primary spacecraft structure.

Frequency Considerations

Of more concern than the dynamic loading that the solar panels must bear is their natural frequency. The values of material properties and dimensions used in calculating frequencies are listed in **Error! Reference source not found.**.**Error! Reference source not found.**.

Parameter	Value	Source/Notes
Panel dimensions	48.6cm x 60cm	Constrained by UNP

[2] www.matweb.com. Accessed: 11/18/09.

[3] Paik, Jeom Kee, et al. "The strength characteristics of aluminum honeycomb sandwich panels". www.sciencedirect.com. Accessed: 11/18/09.

Panel thickness	0.678cm	Manufacturer's specifications
Density	210 kg/m^3	Experimentally determined
Mass per area (gamma)	14.2 kg/m^2	Experimentally determined
Modulus of Elasticity of Aluminum	1.3 GPa	Manufacturer's specifications
Modulus of Elasticity of Carbon Fiber	10 GPa	Manufacturer's specifications
Combined effective modulus	4.4 GPa	Calculated
Poisson's ratio (nu)	0.3	Assumed

TABLE 2.8-2: SOLAR PANEL PROPERTIES

Given the above parameters and assuming that the panel's frequency can be modeled as a rectangular pinned plate as in Figure 2.8-7, the frequency may be determined by the formula:

$$f = [\lambda^2 / (2\pi a)]*[Eh^3 / 12(\gamma(1 - \nu^2)]^{1/2}$$

Where E is the modulus of elasticity, γ is the mass per area, h is the panel thickness, ν is the Poisson's ratio, and λ^2 is a tabulated value based on geometric considerations[4].

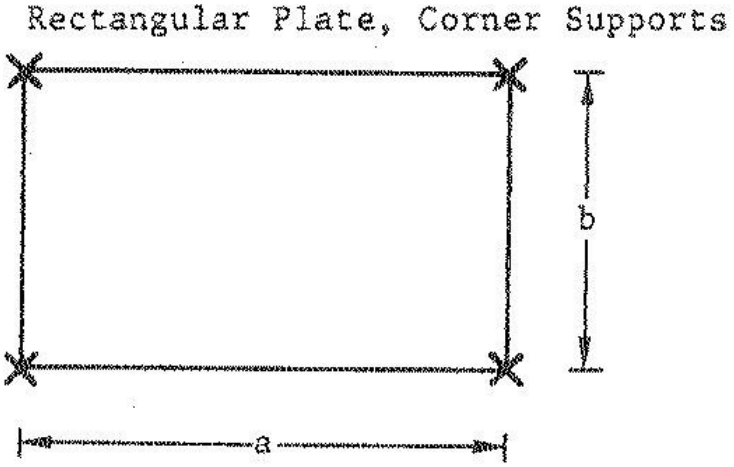

FIGURE 2.8-7. PLATE MODEL

With this model, the calculated frequency of the whole panel is 57 Hz. This model does neglect the fact that the plate is pinned in several locations on each side, but the calculated frequency for

[44] Blevins, Robert D. *Formulas for Natural Frequency and Mode Shape*. Krieger Publishing Company, Malabar: 2000. p. 269.

one bay (the rectangular area in between two horizontal sets of bolt holes) is only 41 Hz. If the two sides of length a in Figure 2.8-7 are considered simply supported or clamped (corresponding to reinforcing the panels across their span at each set of bolt holes with horizontal struts), the calculated frequencies are 285 Hz and 666 Hz, respectively. On the other hand, if the two sides of length b are simply supported or clamped (corresponding to attaching the panels to the fins along their length rather than at only three brackets), the corresponding calculated frequencies are 42 Hz and 98 Hz. Also, if the solar panels were made thicker, with 1.27cm thick honeycomb, the calculated frequency for the original pinned model is 101 Hz. Several design options available were assessed; additional horizontal aluminum struts and clamped vertical edge scenarios were analyzed with Patran and Nastran. Once more accurate models were obtained in this fashion, the three options—thicker composite, horizontal struts, or clamped edges—were assessed from a mass standpoint. All options require additional mass; however, horizontal struts also require some redesign of the solar panel brackets and release mechanisms, as does clamping the edges of each panel. Clamped edges also cut into available surface area for solar cells. These factors were taken into account, and the final solar panel design calls for two horizontal struts per panel, as well as solar panels supports along the bottom of each panel for additional stiffening.

Establishing Vibration Testing Capability

In order to compose a recommendations report for materials selection, the structures team must take into consideration the thermal properties and fundamental frequencies of the materials/composites under consideration, as well as their masses and certain subjective factors, such as ease of manufacture. To this end, it is necessary to design a low-cost and accessible vibration testing platform. The vibration experiment design is outlined in Figure 2.8-8.

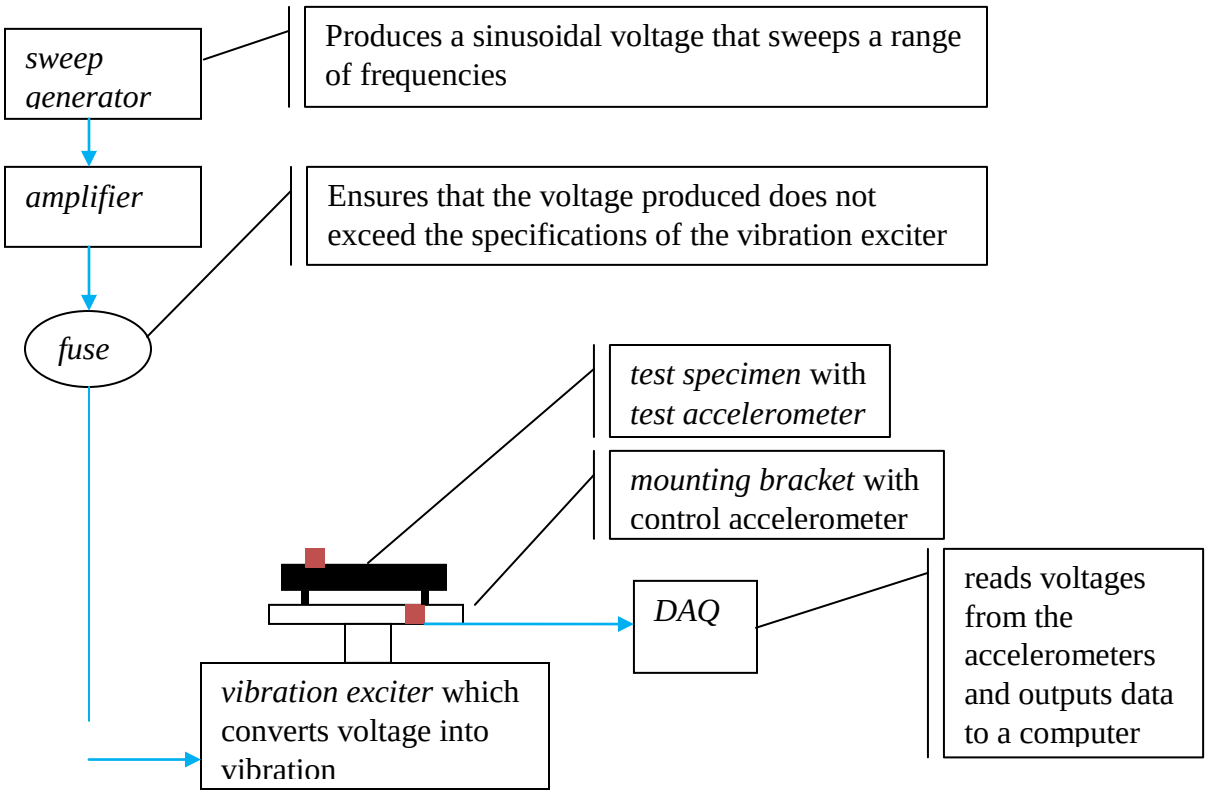

FIGURE 2.8-8: VIBRATION EQUIPMENT SETUP

Composite Testing

Three sample panels were fabricated for testing: aluminum face sheets on ¼" aluminum honeycomb, carbon fiber face sheets on ¼" aluminum honeycomb, and a ¼" thick aluminum isogrid with four bays. The purpose of testing these panels was threefold—these were three options considered for the solar panel design of CASTOR and the testing contributed to the final choice of material, (please see), experimental results could be compared to calculations based on tabulated models used to predict the modes of the solar panels during the design process (specific calculations for the carbon fiber composite and the aluminum composite are given below), and this set of tests also allowed reflection on the design of the vibration table setup (results given in the Analysis section below).

Calculations

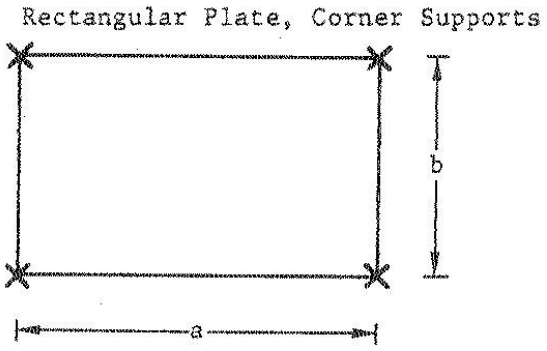

FIGURE 2.8-9: PLATE MODEL

Formula for frequency based on above boundary conditions[5]:

$$f_{ij} = \frac{\lambda_{ij}^2}{2\pi a^2}\left[\frac{Eh^3}{12(1-\nu^2)}\right]^{\frac{1}{2}}, i = 1,2,3\ldots; j = 1,2,3$$

Formula for stiffness factor of a composite plate (Blevins):

$$\frac{Eh^3}{12} = \frac{2}{3} * \sum_{k=0,1} E_k * (d_{k+1}^3 - d_k^3)$$

where E_k is the Young's modulus of each material in the composite layup and d_k is the distance of each material from the centerline of the plate.

TABLE 2.8-3: CARBON FIBER PLATE CHARACTERISTICS

Parameter	**Value**	**Source/Notes**
Plate dimensions (a x b)	6" x 3.25"	Measured
Geometric constant, λ^2	9.29	Approximation based on (a/b) and (Blevins, 283)
Poisson's ratio, ν	0.3	Assumed

[5] Blevins, Robert D. *Formulas for Natural Frequency and Mode Shape*. Krieger Publishing Company, Malabar: 2000.

Mass per area, γ	2.49 kg/m^2	Measured
Stiffness factor, Eh^3	3.13 x 10^4	Calculated using manufacturer's material data and formula listed above

TABLE 2.8-4: ALUMINUM COMPOSITE PLATE CHARACTERISTICS

Parameter	**Value**	**Source/Notes**
Plate dimensions (a x b)	6" x 3.25"	Measured
Geometric constant, λ^2	9.29	Approximation based on (a/b) and (Blevins, 283)
Poisson's ratio, ν	0.3	Assumed
Mass per area, γ	3.97 kg/m^2	Measured
Stiffness factor Eh^3	1.97 x 10^5	Calculated using manufacturer's material data and formula listed above

TABLE 2.8-5: PREDICTED FREQUENCIES

Composite	**Predicted first frequency**
Carbon fiber	2.06 kHz
Aluminum	4.29 kHz

Testing Results

Carbon Fiber Results

There was some sort of response (amplitude response in sample data versus the data from the control accelerometer, though not out of phase) and a definite 180° phase shift between sample accelerometer and control data at around 2.00 kHz (as predicted). The phase shift between the driving frequency (as reported by the control) and the output frequency (recorded by the sample accelerometer) occurs, by definition, at the natural frequency of the sample.

FIRST MODE (all numbers are approximate): 581 Hz (almost three to four times amplification)
Mode at: 720 Hz
Mode at: 2.00 kHz

Aluminum Composite Results

FIRST MODE: begins somewhere around 500 Hz, PEAKS at 860 Hz
Mode at: 1.43 kHz
Mode at: 3.99 kHz

Aluminum Isogrid Results

FIRST MODE: begins somewhere around 340 Hz, PEAKS around 530 Hz
Mode at: 770 Hz
Mode at: 1.87 kHz
Mode at: 2.06 kHz
Mode at: 3.32 kHz

Analysis

There are clear differences between the results of calculation and those produced by testing the sample composites. Before sources of error are considered, it should be noted that the boundary conditions assumed in the calculation were those shown in Figure 2.8-7—**Error! Reference source not found.**—pinned exactly at the corners of the plates—do not precisely match the actual situation where bolts were used to clamp the plates (with the bolt holes set in from the corners of the samples). That aside, the testing shows that the stiffest sample was the aluminum composite and that both it and the carbon fiber composite were preferable to the aluminum isogrid in this respect. For the actual solar panels, however, stringent mass limitations make carbon fiber composites more attractive than aluminum.

Sources of Error

Several sources of error exist in the testing setup itself; specifically, the use of electrical tape rather than a rigid standoff between the sample plate and the mounting bracket means that the input transfer between the vibration exciter and the sample being testing is neither perfect nor necessarily consistent. This may have some bearing on the accuracy of the measured modes. However, the tape should have damped out some of the input, artificially higher modes, so it cannot account for the discrepancies between the calculated frequencies and those returned by the tests. Also, the panels themselves had small thermocouples glued to them, though the small size of these devices is unlikely to affect the results of the tests. In addition to the thermocouples, the carbon fiber composite had a much larger diagnostic device affixed to one edge which conceivably could have significantly altered the results for this plate. In terms of errors present in the calculations, the effective stiffness factor of each composite plate did not take into account the material properties of the film adhesive in between the face sheets and the honeycomb. To check if this factor was responsible for the errors, calculations for the isogrid (which had no adhesive) should be compared to the modes found empirically.

Documentation of experiment results and user's guide for the testing apparatus is also compiled in DD-SSL_vibration_testing_appendix.pdf (located in 3.10-Structures on the fileshare).

Interfaces

The solar arrays interface with the main satellite structure through the solar panel mounting brackets, hinge mounted brackets, deployment mechanisms, and release mechanisms. Most importantly, since they generate power for the satellite, the arrays also interface with the power and propulsion system.

2.8.7 ESPA MOUNT (E. PETERS)

Requirements

The ESPA ring is located on the launch vehicle, under the primary payload. It allows secondary payloads to be carried by the vehicle without interfering with the primary payload. Integration of the satellite with the ESPA ring is achieved through the use of a motorized Lightband, produced by Planetary Systems Corporation. One side of the Lightband is affixed to the ESPA ring. The satellite is attached to the other side of the Lightband. After reaching orbit, the two portions of the ring detach, and the satellite is released. A method of securing the satellite to this structural device is necessary to ensure successful launch. The current design consists of four quarter-circle brackets that mount between the four trusses and interface all 24 holes of the Lightband. A detailed description of this bracket is the focus of this section.

Survival of launch loads was of primary concern in the design of this part. Solid transfer of loads between the satellite and the launch vehicle requires a rigid connection between the satellite and the Lightband. Separation of the satellite from the Lightband before deployment in space would be considered a catastrophic failure. A reliable interface between the satellite and ESPA Lightband must withstand the static and dynamic loads during launch.

Minimizing component mass, while still withstanding launch loading with the required factor of safety, is the objective of the Structures team. Ease of manufacture and assembly is also a priority, as the bolts on the bracket must be accessible so that they can be tightened down to torque-standards for both testing and launch.

UNP judges expressed concern that previous bracket design did not distribute loads evenly around the entire Lightband ring. As a result, the design was modified to better distribute loads and thus assuage concerns. The advantage of the new design is that it interfaces all 24 holes of the Lightband, as opposed to the former design, which only interfaced 16 holes.

Before a new design is accepted, finite-element modeling (FEM) is used to predict whether the bracket design meets structural specifications. If models show that the bracket design is sufficient, it is manufactured and subjected to static and vibration testing to validate the model. Previous modeling suggested that the initial design would not withstand these margined loads. Analysis of the current design has shown that it will survive launch loads with the required safety margins.

ESPA Bracket Design

The Lightband connection brackets serve as the only interface between the launch vehicle and the satellite. Thus, proper design of these brackets is critical for mission success, as well as launch safety. Prior designs of this part were insufficient to properly transfer loads or were too massive; hence a new bracket system was developed. An iterative process was implemented to factor in effects analyzed in ANSYS to design the part. Each bracket attaches to six Lightband bolts, and has two connection points on the truss. Bolts to the Lightband are 3/8-inch in diameter, to allow for a stiff connection. The L-channel design helps to distribute the moment caused by the cantilevered satellite and provides ample access space for a torque-wrench to tighten the bolts.

Locations of the brackets on the satellite are shown below in Figure 2.8-10 in the red circle.

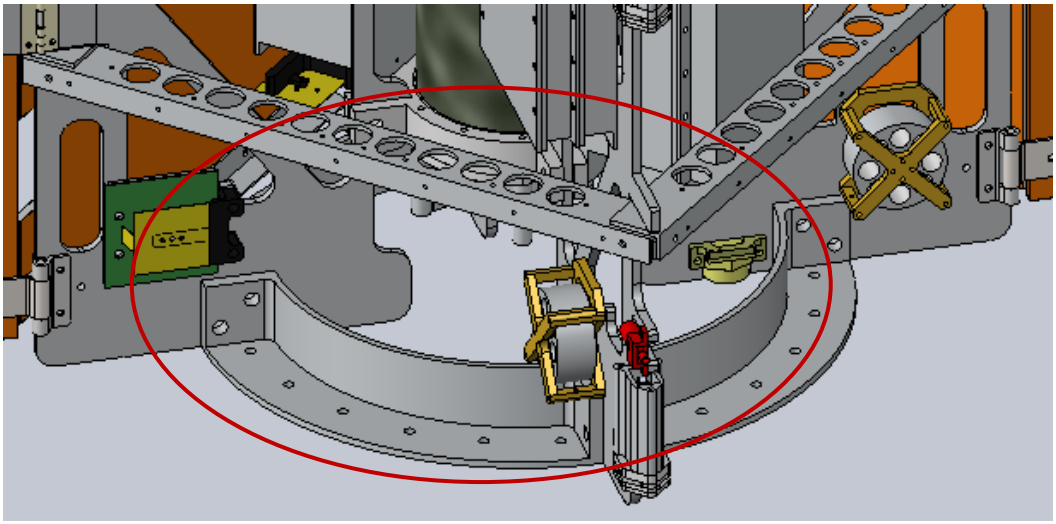

FIGURE 2.8-10: LIGHTBAND BRACKET LOCATIONS ON SATELLITE

The current design partially distributes the load across all of the Lightband holes. Though the load concentration is still greater where the four trusses interface with the brackets, a better distribution across the entire ring has still been achieved, which can be seen in Figure 2.8-19 below. In any loading configuration, loads in the Y-direction or Z-direction will be balanced between the four brackets. PSC (Planetary Systems Corporation), showed the following loading diagram (Figure 2.8-20) Lightband User's Guide.

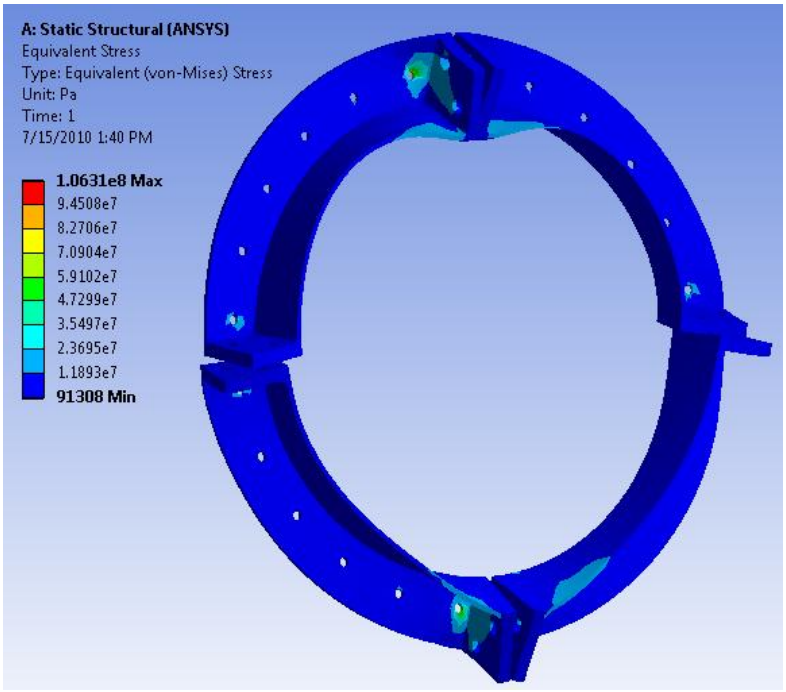

FIGURE 2.8-19: STRESS DISTRIBUTION ON NEW LIGHTBAND BRACKET

Design Considerations

As per UNP specifications, the Lightband mounting brackets must withstand 20-G loading with a factor of safety of 2.0 for yield and 2.6 for ultimate. The brackets must also interface all 24 holes of the Lightband ring.

Due to mass considerations, and the ease of using one material, aluminum was chosen as the base material. The footprint size on the truss was increased from previous designs, to allow for the use of 3/8”-16 bolts rather than 1/4”-20 bolts. This was done to reduce the stresses on the truss-bracket interface, which analysis showed to be the area of highest stress.

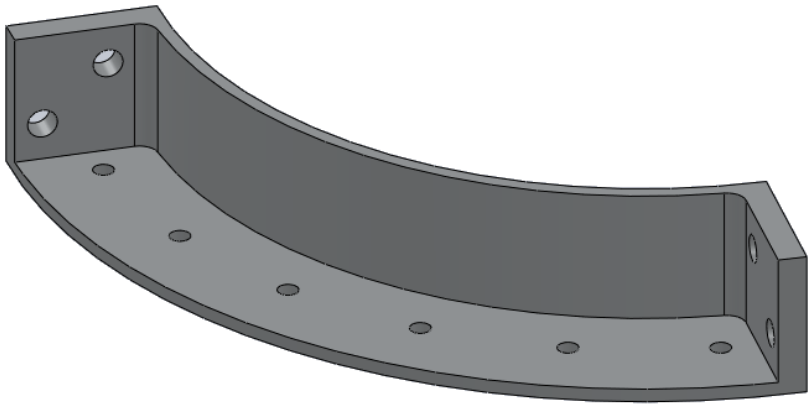

FIGURE 2.8-23: CURRENT BRACKET DESIGN

The previous bracket design was unable to withstand the force and moment produced by the satellite under 20-G loading conditions with the required factor of safety, and needed to be redesigned. Additionally, the full bracket assembly only interfaced with 16 out of the available 24 holes in the Lightband.

Assumptions and Calculations

Due to the 20-G margined launch consideration, each bracket must support a force of:

$$\frac{20 \times (9.8 \, m/s^2) \times (50 kg)}{4} = 2450 N.$$

This places a load of approximately 625N on each truss panel bolt.

Additionally, the moment produced by the satellite under this loading condition must be considered, since the satellite is mounted horizontally to the ESPA ring. The current center of mass of the satellite is 36.78 cm above the Lightband interface plane. Knowing this, the moment imposed on each mounting bracket by the satellite under 20-G loading is:

$$\frac{20 \cdot (9.8 \, m/s^2) \cdot (50 kg) \cdot (0.368 m)}{4} = 902 N \times m.$$

A simplification assumed that all forces are transferred through the bolts in the trusses. In reality, some forces are transferred by surface contact of the panel on the brackets and the panel edge on the Lightband itself. This means that the most critical axis is the X-direction (thrust vector) where these bolts are the sole holding mechanism (no surface contact forces).

ANSYS analysis showed that the new bracket design exceeds safety requirements, with a minimum factor of safety of 2.64.

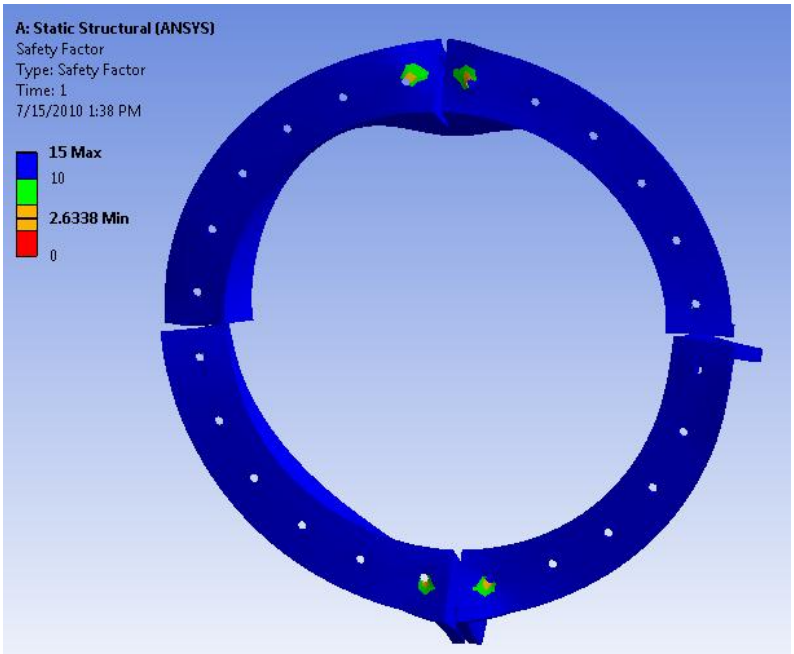

FIGURE 2.8-24: Lightband Analysis Results

2.8.8 LOADS AND MODES (L. SHUMAKER)

Due to the stringent structural requirements placed on this design, it is necessary to submit the spacecraft to a battery of structural testing. This testing is done in four major segments:

- individual component CAD analysis
- individual component empirical testing
- flight modelCAD analysis
- engineering model empirical testing

Individual component analysis is performed on all structural components during design and redesign. This is done using several methods so as to provide corroboration from one result to the next. The primary analysis and results used are those of the ANSYS Workbench Finite Element Model. Secondary analyses are performed using hand calculations, basic principles, and results obtained from literature to corroborate with finite element results. These numbers can be compared to the FEM in order to determine accurate behavior of the model. ANSYS Workbench was chosen to enable rapid iteration and optimization of the design due to its superior interface with Solidworks. The same preparation of a Solidworks model in Patran or ADINA would take many more hours than Workbench, which automates many of the actions, while still allowing the interfaces to be customized as the user wishes.

The individual empirical component testing is performed on components that are either difficult to model or on components that are particularly susceptible to vibration to ensure functionality when on orbit and to serve as benchmarks to validate the finite element models before the full

engineering model is analyzed and tested. This testing can be performed in-house with vibration testing platform developed for the project.

The engineering model analysis is performed to determine how the components interact with each other and what additional nonlinearities arise due to these interactions. Furthermore, many of the boundary conditions assumed in the component analyses do not flow directly to their interfaces with other components in the full engineering model. As a result, this analysis is particularly important in determining if the spacecraft itself is capable of meeting structural design requirements. Furthermore, it is highly desirable to have an engineering model finite element model that (1) can be trusted and (2) predicts that the spacecraft will meet design requirements before performing any integrated structural empirical testing. The analysis used to verify the structural model is described further in the **Error! Reference source not found.** section.

The empirical testing of the engineering model serves as the final structural verification of all models that have been produced and consists of two sets of tests: vibration testing, which was performed at the MIT Lincoln Laboratory shake table, and static testing, which is performed in-house using proof masses. These tests serve to not only prove that that the spacecraft will meet design requirements, but also to validate the finite element model and determine what modifications and additions may be added to the model to increase fidelity and accuracy.

Structural Requirements

There are two key structural requirements placed on the satellite by the University Nanosatellite Program, being the static load requirement and the modal requirement.

- The satellite shall have a fundamental frequency above 100 Hz given a fixed-base condition at the Spacecraft Interface Plane
- The satellite must be able to withstand limit loads of 20 Gs independently in the NS-6 coordinate system. Accelerations should be applied the spacecraft center of mass.

Furthermore, a factor of safety of 2.0 must be used for yield and 2.6 for ultimate failure. Mechanisms must be designed to a factor of 2.0 in analysis and tested to 1.0.

Finite Element Modeling

Finite modeling is performed using the finite element solver ANSYS by ANSYS Corporation. Similarly, the pre/post processor used is ANSYS Workbench V12.0, which interfaces directly with the solver. It should be noted that the software used in previous design iterations was COSMOSWorks, which is a part of Solidworks, which is the CAD tool used. However, the change was made due to licensing issues and that the previous software provided insufficient support to be able to effectively model the satellite. Furthermore, the analysis models and results are stored in an analysis repository that is separate from the main CASTOR subversion fileshare (https://planetx.mit.edu/mitsat_analysis).

As such, the software allows the user to import solids from Solidworks, define appropriate materials, define and create the finite elements and meshes to be used, apply loads and restraints, analyze, and view results. Two types of analyses are used, corresponding to the design requirements imposed. ANSYS's Static Structural analysis is used for the static analyses as the standard linear solver option and Modal analysis is used for the modal analyses as the standard normal modes solver option. Furthermore, the bodies are meshed primarily using tetrahedral elements (the default meshing element), however hex and swept elements are used for many elements (such as solar panels and other shell-like bodies). Fortunately, ANSYS Workbench has a very intelligent meshing algorithm, which is able to determine appropriate mesh type based on geometry. Some custom modifications were necessary in order to decrease the number of elements and degrees of freedom, but this was largely limited to body sizing custom parameters on the trusses, plates, and many of the brackets. This resulted in a mesh with 82,570 nodes and 30,153 elements, which was just below the limit on what ANSYS could solve with its memory allocation.

Contact regions are primarily defined using "bonded" contact interfaces so as to scope out the need for bolt interfaces (to reduce the problem size to a manageable level). The one exception to this rule is in the interface between the solar array braces and the solar arrays, where a frictionless boundary condition is chosen. This is in an attempt to simulate the actual surface, where the panel is unable to move in one direction (is supported by the brace), but is free to move in the other. However, the results discussed below were generated from a model where all contact regions were defined as "bonded" as the complexity of the more accurate model exceeded the computing power currently available for analysis. In the next cycle of analysis and redesign for mass optimization, this scenario will be applied to a simpler model to identify reasonable bounds for the first mode of the satellite.

Boundary conditions are as follows. Six degree of freedom restraints are placed on the bottom faces of the lightband brackets to simulate attachment to the Motorized Lightband and fulfill the UNP requirement of determining the "fixed base natural frequency". In the static analyses, acceleration loads are also placed in each of the orthogonal directions of 400 m/s^2, to simulate 20Gs at a safety factor of 2.

Finite element model point masses are defined as in Table 2.8-6**Error! Reference source not found.**.**Error! Reference source not found.**. Locations are as defined in the CAD model.

Name	Mass (kg)
Bottom antenna and brackets	0.0433
Truss-mounted antenna	0.1568
Magnet and bracket	0.176
Xenon feed system	0.75

Relief valves	0.4
Reaction wheel (3)	0.225
GPS bracket	0.00423
GPS	0.00414
Anode	2.277
Avionics components	2.017
Sun sensor (4)	0.0491
Imaging assembly	0.02674

TABLE 2.8-6: FEM POINT MASSES

Engineering Model Finite Element Analysis

The finite element model for the engineering model is, in general, a compilation of:

- The finite element models of the primary structure components
- Simplified versions of the finite element models of secondary structure components
- Mass models of non-structural components, namely components of other subsystems

Creation of the model is performed as follows.

- The primary structure and simplified models of the secondary structure is assembled and mated in Solidworks
- The assembly is imported directly from Solidworks into ANSYS Workbench using the Workbench interface module
- Any necessary interface conditions are modified to represent the accurate interaction between elements in the FEM
- Loads and restraints are applied to the model to represent the loading conditions applied
- Defining material properties for all components
- Meshing parameters are modified as necessary to allow mesh to proceed
- Defining point masses to represent any non-structural components
- Defining analyses and any desired results

At this point, the model is submitted for analysis and debugged as necessary until it is believed to be reasonably accurate. Then, the geometry is modified as necessary to meet design requirements.

The analysis was performed on the simplified version of the satellite so as to determine the baseline frequency. The resulting mode is shown in Figure 2.8-11: First Modal Analysis, showing a modal deformation plot with a first mode of approximately 131 Hz.

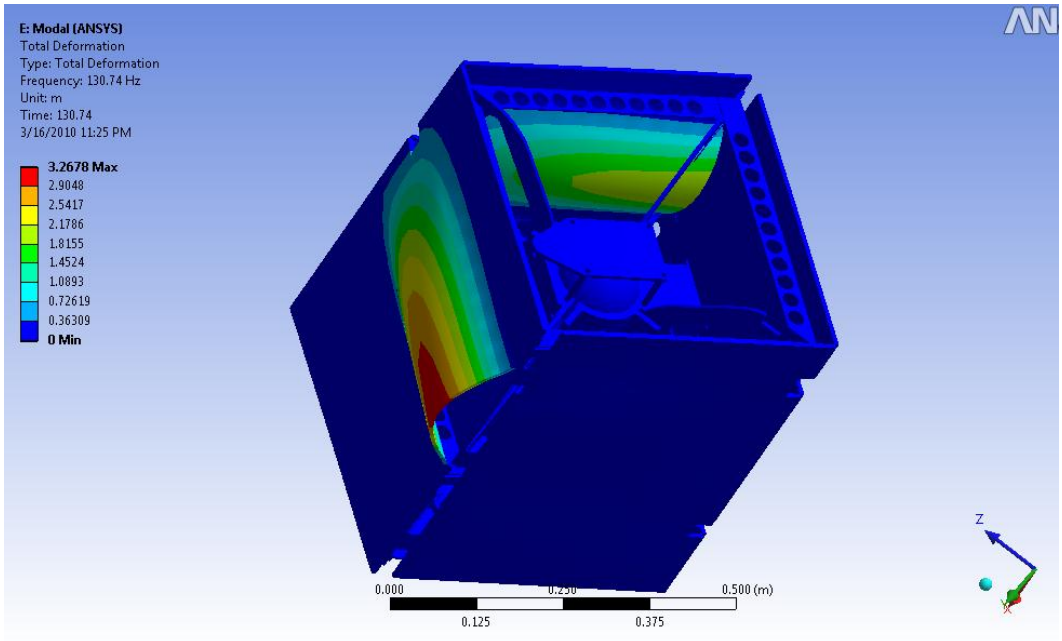

FIGURE 2.8-11: FIRST MODAL ANALYSIS

As can be seen, the first mode is a solar panel mode. This mode has been problematic in the past, but the decision to manufacture the panel composites out of FR4 face sheets on aluminum honeycomb as opposed to carbon fiber face sheets boosted this mode to above the UNP requirement of 100 Hz. The current design, while under the 50 kg total mass requirement, could afford improved mass savings. Areas which will be modified and analyzed again for mass optimization are listed below:

- Re-organization of components on trusses and optimization of truss speedholes
- Experimental removal of a solar array stiffener to the bottom of each of the solar panels (originally added when the design included carbon fiber face sheets)
- Reducing the height and thickness of various component brackets that are currently conservatively designed in order to meet frequency requirements but the analysis indicates that they affect this requirement less than expected

The second iteration of the simplified model, wherein SPRMs, SPDMs, and HMBs were much simplified in order to reduce the amount of computation needed in ANSYS and the solar panel brace interface was modeled as frictionless, showed a torsional mode in the trusses with a first fundamental frequency of approximately 85 Hz. With a frictionless interface with a normal Lagrange formulation, the frequency remained at 85 Hz and the problematic mode was still in the trusses (ANSYS defines normal Lagrange as follows: enforces zero penetration when contact is closed making use of a Lagrange multiplier on the normal direction and a penalty method in

the tangential direction). Further investigation is necessary to identify how to best model the panel-brace interface and then optimization will begin to minimize mass usage while eliminating modal issues in both the trusses and solar panels.

The configuration analyzed has the safety factors and stress plots as shown in Figure 2.8-12 through Figure 2.8-13. Since this analysis was for 40 G loading, for 20 G loading (the UNP requirement), the factor of safety is twice that shown in the image, or 3 rather than 1.5.

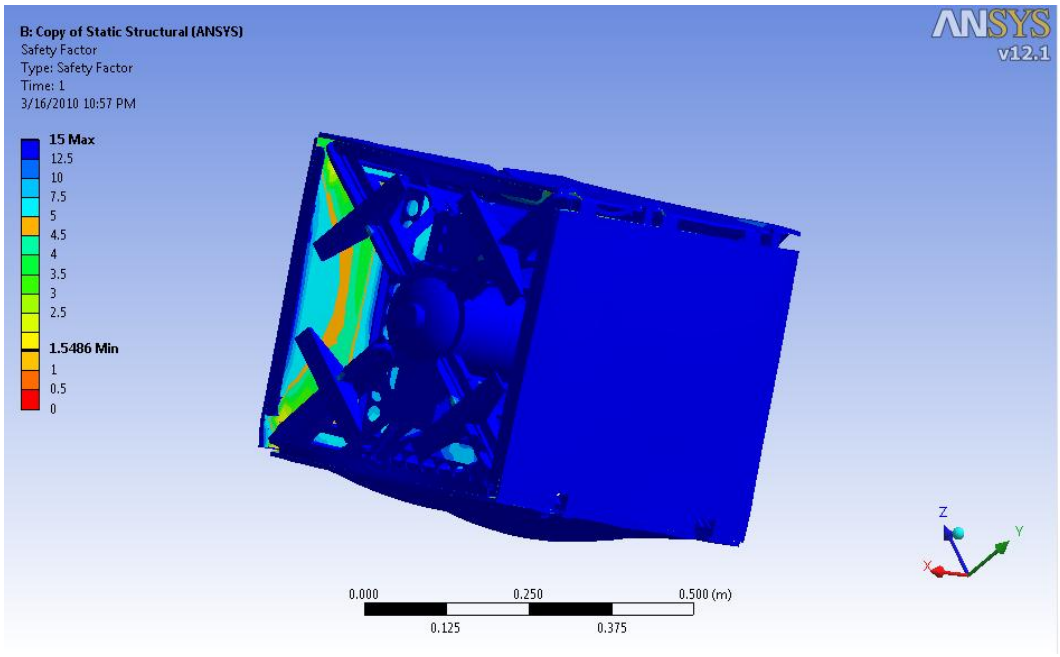

FIGURE 2.8-12:40 G STATIC LOADING PERPENDICULAR TO THE THRUST AXIS (REPRESENTATIVE OF BOTH Y- AND Z-DIRECTIONS)

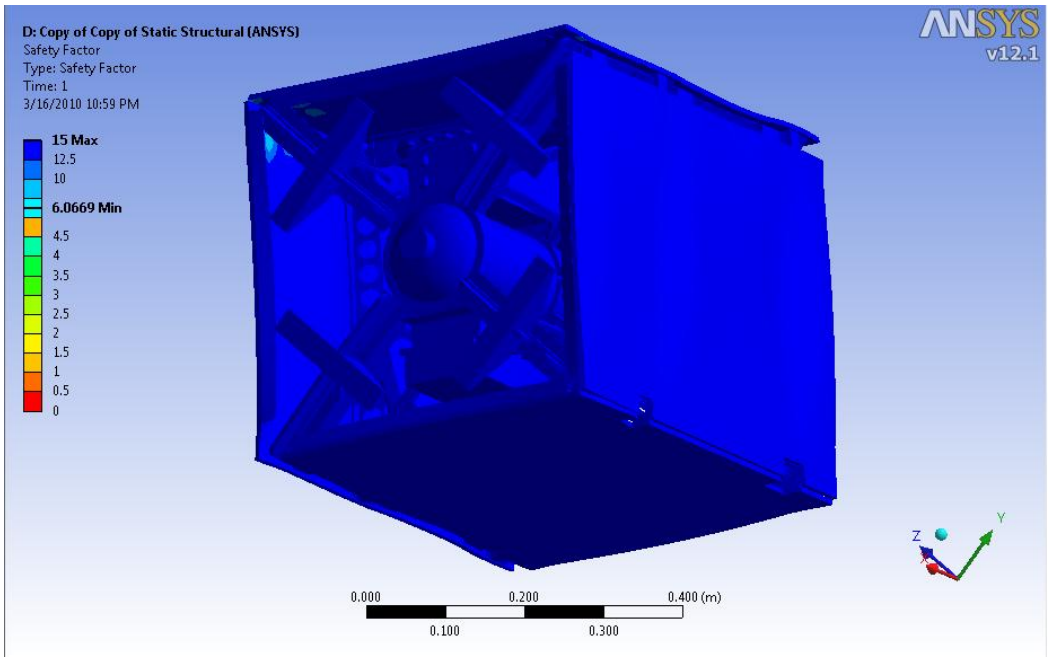

FIGURE 2.8-13: STATIC LOADING PARALLEL TO THE THRUST AXIS

The greatest stress occurred in the corners of the solar panels, as can be seen in the top left.

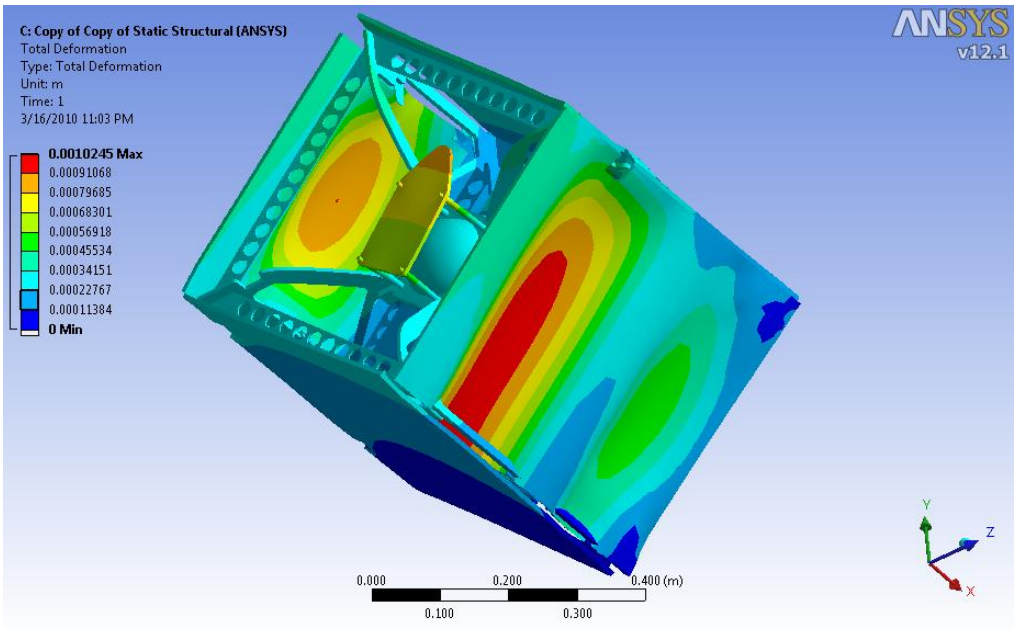

FIGURE 2.8-14: DEFORMATION DUE TO STATIC LOADING PERPENDICULAR TO THE THRUST AXIS

As can be seen, the safety factors given by stress analyses in three different dimensions were about 3 for loads perpendicular to the thrust axis (recall that the plots above were for 40 Gs loading, which is twice the UNP requirement, and thus the safety factors given in the plots should be doubled). The final image demonstrates the total deformation expected of the satellite structure, with a maximum deformation in the solar panels of approximately 1 mm.

Analysis was performed separately on several key component brackets that were overdesigned, most importantly on the Lightband brackets that attach the four structural trusses to the Lightband interface. Originally, the brackets did not meet the factor of safety requirements, but appropriate design changes were made to address this. A detailed discussion of the results can be found under 2.8.7 ESPA Mount.

More representative of the other components, the magnet bracket assembly was shown to be overdesigned and has undergone two cycles of analysis. Analysis showed that the bracket was overdesigned, and that its mass could be reduced by decreasing the thickness of the support arms, while still maintaining a factor of safety greater than what is required. Though the first fundamental mode of the new design decreased from over 1400 Hz to 830 Hz, this is still well over the 100 Hz requirement. The new design still has a factor of safety greater than 10. Future revisions may include a material switch from aluminum to Delrin, for greater mass reduction.

The Solar Panel Release Mechanism (SPRM) and solar panel deployment mechanism (SPDM) were also shown to be overdesigned. The SPRM currently has a factor of safety greater than 10, while the SPDM has a factor of safety of 6.4. These designs may be modified in the future to reduce mass, if needed.

Large safety factors are mostly due to the need to meet frequency requirements and are thus not considered excessive from a design perspective. Based on the total model's modal and static analysis results given above, this design is deemed acceptable pending future analysis and revision based on CDR feedback to increase the mass margin while retaining a favorable first mode and structural integrity.

Engineering Model Empirical Testing

Empirical testing of the engineering model is performed as the final structural verification of the satellite. The purpose is to both prove that the physical model can withstand loads and to verify the fidelity of the model. As mentioned above, this is done in two phases: static testing and vibration testing.

For static testing, this is performed by mounting the model of the satellite to the strongback in the hanger in building 33 using a Lightband interface mockup. Then, loading may be applied using a series of proof masses to test the satellite in each of the required directions.

Vibration testing is performed at the MIT Lincoln Laboratory environmental testing facility. It consists of a series of tests that are performed in the order specified below for each axis:

1. Low Random vibe to identify modes and points of resonance
2. Sine sweep test to verify the natural frequency
3. Sine burst test to verify structural strength
4. Sine sweep test to re-verify the natural frequency
5. High Random vibration test

6. Sine sweep test to re-verify the natural frequency
7. Shock test
8. Sine sweep test to re-verify the natural frequency

In previous test campaigns, the shock testing (7) had never been performed due to uncertainty in what loads should be applied and since the table at the facility was incapable of providing the shock levels as specified in the User's Guide. Further information regarding vibration testing procedures may be found in section 2.4.1.2 of the fileshare.

2.9 GROUND SYSTEM EQUIPMENT

2.9.1 GSE OVERVIEW (D. ROCKWELL)

The ground support equipment section will describe the requirements of mechanical and electrical ground support equipment, detail the conceptual designs made to fulfill some, not all requirements, and will also briefly make references to the design constraints made by the limited availability of interfaces on the satellite for ground support equipment. The ground support equipment will be used for transportation, handling, and preparation of CASTOR at testing and launch sites, and is still in a conceptual design phase as other subsystems finalize their design.

2.9.2 GSE REQUIREMENT (D. ROCKWELL)

The shipping container shall:

- Contain the entire satellite or satellite stack
- Maintain class 100,000 clean conditions
- Provide ESD protection to the satellite
- Have a means for grounding the container from an external grounding point before opening container
- Enable shipping both with and without the PSC Lightband integrated to CASTOR.
- Measure the shock environment experienced by the satellite during shipping through the use of shock sensors in all 3 axes. Approved shock sensor styles are ball and spring or data-logger type shock sensors, sticker-type shock sensors are not allowed. Shock sensors shall be placed on the primary mounting plate/interface to the satellite so as to accurately measure the shock as experienced by the satellite

It is also recommended that the shipping container:

- Separate into two pieces at the interface plane between the satellite and the container. The intent here is to allow easy access to the bolts that mate the satellite and the container.
- The shipping container should incorporate full height posts that are affixed to the outside corners of the interface plate. These corner posts protect the satellite from the lid while opening and closing
- Incorporate a shock isolation system, usually between the plate on which the satellite is mounted and the box.
- Incorporate means for pressure equalization during shipment (significant bowing of container walls can occur due to differential pressure)

- 48 point bolt circle for the 15" Lightband. Doubling the Lightband interface bolt circle allows for flexibility during installation of satellite in the container. It resolves clocking issues.
- Have wheels for ease of movement
- Incorporate means of restraining motion of container, through locking wheels, retractable wheels, etc.
- Pallet jack/fork lift compatible
- Handles for lifting by hand
- The shipping container can be used as a display case

Mechanical Ground Support Equipment (MGSE) shall:

- Consist of a lifting harnesses that shall be designed to lift CASTOR from a single point above its center of gravity, in every orientation except upside down (+X, -X, +Y, -Y, +Z, and not -Z). Lifting equipment shall be designed such that it will not contact the Lightband during integration and ground handling operations.
- Consist of tabletop MGSE stands that must be able to support CASTOR with, without, and with only half of the Lightband.
- Be designed using a factor of safety of 5.0 for ultimate failure, and be proof loaded to twice the design load.
- Meet all requirements for flight hardware as prescribed in KHB 1700.7C, if it shall remain attached to CASTOR for flight.

Electrical Ground Support Equipment (EGSE) shall perform the following functions:

- Battery charging and discharging while satellite is inhibited.
- Inhibit actuation (inhibit/enable satellite).
- Power satellite while satellite is inhibited.
- Support functional testing of satellite, including subsystem level and full "day in the life" testing

EGSE will also meet the following requirements:

- EGSE shall be self contained and portable.
- EGSE shall be capable of command and control of the satellite without free radiation of RF energy, i.e. through harnessing and/or with RF hats.
- EGSE shall also be capable of command and control of the satellite through radios and RF. (Note that antenna hats satisfy both of these requirements.) Both communications channels must be available.
- Functional testing after integration to the launch vehicle must be performed without free radiation of RF energy.
- Battery charging equipment in the EGSE shall be current limited by design and shall provide monitoring and protection to prevent battery damage or failure.
- The ability to discharge the battery without enabling the satellite bus/loads is required, i.e. through resistors contained in the EGSE.
- A main power switch shall be provided, with indicator light.

- All switches or buttons shall be clearly labeled.
- Separation between switches/buttons shall be sufficient to avoid accidental actuation.
- Switches shall include covers, with an automatic-off feature, such that when the cover is closed the switch is in the off position.
- Circuit protection (fuses or circuit breakers) shall be installed on primary circuits, on the load (not ground/return) lines.
- Circuit protection devices shall be readily accessible for inspection, reset, or replacement.
- Circuit breaker trips and fuse blows shall be readily detectable by visual inspection.
- Circuit protection shall be clearly marked with voltage present and rated amperage.
- All wiring shall be copper and contact with dissimilar metals shall be avoided. Aluminum wire shall not be used.
- Connectors used in the harnessing between the satellite and the EGSE shall be scoop-proof.
- EGSE shall use standard 120 V, 60 Hz, 3 prong "household" power, preferably through a single plug.
- If batteries are included as part of the EGSE, polarity of battery terminals shall be clearly marked and ventilation shall be provided to ensure concentrations of vapor do not reach 25% of the lower explosion limit.
- Equipment shall be designed, fabricated, inspected, and tested in accordance with NFPA 70.
- All electrical ground support equipment (EGSE) shall meet the safety requirements of KHB 1700.7C and AFSPC 91-710 Vol 3 Sec 14.2.
- EGSE components and/or interfaces that remain attached to CASTOR for flight must meet all requirements for flight hardware.

It is also recommended that EGSE:

- Should support discharge and charge state verification of individual cells.
- Should be designed with fuses and diode protection to ensure that failures in ground support equipment or procedural mistakes will not damage CASTOR's hardware or cause other hazardous conditions.
- Should not have connectors with exposed pins. This applies to both the EGSE itself and the flight hardware.

2.9.3 SHIPPING CONTAINER (L. MCCARTHY)

The shipping container will house CASTOR during transport. Along with all other MGSE, it will maintain a factor of safety of 5.0 for ultimate failure. It will be approximately 95 cm x 95 cm x 110 cm in size, and will provide a space of approximately 90 cm x 90 cm x 95 cm in which to house the 50 cm x 50 cm x 60 cm CASTOR. The extra space ensures accessibility to the satellite, and provides space for environmental monitors, shock sensors, MGSE, EGSE, and harness equipment.

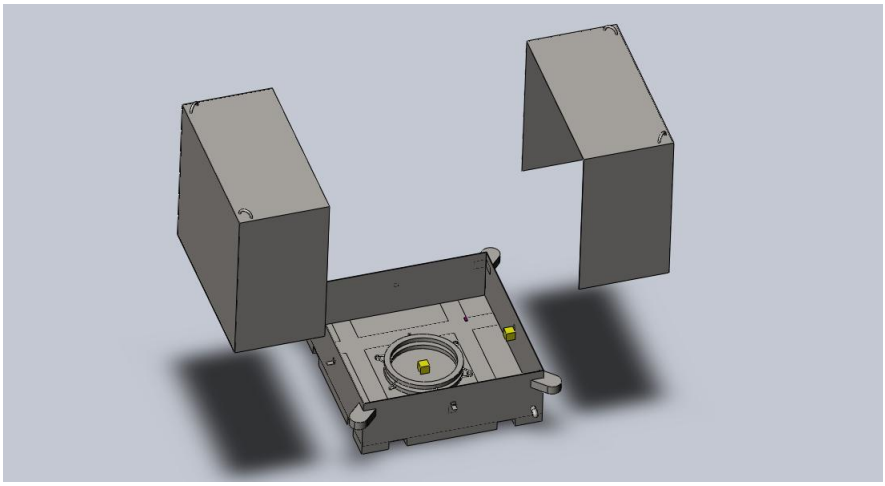

FIGURE 2.9-1 SHIPPING CONTAINER OPEN CONFIGURATION

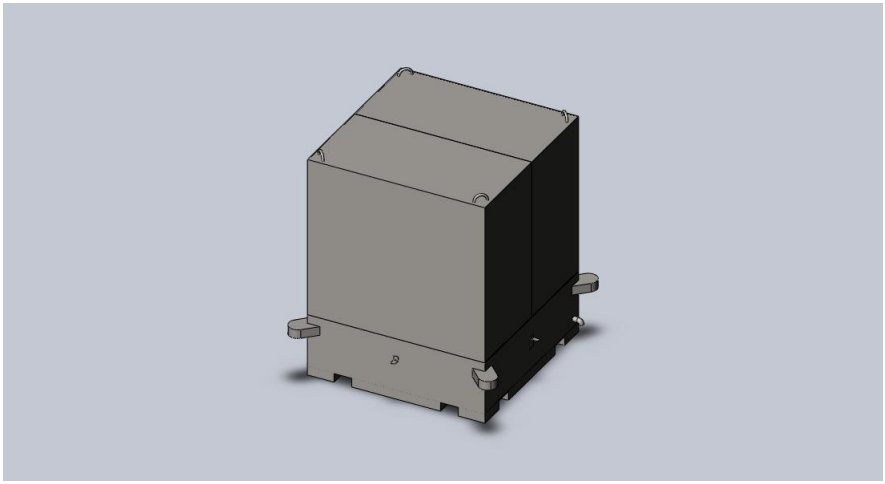

FIGURE 2.9-2SHIPPING CONTAINER CLOSED CONFIGURATION

A High Efficiency Particulate Air (HEPA) filter will be installed to maintain class 100,000 clean conditions. Environmental monitors will confirm these conditions by recording temperature, humidity, and air pressure. Shock isolating feet will also be incorporated, and shock sensors will determine the amount of stress that has been exerted on the satellite during transport. Grounding points will be reachable from all sides to protect against electrostatic discharge (ESD).

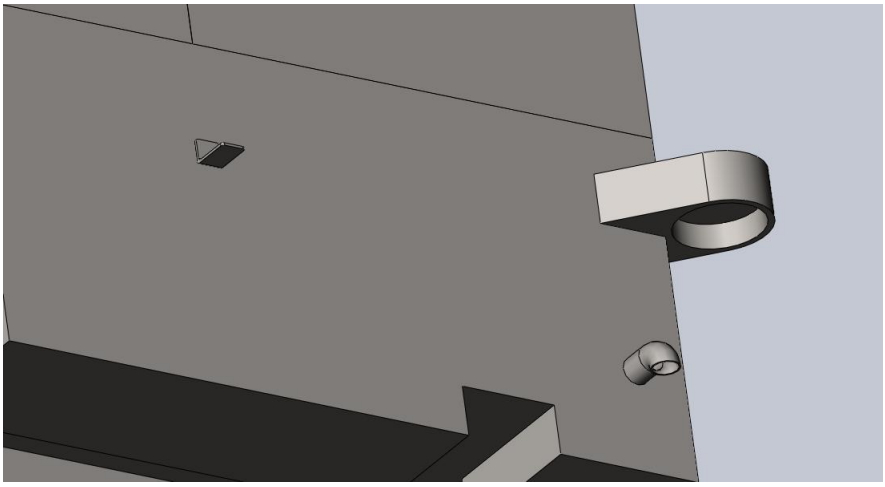

FIGURE 2.9-3: FILTERED VENT, GROUND AND JACK POINT

The shipping container will also be pallet jack/forklift compatible. Lifting handles at the top can be accessed by a crane, or used to lift the container by hand. Wheels may be installed for ease of mobility along the ground.

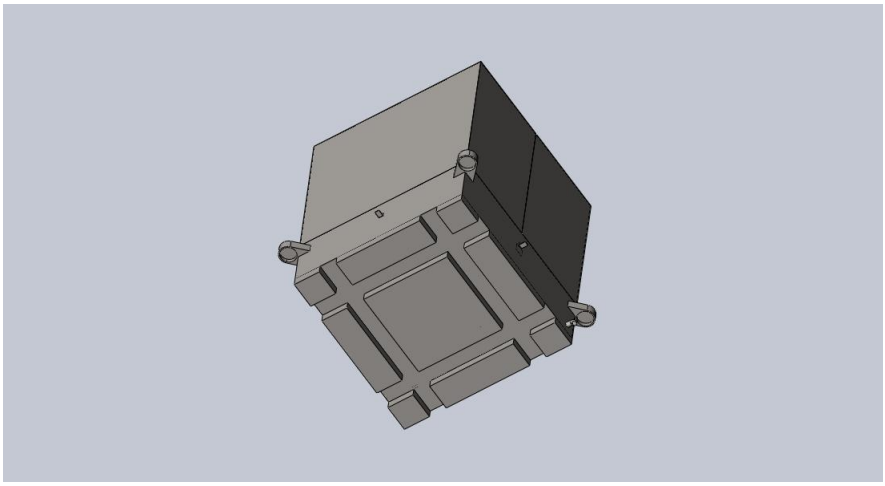

FIGURE 2.9-4: PALLET JACK/FORKLIFT SOCKETS

2.9.4 LIFTING HARNESS (D.ROCKWELL)

The lifting harness will consist of four top lifting harness clamps, four bottom lifting harness clamps (of similar design as the top lifting harness clamps), HT Series Aluminum framing, joining strips, and corner brackets, plexiglass or acrylic sheet, 24- ¼" eyebolts with shoulders, 8- ¼"shoulder bolts with an aluminum wire pulley system.

The lifting harness clamps shown in (Figure 2.9-5: Lifting Harness Clamp) will engage the four trusses of the satellite. The lifting harness clamps will be attached to the trusses shown in (Figure 2.9-6: Lifting Harness Clamp with satellite and Braced structure) with 8- ¼"shoulder bolts

shown in (Figure 2.9-8). The lifting harness clamp will be attached to the braced structure constructed of HT Series aluminum the structure will be 54 cm x 54 cm x 64 cm modeled in (Figure 2.9-6)with 16 of the 24- ¼" eyebolts with shoulders shown in (Figure 2.9-8). HT Series aluminum framing was chosen to minimize the need for welding and make assembly and disassembly much easier for this frame. The lifting harness attach points that will be used for lifting will be the eyebolts jutting out of the framed structure and the top/bottom of the lifting harness clamps. The number of eyebolts ensures that there are at least 8 eyebolts pointing in all 3 axial directions. The aluminum wiring will be threaded through the eyebolt and connect to an as of yet unspecified pulley system. The framing will also have plexiglass or plastic acrylic sheet covering to protect the satellite's solar panels.

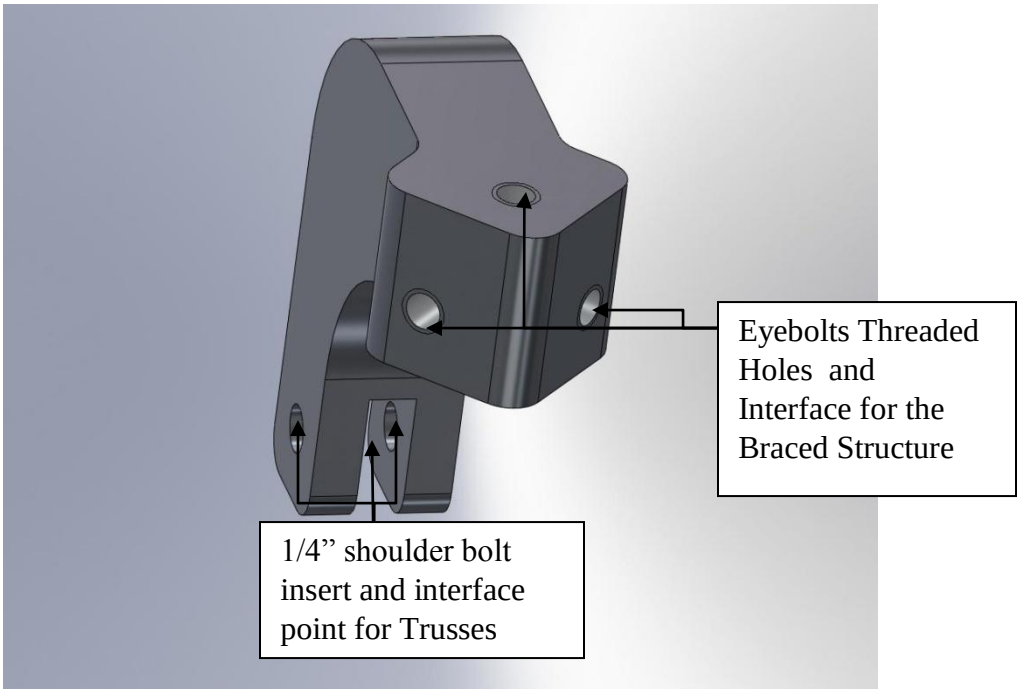

FIGURE 2.9-5: LIFTING HARNESS CLAMP

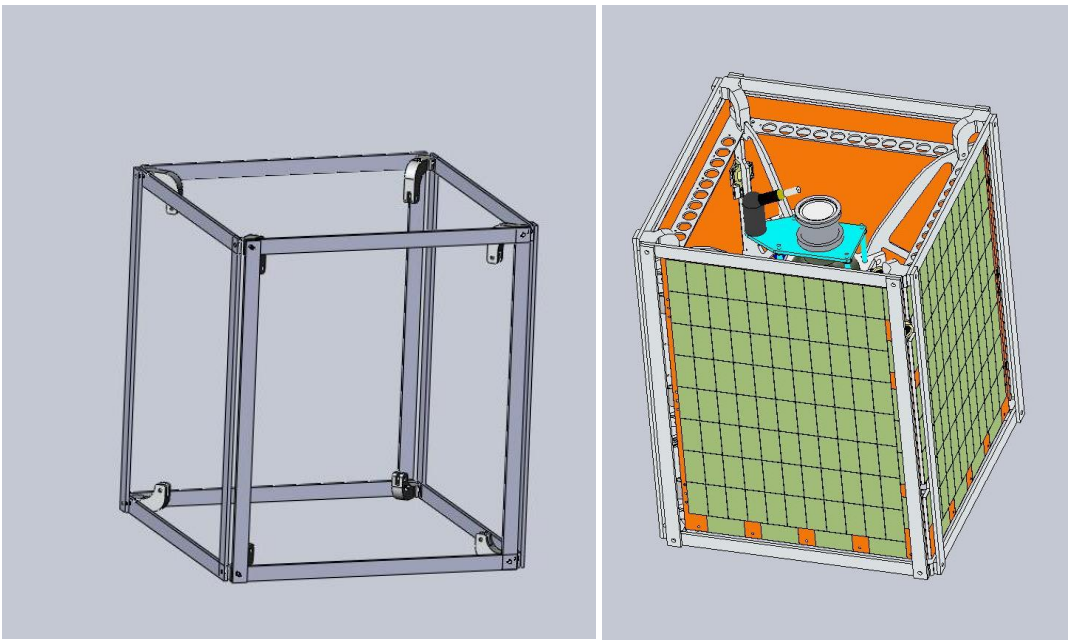

FIGURE 2.9-6: LIFTING HARNESS CLAMP WITH SATELLITE AND BRACED STRUCTURE

FIGURE 2.9-7: HT SERIES ALUMINUM FRAMING, JOINING STRIPS, AND CORNER BRACKETS

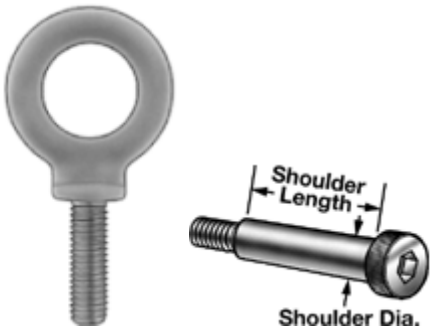

FIGURE 2.9-8: EYEBOLT WITH SHOULDER AND SHOULDER BOLT

2.9.5 EGSE (D. AINGE)

To minimize the complexity of the EGSE, our design will utilize as few in-house products as possible. The main components of this system are the inhibitory controls and the battery charger; good off-the-shelf solutions already exist for these components. Because the EGSE will be powered with a single household three-prong plug, power usage is not a concern. AC/DC converters will be implemented to allow us to use an identical charging circuit as on-board the satellite, again minimizing complexity and risk. Circuit protection will be used on the AC line coming into the EGSE, as well as on the DC line headed to CASTOR to prevent damages from any accidental loads in either direction.

2.10 THERMAL (W.PINO & A.ESPITIA)

2.10.1 THERMAL SYSTEM OVERVIEW (W. PINO)

The thermal section of the design document describes the thermal control techniques that are used on the satellite, the requirements that must be met, the methods that have been used to analyze the system, and the interfaces that exist between the various systems that are affected by the thermal design. Thermal control is essential in order to secure the performance of all components on the satellite during the various mission phases. The CASTOR thermal system includes the design and implementation of thermal control as well as the necessary hardware. To measure temperatures, there are 20 analog thermal sensing devices on the satellite. Of those 20, 14 are temperature sensors and 6 are thermocouples.

There are several methods of implementing thermal control. The CASTOR satellite makes use of passive thermal control by implementing a reflective surface coat. After studying the results from the thermal analysis described in the modeling approach section, it was determined that Alodine should be applied to all the aluminum surfaces and that Z93 should be applied on the back of the panels and on the engine. Z93 is a type of white paint that has a low absorptive coefficient and can reflect the short wavelength infrared light emitted by the sun. The paint also has a high emissivity factor and can expel longer wavelength radiation such as heat emitted by components onboard the satellite. The use of these materials allows the satellite to stay within desired temperature ranges for optimal functionality.

2.10.2 THERMAL SYSTEM REQUIREMENTS (W. PINO)

The thermal system team is required to provide adequate thermal control for the satellite for all stages of the mission. This includes a range of altitudes within low earth orbit as well as a range of incidence angles. Thermal models of the satellite must also be presented to the AFRL. There are temperature limit requirements that must be satisfied. The calculated temperature ranges for each component must fall within those requirements. It is necessary to include

operational temperatures ranges that span temperatures where the component can be turned on and used. Additionally, survival temperatures ranges must be provided. These output values for temperature ranges span temperatures that the component can endure without suffering damages when it is turned off.

TABLE 2.10-1: TEMPERATURE LIMIT REQUIREMENTS

Component	Operating Range ^{o}C	Survival Range ^{o}C	Component	Operating Range ^{o}C	Survival Range ^{o}C
NiCad	0 to 70	-20 to 75	Camera	-20 to 60	-35 to 85
MPPT	-40 to 60	-45 to 85	Reaction Wheels	-20 to 60	-35 to 70
PDU	-55 to 100	-65 to 110	GPS	-20 to 50	-30 to 60
PPU	-45 to 85	-45 to 90	DCFT	0 to 200	-50 to 300
MEMS IMU	-40 to 85	-55 to 85	Xenon Gas	0 to 127	-50 to 127

As part of the requirements, it is necessary to provide a table listing the thermophysical properties of all the materials that are used on the satellite. The following table lists the name of the material, the conductivity (W/mm/K), the density (kg/mm^3), and the specific heat (J/kg/K) in units compatible with the way the Thermal Desktop program accepts inputs.

TABLE 2.10-2: TABLE OF THERMOPHYSICAL PROPERTIES

Material Name	Conductivity (W/mm/K)	Density (kg/mm^3)	Specific Heat (J/kg/K)
50% Alum 6061-T6	0.001	1.36E-06	1
Air	2.57E-05	1.21E-09	1.005
Aluminum	0.22	2.71E-06	896
Aluminum 6061	0.1679	2.77E-06	1256
Aluminum Alloy 6061	0.12134	2.74E-06	795
Black Plastic	0.00023	1.25E-06	1930
Carbon Composite	0.0002	1.49E-06	1880
Chip	0	2.00E-06	837.32
Copper Alloy	0.388	8.93E-06	385
Copper C19400	0.26	8.86E-06	385
Fr4 2oz Copper	0.0177	1.91E-06	600
Glass	0.002	2.40E-06	840
Gold	0.318	1.89E-05	130
Lead	0.035	1.14E-05	130
M1	0.001	2.59E-13	1

Magnesium	0.15062	1.74E-06	1004
MLI	0.001	1.00E-09	0
Silicon Solar Cells	0.025	2.33E-06	712
Stainless Steel 316	0.01626	8.03E-06	502.1
Stainless Steel, AISI 301	0.001	7.92E-06	1
Water	0.0006	1.00E-06	4200
Xenon Gas	5.65E-06	5.89E-09	158.32

TABLE 2.10-3: TABLE OF OPTICAL PROPERTIES

Material Name	Solar Absorptivity	IR Emission	A/E
Aluminum (anodized)	0.140	0.840	0.167
Aluminum (polished)	0.090	0.030	3.000
Aluminum (quarts overcoated)	0.110	0.370	0.297
Aluminum Alodine	0.230	0.030	7.667
Aluminum Foil	0.150	0.050	3.000
Aluminum (heavily oxidized)	0.130	0.300	0.433
Anodize Black	0.880	0.880	1.000
Black Plastic	0.250	0.850	1.129
Brass	0.550	0.525	0.476
Copper Foil Tape	0.960	0.040	13.750
Delrin Black Tape	0.250	0.870	1.103
Dull Brass, Copper, Steel, Alumi	0.550	0.250	2.100
FR4	0.960	0.800	1.200
Gold (highly polished)	0.090	0.030	3.000
Graphite Epoxy	0.930	0.850	1.094
Kapton Film	0.340	0.550	0.618
Metal, plated nickel oxide	0.920	0.080	11.500
MLI (inner surface)	0.000	0.950	0.000
MLI(outer surface)	0.380	0.850	0.447
Opal Glass	0.280	0.870	0.322
Silver (highly polished)	0.075	0.025	3.000
Solar Cells	0.850	0.850	1.000
Tedlar Black	0.940	0.900	1.044
Tedlar White	0.390	0.870	0.448
Teflon (silver, 5mil)	0.080	0.810	0.099
Xenon Gas	0.250	0.250	1.000
Zerlauts S-13G White Paint	0.200	0.900	0.222
Zerlauts Z-93 White Paint	0.170	0.920	0.185

2.10.3 THERMAL MODELING APPROACH (W. PINO)

There are three facets to the modeling approach used on the CASTOR satellite. The first one involves hand calculations that make use of the governing equations that affect the system. The hand calculations are used to solve for the resulting temperatures of the satellite components. In order to capture the full behavior of the system, all phases of the mission were analyzed. This includes polar orbit configurations, where the satellite experiences the most extreme hot case due to continuous sun exposure as well as equatorial orbit configurations, where the satellite faces the sun for only a portion of the orbit. The mathematical model also includes the effect of reflected sunlight from the earth, or albedo, and the effect of sunlight absorbed by the earth that is then emitted as infrared radiation. These calculations were written into a MATLAB script that contains the hand calculation analysis.

The second form of analysis makes use of the Thermal Desktop modeling software. Given a 3D Computer Aided Design (CAD) model, this software has the capability of simulating various orbiting conditions. Nodes and heat loads can be added to the CAD model as needed in order to capture the full behavior of the system. The current thermal model has 460 nodes. Using the Thermal Desktop software, simulations have been run at various orbits and sun incidence angles. It has been used to model the hottest and coldest cases. The cases include polar orbits where the satellite is exposed to the sun for the entire duration of the orbit as well as equatorial orbits.

The last aspect to the thermal modeling approach involves thermal vacuum testing conducted at MIT Lincoln Laboratory. The main purpose of the thermal vacuum test is to observe the thermal behavior of the satellite and then compare those findings with the results from the calculations and the simulations from the previous analyses. The entire satellite structure and its subcomponents are put into the vacuum chamber and the pressure is brought down to 10^{-9} torr. In order to simulate heat loads from components, 23 resistors are mounted on the satellite. The chamber temperature is then fluctuated from -20 degrees Celsius to 20 degrees Celsius and the LabView software is used to collect data. The output data then gets correlated to the results from our first two methods of analysis. It is used to assess the validity of our models.

2.10.4 ENGINE MOUNT DESIGN (A. ESPITIA & W. PINO)

The structures team has completed their redesign of the structural model. One of the questions that the design had brought out was the effect of reducing the size of the radiation plate. This reduction would result in heat to be dissipated from the engine more slowly than before. The concern the thermal team had was whether this reduction would result in more heat to be transferred down the engine mount posts to nearby electronic equipment and potential cause them to reach high temperatures. In order to determine if this design would present a thermal problem, the new design was subjected to orbital simulation. The results of an orbital simulation of 10 orbits around the equator at 550 km above the earth's surface with no thermal control can be seen in Figure 2.10-2. The different lines represent different nodes along the four engine posts. Note: The posts corresponding to the nodes can be seen in Figure 2.10-1. The nodes that are in T20's correspond to Post 1. Similarly, the T40's are for post 2, T50's are for post 3, and the

T60's are for post 4. Due to graphing limitations on Thermal Desktop, only 14 nodes can be plotted at once.

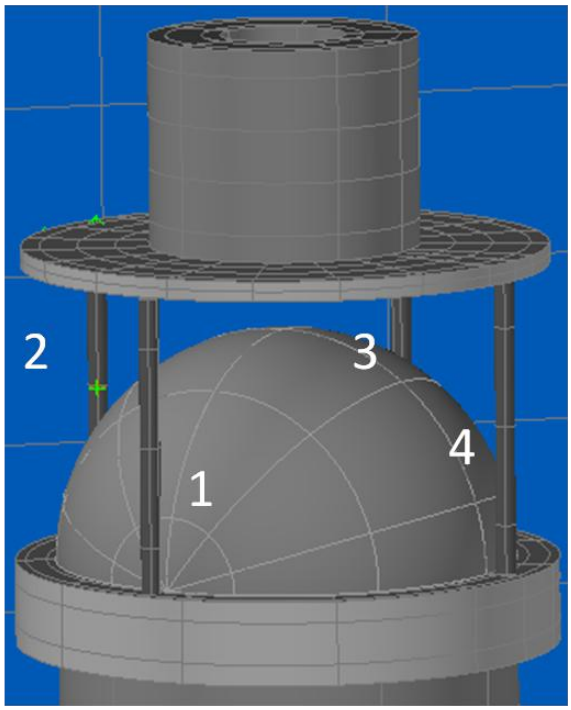

FIGURE 2.10-1: ENGINE MOUNT DESIGN

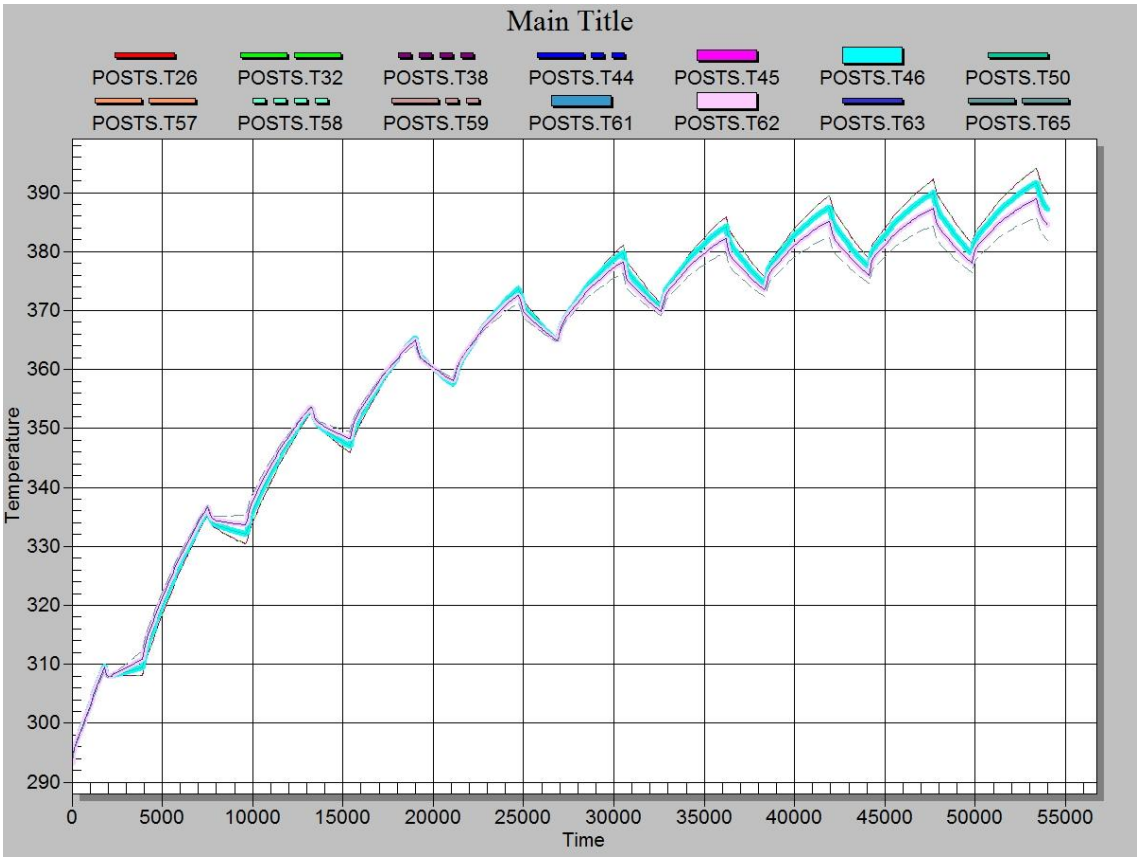

FIGURE 2.10-2: TEMPERATURE (K) VS. TIME(S) FOR ENGINE POSTS

The results above show that the engine posts tend to level off at a temperatures of 390K, which could result in a significant amount of heat being transferred to key electronic equipment that is mounted on the tank clamps (such as the battery box, avionics stack, and a reaction wheel).

In order to address this problem, the thermal team applied Z-93 white paint on the bottom of the engine mount and the four posts supporting the mount. The simulation was run once again and the results can be seen in Figure 2.10-3.

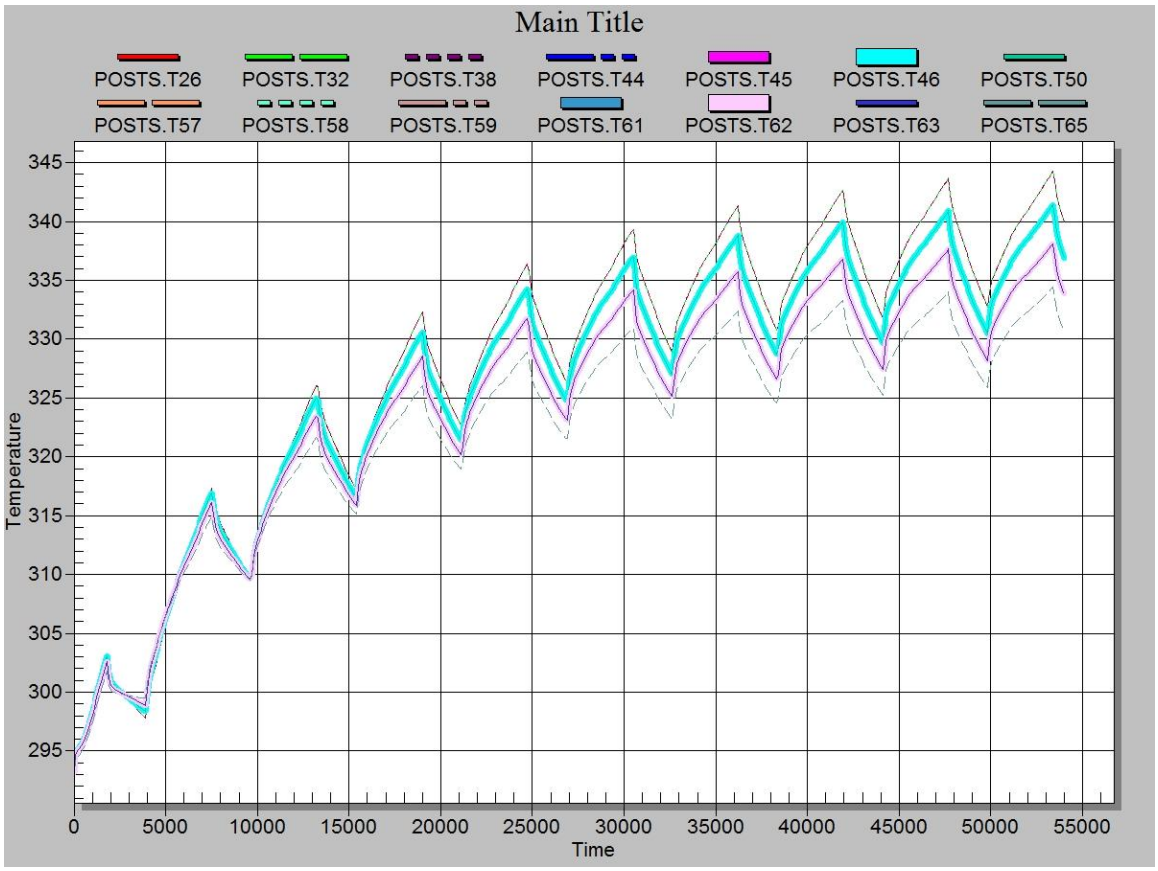

FIGURE 2.10-3: TEMPERATURE (K) VS. TIME(S) FOR ENGINE POSTS WITH Z93

The results show a significant improvement. The engine posts all level off between 330K and 340K. Additionally, the nearby electronic equipment did not show any significant increases in their temperatures (as compared to the previous engine mount design with a larger size). The above results show that the new engine mount design should not create any significant thermal issues that cannot be resolved with the use of thermal control.

2.10.5 INTEGRATED MODELING (A. ESPITIA & W. PINO)

The thermal modeling requirement set in place by the UNP program was to have a 100 node SINDA model of the satellite. In order to achieve this requirement the Thermal Team has begun by modeling individual components (battery box, anode, avionics, composites). The individual components are aggregated to the assembly level and reanalyzed to ensure the interfaces between components accurately represent the truth. Finally the assemblies are being combined into an integrated CASTOR thermal model. Components requiring >1W continuous will be included in the integrated thermal model. All components operating at less than 1W are assumed to approach the temperature of their adjacently mounted component. Though unspecified, components that require <10 W sporadically (such as the DCFT) will also be modeled. The CASTOR SINDA

model currently has over 400 nodes dispersed between 20 different components. Analysis of the assembly and integrated models has been made and is still ongoing as component and the structural layout change.

The comments and suggestions gathered at the preliminary design review led to a structural redesign of CASTOR, which was completed at the beginning of 2010. As a result, the thermal team also adjusted its thermal model in order to best resemble the new design. The new thermal model can be seen inFigure 2.10-4. Aside from the solar array configuration change, two new boxes (which will house a majority of the electronic components) were placed on the tank clamps on either side of the satellite (only one is visible in the figure below). Though this model is simply the previous model adjusted for the redesign, the thermal team has planned another TVac test to once again validate its model as well as apply some thermal control.

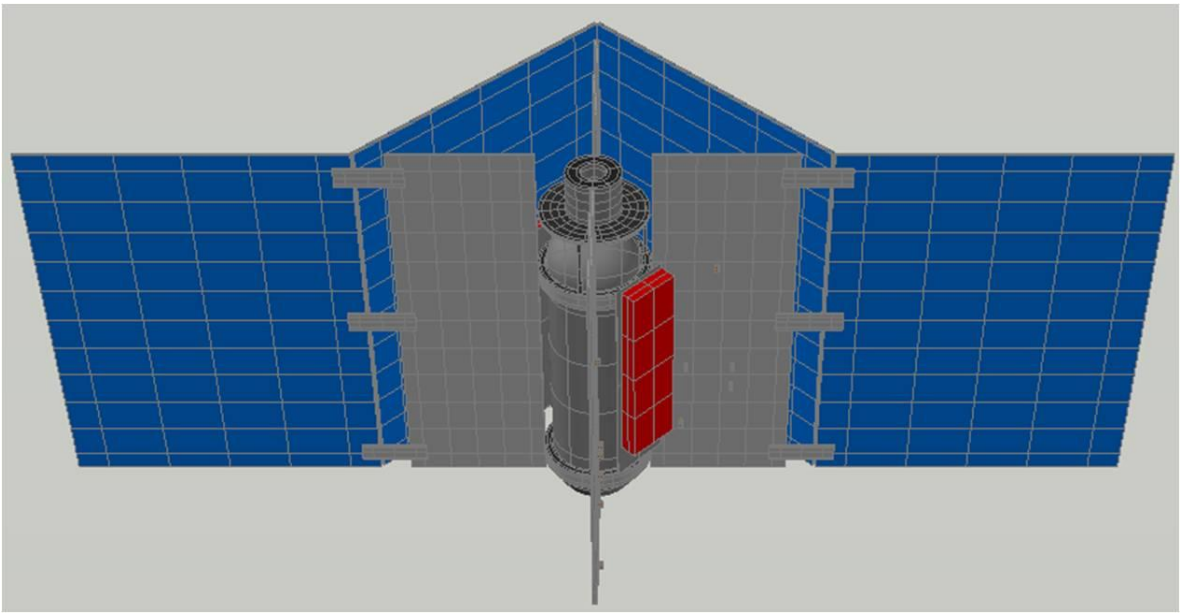

FIGURE 2.10-4: INTEGRATED THERMAL DESKTOP MODEL

Using the updated thermal model (which has been validated at an earlier design), the team has run simulation in order to determine the areas in need of thermal control. A simulation of 10 orbits (so that it would reach steady state) at 550 km (see Figure 2.10-5) was run. The results are in Figure 2.10-6.

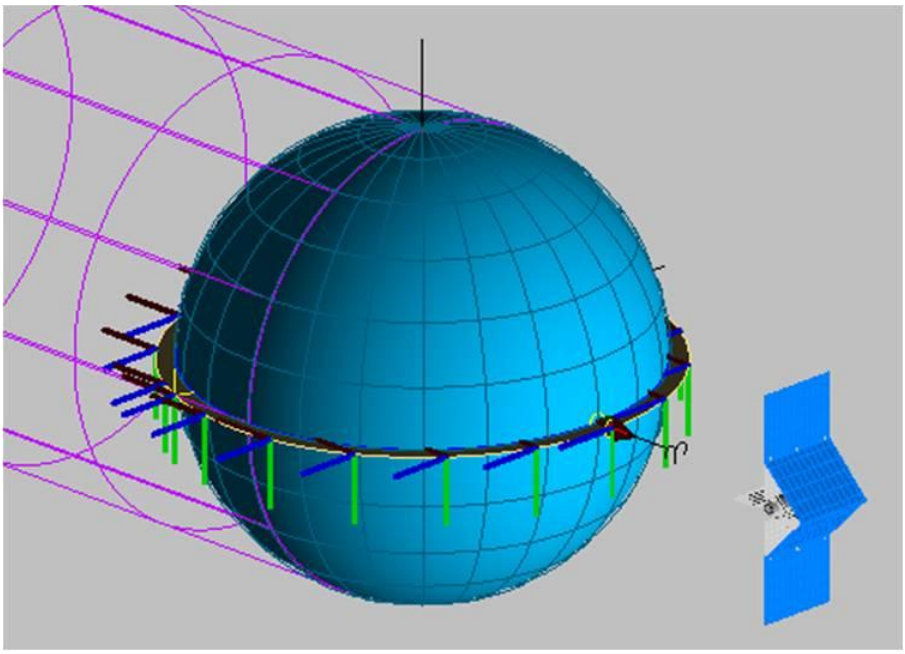

FIGURE 2.10-5: SIMULATION ORBIT

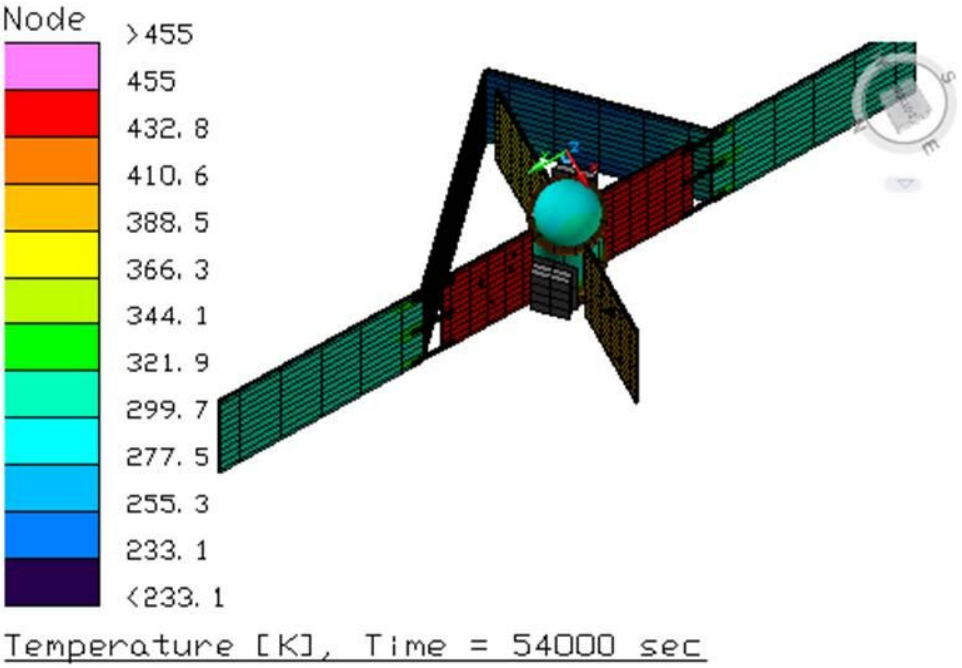

FIGURE 2.10-6: SIMULATION RESULTS

The results show that the majority of the satellite tends to heat up too quickly. To address this, the team decided on using a highly emissive paint, Z93 white paint ($\varepsilon = 0.92$). Since solar cells operate better in the cold than in the heat, the back of all 4 solar arrays and the engine (mount included) were covered in Z93. Also, a mounting plate was placed behind the two main

electronic boxes to provide additional structural integrity as well as a conduction path so heat can be dissipated away from them. After adjusting the thermal model for the proposed thermal control, the same simulation was run. The results are shown in Figure 2.10-7.

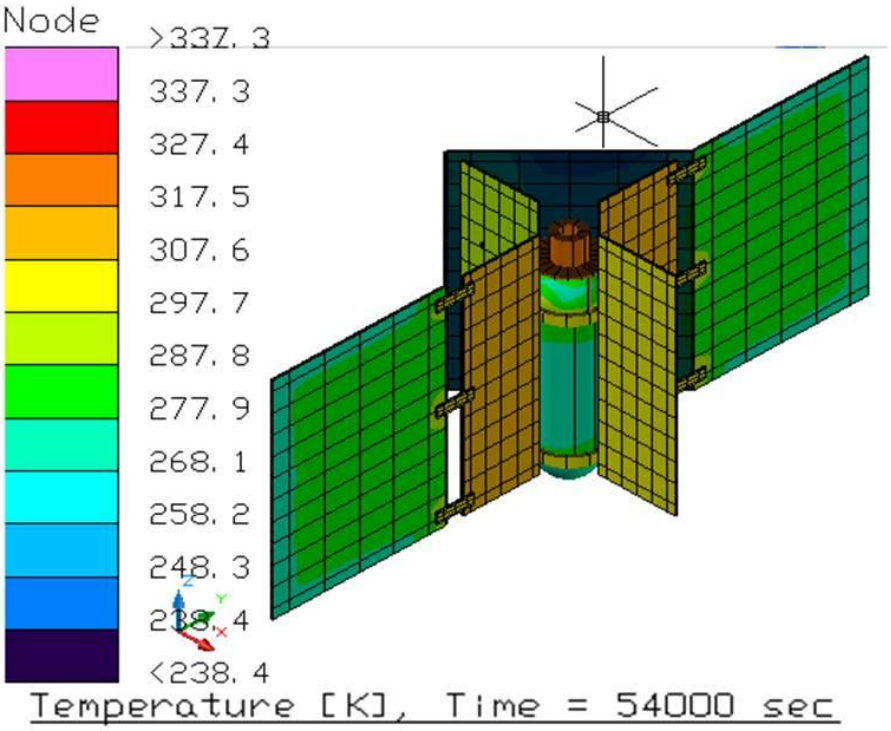

FIGURE 2.10-7: SIMULATION RESULTS WITH THERMAL CONTROL

With thermal control, the results that were yielded were significantly better. Only the engine exceeded 50°C and only the solar panels fell below 0°C. This simulation however, was only for an equatorial orbit. In order to have range of possible temperature components could see due to various orbits, additional simulation were run. The altitude, inclination, and beta angle were all adjusted. A graphic representation of the hottest and coldest cases for the components can be seen in Figure 2.10-8 where the bars represent the predicted temperature ranges while the lines represent the operating temperature ranges.

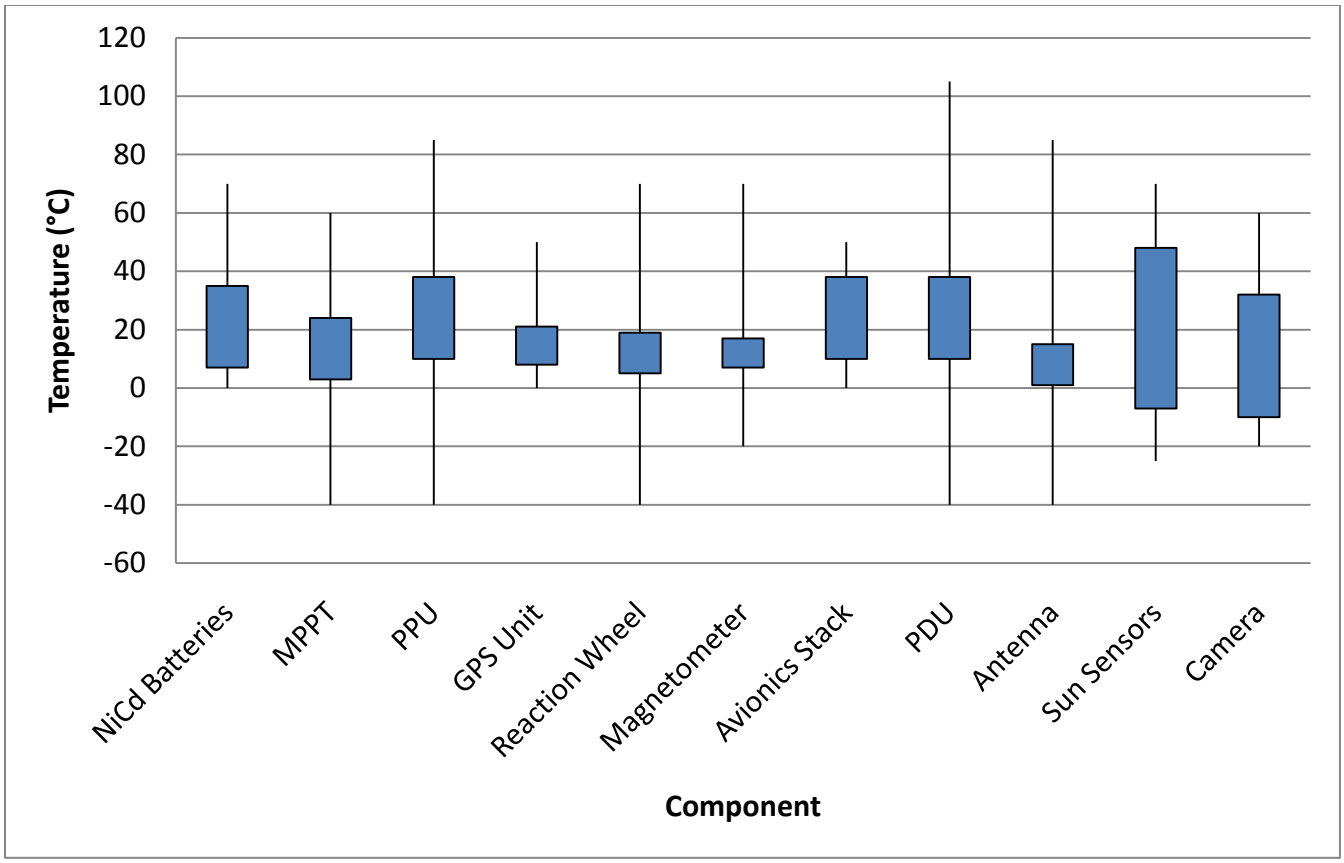

FIGURE 2.10-8: PREDICTED AND OPERATING TEMPERATURE RANGES

Some components have the same cold/hot temperature since they are located in the same place (i.e. inside one of the boxes). Additionally, some margins are large due to the large operating temperature ranges of some of the components. The model indicates that the requirement of giving the satellite adequate control will be met.

2.10.6 THERMAL TESTING (A. ESPITIA)

The thermal team aims to validate models created in Thermal Desktop with hand calculations in MATLAB and test data collected from a variety of test. In order to create fidelity in the models created in Thermal Desktop, preliminary modeling of a structural fin was done in both Thermal Desktop and MS Excel, and then tested in the clean room. The model predicts the temperatures at the various sensor locations to within 3 degrees Kelvin. The stated tolerance on the specification sheets is 3 degrees at the temperature range that the sensors were operating within. The first round of analysis indicated that the model was significantly off of the actual test data. Figure 2.10-9 through Figure 2.10-13show the fin sensor layout (denoted by the black circles) and resistive heater (in yellow), test setup pictures, thermal desktop meshed model, the transient response of the test, the thermal desktop model results, and finally the actual test data results.

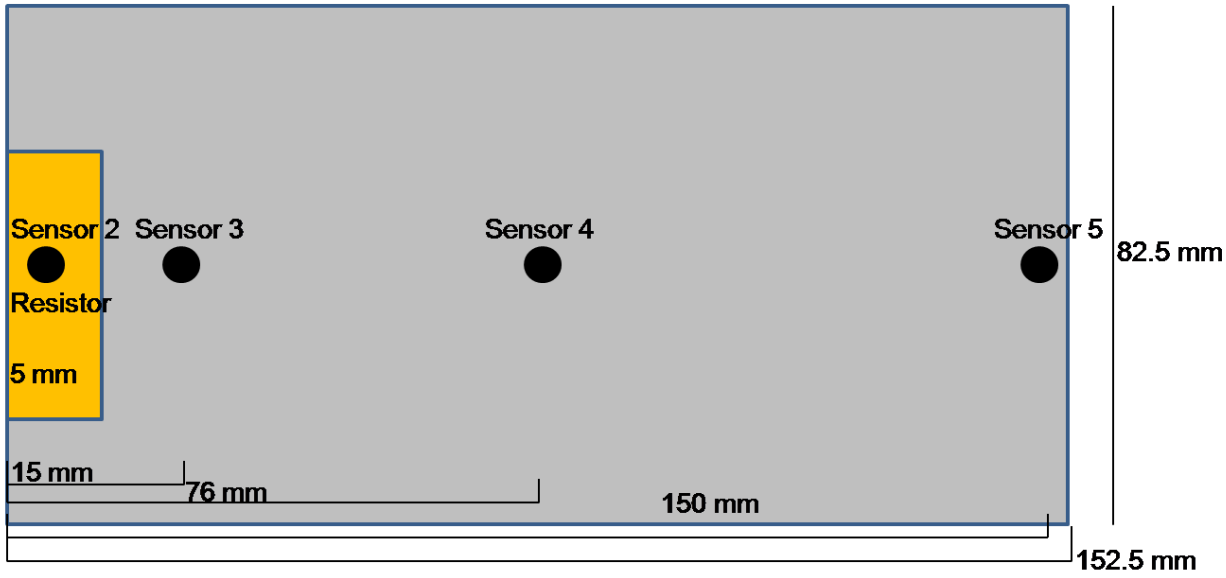

FIGURE 2.10-9: THERMAL FIN SENSOR LAYOUT

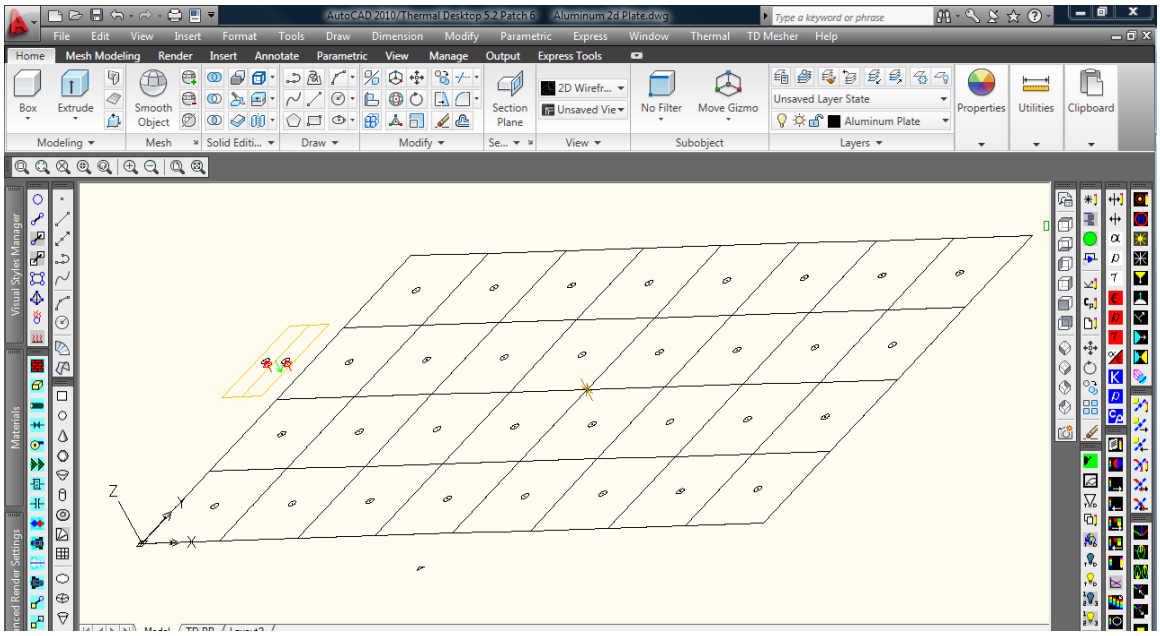

FIGURE 2.10-10: THERMAL DESKTOP FIN MODEL

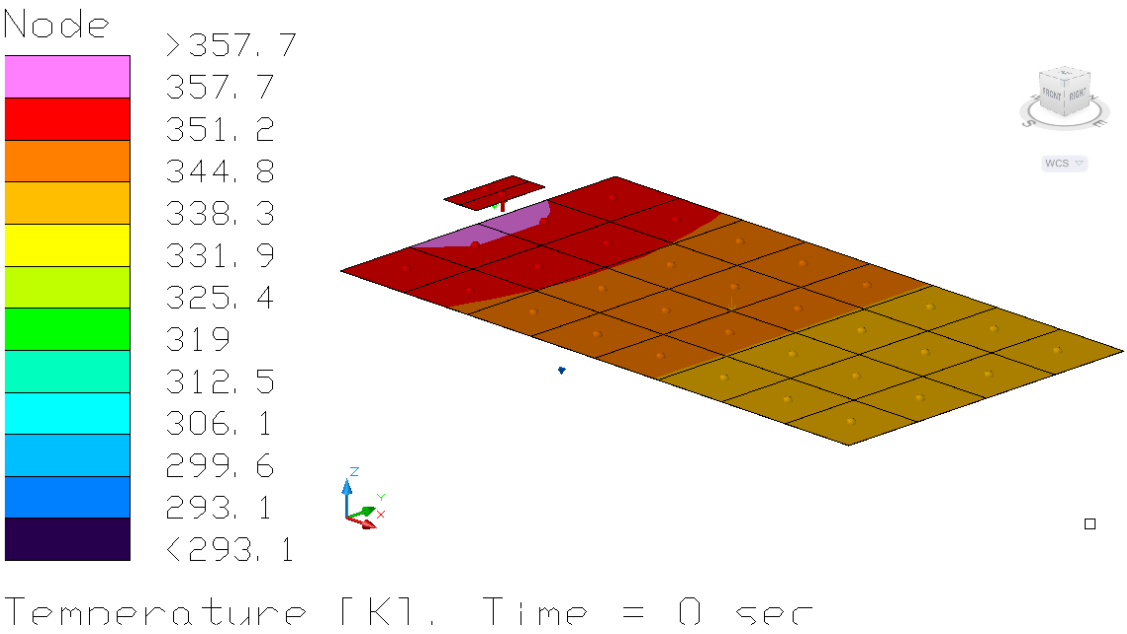

FIGURE 2.10-11: THERMAL DESKTOP TRANSIENT TEST RUN

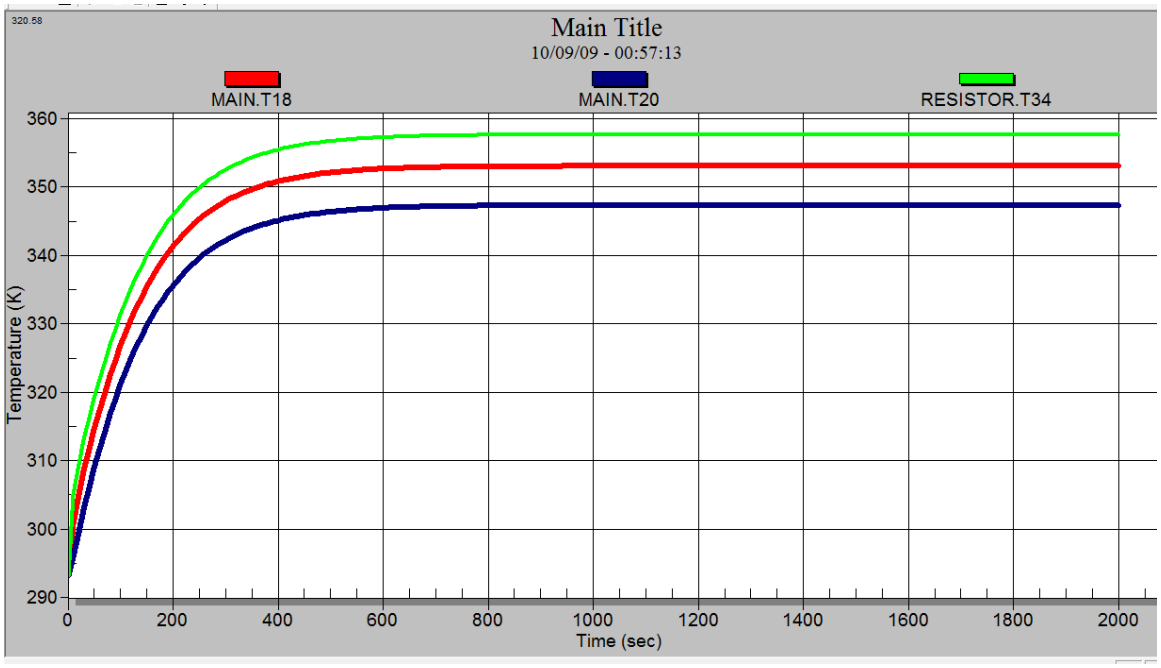

FIGURE 2.10-12: THERMAL DESKTOP FIN MODEL DATA

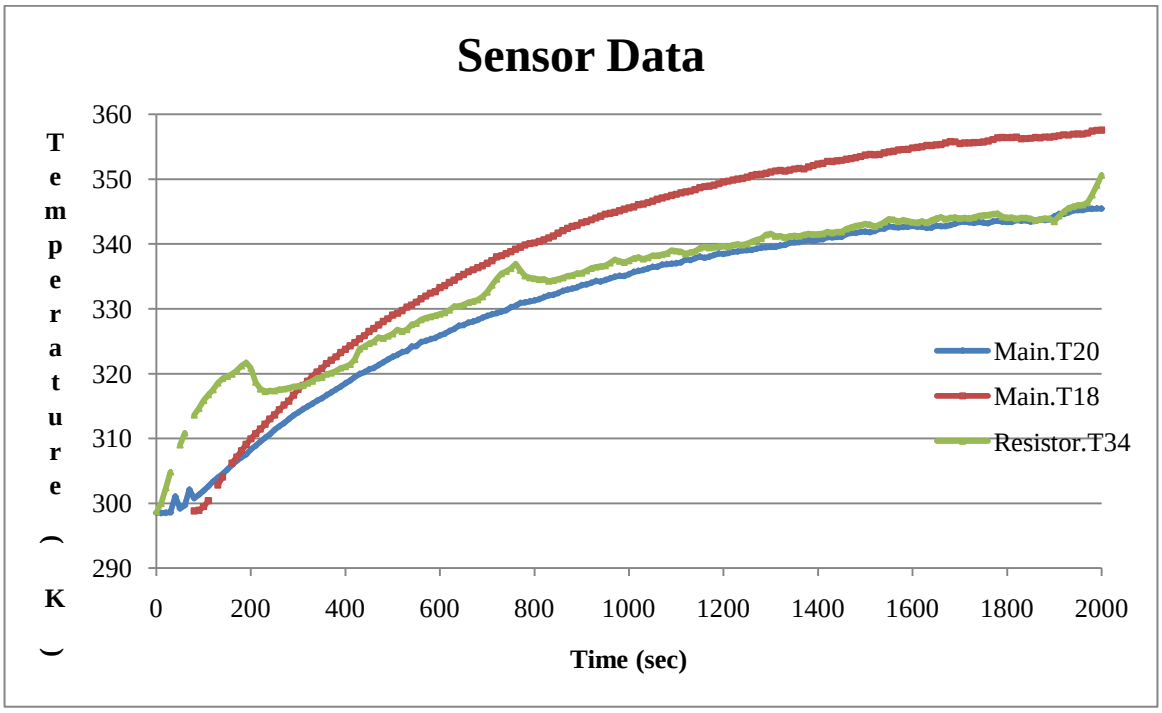

FIGURE 2.10-13: THERMAL FIN SENSOR DATA

The spikes in the resistor sensor were due to accidental changes in the current going to the sensors in combination with the error in the output of the sensor. The following are the input conditions given to Thermal Desktop in order to properly model the test environment.

- Conduction, convection, radiation, heat input
  - Same conditions as the steady state
  - Resistor initial temp @ 293.15K
  - Aluminum plate initial temp @ 293.15K
  - Ambient environment @ 293.15K
  - Test case run for 3600 sec (1 hour) at 100 sec intervals (5000 rays per surface)
    - Final temp mimics steady state as expected
    - Initial temp for all objects is as stated
- Model predicts a faster rise in temperature than the sensors display
- Model final temperatures are accurate to within 3 degrees of data
- Sensors are rated to +/- 3 degree accuracy

Clearly there is a significant discrepancy between the actual and model data. While the steady state temperatures only vary by a few degrees the time constant of the model is much higher than that of the actual data. This led to a resulting investigation of the sensors themselves. It is believed that the sensors naturally see a time lag in the temperatures that they record due to the resistance of the plastic material. Adding in the sensors to the Thermal Desktop model resulted in far closer model/data correlation. Additionally, accurately modeling the ambient temperature brought the steady state temperatures even closer than in Test 1.Figure 2.10-14 through Figure 2.10-16show the data for the ambient environment that was added to the Thermal Desktop fin model, the 4 sensor additions to the mesh layout, and finally the resulting model/data correlation.

Potential Error Sources:

- Sensor time lag
- Resistance of the sensor not taken into account
- Material properties were not exact
- Ambient temperature was a constant
- Glue did not hold sensors on aluminum well
- Thermal resistance of the glue not considered
- Radiating to black body instead of room temp

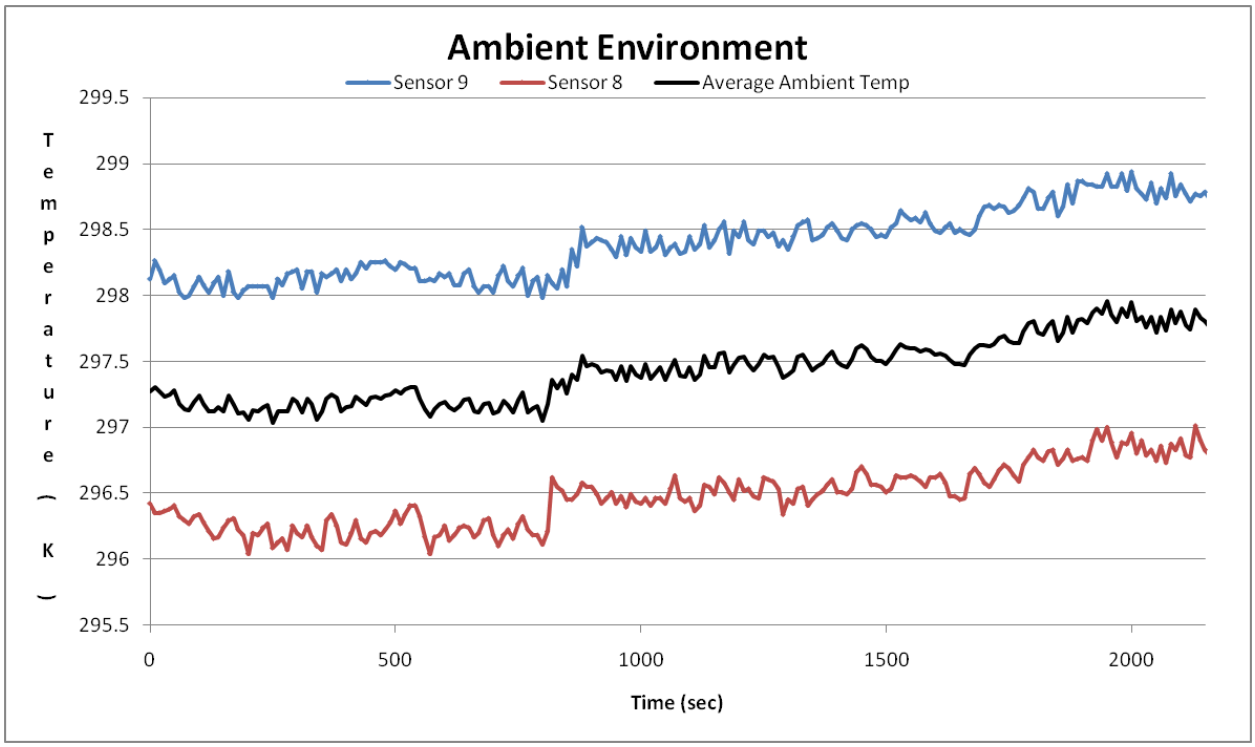

FIGURE 2.10-14: AMBIENT ENVIRONMENTAL DATA

- Added 4 sensors to the model
  - Black Plastic radiates with solar absorptivity 0.96 and IR emissivity 0.85 (α/ε = 1.129)
- Sampled model at sensor nodes
  - Resistance of plastic resistors should affect the time constant of the temperature response
- Changed aluminum material property to Al 7079 (K=121.34)
  - Heavily oxidized aluminum has solar absorptivity 0.96 and IR emissivity 0.85 (α/ε = 1.129)
- Matched ambient temperature profile, which shows our model is consistent with the test data.

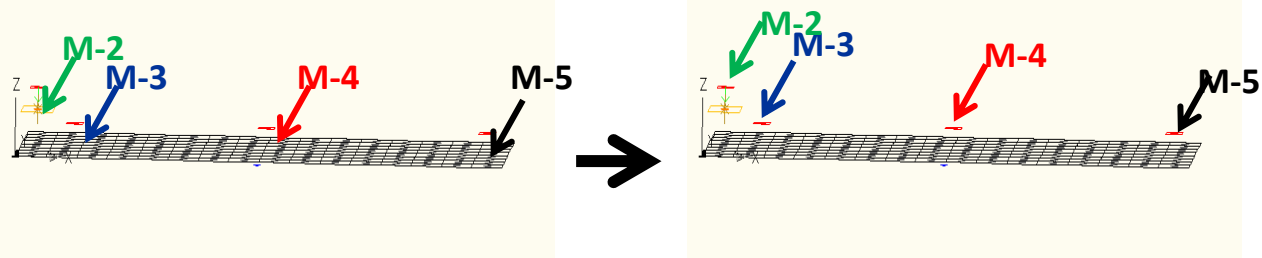

FIGURE 2.10-15: THERMAL DESKTOP MODEL CHANGES

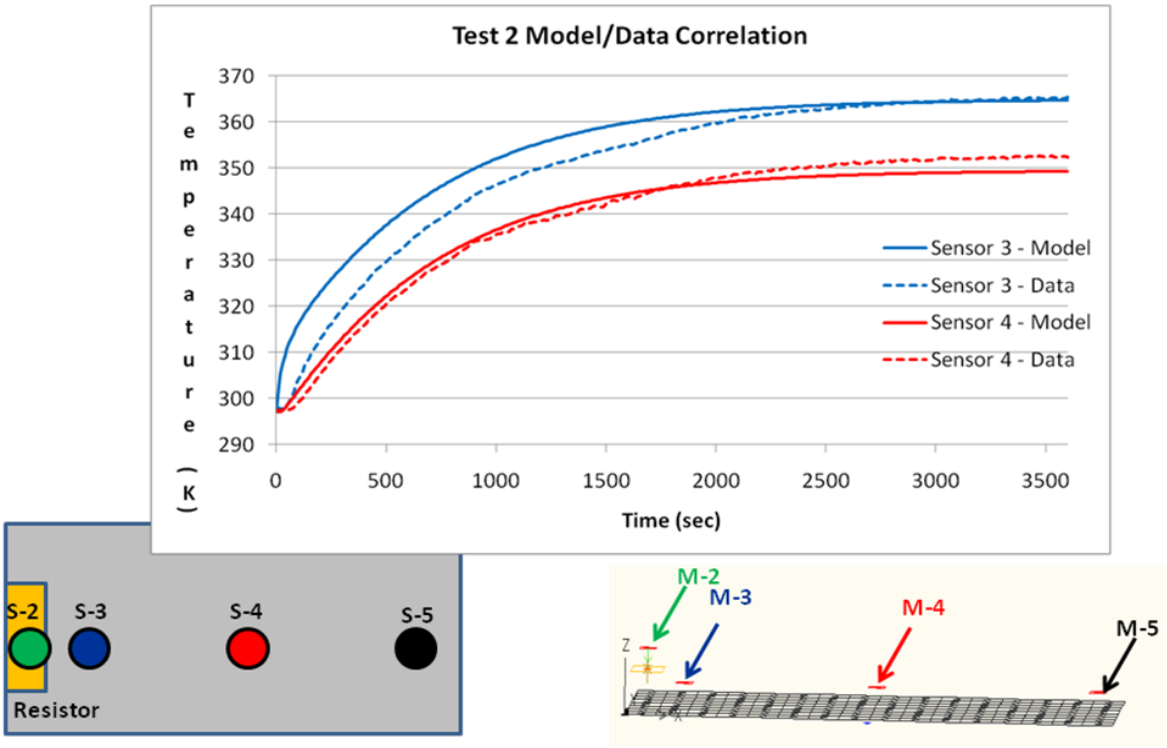

Figure 2.10-16: Test 2 Model/Data Correlation

2.10.7 SOLAR ARRAY COMPOSITE TESTING (A. ESPITIA)

2.10.7.1 PURPOSE

The structures team has assembled three potential layouts that will be thermally and structurally tested and analyzed to determine the best (most mass efficient, best thermal characteristics to keep cell temperatures in the right range, and meeting the ESPA and UNP launch load structural requirements.The purpose of the solar array composite testing was to determine which composite performed 'best' from a thermal perspective. 'Best' performance can be defined as keeping the critical components within their optimal range while maximizing their lifetime. Solar cells prefer to operate at ~-25C. The three design possibilities are identified and shown below.

- Design 1: Carbon fiber/Aluminum honeycomb composite, Fr4 PCB board, cells
- Design 2: Aluminum sheet/Aluminum honeycomb composite, Fr4 PCB board, cells
- Design 3: Aluminum 2D isogrid, Fr4 PCB board, cells

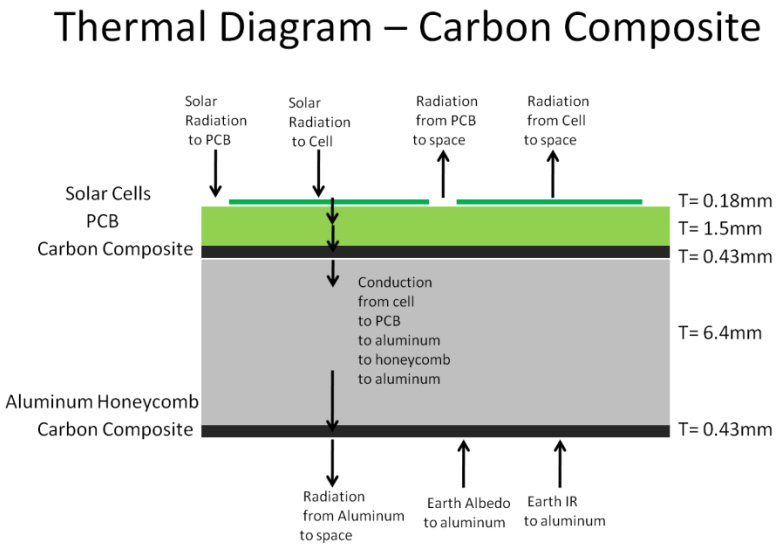

FIGURE 2.10-17: CARBON COMPOSITE LAYOUT

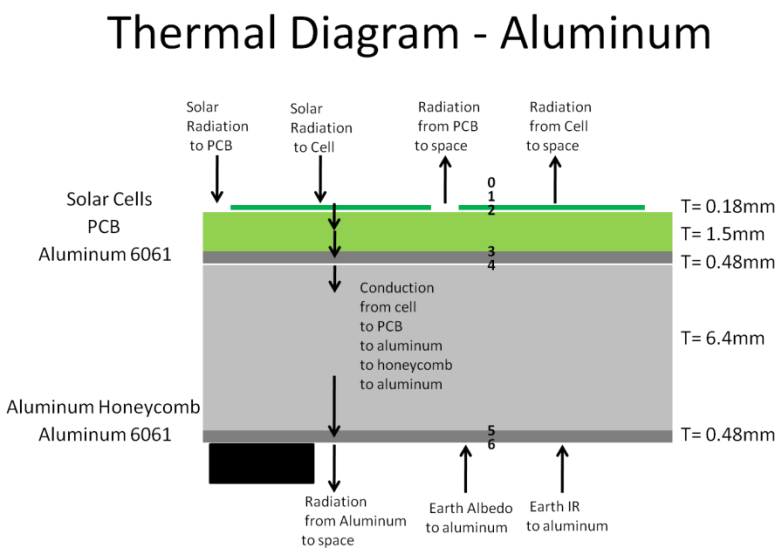

FIGURE 2.10-18: ALUMINUM LAYOUT

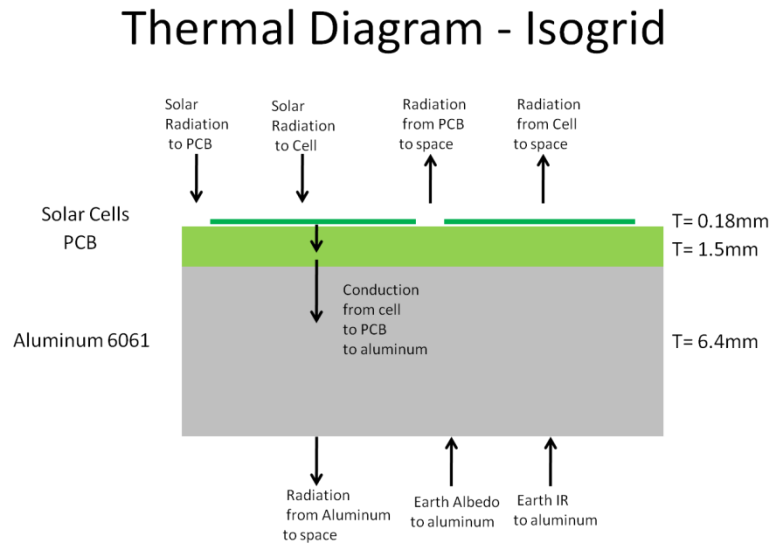

FIGURE 2.10-19: ALUMINUM ISOGRID

2.10.7.2 TEST PLAN

A Thermal desktop model of three different composite layouts was developed and analyzed. The three options included the carbon honeycomb composite layout, the aluminum phase sheet and honeycomb layout, and the solid aluminum sheet. Each of the three designs was also tested with the addition of the PCB board and four solar cells. The thermal desktop models were compared

to temperature data collected at room temperature. The test setup can be seen in Figure 2.10-20 and Figure 2.10-21.

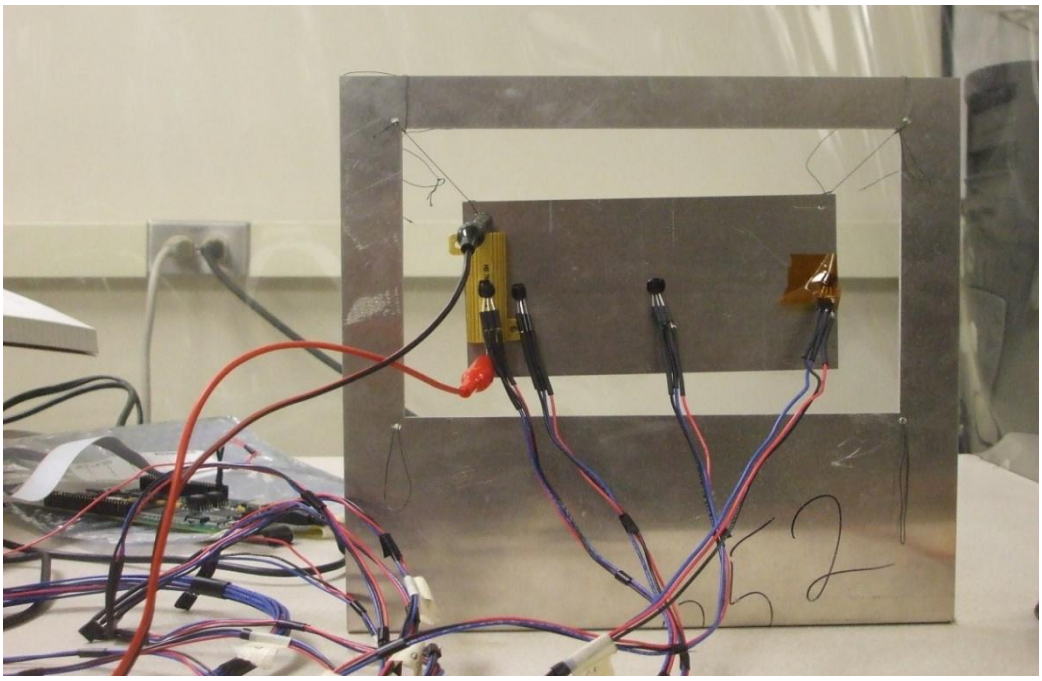

FIGURE 2.10-20: THERMAL FIN TEST SETUP 1

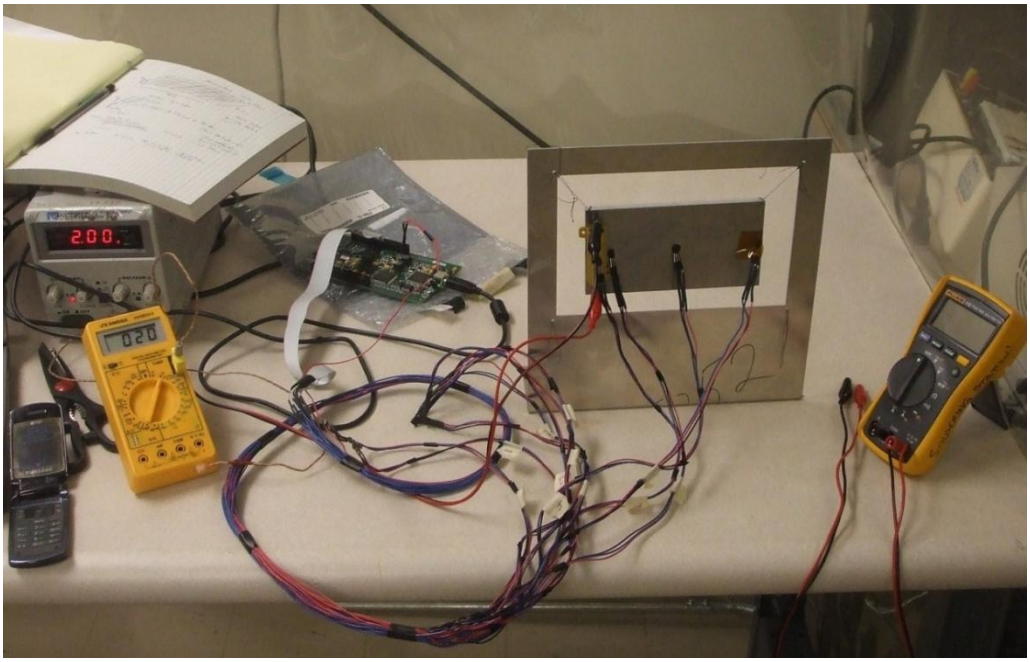

FIGURE 2.10-21: THERMAL FIN TEST SETUP 2

2.10.7.3 RESULTS

After analyzing the results, the aluminum sheet performed best with the aluminum phase sheet and honeycomb at a close second. According to the composite MATLAB models we can expect to see temperatures in the range of -46 to 25 degrees Celsius using the aluminum phase sheet and honeycomb design. While this design is nearly twice as heavy as the carbon composite and honeycomb design, it will keep the solar cells within the desired temperature range allowing them operate at their maximum efficiency point.

2.10.7.4 CONCLUSION

The Thermal Team's conclusion is that the aluminum sheet with honeycomb design will give the best thermal performance at the lowest mass cost.However, the structures team has decided to use an aluminum honeycomb composite with PCB on both sides, which benefit the power team's wiring of solar cells and found to the best panel design during vibration test. Though it is not the best thermal design in terms of conduction, the proposed design was still shown to perform well thermally and keep the solar cells near their optimal operating range of -25°C.

2.10.8 AVIONICS FLATSAT TESTING (A. ESPITIA)

2.10.8.1 PURPOSE

In order to monitor the temperature of various components of the satellite, the thermal subsystem will use 20 sensors to do so. The figure below outlines the sensor locations. Fourteen (in red) are LM19 analog sensors (see page 276) that will be able to connect and obtain power from one of the PICs in the avionics system. The six (in yellow)others are K-type thermocouples, which are more robust and have a larger range of temperatures it can monitor. The thermocouple will also interface with the avionics system through a PIC.

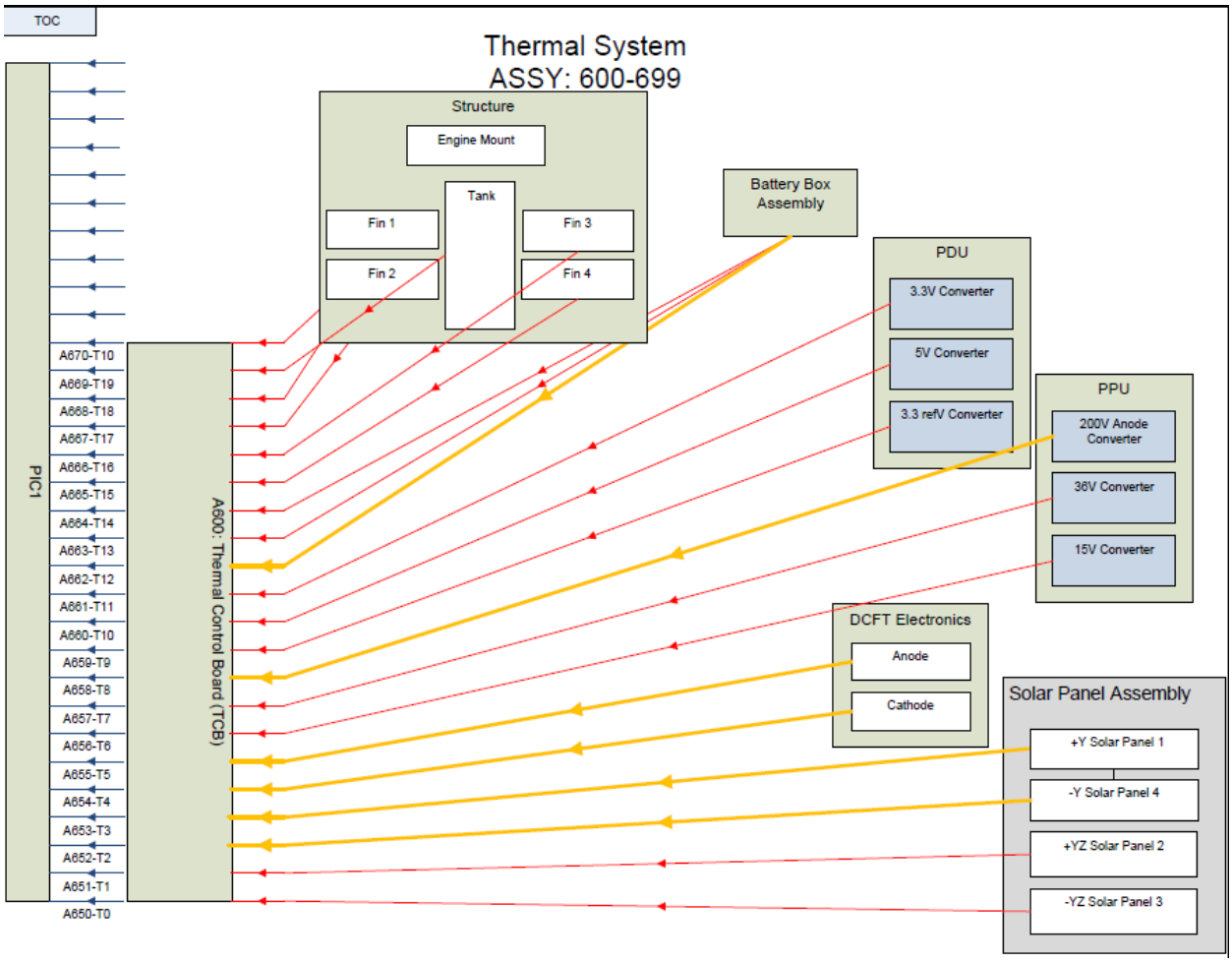

FIGURE 2.10-22: SENSOR LOCATION DIAGRAM

The purpose of the Avionics Flatsat testing is to show that the Avionics system, in particular the Pic, can read, store, and transmit data from the thermal sensors that are to be used to monitor the temperatures of components of the satellite throughout its mission lifetime.

2.10.8.2 TEST PLAN

The LM19 sensors and the K type thermocouples will be connected to one of the PICs on the Avionics system, where they can transmit data and receive power and ground (if necessary). Once properly connected, the code that runs the Avionics system will begin to run and start reading the data. It will continue to read the sensor data throughout the duration of the test, which will be TBD minutes. The PIC will store and transmit the data as commanded/necessary.

2.10.8.3 SCHEDULE

The Avionics Flatsat testing will be broken down into three main phases. The first is to show that the PIC is able to read one of thermal sensors. That part has been partially completed since the PIC was able to read one of the LM19 analog sensors. The team still must test its ability to read a thermocouple. That is scheduled to be done in June 2010 once the proper thermocouple

interfaces are designed. The second main phase is the ability to store the sensor data in proper files in the allocated memory. This is tentatively scheduled to take place in late June 2010. The third phase of the testing is the ability to transmit the stored data back to the ground, where the data can be processed/used as necessary. The test date for this is tentatively also scheduled in late June 2010.

2.10.9 LAB WORK: ENGINE TESTING (A. ESPITIA & W. PINO)

2.10.9.1 PURPOSE

The purpose of the Engine Testing is to monitor the temperatures the engine experiences during operation, ensure that they are below 327°C, the critical temperature of the engine, and to record this data and incorporate it into current thermal models of the engine. Additionally, the test results will aid in the thermal design over the engine, the mount it's placed on, and the four posts that connect the mount to the top tank clamp. Currently, the thermal design has Z93 paint on all components in order to keep the temperature the components will experience at low temperatures (less than 450K).

2.10.9.2 TEST PLAN

A thermal model based on known values of the engine was developed in Thermal Desktop and MATLAB (see Section 5.9.2) and evaluated. The engine will be placed in a vacuum chamber at room temperature, 22°C, and turned on. As it will be on the satellite, a Type K Thermocouple will be placed at the base of the anode and at the base of the outer shell of the engine. The temperature readings will be monitored and recorded until the engine has reached a steady state. The actual temperature readings measured will be compared to the results from hand calculations and Thermal Desktop. The thermal models will then be adjusted as needed.

2.10.9.3 SCHEDULE

The Engine test is currently ongoing in the Space Propulsion laboratory in coordination with the Propulsion team. Four K-type thermocouples (provided by Aurora Flight Sciences) will be placed in various locations on the engine. The engine first must be conditioned for four hours prior to firing.

2.10.9.4 SKILLS ACQUIRED

Similar to the solar array composite testing (described earlier) and the TVac test, the thermal team has and is still developing important skills. The main skill the team has learned from lab work is validating Thermal Desktop models by correlating prediction the model makes with actual test data. The team has learned how to properly carry out a test from start (writing the test plan) to end (analyzing the data). Additionally, the team gained the skills of modeling test environments in Thermal Desktop, such as creating a vacuum chamber to place the engine in order to accurately model the actual test setup. This also included specifying the proper input variables (ambient temperature, conductivity, convection coefficient, any boundary conditions). This will allow the team to have model prediction in conjunction with test data so the two sets

data can be correlated and the Thermal Desktop models can be validated. After validation, the team is able to revise/make a final design choice in the thermal design of the components/satellite.

3 BEYOND PQR

3.1 FCR (L. JOHNSON)

FCR will be held in Albuquerque, NM on January 17th, 2011. Due at FCR are a set of documents that full describe and analyze the satellite design. These documents are due to UNP by December 27th, 2010. At FCR the Satellite Team will have 15 minutes to present on the design and 20 minutes to demonstrate the satellites functionality at a booth. The winning satellite will be chosen at the end of the day. If CASTOR is chosen, we will enter Phase 2 of the University Nanosat Program and will need to deliver a completed satellite to AFRL by June for complete environmental and functionality testing. The required documents are listed on the fileshare.

[The Deliverables List will found in Section 42.78 of the Fileshare as

Deliverable_Status.xlsx]

3.2 ASSEMBLY PLANS (L. JOHNSON)

The purpose of this document is to describe the specifications and methods by which parts of the spacecraft will be reassembled when dismantled for testing.

Each subteam is responsible for the development of assembly plans for their subsystem. Structures and Systems team are responsible for the system wide assembly plan. These plans will be used once the satellite has been handed over to AFRL for testing and launch.

[The Assembly Plans will found in Section 4.2.7.1 of the Fileshare in the

Assembly Plan Documentation folder]

3.3 VEHICLE INTEGRATION PLAN (A. FUHRMANN)

The purpose of this document is to describe the plan and methods that will be used for integrating the various subsystems into a cohesive vehicle. It provides the overarching procedures and schedule to be used. Supplemental documentation, primarily the ICDs and mechanical drawings, further defines how the integration must be performed.

For each subsystem, it will first be tested per the integration plan functionality tests by the "ready for integration" date. Then it will be integrated per the procedure described with the help of the relevant ICDs by those listed under tasking by the "integrated" date. To this end, the relevant mechanical ICD can be used to find the appropriate mounting information (such as bolt hole pattern). Further physical envelopes of the different parts are provided in the mechanical drawings. The data and power ICDs can be used to find the specifications and connections to the data and power connections. Finally, the system will be wired with both data and power per the

ICDs and tested again for functionality by the "wired" date. See the Integration Plan section of the Design Document for full details on the general procedures and standards.

[The Integration Plan may be found in Section 2.7 of the Fileshare as

CASTOR-Manufacturing_Plan.doc]

3.4 TESTING PLAN (K. ANDERSON)

All test plans can be found in the associated test plans. The three system level tests are the Balloon SHOT (II), Vibration, and Thermal Vacuum test and are listed with the subsystem performing them.

Index of tests (all plans and results are available in Appendix 5.6.

- Avionics
  - EMC/EMI (August 2010)
  - FlatSat I (Ground station Communications) (November 2009)
  - FlatSat II (Read Thermal/Power Sensor Data) (May 2010)
  - FlatSat III (Read/Operate ACS sensors) (May 2010)
  - FlatSat IV (PPU/Linear Actuators/Inhibits) (May 2010)
  - FlatSat V (Operate XFS) (May 2010)
  - FlatSat VI (Radiation effects) (May 2010)
  - Balloon SHOT (II) (June 11-13th 2010)
- Communications
  - Antenna (April 2010)
- ACS
  - GPS (November 2009)
  - Magnetometers (March 2010)
  - Reaction Wheels (March 2010)
  - Torque Coils (June 2010)
  - Sun Sensors (October 2010)
- Power
  - Integrated PPU (May 2010)
  - MPPT (July 2010)
  - On-board Charger (May 2010)
  - PDU (April 2010)
  - FlatSat (August 2009)
  - Solar Power (April 2010)
  - PDU converter (Summer 2010)
- Structures
  - Vibration (March 2009, February 2010, October 2010)
  - Thermal-Vacuum (March 2010, October 2010)
- Science
  - Camera Avionics (May 2010)
  - Camera Functional (September 2010)
  - Camera Thermal-Vacuum (April 010)

    - Camera Vibration (April 2010)
- Propulsion
    - DCFT Efficiency (April 2010)
    - Feed System (June 2010)
    - Integrated PPU (May 2010)

4 REFERENCES

[1] “Schedule,” https://planetx.mit.edu/svn/83_fileshare/1-Management/1.1-Schedule/

[2] “ICD Management,” https://planetx.mit.edu/svn/83_fileshare/2-Systems/2.2-Interfaces_Management/

[3] “NASA Systems Engineering Handbook,” URL http://education.ksc.nasa.gov/esmdspacegrant/SystemsEngineering.htm. (Visited February 2010).

[4] “Risk Management,” https://planetx.mit.edu/svn/83_fileshare/2-Systems/2.5-Risk/RiskManagements.xls

5 APPENDICES

5.1 REQUIREMENTS (K. ANDERSON)

[The RVM may be found in Section 2.6 of the Fileshare as CASTOR-RVM-clean]

5.2 MASTER EQUIPMENT LIST (G. FRITZ)

[The MEL may be found in Section 2.1.2 of the Fileshare as UNP-MEL-Current]

5.3 INTERFACE CONTROL DOCUMENTS (A. FUHRMANN)

[The ICDs may be found in Section 2.2-Interfaces Management of the Fileshare.]

5.4 SCHEDULE (G. FRITZ)

[The Schedule may be found in Section 1.1 of the Fileshare as Full Schedule]

5.5 RISK MATRIX (J. JAMES)

[The risk matrix may be found in Section 2.5 of the Fileshare as Risk_Mitigation]

5.6 TESTING PLANS (K. ANDERSON)

[The testing plans may be found in Section 2.4.1 of the Fileshare as Testing_Plans]

5.7 CAD DRAWINGS (E. PETERS)

*[Larger versions of the CAD Drawings may be found in Section 5.3.12.3 of the Fileshare as *.pdf]*

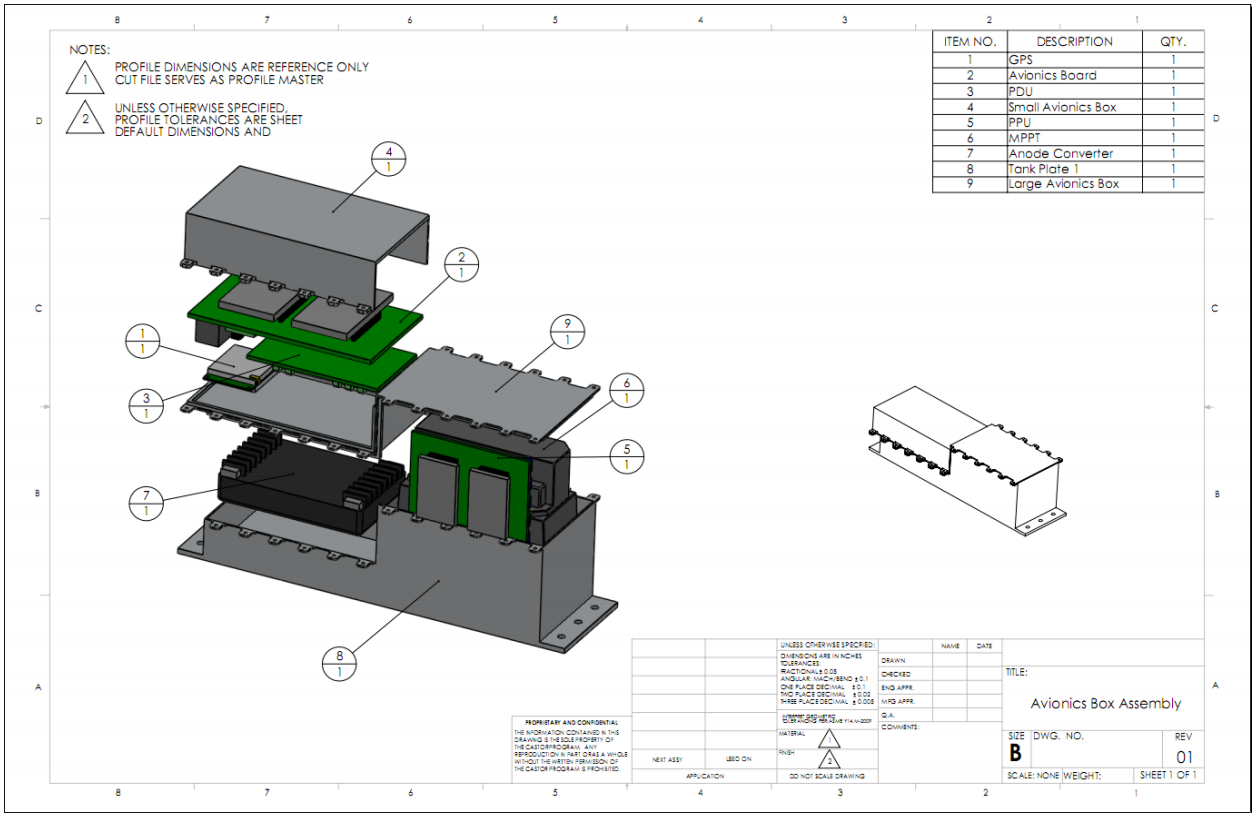

Figure 4.9 - 1: Avionics box assembly

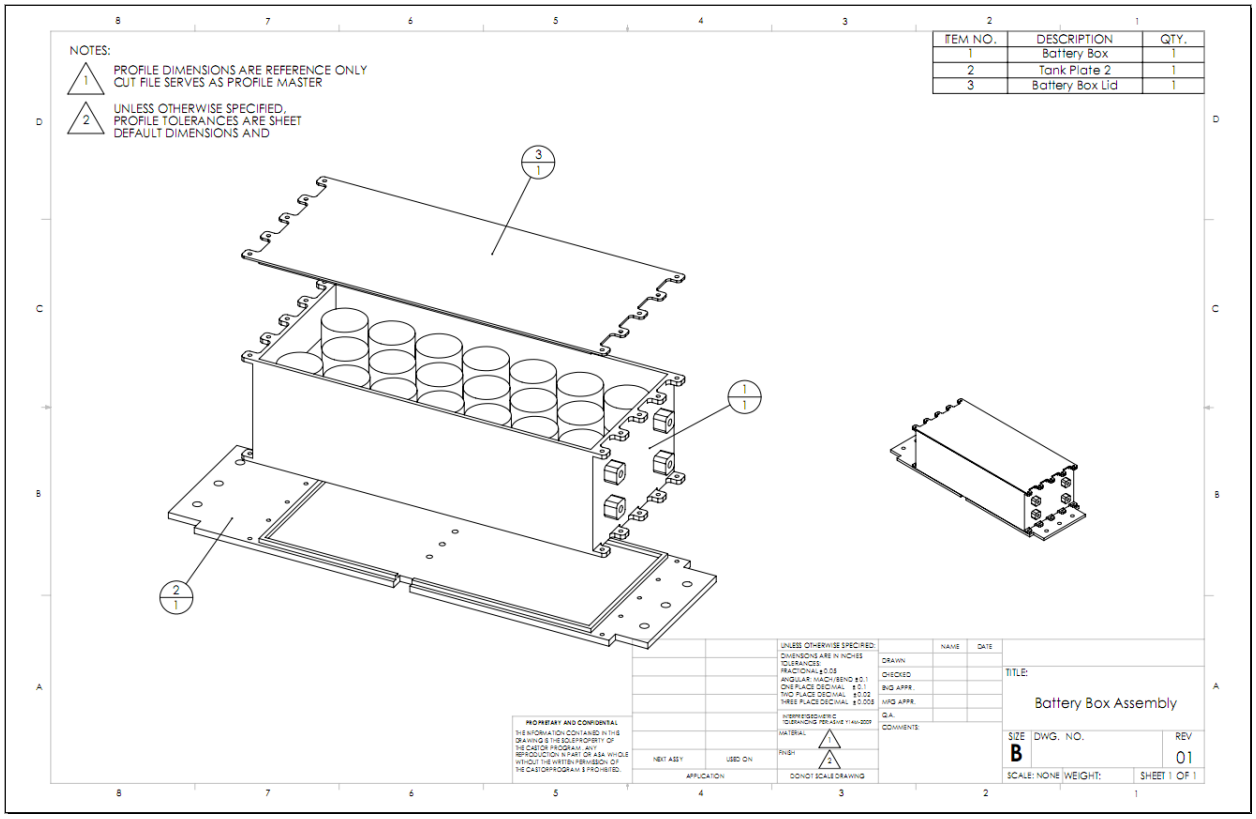

Figure 4.9 - 2: Battery box assembly

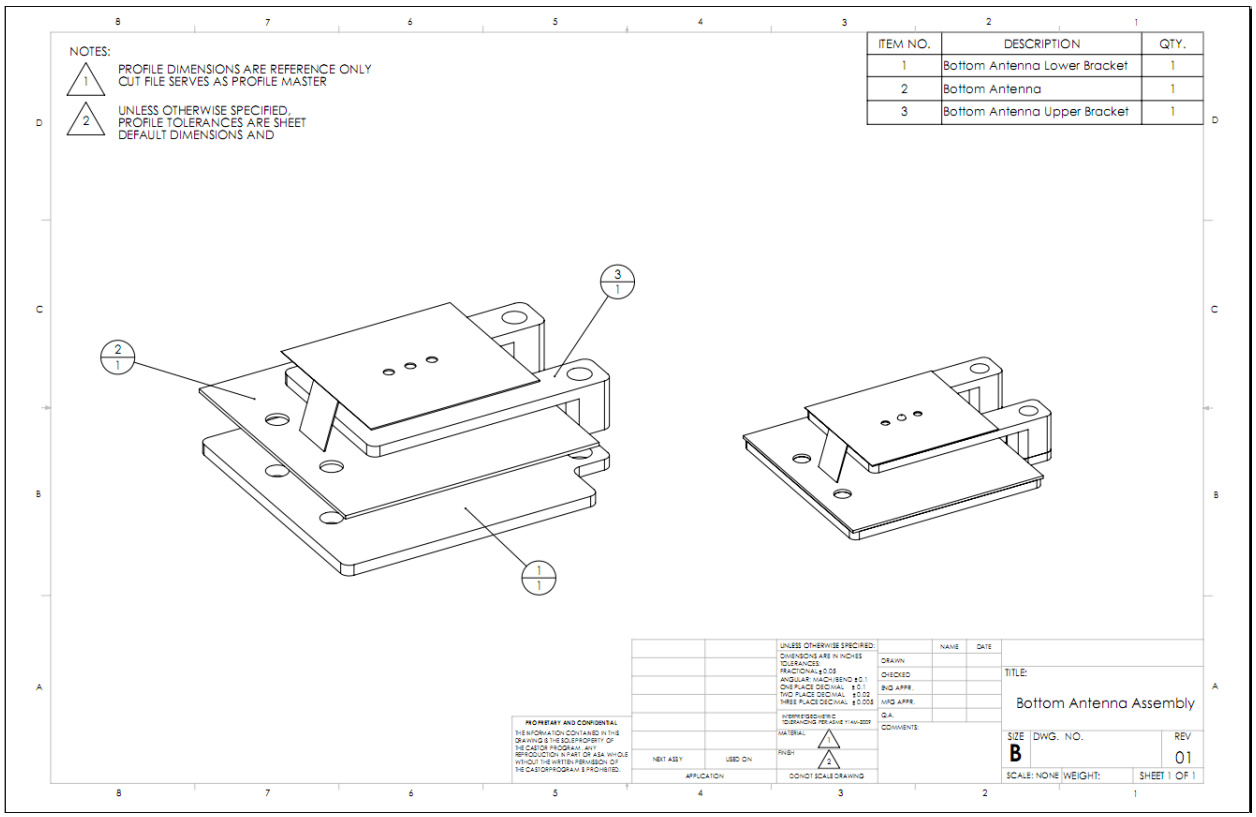

Figure 4.9 - 3: Bottom antenna assembly

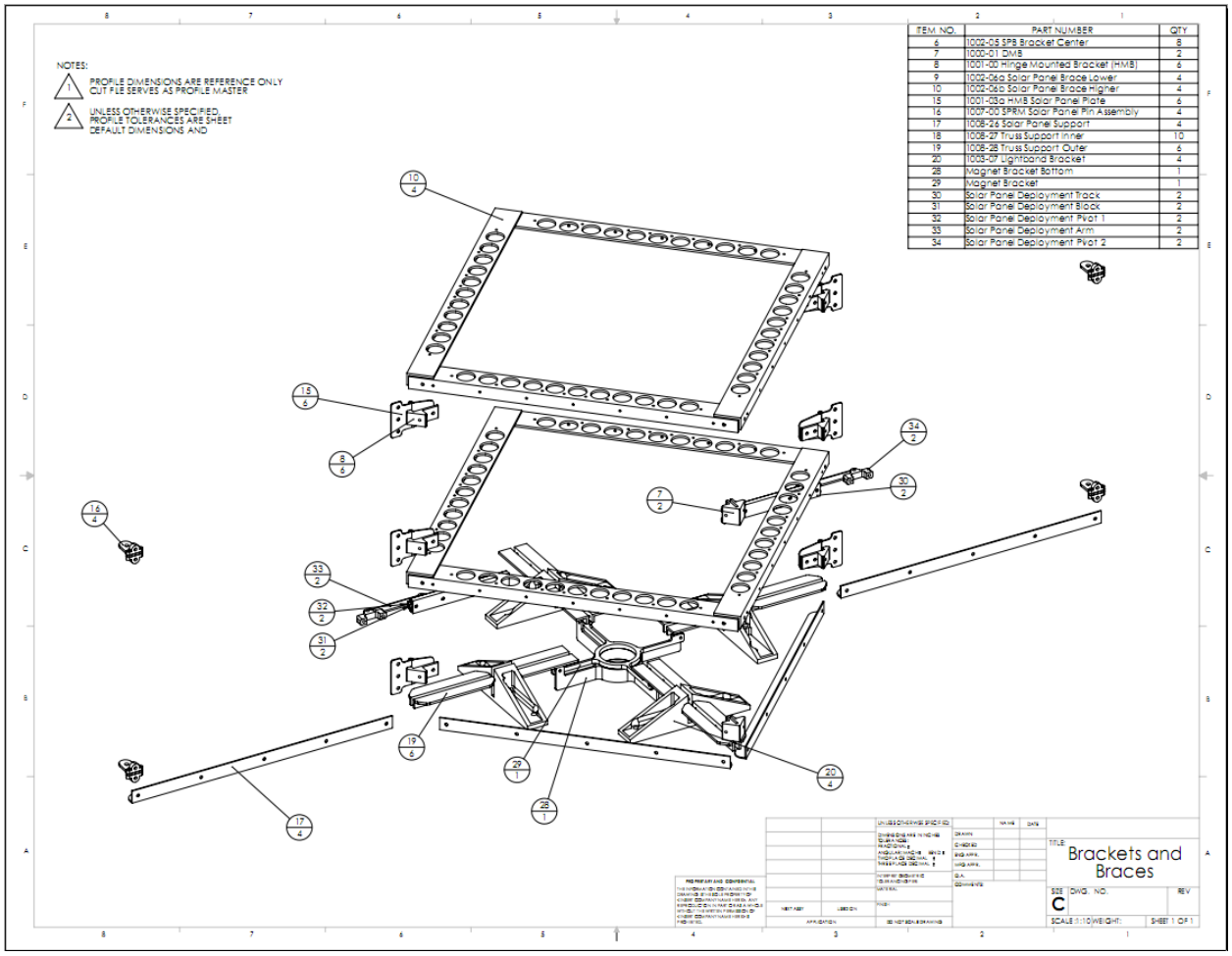

Figure 4.9 - 4: Brackets and braces assembly

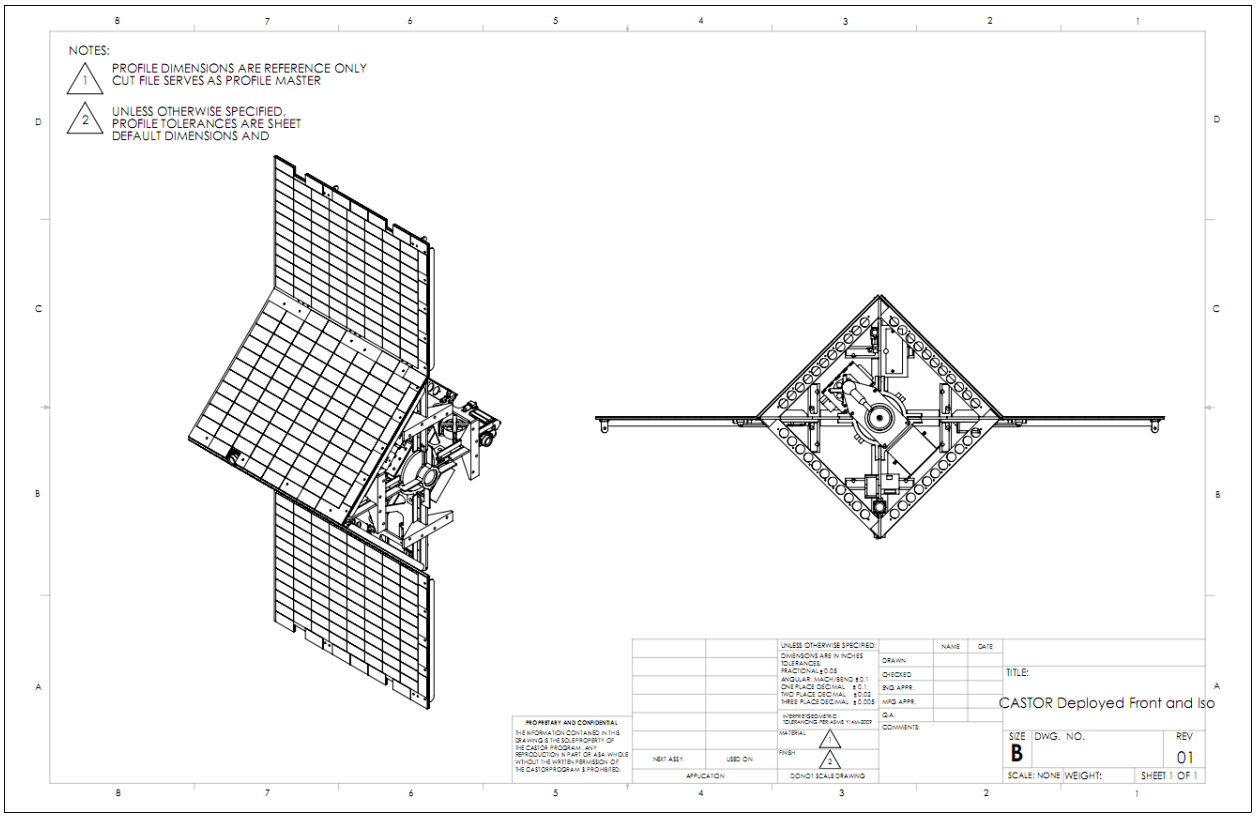

Figure 4.9 - 5: CASTOR Deployed Configuration

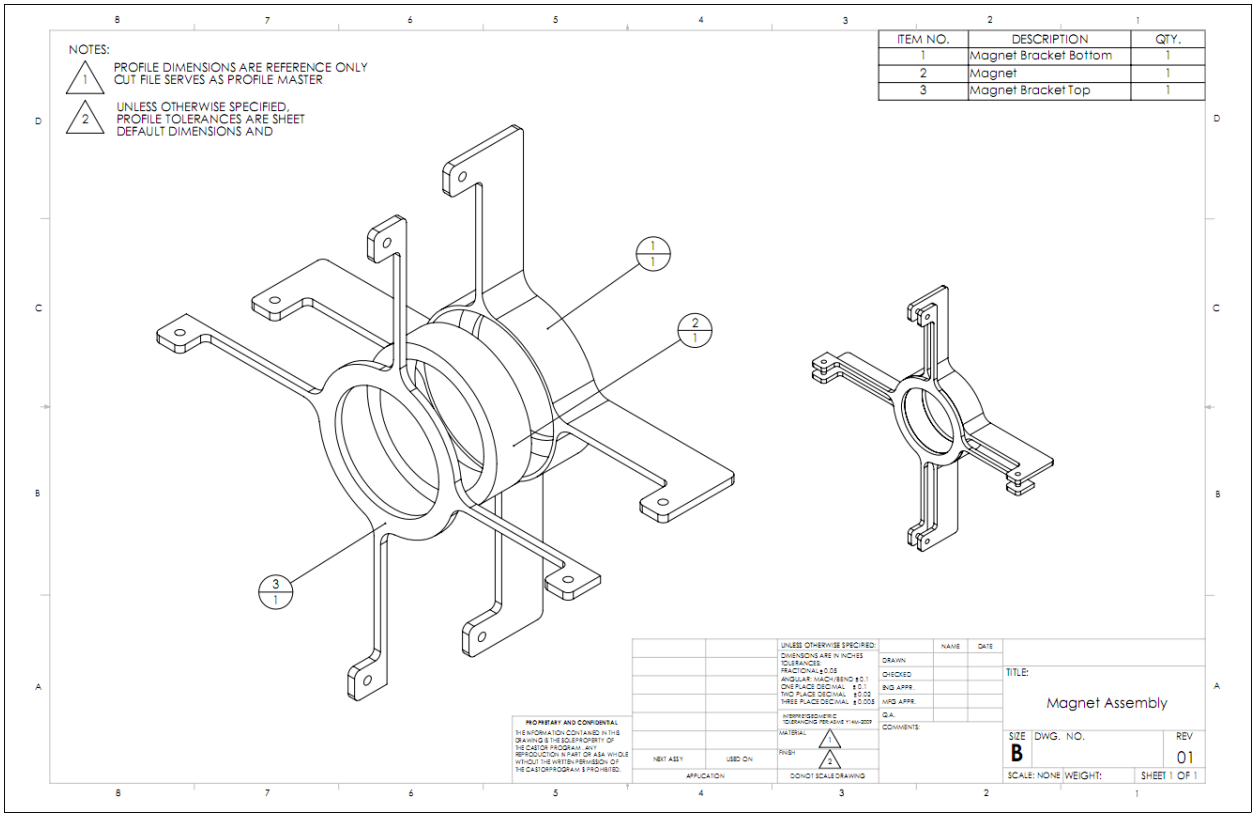

Figure 4.9- 6: Magnet bracket assembly

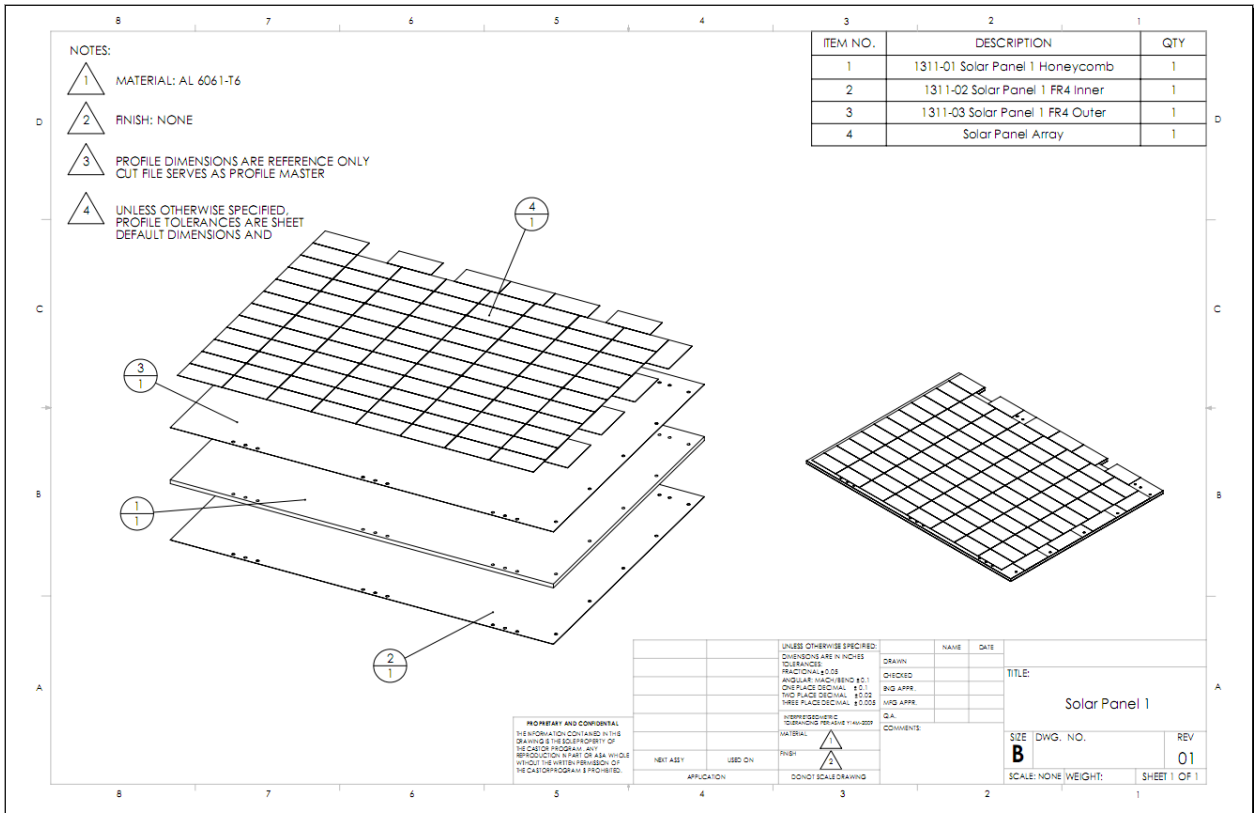

Figure 4.9 - 7: Solar panel 1

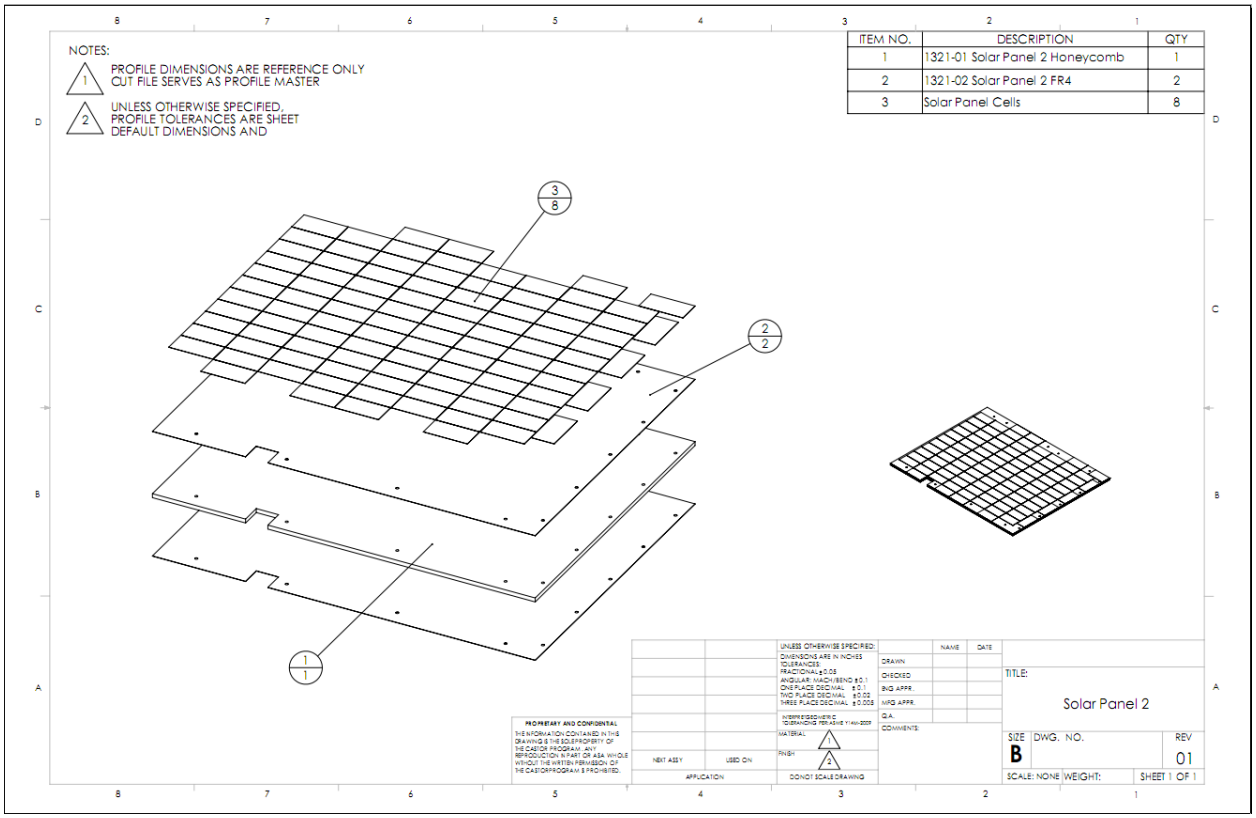

Figure 4.9 - 8: Solar panel 2

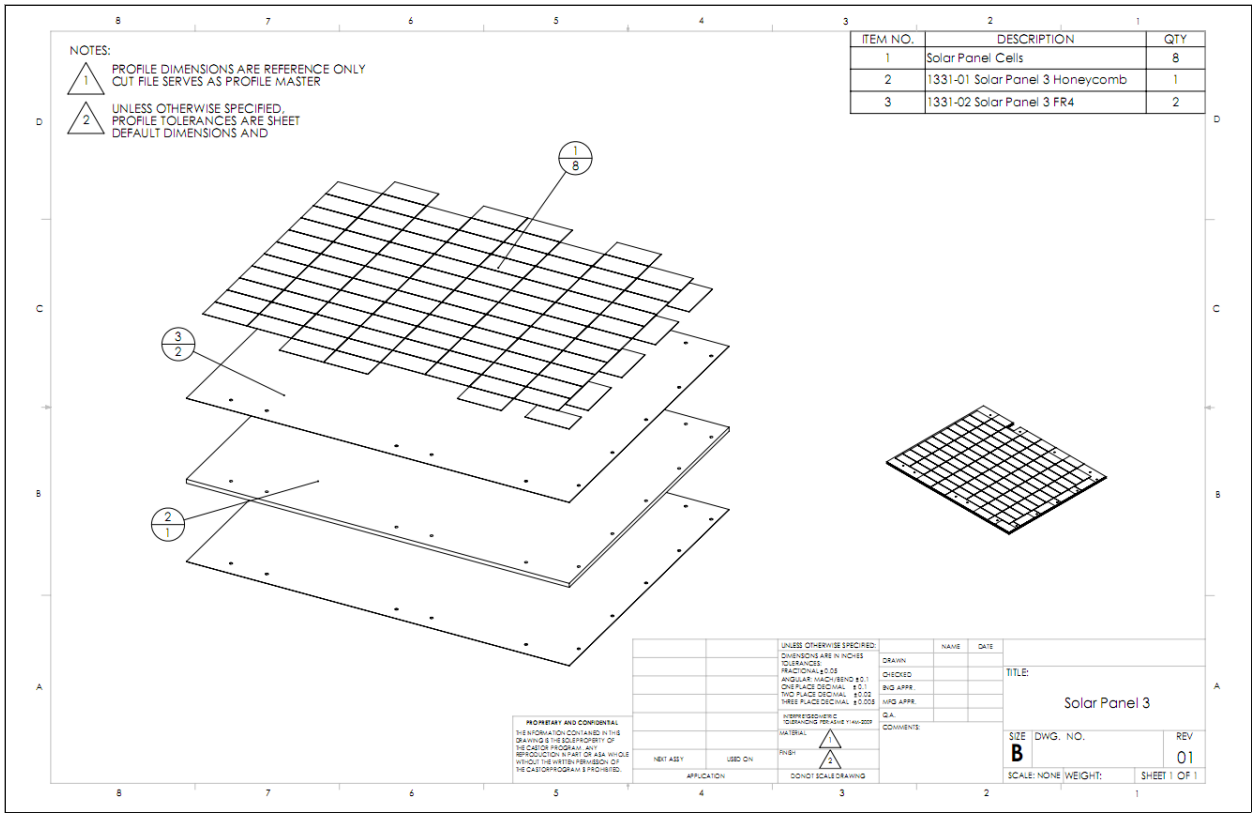

Figure 4.9 - 9: Solar panel 3

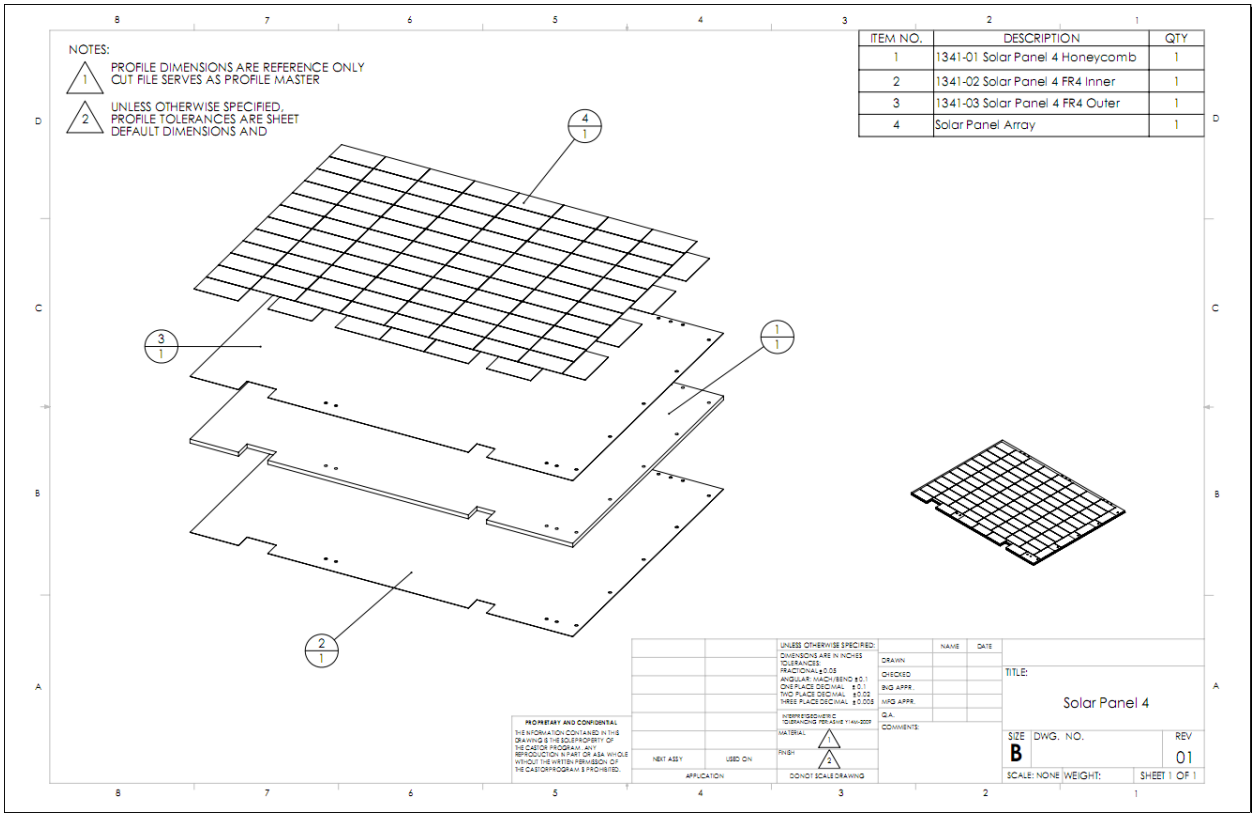

Figure 4.9 - 10: Solar panel 4

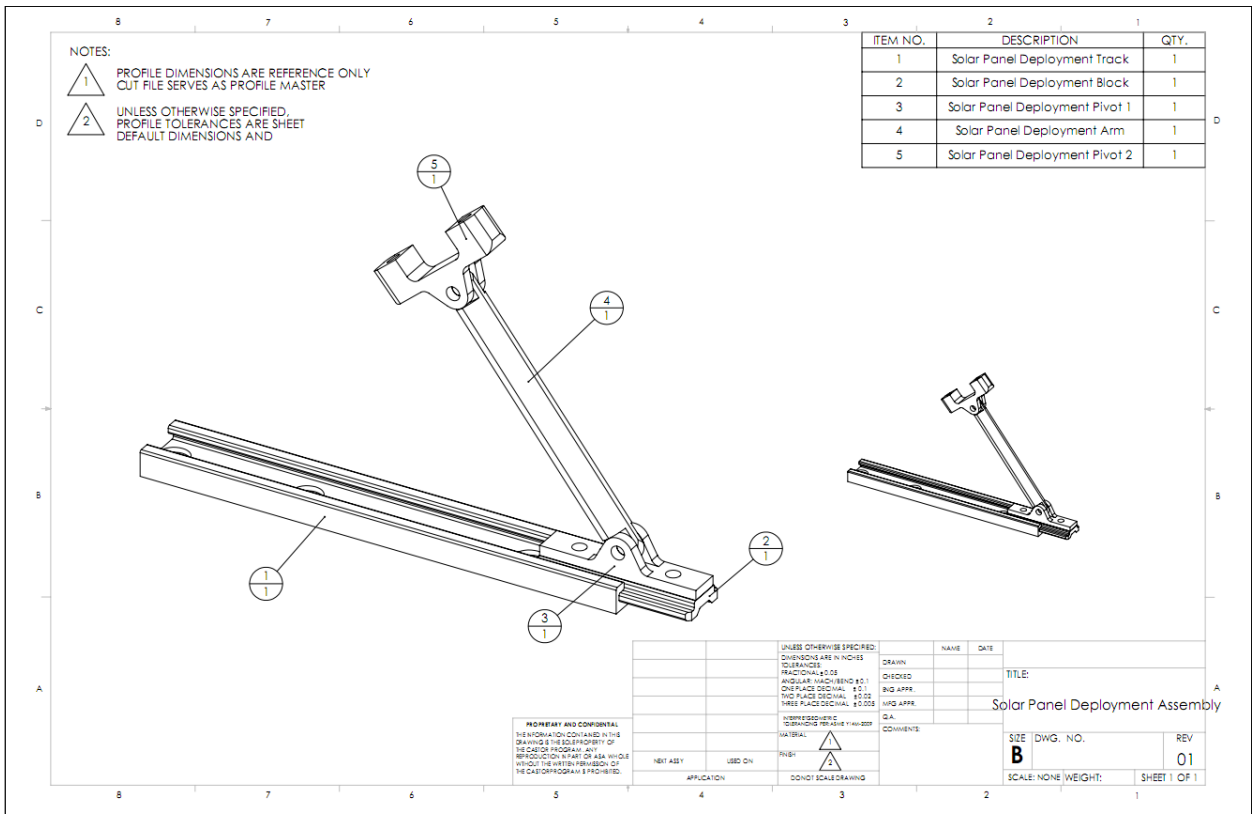

Figure 4.9 - 12: Solar Panel Deployment Mechanism assembly

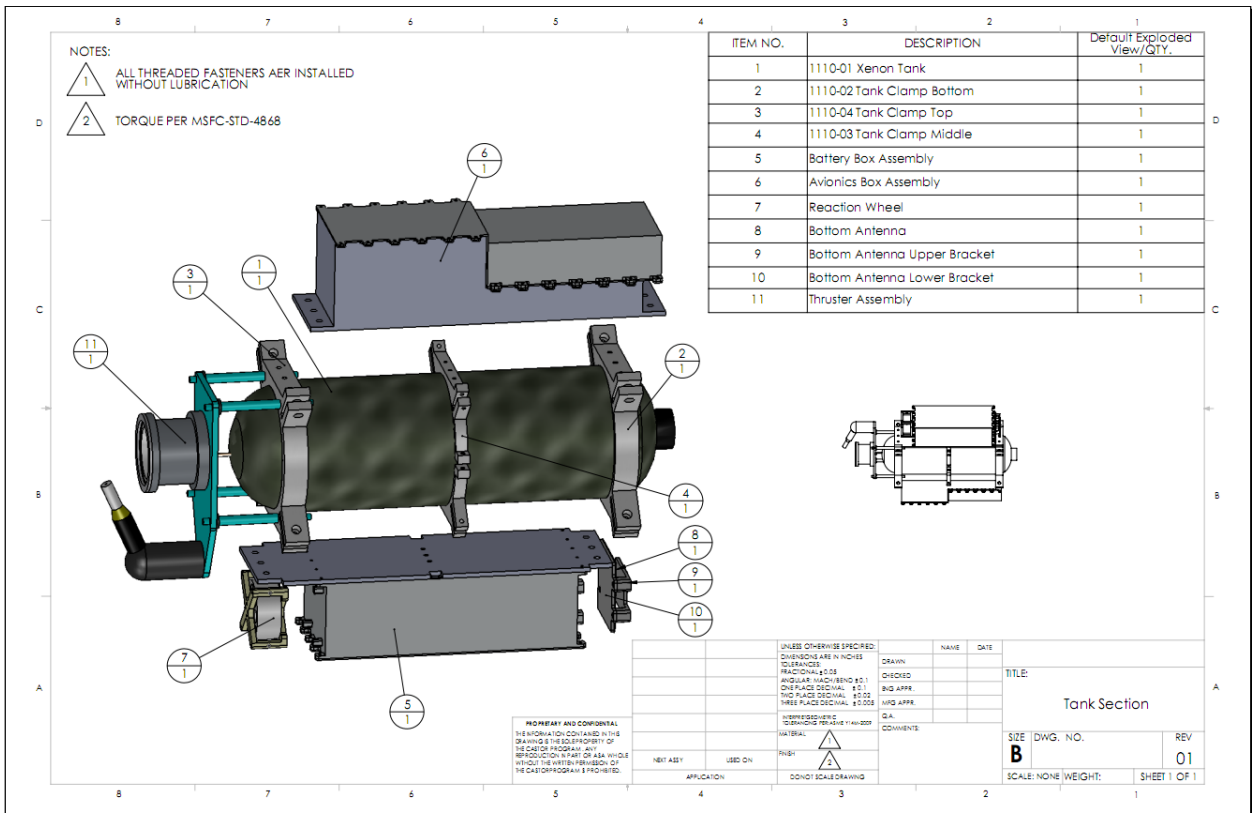

Figure 4.9 - 13: Tank section

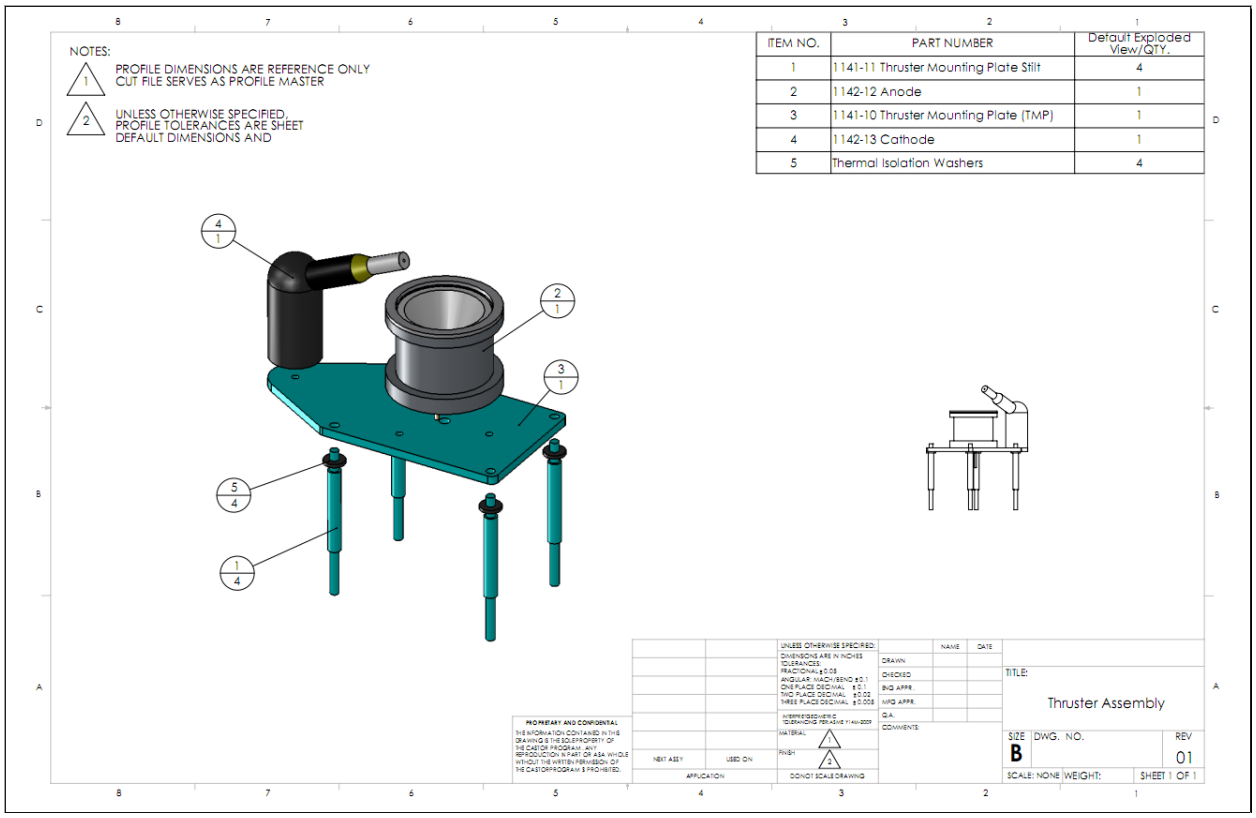

Figure 4.9 - 14: Thruster assembly

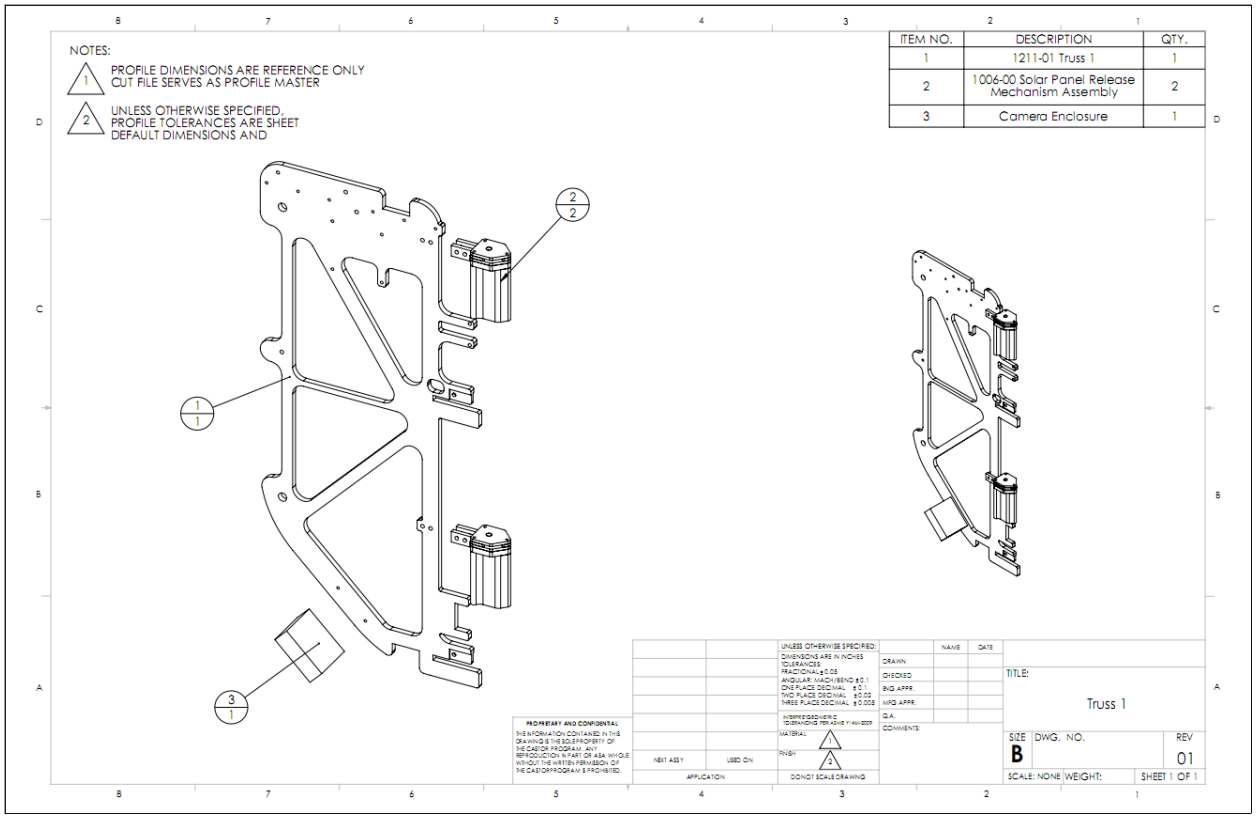

Figure 4.9 - 15: Truss 1

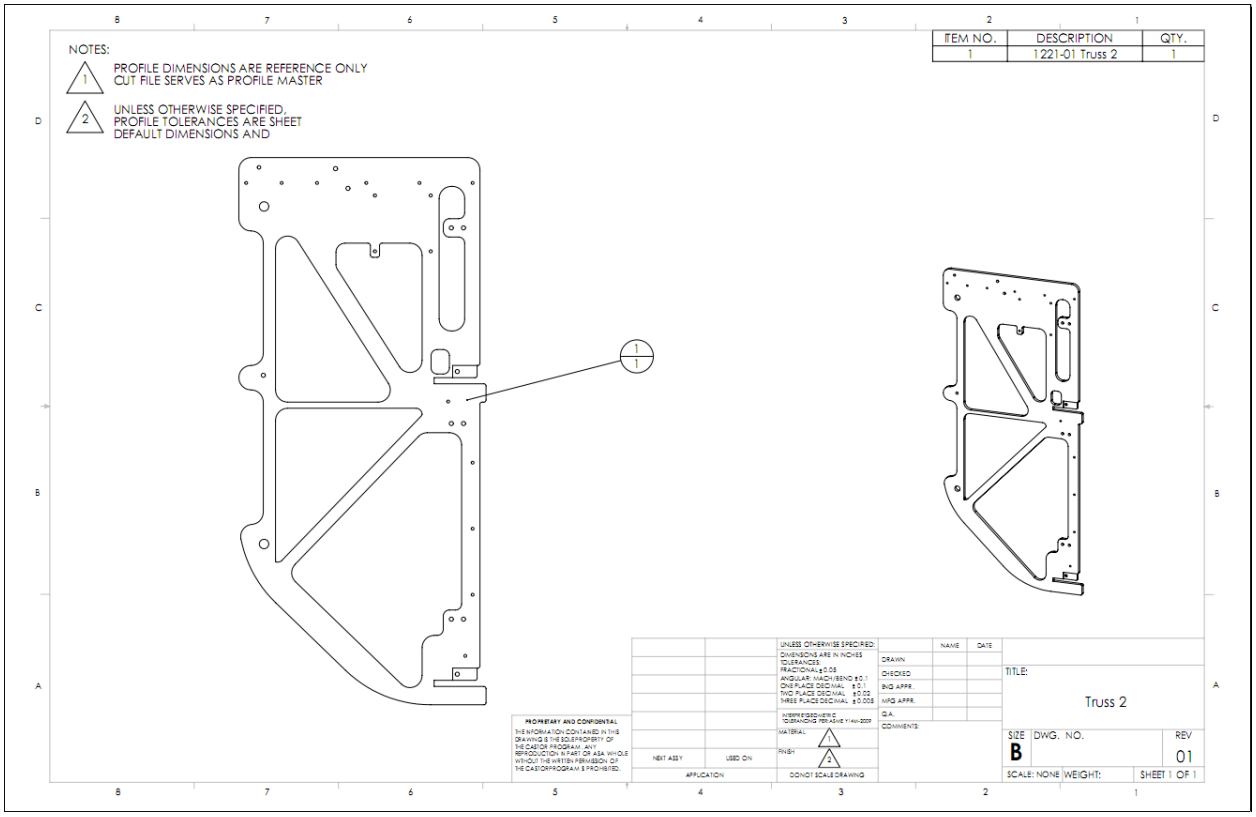

Figure 4.9 - 16: Truss 2

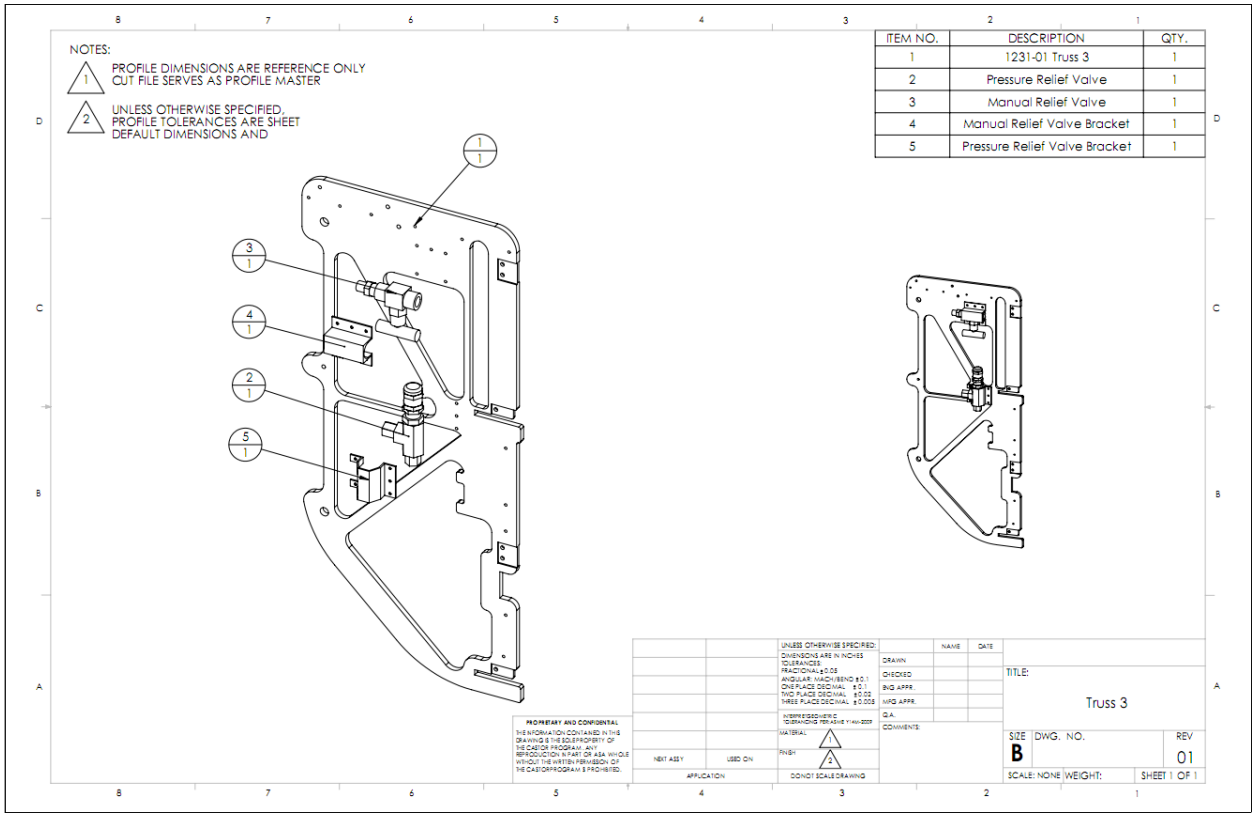

Figure 4.9 - 17: Truss 3

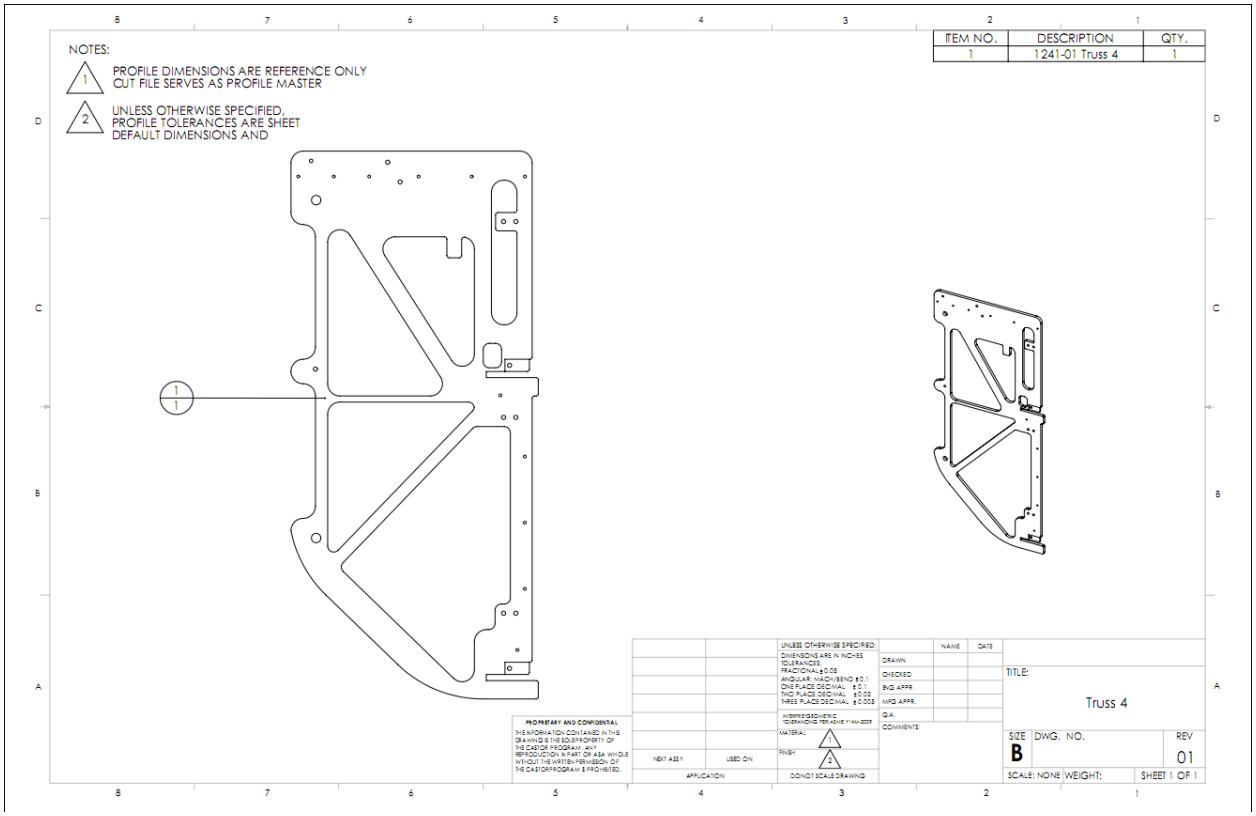

Figure 4.9 - 18: Truss 4

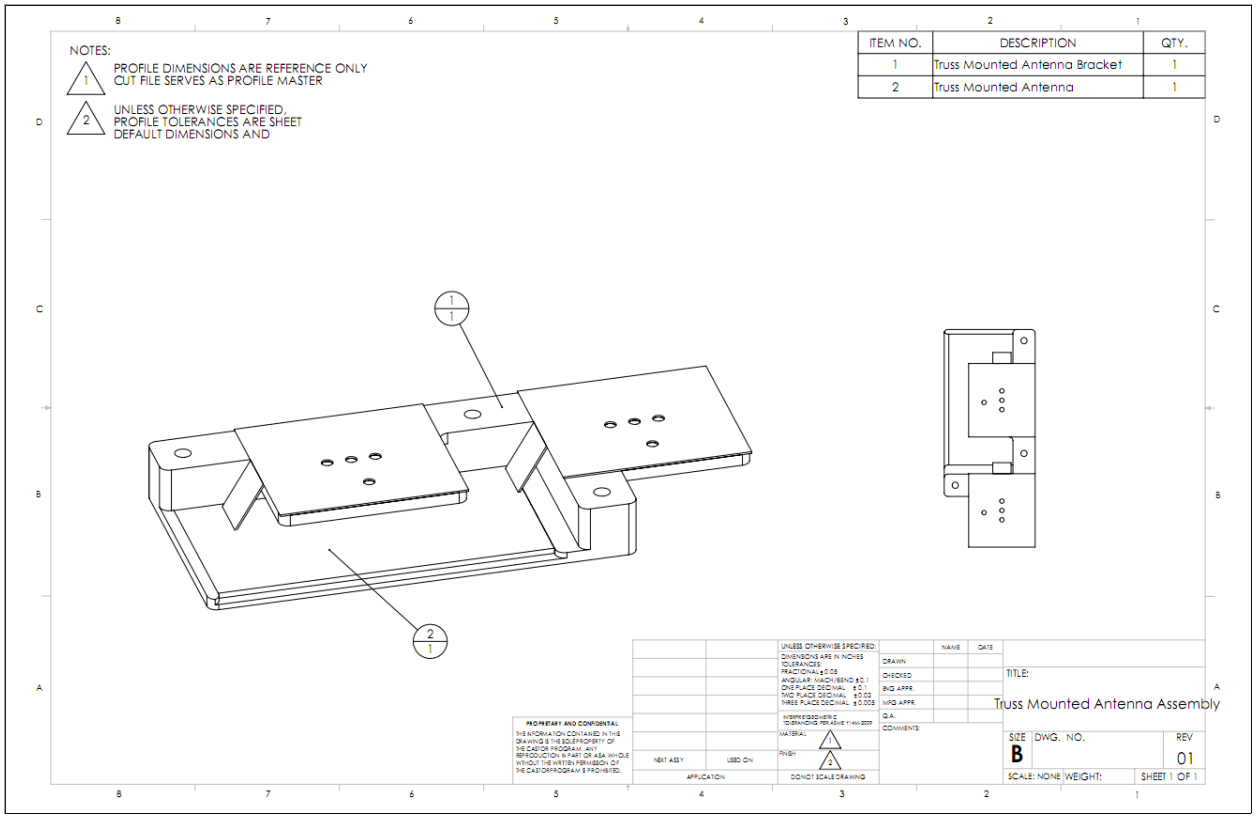

Figure 5.7 - 19: Truss-mounted antenna assembly

5.8 ALTERNATIVE SCIENCE MISSIONS (L. TAMPKINS)

5.8.1 CASTOR ALTERNATIVE SCIENCE GOALS

The main mission of the CASTOR Science and Payload Team is to design and engineer devices that are properly integrated with the satellite's system whose main function is to collect scientific data during the CASTOR mission. Possible missions that would collect science worthy data and measurements will be outlined here. The possible missions are divided into three categories based on the locations of observations; these categories are near-earth, lunar (which includes asteroids), and exosolar. The technique of synthesis imaging will be used in missions that involve radio or ultraviolet astronomy; hence, a brief outline of synthesis imaging and how it applies to the capabilities of the CASTOR satellite is given.

5.8.2 NEAR EARTH MISSIONS

Earth radiation belts: Understanding the extent and magnitude of various sections of the belts, as well as accurately forecasting space weather, will increase the safety of manned space missions and the efficiency of satellites. Possible studies include investigating how the whistler mode chorus and its interaction with charged particles within the belts. Examples include how they

might relate to magnetic storms, sub-storms, and aurora displays. Another study includes understanding very low frequency (VLF) waves in the belts to create models to predict space weather.

Space weather with a focus on substorms: Little data has been collected on substorms because of their distance from Earth and their large size. Multiple passes by a single satellite studying the region has yet to be recorded. One study could be devoting the satellite to orbits that continuously cross the magnetotail region and perform various measurements. Such measurements could include data collection on how substorms disrupt orderly flow of plasma in the cross-tail current.

Cosmic rays with a focus on shock acceleration:Like radiation, cosmic rays,energetic particles in space, are a threat to manned spacecraft and electrical components. Scientists still do not know where cosmic rays originate from. This also means that the origin of the particles' energies is unknown. However, one theory suggests that shock acceleration may contribute particles energy. Unlike the particles origin shock acceleration can be observed in the magnetosphere. A study could be done in the magnetosphere measuring various aspects of shock acceleration and cosmic rays in order to find a correlation.

Magnetosphere waves:The magnetosphere contains many "waves" that vary in frequency due the density of the surrounding plasma and magnetic field. Such waves include whistlers, Alfvén waves, micropulsations, hybrid wave modes, auroral kilometric radiation etc.This is still a pretty open field of research for many the roles that these waves play in space have yet to be fully understood. One study could be inserting the satellite in the magnetosphere with the proper instruments to investigate the waves (one type of wave) and how they interact with their surrounding environment.

5.8.3 LUNAR MISSIONS

Lunar gravitational fields:The Moon has a weak gravitational field that drastically varies in some areas. The current theory is that the gravitational anomalies are due to dense lava flows called mascons that are found in some impact basins. Since it affects the orbits of spacecraft travelling near or around the moon scientists have mapped out the gravitational field of the moon; however, the exact cause of the variations are still unknown. Further study could be done on how various surface features, such as mascons, contribute the lunar gravitational field. Any data collection and analyst would have to go beyond simple mapping or measuring the field or surfaces, but creating an active model showing how specific sources contribute the overall field.

Lunar outgassing and transient lunar phenomenon: Outgassing is the venting of elements and molecules such as radon, nitrogen, carbon monoxide, and carbon oxide from the moon's surface. Scientists are not completely sure about the origin of these gases; however, theories suggest that they are the result of volcanic or tectonic activity underneath the moon's surface. Since these compounds that are emitted are the main components of the lunar atmosphere, understanding what causes outgassing, and where it is most likely to occur is important in understanding not only the activities below the lunar surface but also the lunar atmosphere. Nitrogen and Carbon are important substances that will be needed in sustained missions on the moon. Possible studies

include radio scans that penetrate more than 20 meters into the lunar surface, spectroscopy measurements to study the connection between lunar outgassing and transient lunar phenomenon, and very low lunar orbits for in situ studies of outgassing. Examples of spectroscopy measurements are be done by alpha particle spectrometers, mass spectrometers; also, radon and muon emissions could be measured as well. Various techniques to triangulate outgassing sources are also within the capabilities of CASTOR.

5.8.4 EXTRASOLAR

Magnetic field interactions between exoplanets and their respective star: Detecting and measuring an exoplanet's magnetic field is a suggested science mission that could help determine if a planet is habitable, for magnetic fields shield against radiation which is necessary for life to thrive. The emission of heat, hydromagnetic waves, and accelerated particles is an effect of the interaction between an exoplanet's magnetic field and its nearby star; thus, these effects can be measured and analyzed in order to model the observed exoplanet. Another study includes measuring the chromospheric flux, x-ray and/or radio emissions of photospheric magnetic fields.

Ultraviolet astronomy and radio astronomy:Further ultraviolent studies of exoplanets have been suggested by researchers wishing to model various aspects of exoplanets. One aspect of ultraviolet research is the measurement of auroral and/or dayglow emission by large exoplanets.

5.8.5 SYNTHESIS IMAGING

Synthesis imaging is a technique performed by multiple satellites/telescopes where the distance between individual telescopes, the time lag, and the angle of the incoming signal are used to analyze the signal. Synthesis imaging is used in visual, infrared, ultraviolet and radio astronomy; however, ultraviolet and radio astronomy missions are more practical due the size and mass constraints on CASTOR. The use of this technique is suggested because it will increase the resolution of a targeted signal. The main idea is to have CASTOR act as multiple receivers in an array. By measuring a targeted signal at equal intervals, creating a "grid", and calculating the time delay of the signals it is possible to treat CASTOR as a static array of satellites.

5.8.6 CONCLUSION

Once research has been completed, discussions with colleagues, faculty members, and professionals in their respective fields will commence to determine what science mission, if any, could be performed by CASTOR. Then the specifics of the mission will be planned out to fit the capabilities of the satellite. Following this stage design and testing of instruments needed to collect data will be performed. It is important to note that all instruments must weigh less than one kilogram, contain a volume less than 10 cm^3, and use at most 5 watts of power. This will enable to add the component to the satellite without changing its overall mass or structure.

5.9 THERMAL TEAM DATA

5.9.1 LM19 THERMAL SENSOR SPECIFICATION SHEET

National Semiconductor

October 2007

LM19
2.4V, 10µA, TO-92 Temperature Sensor

General Description

The LM19 is a precision analog output CMOS integrated-circuit temperature sensor that operates over a −55°C to +130° C temperature range. The power supply operating range is +2.4 V to +5.5 V. The transfer function of LM19 is predominately linear, yet has a slight predictable parabolic curvature. The accuracy of the LM19 when specified to a parabolic transfer function is ±2.5°C at an ambient temperature of +30° C. The temperature error increases linearly and reaches a maximum of ±3.8°C at the temperature range extremes. The temperature range is affected by the power supply voltage. At a power supply voltage of 2.7 V to 5.5 V the temperature range extremes are +130°C and −55°C. Decreasing the power supply voltage to 2.4 V changes the negative extreme to −30°C, while the positive remains at +130°C.

The LM19's quiescent current is less than 10 µA. Therefore, self-heating is less than 0.02°C in still air. Shutdown capability for the LM19 is intrinsic because its inherent low power consumption allows it to be powered directly from the output of many logic gates or does not necessitate shutdown at all.

Applications

- Cellular Phones
- Computers
- Power Supply Modules
- Battery Management
- FAX Machines
- Printers
- HVAC
- Disk Drives
- Appliances

Features

- Rated for full −55°C to +130°C range
- Available in a TO-92 package
- Predictable curvature error
- Suitable for remote applications
- UL Recognized Component

Key Specifications

Accuracy at +30°C	±2.5 °C (max)
Accuracy at +130°C & −55°C	±3.5 to ±3.8 °C (max)
Power Supply Voltage Range	+2.4V to +5.5V
Current Drain	10 µA (max)
Nonlinearity	±0.4 % (typ)
Output Impedance	160 Ω (max)
Load Regulation	
0 µA < I_L < +16 µA	−2.5 mV (max)

Typical Application

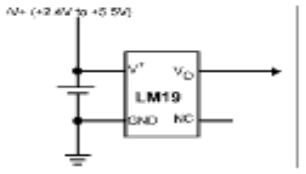

$$V_O = (-3.88 \times 10^{-6} \times T^2) + (-1.15 \times 10^{-2} \times T) + 1.8639$$

or

$$T = -1481.96 + \sqrt{2.1962 \times 10^{6} + \frac{(1.8639 - V_O)}{3.88 \times 10^{-6}}}$$

where:
T is temperature, and V_O is the measured output voltage of the LM19.

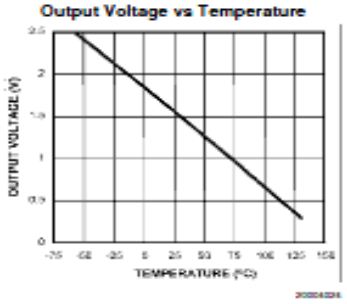

FIGURE 1. Full-Range Celsius (Centigrade) Temperature Sensor (−55°C to +130°C) Operating from a Single Li-Ion Battery Cell

 200040 www.national.com

LM19 2.4V, 10µA, TO-92 Temperature Sensor

Temperature (T)	Typical V_O
+130°C	+303 mV
+100°C	+675 mV
+80°C	+919 mV
+30°C	+1515 mV
+25°C	+1574 mV
0°C	+1863.9 mV
−30°C	+2205 mV
−40°C	+2318 mV
−55°C	+2485 mV

Connection Diagram

TO-92

See NS Package Number Z03A

Ordering Information

Order Number	Temperature Accuracy	Temperature Range	NS Package Number	Device Marking	Transport Media
LM19CIZ	±3.8°C	−55°C to +130°C	Z03A	LM19CIZ	Bulk

5.9.2 ENGINE THERMAL ALGORITHM

```
%Engine Thermal Model - Programmed in MATLAB

%% Constants
sig = 5.670400*10^-8;  %Stefan-Boltzman Constant W/m^2K^4
e=1;a=1;t=0;
```

```
%% Material Properties  (1.Emissivity, 2.Absoptivity, 3.Thermal Conductivity
W/mK)
css = [e, a, 37];      %CastStainlessSteel
tungsten = [.23, .38, 200];
aisi304 = [e , a, 16];
cp = [e , a, 1.495];       %CeramicPorcelain
alloy = [.11, .17, 180];    %6061 Alloy
silicon = [e, a, 124];

%% Parts (1.Material, 2.Thickness m, 3.Height m, 4.Top Area m^2, 5.Side Area
m^2, 6.Temperature K)
%note:Values set as a and e are not actual values. The correct values will
%be substituted as soon as they are determined.
bp =  [alloy,    .231, .006, .042, .004, t];    %Baseplate note:approximated
as a disk with radius=.231m and height=.006m
os =  [aisi304,  .012, .061, .002, .014, t];    %Outershell note:approximated
as a cylinder with outer radius=.036m, inner radius=.025m, height=.061m
bc =  [css,      .025, .010, .121, .001, t];    %Base Core
lm =  [tungsten, .020, .012, .003, .002, t];    %Large Magnet
ls =  [aisi304,  .017, .003, .002, .001, t];    %Large Spacer
mm =  [tungsten, .013, .012, .002, .002, t];    %Medium Magnet
ss =  [aisi304,  .010, .003, .002, .001, t];    %Small Spacer
sm =  [tungsten, .007, .012, .001, .002, t];    %Small Magnet
cic = [cp,       .003, .046, .0003,.006, t];    %Ceramic Insulator-Cone
Section note:approximated as a cylinder with outer radius=.021m, inner
radius=.018, height=.046m
cit = [cp,       .010, .003, .002, .001, t];    %Ceramic Insulator-Top
Section
tr =  [allloy,   .008, .003, .002, .001, t];    %Top Ring
pd =  [silicon,  .002, .002, .0001,.0001,t];    %Porous Disc

%% Thermal Sources W/m^2

sfh = 1414;     %Solar Flux Hot
eah = 381.78;   %Earh Albedo Hot
eih = 257;      %Earth IR Hot
sfc = 1322;     %Solar Flux Cold
eac = 224.74;   %Earth Albedo Cold
eic = 218;      %Earth IR Cold
ca  = 20;       %Cathode note:in Watts

%% Resitance
%This section currlently breaks the engine down into layers starting with
%the inside and moving out.  Eventually this section will be broken down
%and each will be shown on it's own.

r1 = cic(2)/(cp(3)*cic(5))+pd(2)/(sillicon(3)*pd(5));
r2 = ((cp(3)*cit(5))/cit(2) + (lm(2)/(tungsten(3)*lm(5))+
mm(2)/(tungsten(3)*mm(5))+ sm(2)/(tungsten(3)*sm(5)) +
ls(2)/(aisi304(3)*ls(5)) + ss(2)/(aisi304(3)*ss(5)))^(-1))^(-1);
r2 = os(2)/(aisi304(3)*os(5));

%% Temperatures K
%This section currlently breaks the engine down into layers starting with
```

```
%the inside and moving out.  Eventually this section will be broken down
%and each part's temperature will be shown.

dT1h = (.5*os(5)*(sfh+eah+eih)*aisi304(2) + ca*cp(2))*(r1+r2+r3);
%Temperature difference between Layer 1 and Layer 3 for hot case
dT1c = (.5*os(5)*(sfc+eac+eic)*aisi304(2) + ca*cp(2))*(r1+r2+r3);
%Temperature difference between Layer 1 and Layer 3 for hot case

T1 = (ca/(cic(5)*cp(2)*sig))^.25; %Temperature of inside layer.
T3h = T1 - dT1h;                  %Temperature of outside layer for hot case.
T3c = T1 - dT1c;                  %Temperature of outside layer for cold
case.
T2h = (T1/r1 + T3h/(r2+r3) + .5*os(5)*(sfh+eah+eih)*aisi304(2))/(1/r1 +
1/(r2+r3)) %Temperature of middle layer for hot case.
T2c = (T1/r1 + T3c/(r2+r3) + .5*os(5)*(sfc+eac+eic)*aisi304(2))/(1/r1 +
1/(r2+r3)) %Temperature of middle layer for cold case.
```

6.1 ACS LAB (D. DELATTE)

Laboratory work in Space Systems allows students to practice skills necessary for building and testing the satellite. By working on these projects, students are able to use the equipment in the lab and can gain experience with the components. By having this experience, risk of errors is reduced and familiarity is gained.

6.1.1 BEACON FRAME (D. DELATTE)

The design of the beacon frame was completed and the beacons were put in place (not pictured). The inventory analysis from a previous week was used to determine the most efficient and least wasteful use of the available green U-bars. The air bearing is a four by four foot granite block. The frame needs to clear the top of CASTOR on the air bearing, which would be approximately eighty-seven inches. Given these constraints and the knowledge that the inventory had four eight foot green U-bars and four ten foot U-bars, it made the most sense to cut the ten foot pieces into five foot segments and use these for the top and bottom pieces (parallel to the ground).

FIGURE 6.1-1: GREEN BEACON FRAME AROUND AIR BEARING

FIGURE 6.1-2: CORNER CONNECTION OF BEACON FRAME WITH DIAGONAL SUPPORT BAR

After the construction of the main frame (pictured in figures above), five aluminum beacon holders were placed appropriately around the periphery of the frame. Three were placed in a vertical orientation on the top plane and two were placed on vertical poles further down. Initially there was an issue getting the beacons to fin inside their mounts, but a combination of using a Dremel tool and loosening the screws holding the plate together allowed enough slack to fit the beacons in the mounts. Measurements were taken of the positions and these positions were used to create a beacons.dat file for SPHERES so that the air bearing can be used in future testing. The final modification was to turn the beacons so that they were at 35º from their holders and point directly into the center where SPHERES will be on top of the air bearing. This construction and modification process completed the lab for the creation of the beacon frame.

6.1.2 SPHERES (D. DELATTE)

For SPHERES, a control was written that would make spheres travel in a polygon around the glass table. Initial testing of the program was moderately successful for a first try. The code did compile, SPHERES was successfully controlled, and it did move, but it did not travel in a perfect polygon.

Another demo called "StopAndStare" focused on the attitude control instead of the position control. This demonstration showed the ability to control the attitude as well as the gain. In the demo, SPHERES was controlled to have only 10º of overshoot in its attitude. These two demos were good experience for when SPHERES will be used to test components on the air bearing.

The final laboratory work focused on sending and receiving data between SPHERES and a computer station.

6.1.3 MAGNETOMETER (S. VEGA)

Component testing will aim to prove that the magnetometer is capable of meeting accuracy requirements. The ADCS requirement for attitude determination is within 1˚ of accuracy in each axis. To determine this capability, the magnetometer will be tested in a magnetic field created by a Helmholtz coil, so that the 1-axis magnetic field vector is known. When placed between the coils, the reading from the magnetometer should then confirm the known magnetic field, showing a vector component of the field in one axis. ADCS will also be able to rotate the magnetometer to specified angles to confirm the correct vector component measurements in each axis, and determine to what degree the magnetometer's readings remain accurate. This next

immediate step of this stage in testing requires finalization machining parts and assembly of the Helmholtz coil.

6.1.4 AIR BEARING (S. VEGA)

Once this test is completed, the next stage of testing will be to test the component on the air bearing test bed, using the SPHERES satellite to give a true attitude reading to compare to the reading from the magnetometer. A larger Helmholtz coil is also being constructed around the air bearing, such that a similar test to the tabletop Helmholtz coil test can be run on the air bearing with greater degrees of freedom available to position the magnetometer. The goal is for the magnetometer reading to be within 1˚ of accuracy in each axis. ACS will create an estimation process for the magnetometer readings to attain this accuracy. The air bearing will need to be redesigned by this point in testing in order to accommodate SPHERES and magnetometers with ease in new mounting points. A concept drawing has been created as a detailed design with specific dimensions.

6.1.5 REACTION WHEEL (C. DEVIVERO)

Closed loop reaction wheel control reduces overall risks associated with hardware by enhancing the air bearing capability to provide an adequate test facility. The test facility can be used by CASTOR's ACS components for integration testing and performance verification. These components need a reliable actuation system in order to apply test results to CASTOR.

A closed loop Position-Integral (PI) controller shall be used on the reaction wheel speed state. The controller is of the form

$$\dot{\boldsymbol{x}} = A\boldsymbol{x} + B\boldsymbol{u} \quad \text{(Equation 1)}$$

$$A = \begin{bmatrix} 0 & 1 & 0 \\ 0 & -\frac{b}{I} & \frac{K_t}{I} \\ 0 & -\frac{K_t}{L} & \frac{R}{L} \end{bmatrix} \quad \text{(Equation 2)}$$

$$B = \begin{bmatrix} 0 \\ 0 \\ \frac{1}{L} \end{bmatrix} \quad \text{(Equation 3)}$$

$$\boldsymbol{y} = C\boldsymbol{x} + D\boldsymbol{u} \quad \text{(Equation 4)}$$

$$C = [0 \quad 1 \quad 0], D = 0 \quad \text{(Equation 5)}$$

$$\boldsymbol{x} = \begin{bmatrix} \int \omega \\ \omega \\ i \end{bmatrix} \quad \text{(Equation 6)}$$

$$\boldsymbol{u} = \begin{bmatrix} 0 \\ 0 \\ V_c \end{bmatrix} \quad \text{(Equation 7)}$$

where b is the friction coefficient of the reaction wheel, K_t is the current constant, R is the resistance, L is the inductance, ω is the speed, i is the current, and V_c is the commanded voltage.

In order for the reaction wheels to be effective, the rise time of the speed must be less than the time between control loop executions (0.050 seconds), and there should be no overshoot because the braking system of the reaction wheels is relatively unpredictable and thus undesirable. The figure below shows the ideal performance of the reaction wheel.

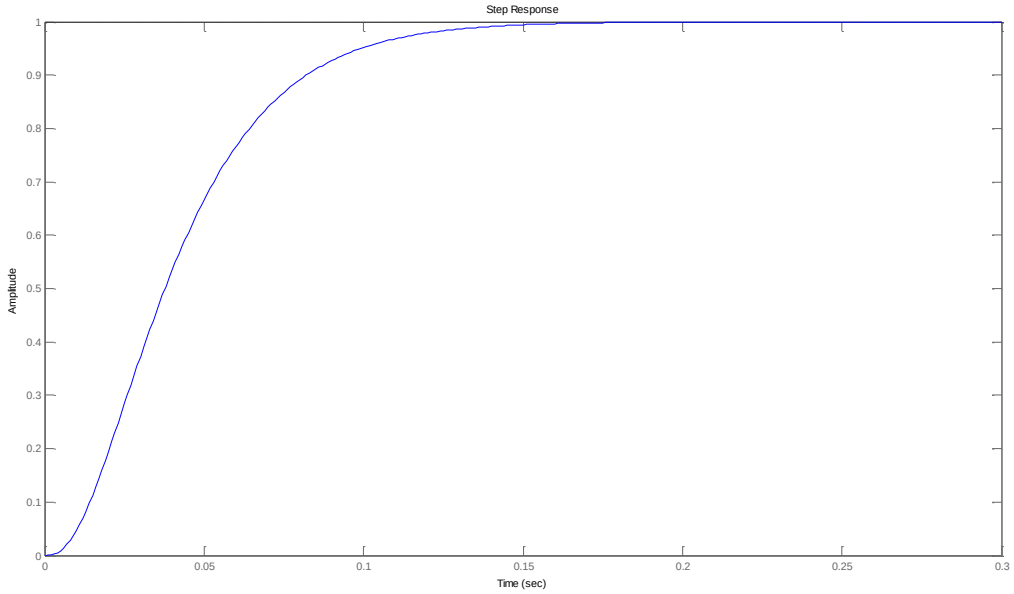

FIGURE 6.1-3: IDEAL REACTION WHEEL RESPONSE

In Figure 1, the y axis represents the speed of the reaction wheel and the x axis represents time.

Figure 2 shows the originally proposed controller. While the rise time is acceptable, there is excessive breaking, as well as cyclic breaking once in steady state.

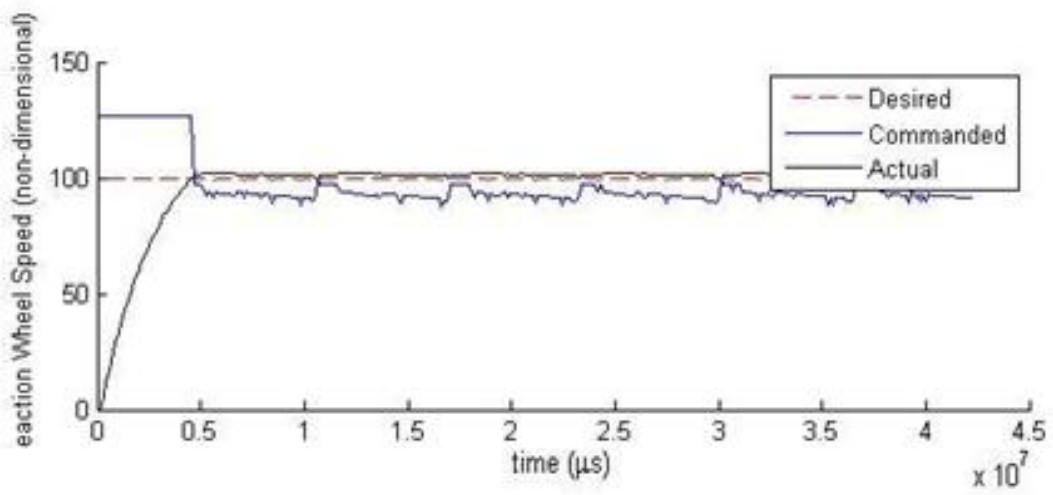

FIGURE 6.1-4: REACTION WHEEL RESPONSE (WITH ORIGINAL CONTROLLER)

The Figure 3 shows the current state of the redesigned controller. The rise time is slower than desired, but the breaking problem has been removed.

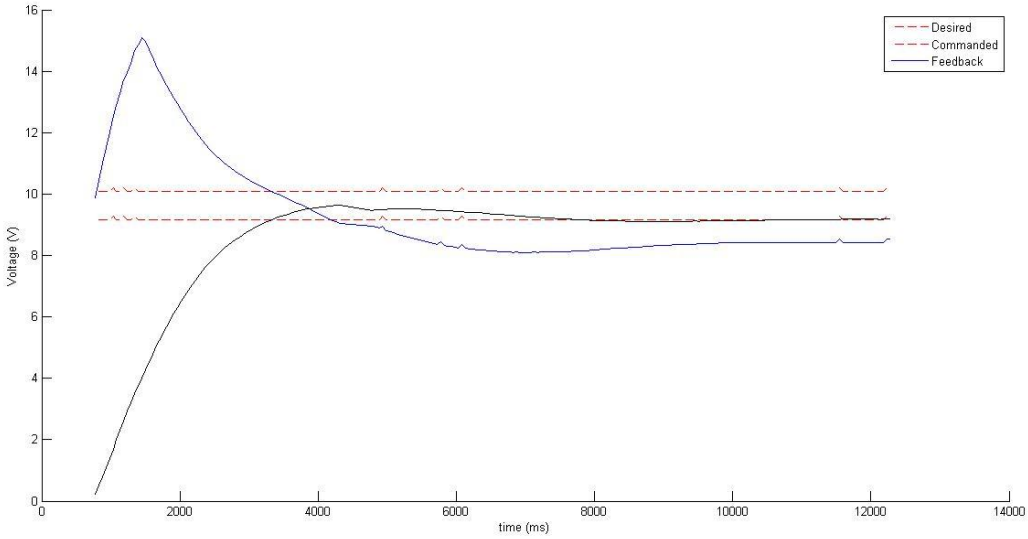

FIGURE 6.1-5: REACTION WHEEL RESPONSE (WITH IMPROVED CONTROLLER)

Further work to be done is to reduce the system rise time, overshoot, as well as better characterize the friction of the reaction wheel.

6.1.6 HELMHOLTZ COIL (N. CONDUAH)

To adequately test the torque coils and magnetometer, the presence of a magnetic field stronger than the earth's magnetic field is required. The ACS team thus decided to build a Helmholtz coil that could be used to provide a stronger magnetic field to tests against. Building an Electromagnetic Field Simulator (EMFS) would also be beneficial in the long term for the Space

Systems Lab since this can be used in numerous tests of magnetic components placed on the air bearing. The following documents describes the methodology over the semester used to achieve this goal.

For CASTOR the needed magnetic field is desired to be in the range of 10-100 times stronger than the earth's magnetic field. The final strength will be dependent on cost. To achieve this, research was performed and the idea of building Helmholtz coils was agreed upon. The next step is thus to propose and finalize the specification of the coils.

After some consideration it was agreed to start off with a 1-D EMFS, that is a one Helmholtz coil. For reasons of symmetry of the air bearing and the availability of maneuverability of the coil up and down the air bearing, the coil will be placed with the air bearing at the center of the circumference of the coil.

That is along the z-axis, this would be a -90 degree rotation of the below depiction.

6.2 PROPULSION LAB (K. LOEBNER)

6.2.1 ACTIVITIES OVERVIEW (K. LOEBNER)

The Propulsion Laboratory team is responsible for one primary area of investigation for the Spring 2010 semester. This is to conduct efficiency testing on the Diverging Cusped Field Thruster (DCFT) to determine the highest efficiency operating line at a variety of power levels and flow rates. All additional and preparatory work is dedicated to this goal.

6.2.2 TESTING EQUIPMENT (K. LOEBNER)

The primary piece of testing equipment that is essential for the successful execution of the Efficiency Testing is the thrust balance. The key piece of equipment needed to execute the DCFT Efficiency Test is the thrust balance. The thrust balance is an apparatus, depicted in Figure 6.2-1: Thrust Balance below, consisting of a pendulum, frame, and several electrical sensors and actuators.

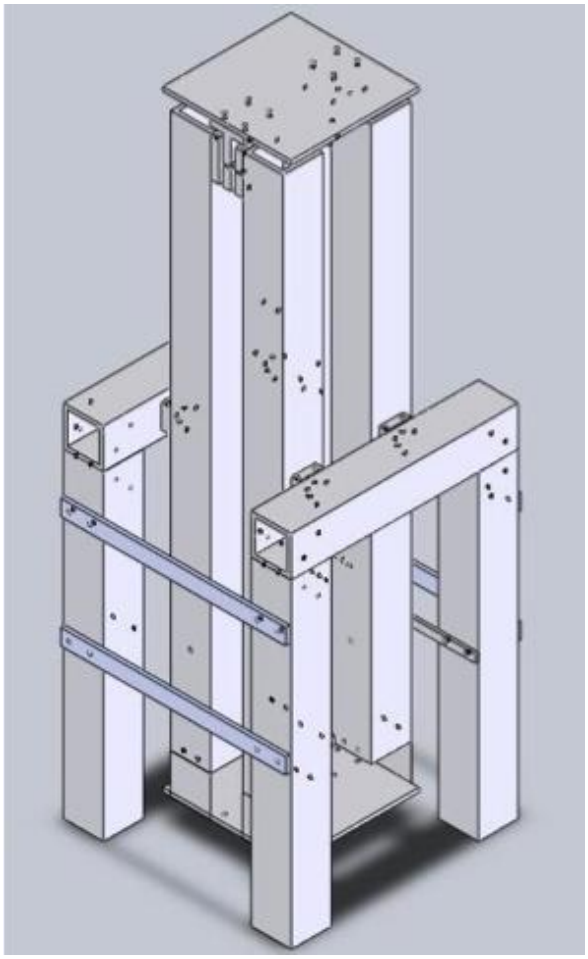

FIGURE 6.2-1: THRUST BALANCE

The balance is controlled and operated by a Labview program created by Randy Leiter. Details on how to use the control software are contained in Section 6.2.2.1. The thrust balance is designed to operate as follows: when a thrust is applied to the upper plate by the DCFT, the entire pendulum rotates such that the top and bottom plate remain parallel. The bottom of the pendulum contains a weight equal to that of the DCFT. A pendulum design of this form is preferable because it ensures that the system remains in equilibrium when perturbed from its rest position, and it is far less expensive than an electronic scale of the requisite sensitivity. The top and bottom plates are held parallel and horizontal using four precision-machined bearings at both the upper and lower plate, and the entire pendulum rotates about another four bearings at the centerline. These high precision parts require no lubricant, so they are safe for use in a vacuum. They are also essentially frictionless, which means they contribute a negligible amount to the overall system stiffness, easing calibration.

Measurements are recorded as follows: A thrust causes the balance to move relative to its equilibrium state. The position change is recorded as a voltage by a linear variable differential transformer (LVDT) at the pivot point and sent back to the control software, which determines the displacement and then applies a voltage to the primary voice coil, which is an electromagnetic actuator located on the thrust balance that applies a force which restores the pendulum to a neutral position. This process is governed by a PI control loop operating at relatively high frequency, so in practice the balance will be significantly displaced while experiencing a thrust. The voltage necessary to restore the pendulum to its original position corresponds directly to a thrust value.

Before the thrust balance can be placed in the chamber, it must undergo a cleaning procedure to prevent it from causing excess contamination. The cleaning procedure is as follows:

1) Disassemble the thrust balance in its entirety. All fasteners must be removed, and placed in the sonic cleaning system for 8-10 minutes.
2) Any metal components too large to be placed in the sonic cleaner must be wiped down on all surfaces with acetone to remove any robust residues, such as ink or adhesive. **Note: non-metal components such as nylon washers should NOT be cleaned with acetone, as it could dissolve them.
3) All components must then be wiped down with isopropyl alcohol to remove any soap, acetone, or other residues.
4) The thrust balance must then be reassembled, using tools that have been cleaned using the same procedure outlined above in steps 2 and 3. **Note: all cleaned components should remain on the laminar flow bench when not specifically in use in order to maintain their decontaminated state.

In order to obtain accurate data from the thrust balance during testing, it must to be calibrated after being placed in the vacuum chamber with the thruster mounted to it and connected to the Xenon feed lines. This is because the experimental setup, when fully operational, will cause a slight offset in the position of the thrust balance and the stiffness of the system. Thus, the secondary voice coil must be used to return the thrust balance to zero displacement, and then a calibration curve must be created corresponding to how the thrust balance responds to the stiffness of that particular configuration.

In the configuration typically used for prior testing of the DCFT, heavy steel flex hoses were used to deliver Xenon to the thruster anode and cathode. These hoses were too stiff for use with the thrust balance, so Teflon tubing was used instead. However, if left hanging from the rear of the thruster, the weight of the feed lines would displace the thrust balance to such a degree that data collection would not be possible. Therefore, a method of suspending the Xenon feed lines and cathode wiring from the ceiling of the vacuum chamber was devised to mitigate that effect. By hanging all thruster connections from two hooks located directly above the thrust balance, they displace the thrust balance a small enough amount that it is possible to correct it using the secondary voice coil. Using the LabView software, the power delivered to the secondary voice coil is adjusted until the LVDT reads zero displacement, and then calibration can begin.

In order to calibrate the balance inside the chamber, the calibration rig is placed at the edge of the chamber such that calibration weights can hang down outside while exerting a force on the thrust balance within. The calibration weights apply a known force, and using the LabView

software we measure the voltage delivered to the primary voice coil in order to counteract that known weight, taking 5-10 data points at each weight increment. By following this procedure over the range of thrust-force values we expect to achieve, we can generate a linear fit to the data as shown in Figure 2 below. In this figure, the x-axis represents a non-dimensional percentage of the possible resistance the voice coil can provide, and the y-axis represents the force in milli-Newtons.

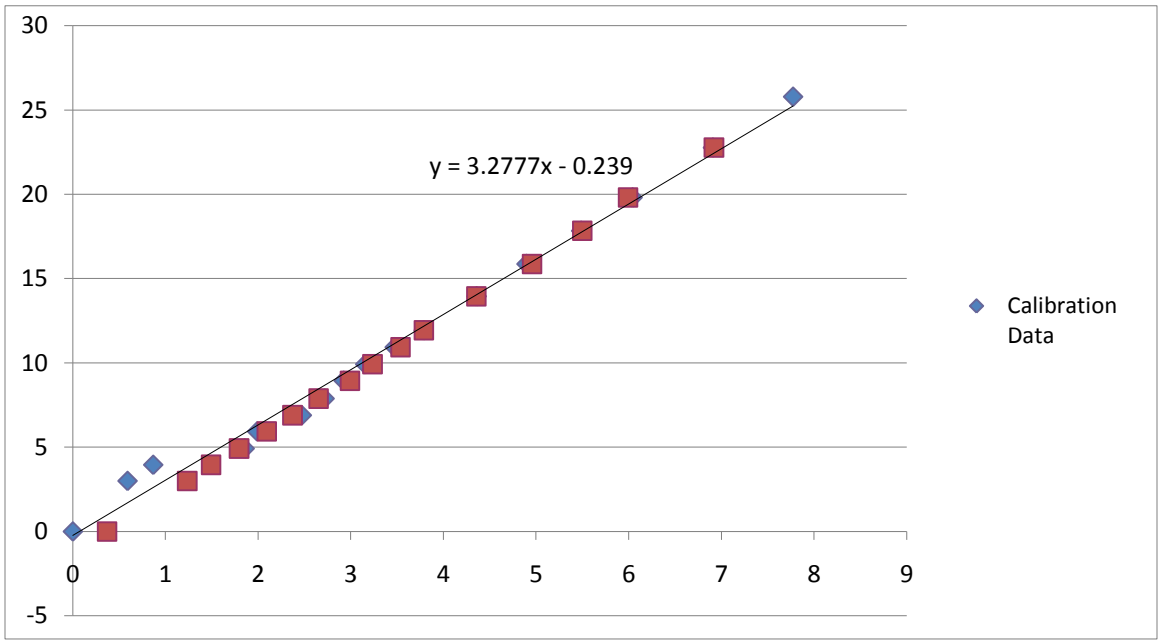

FIGURE 6.2-2: MILLI-NEWTONS VS. % FORCE APPLIED

Using this linear relationship derived from the calibration, the data from the thrust balance can be mapped to actual thrust values, and the DCFT efficiency can thus be calculated.

6.2.2.1 THRUST BALANCE CONTROL SOFTWARE GUIDE

Hardware Setup:

1) Parts required:
   - DCF Thrust Balance
   - Control Box
   - 9 pin vacuum ready cable
   - 9 pin cable
   - Power cord for control box
   - USB cable
2) Connect the vacuum ready 9 pin cable to the 9 pin connector on the thrust balance.
3) Connect the other end of the vacuum cable to the ordinary 9 pin cable. DO NOT connect the 9 pin cable to the control box yet
4) Connect the power cord to the control box and to a wall socket. DO NOT turn on the control box yet.
5) Connect the usb cable to the computer.

Diagnostic Steps:

1) Connect the DAQ card to the computer through the usb cable. Do NOT turn on the control box.
2) Open the "Measurements & Automation Explorer" by double clicking its icon on the desktop
3) Under the toolbar on the left, expand "Devices and Interfaces"
    - Expand "NI-DAQmx Devices"
    - Select USB 6009 Dev 3 (if the computer sees the DAQ card it will be in green) and click on the button that says "test panel" (see Figure 6.2-3)

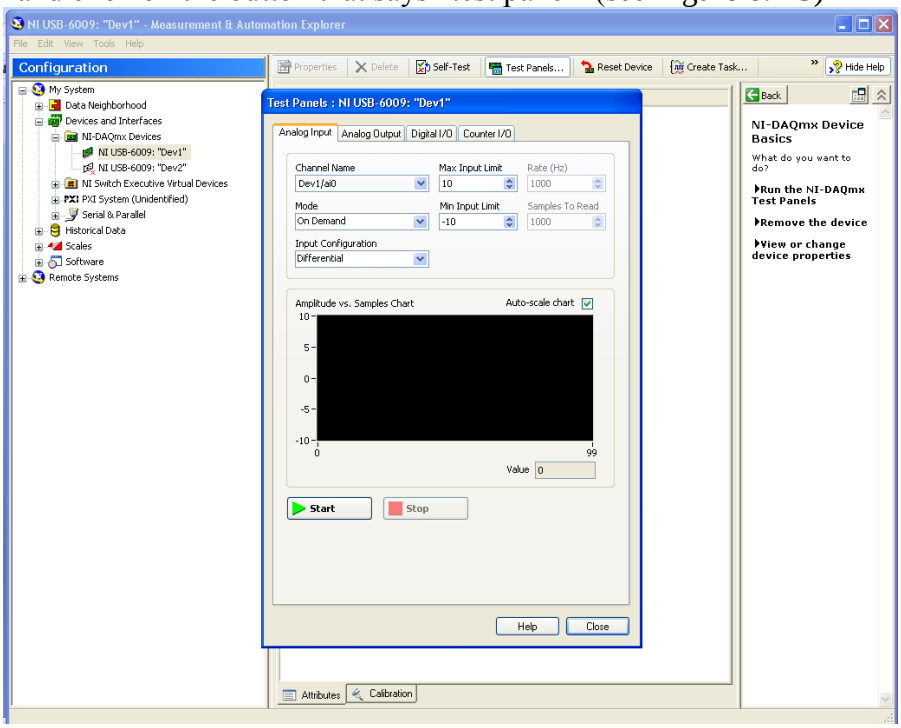

FIGURE 6.2-3: DIAGNOSTIC

4) While keeping the control box switch in the "off" direction and with no connection to the thrust balance:
    - Select the Analog Output Tab, set the channel to "ao0", and set the voltage to 2.5V. Click the update button.
    - Go back to the Analog Input tab and set the following:
        - Channel Name- ai2
        - Mode- continuous
        - Rate- 10,000 Hz
    - Click the Start button and verify that the DAQ card is sending a 2.5V signal as expected (a small 60Hz oscillation may be present, but it will have a small voltage). Repeat by setting the voltage to 0V and 5V. This will confirm that the DAQ card is working as expected. See Figure 6.2-4.

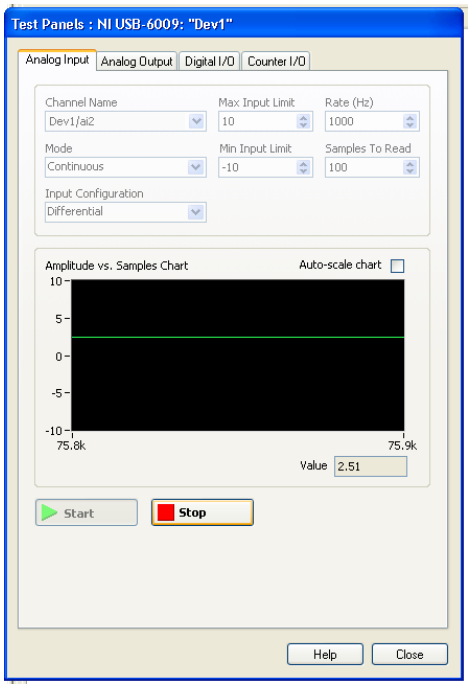

FIGURE 6.2-4: GUI

5) Now that the DAQ card is working as expected, the amplifying circuits will be tested. First, go to the analog output tab.
    - Go to channel "ao0", adjust the voltage to 2.5V and click update. Go to channel "ao1" and adjust the voltage to 2.5V and click update as well.
6) Now connect the 9 pin cable to the box and turn the power to the control box on by flipping the switch to the "on" position.
    - On the analog input tab, hit the stop button and change the channel name to "ai1". This channel monitors the voltage coming out of the first amplifying circuit. Go ahead and click start.
    - Now go to the analog output tab. Make sure to select channel "ao0". Set the voltage to 5.0V and click update. You should see the voice coil pull or push the pendulum thrust stand slightly.
    - Go back to the analog input tab and verify the voltage is no longer 0V. It should be about 0.7 or 0.8V.
    - Go back to the analog output tab and set the voltage to 0V (and click update). You should see the voice coil move the stand in the opposite direction this time.
    - Go back to the analog input tab and verify the voltage is now around -0.7 to -0.8V.
    - Go back to the analog output tab and set the voltage back to 2.5V.
    - The first amplifying circuit and voice coil are working appropriately. Now repeat these steps for the output channel "ao1" and input channel "ai3" to verify the second amplifying circuit and voice coil are also working.
7) The next set of steps will verify the LVDT is working appropriately.
    - On the analog input tab, set the channel name to "ai0" and click start. This channel monitors the voltage signal coming from the LVDT.

- Simply tab the balance so that it oscillates slightly and you should see the signal fluctuate (see Figure 6.2-5).

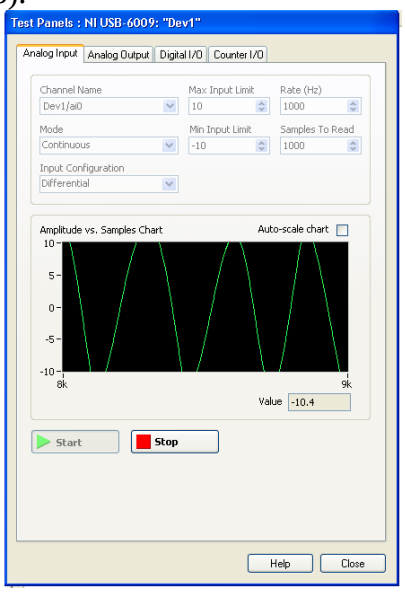

FIGURE 6.2-5: MONITOR LVDT

- When the balance is settled, the LVDT should be reading as close to 0V as possible (the neutral balance reading). If the LVDT is not reading close to 0V when the balance is still, adjust the LVDT by loosening the screw that holds it in place and move it appropriately.

8) The diagnostic steps are now complete. The control box, LVDT, and both voice coils are now working as they should. Close the Measurement & Automation Explorer.

Operation Steps:

1) Go to start, search, files and folders. Search for the VI file called MIT-SPL Thrust Balance-5
2) Open the program. You should see the screen indicated in Figure 6.2-6.

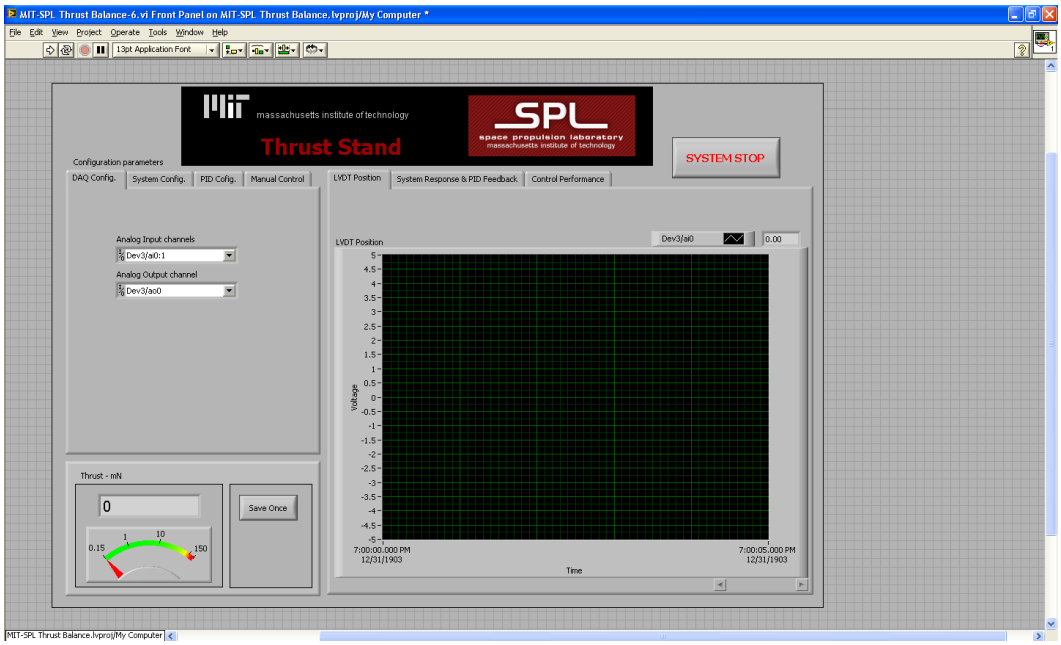

FIGURE 6.2-6: SPL THRUST BALANCE

3) First the DAQ card needs to be configured. Select the tab which reads "DAQ Config.".
   - For the analog input channels, select ai0 (LVDT), ai1 (first voice coil), and ai3 (second voice coil). (see Figure 6.2-7)

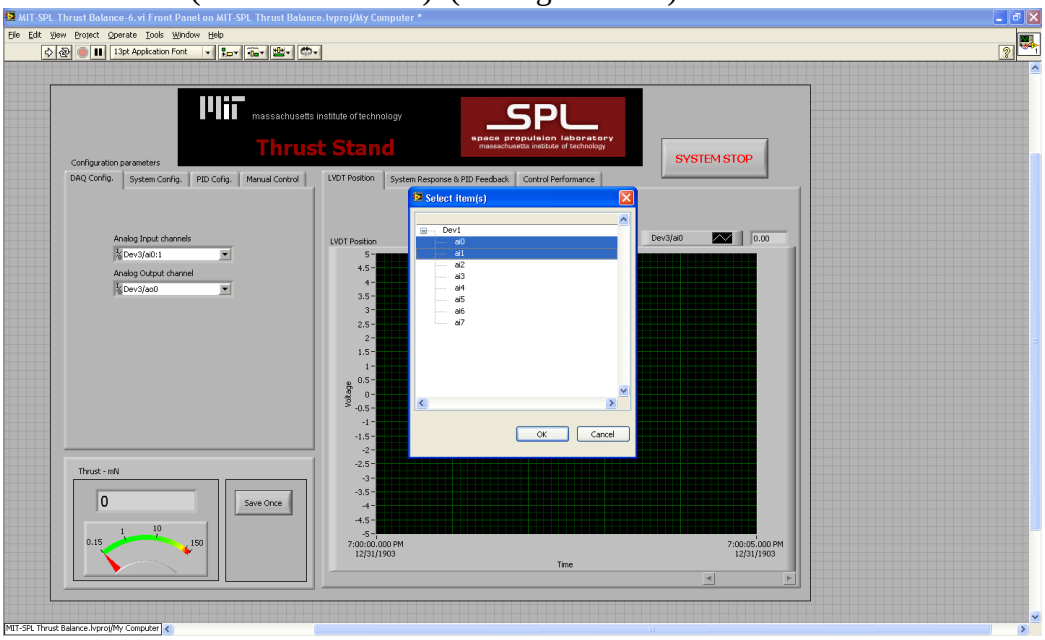

FIGURE 6.2-7: CONFIGURING DAQ CARD

   - For the analog output channels, select ao0 (first voice coil) and ao1 (second voice coil). (see Figure 6.2-8)

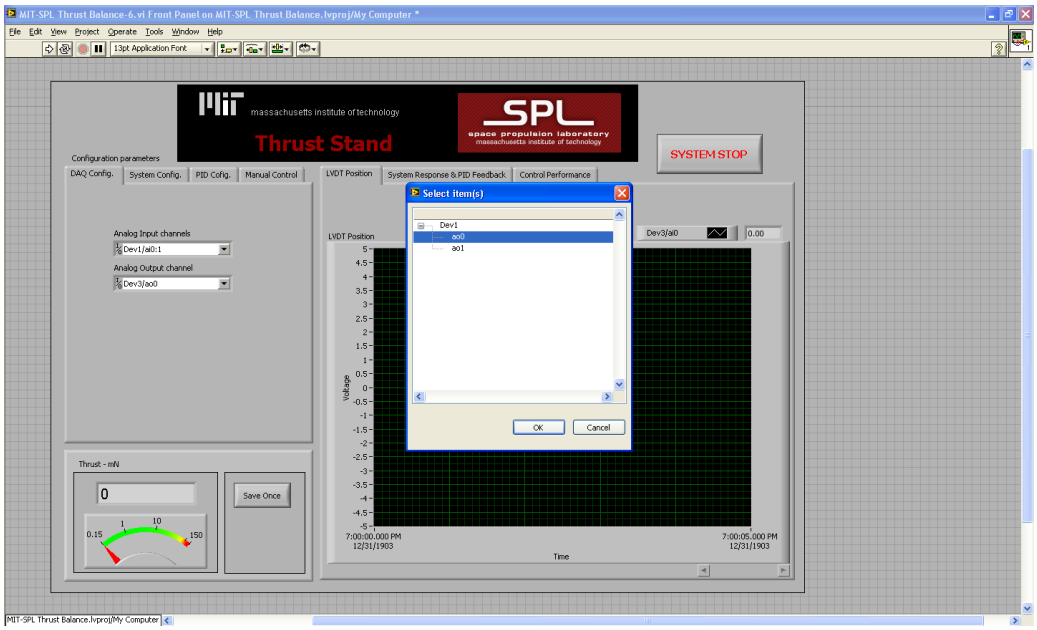

FIGURE 6.2-8: ANALOG OUTPUT CHANNELS

4) Now go to the manual control tab.
   - Turn the PID control off. You will know that it is off when the button is red. (see Figure 6.2-9)

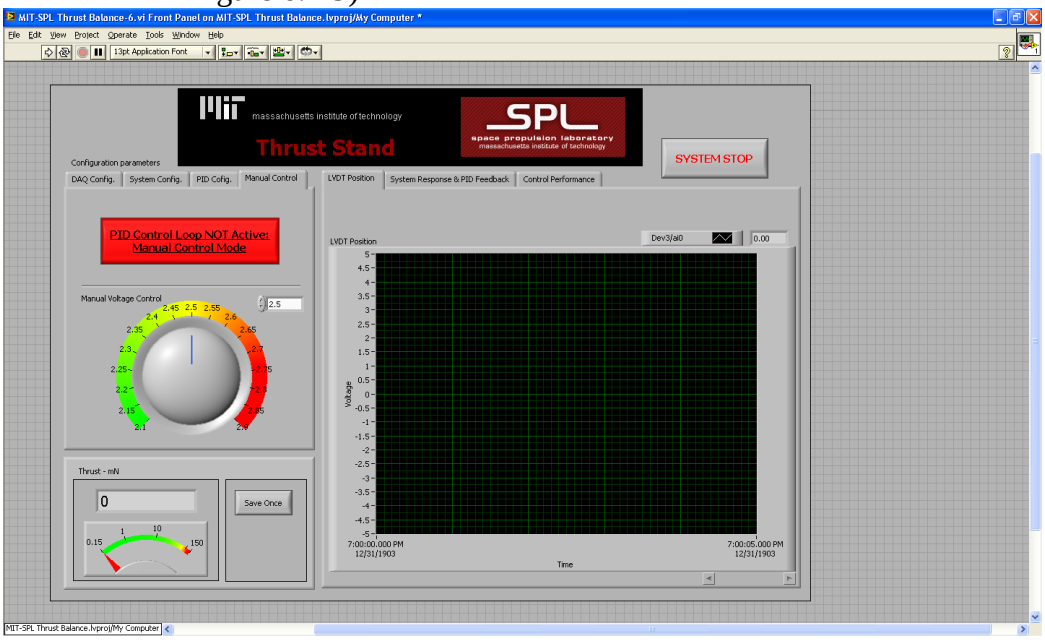

FIGURE 6.2-9: TURN PID OFF

5) Now the program is ready to start. Make sure the manual voltage control is set to 2.5V and select the run button (the arrow button just below the view menu).
   - Select the LVDT position tab. The position should be at 0 for 2.5V. If it is not, some adjustment of the LVDT may need to be made. See Figure 6.2-10.

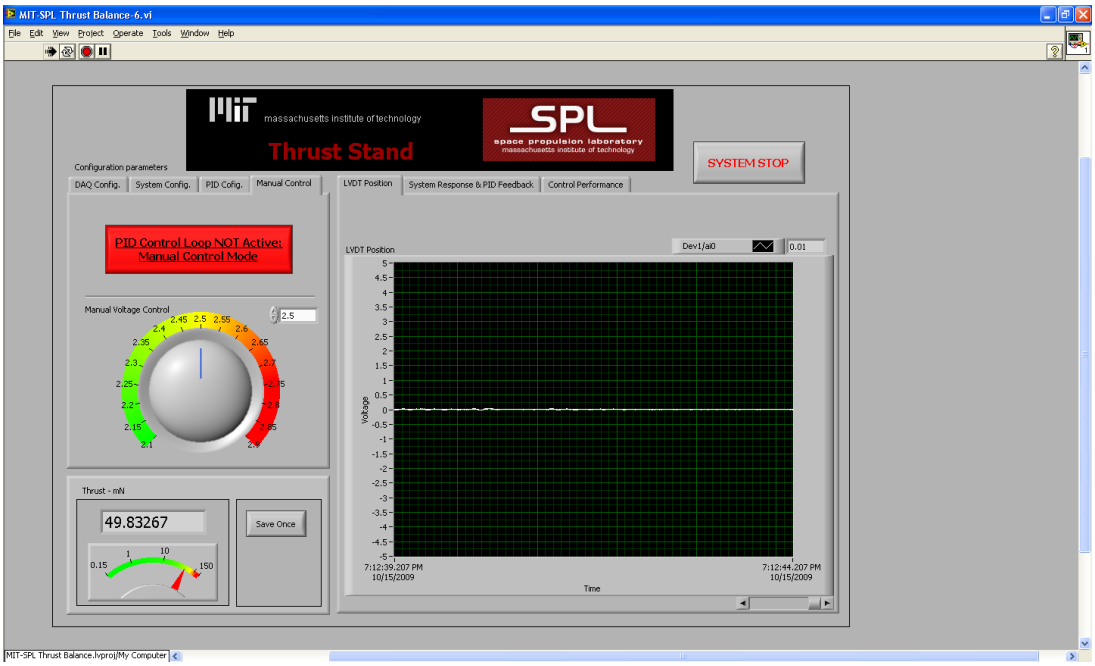

FIGURE 6.2-10: LVDT POSITION TAB

- Now go to the System Response & PID Feedback Tab. You will see a series of lines on this graph
    - The white line is the LVDT position.
    - The green line is the set point.
    - The red line is the power the PID software is commanding to the voice coil.
- The computer will work to match the white line with the green line.

6) Turn the PID control on (button should now be green). Allow the system to settle and reach steady state. Baseline readings of the thrust force should be taken at this point and subtracted from the data later.
7) Apply a force to the balance. First the white line which represents the LVDT signal will begin to move away from 0. Next, the red line (power to the voice coil) will begin to move away from zero as well (power being sent to the voice coil) and the LVDT signal (white line) will slowly move back to the green line. See figure below. Eventually, the system will reach steady state, with the red line offset from 0 by a certain amount (this is the thrust force) and the white line will sit on top of the green line. See Figure 6.2-11.

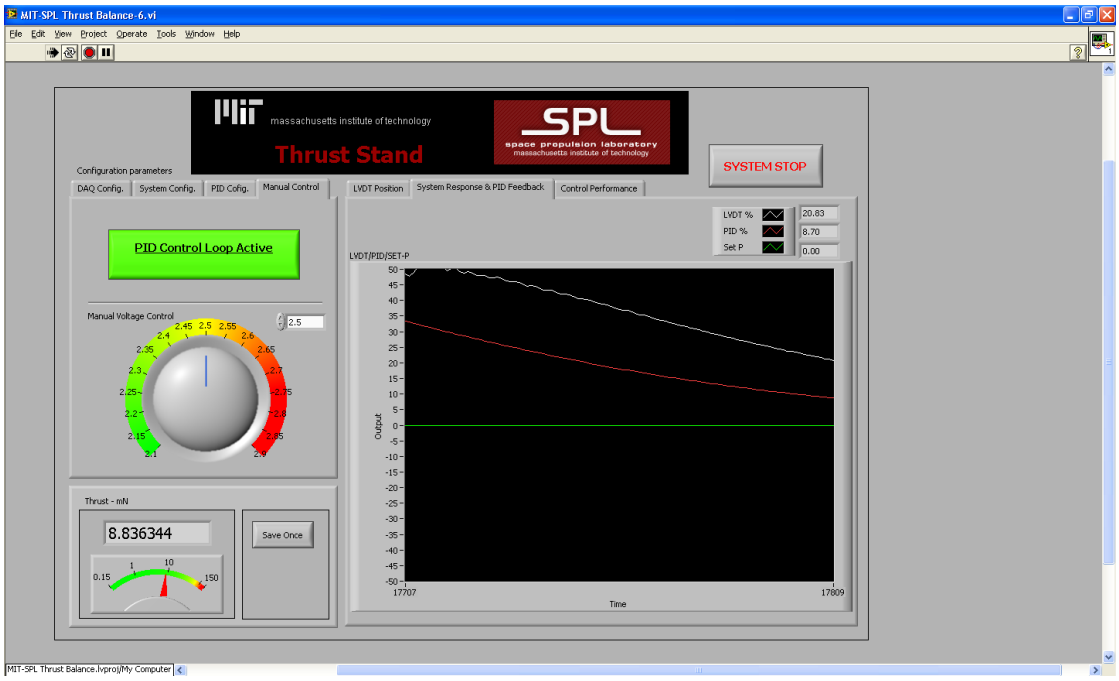

FIGURE 6.2-11: LVDT FORCE BALANCE

6.2.3 DCFT EFFICIENCY TESTING (K. CHOU)

As of the end of Spring 2010, the Propulsion Laboratory Team has completed the first round of data collection. Further testing will determine the accuracy of the first data set and obtain higher resolution information.

6.2.3.1 DATA ANALYSIS

After analyzing the first data set, correlations between the different state variables can be made. Of interest are the correlations between: anode power and thrust, anode power and efficiency, and thrust and efficiency. The main equation during this testing is:

$$\eta = \frac{F^2}{2P\dot{m}} \quad (1)$$

From the plot of anode power and thrust, a direct correlation can be made between the two variables.

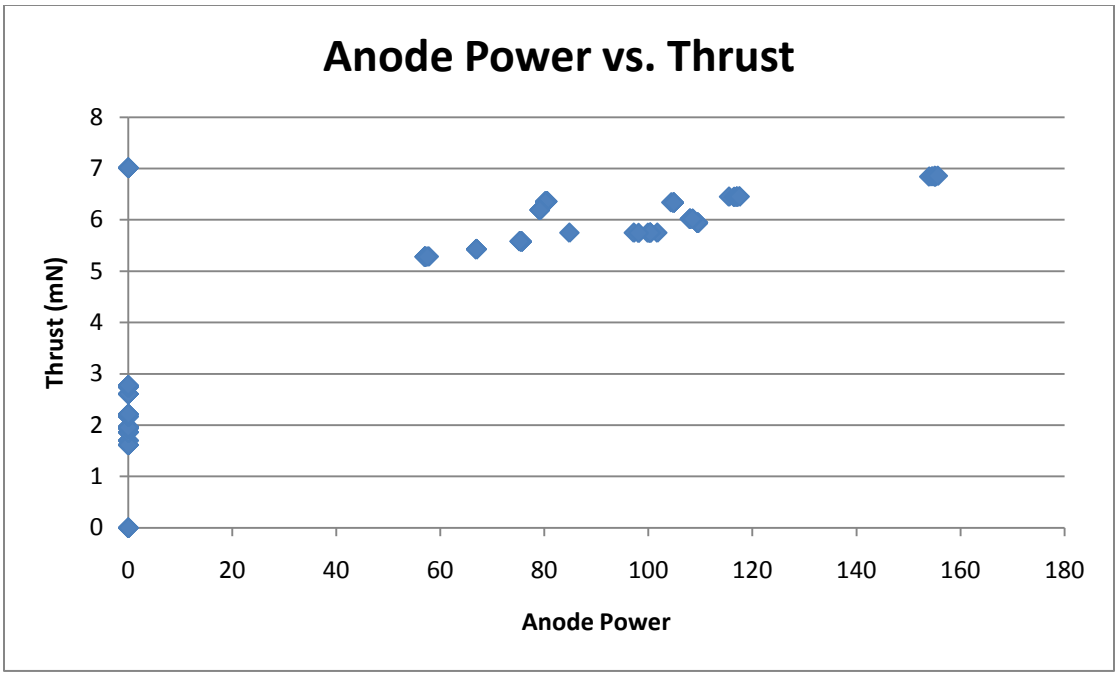

FIGURE 6.2-12: ANODE POWER VS. THRUST

Figure 6.2-12 shows that as the anode power increases, the thrust produced increases as well, as can be explained from Equation 1 if rearranged to solve for thrust:

$$F = \sqrt{2\eta P\dot{m}}$$

The next relation of importance is between anode power and efficiency. Looking at Equation 1, it can be determined that an increase in power will decrease efficiency. This is confirmed in Figure 6.2-13, shown below:

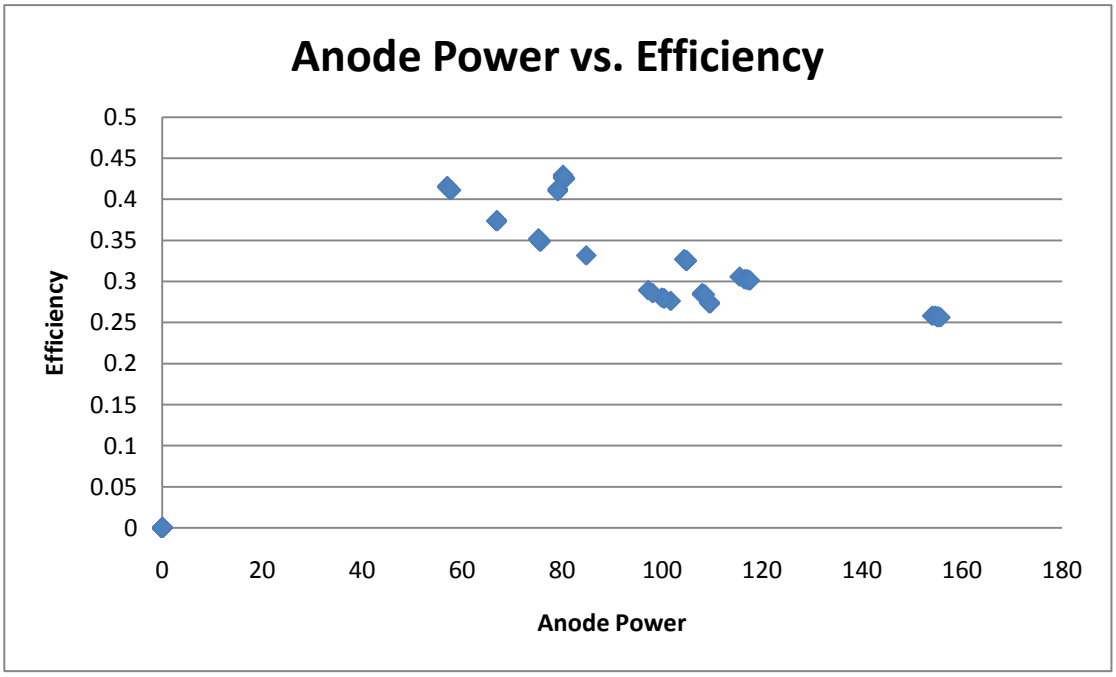

FIGURE 6.2-13: ANODE POWER VS. EFFICIENCY

Lastly, it is important to determine the relation between thrust and efficiency. It can be seen in Equation 1 that an increase in thrust will produce a decrease in efficiency.

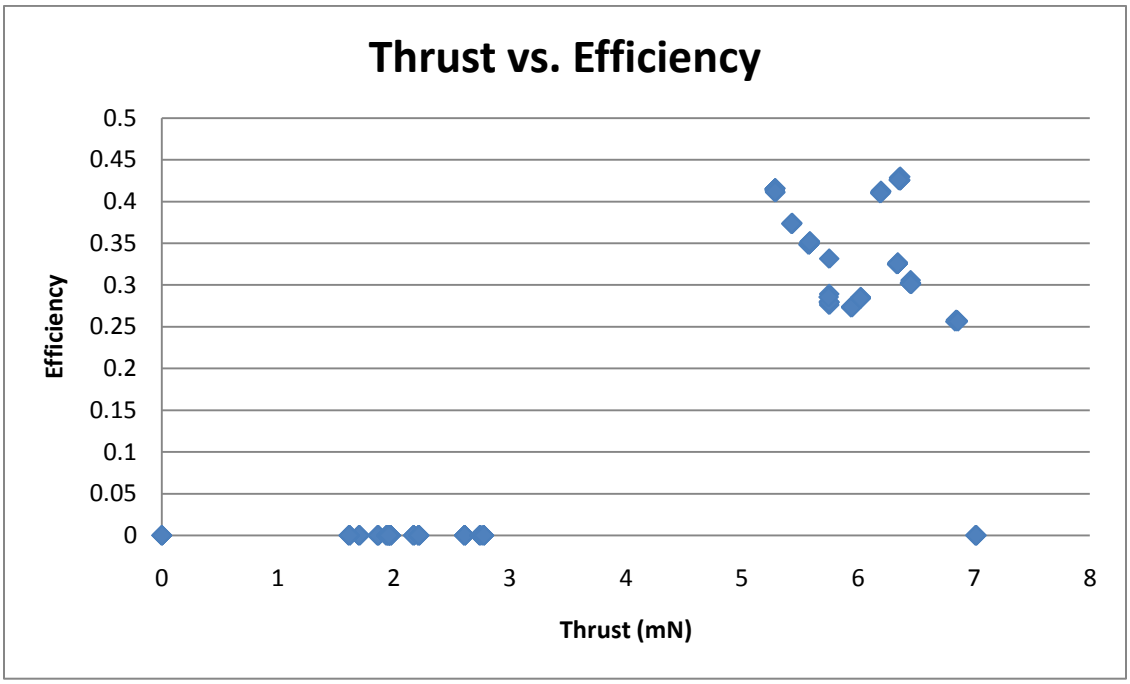

FIGURE 6.2-14: THRUST VS. EFFICIENCY

From Figure 6.2-14, it is difficult to determine this relation, but if the outliers at (6.197, 0.413) and (6.364, 0.426) are not taken into consideration, it can be seen that an increase in thrust will produce a decrease in efficiency.

Because anode power influences efficiency and thrust in opposite ways, it is crucial to determine how much thrust or efficiency to give up. If a large amount of power is provided, the DCFT will provide higher thrust but have lower efficiency. However, if a smaller amount of power is provided, the DCFT will have a lower thrust but higher efficiency.

Further DCFT testing will provide more data that allows for the determination of power levels with optimal thrust and efficiency. After this testing has been performed, DCFT testing with varying fuel mass flow rates will be executed in a similar manner to power level testing to determine the optimal fuel mass flow rate. With the information received from power and fuel mass flow rate testing, the power and fuel mass flow rate setting can be determined that allows for DCFT peak performance.

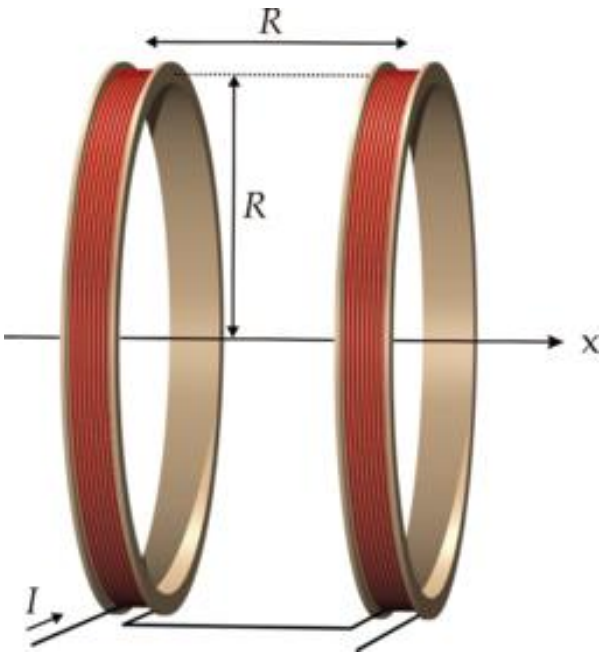

Characteristics of the coil are specified using the following field strength equation.

$$B = \left(\frac{4}{5}\right)^{3/2} \frac{\mu_0 n I}{R}$$

where

μ_0 is the permeability of free space 1.26 x 10-6 (Tm/A), n is the number of turns of wire in each coil, I is the current in A flowing through each coil and *R* is in meters

The magnetic field strength is desired to be about 10-100 times stronger than the earths magnetic field. Earths magnetic field ranges between 30 microteslas and 60 microteslas however a value of 50 microteslas was used for calculations. For reference 100 times the strength of the earths magnetic field would is about the strength of a refrigerator magnet.
Thus the need for specific values of current(I), number of turns(n), type of coil and cost thus became apparent to finalize a design.

To make this assessment I created a matlab script that would take the radius of the coil, current, field strength and wire gauge as inputs. It would then produce the number of turns needed, total length of each coil and power.

Below are some simple combinations explored, with a radius of 2.5 feet for the coil which gives an area of about 1.8241m^2 and a perimeter of 4.787 m.

TABLE 6.2-1: HELMHOLTS COIL PARAMETER TEST RESULTS 1

Strength Desired /Earth Mag Field	Earth Mag Field Strength / microteslas	Current / A	Wire Gauge	# of turns	Total length/km	Power/ Watts	Cost/~$ (from reliable vendor)
100	$3*10^{-5}$	10	11	305	1.75	724.39	-
100	$6*10^{-5}$	10	11	610	3.51	1448.8	-
100	$5*10^{-5}$	10	11	508	2.92	1207.3	-
10	**$5*10^{-5}$**	**5**	**14**	**102**	**0.58**	**120.97**	**474**
10	$5*10^{-5}$	2.5	17	203	1.17	121.3	-
10	$5*10^{-5}$	1.5	20	339	1.95	145.9	362
10	$5*10^{-5}$	1	21	508	2.92	122.6	-
10	$5*10^{-5}$	0.5	24	1017	5.84	122.98	550
10	$5*10^{-5}$	0.25	27	2034	11.68	123.29	-

Depending on the value of current used the optimal gauge of wire was used to reduce the amount of resistance in the coil.
The idea was to try and obtain the smallest amount of current and use greater values for voltage since the power supply is not greatly limited. Also costs of coils with a "-" value imply that the current vendor did not provide the gauge of wire specified. However the order of the cost may be estimated from the scenarios surrounding it. This may imply that our final choice may have to be edited in terms of gauge to ensure the vendor can provide them.

From the options covered, a Helmholtz coil of 5 A, 102 turns seems to be the most viable option.

Another set of calculations were performed after realizing the frame around the air bearing would put a dimensional limit on the coils radius. Thus a coil with a radius of 3 feet for the coil which gives an area of about 2.6268 m^2 and a perimeter of 5.745m

TABLE 6.2-2 – HELMHOLTZ COIL PARAMETER TEST RESULTS 2

Strength Desired /Earth Mag Field	Earth Mag Field Strength / microteslas	Current / A	Wire Gauge	# of turns	Total length/km	Power/ Watts	Cost/~$ (from reliable vendor)
10	$5*10^{-5}$	5	14	68	0.26	53.76	209
10	**$5*10^{-5}$**	**2.5**	**17**	**136**	**0.52**	**53.91**	-
10	$5*10^{-5}$	1.5	20	226	0.87	64.83	204
10	$5*10^{-5}$	1	21	339	1.30	54.51	-
10	$5*10^{-5}$	0.5	24	678	2.60	54.66	244
10	$5*10^{-5}$	0.25	27	1356	5.19	54.8	-

With these additional calculations we realize that reducing the radius of the coil tends to decrease a lot of the other costly variables. From the options in the second table a current of about 2.5 A, using a 17 gauge wire, with a total of 136 turns and a power rating of 53 watts seems to be a balance of both cost and yield.

The next stage for action in terms of specifications, is to consider our resources and judge what costs we can incur, and what voltages can be provided easily and safely. These will help finalize the specifications of the helmholtz coil.

Like any good process refining and checking achieved measures is very important. As such the code for optimization of parameters was revised. This time focus was given to current as the deciding factor. Together with the desired field strength all other parameters such as gauge, number of turns, total length of coil, total resistance, power and the actual field strength resultant could be calculated. Notably we will most likely be making use of a power supply plugged into a mains socket and thus a maximum power rating of about 120W would be applied. Also the power supply in question has an upper bound of 40V. Thus setting a unit current of 1.73 amps.

Using this methodology the following results were produced considering 0-12 Amps.

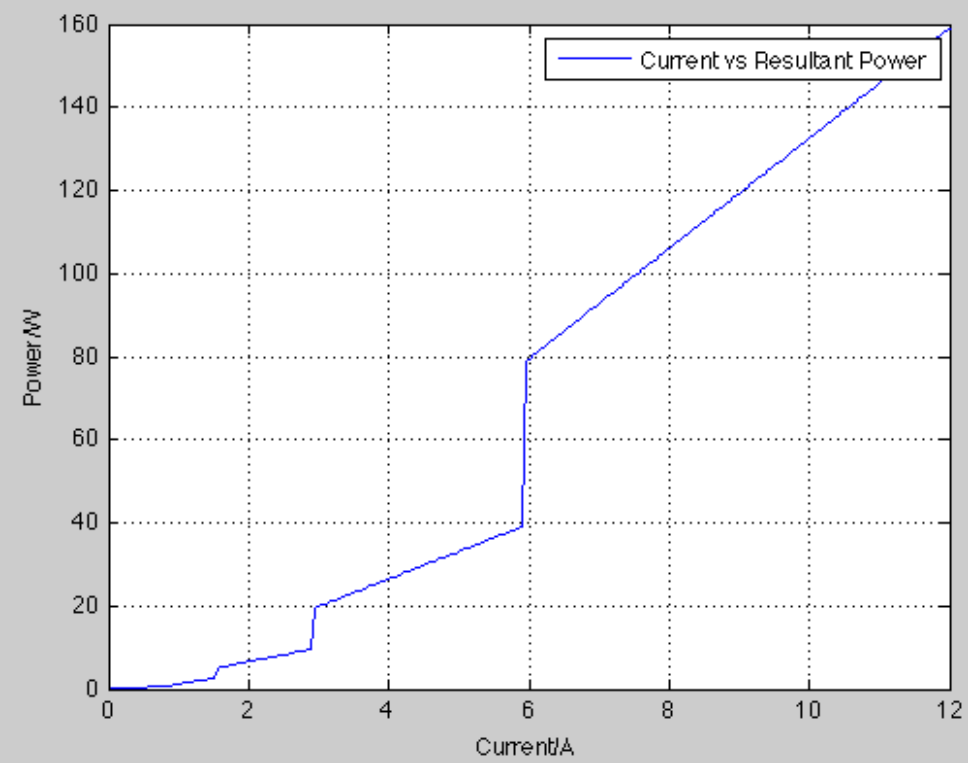

FIGURE 6.2-15: HELMHOLTS COIL PARAMETER OPTIMISATION: CURRENT VS POWER

Here we see that at the max power value the current is about 9A.

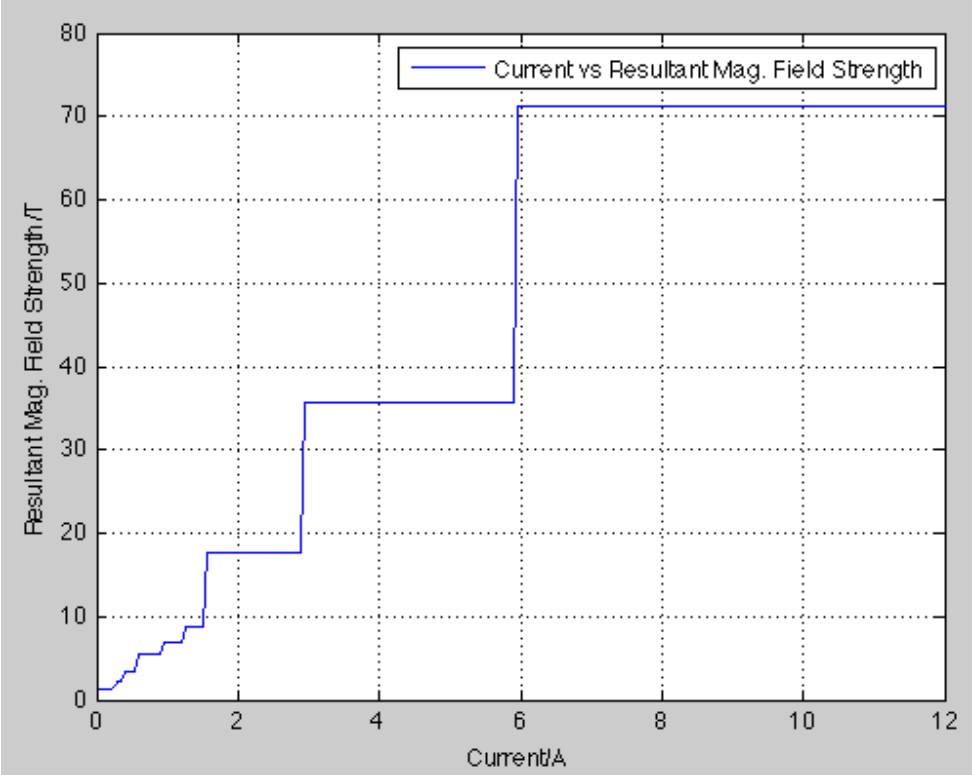

FIGURE 6.2-16: HELMHOLTS COIL PARAMETER OPTIMISATION: CURRENT VS ORDERS OF EARTH MAG FIELD

Interestingly we can see that the variation converges to a value of ~ 71 times the earths magnetic field at about 6A.

In my previous portfolio I presented 5A as a viable option. This gives 1016.9 turn, a total length of 5.8426km, a total resistance of 48.3886 ohms, a power reading of 33.0657W and a magnetic field strength ~ 60 times that of earths.

Similarly, a current of 1.7A gives 2991 turns, 17.1km, 285.4 ohms, 5.6056 W and 17.73 time the earth strength.

Given the results from the previous iterations and the cut off of true magnetic field strength 6amps may be a viable specification to consider when a higher field strength is desired. For the lower field strength roughly 1,5 amps should be sufficient.

Eventually it will be the ACS budget that will decide how much we can spend and thus how much wire can be purchased.

The following additional graphs may also provide insightfulness in deciding the final parameters.

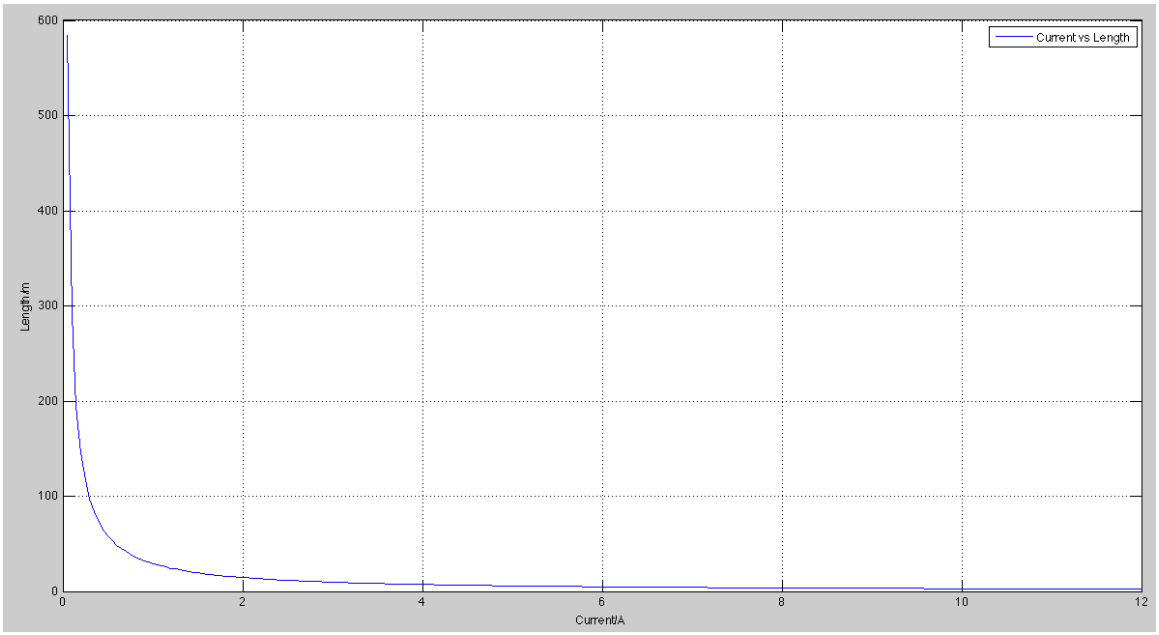

FIGURE 6.2-17: HELMHOLTS COIL PARAMETER OPTIMISATION: CURRENT VS LENGTH

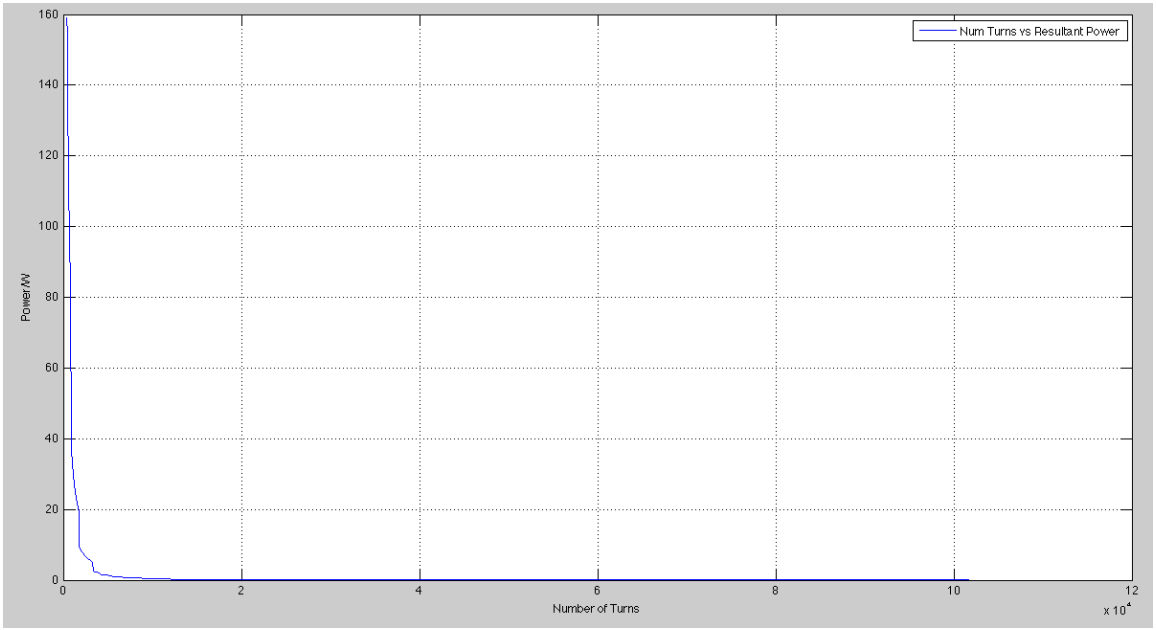

FIGURE 6.2-18: HELMHOLTS COIL PARAMETER OPTIMISATION: NUMBER OF TURNS VS POWER

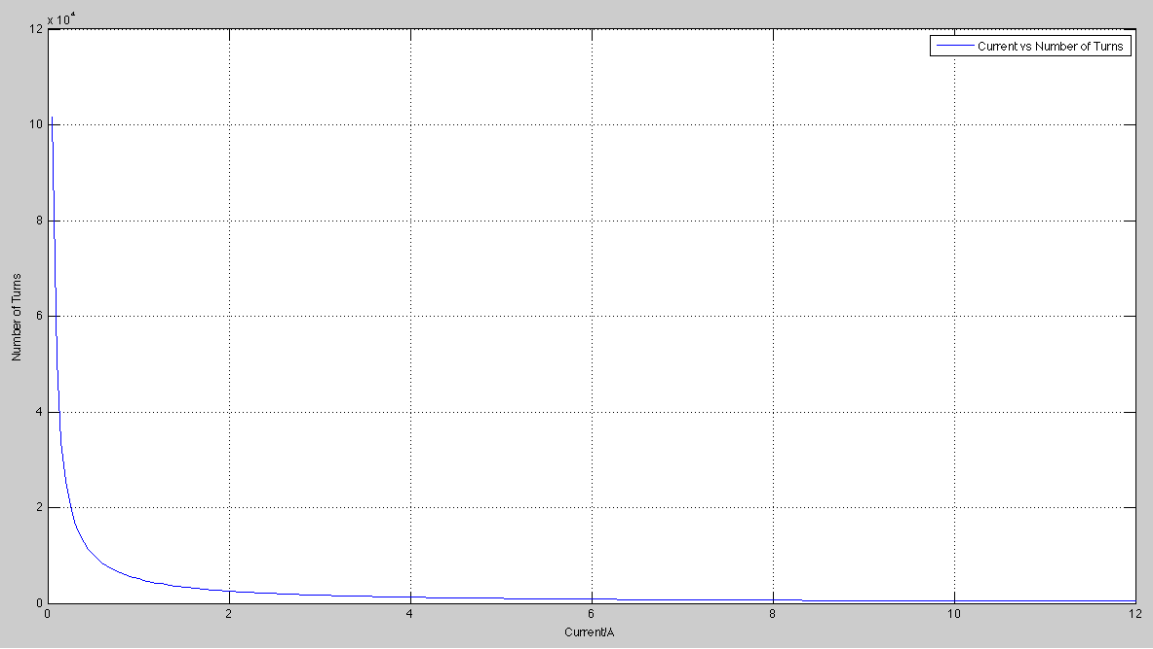

FIGURE 6.2-19: HELMHOLTS COIL PARAMETER OPTIMISATION: CURRENT VS NUMBER OF TURNS

Finally a table of results is presented below, allowing for simpler comparison.

TABLE 6.2-3: RESULTS

Current/A	Gauge/ AWG	#of Turns	Length of coil/ km	Resistance	Power/ Watts	Strength of Magnetic Field/EMG Strength
0.5	24	10169	58.43	4919.3	0.325	3.4991
1	21	5084.7	29.21	1226.5	1.304	7.017
1.5	20	3389.4	19.47	648.37	2.46	8.85
2	17	2542.3	14.6	242.6	6.59	17.73
2.5	17	2033.9	11.69	194.09	8.24	17.73
3	14	1694.9	9.74	80.65	19.84	35.58
3.5	14	1425.8	8.37	69.13	23.15	35.58
4	14	1271.2	7.3	60.49	26.45	35.58
4.5	14	1129.9	6.49	53.76	29.78	35.58
5	14	1016.9	5.84	48.38	33.06	35.58
5.5	14	924.84	5.31	43.99	36.37	35.58
6	11	847.44	4.868	20.12	79.515	71.287

The above values however are rather large in terms of length of coil. As such the ACS team will access the validity of the calculations before finalizing the specification.

Whiles this is being finalized it is possible to go ahead and consider the structure of the EMFS. Considering questions like, what will the coil be wound around; should the twin coils be connected and if so how; how will the coils be attached to the frame? The answer to all these questions will mark the final parameters needed to conclude on the EMFS design.

Construction Issues

I found it important and necessary to first explore possible issues of contention that may be faced before finalizing on a form and plan of construction.

Form & Coiling Issues

What kind of a form and structure should the final coil have? Considering that the coil is to be mounted around the air bearing and to the frame it may be a good idea to make it as small as possible and with some sort of the capability to be attached to leads from the frame.

Specifically what kind of material should be used to ensure the circle shape. Possible options were aluminum channels, plexy glass and no form assuming the wound coil is structurally stable. Note that these materials must be non-ferrous materials t avoid any interaction with the produced magnetic field.

Exploring the aluminum channel a feasible option would be the rings, as depicted below from - www.johnsonrollforming.com

Rings: Channel, Angle or Special Shapes
(as Illustrated)

Given the above, the question of how to go about effectively wounding the coil becomes apparent. Especially since the number of turns ranges on the order of 10^2. After some consideration and referencing, an easy and effective solution will be to just cut out a circular disk of ply wood larger than the needed 6 ft diameter. Bolts can then be placed along the circumference of the proper coil shape. The disk can then be placed on a base with a pin at the center, thus allowing the disk to spin and simultaneously wind the coil. Zip ties or any other locking snippets could be used to keep the collection of coils. This scenario saves time and allows for improved winding. However it assumes the coil is not heavily insulated.

Thermal Issues

Depending on the resistance produced by the wire and the time, we must consider whether there would be dire thermal consequences. That is the wire melting, or reaching high temperatures to significantly increase resistance. Particularly, the windings closest to the center since they will build up the most heat. We must thus then see what kind of thermal specification could be established to avoid this, such as not running the simulation for longer than a certain period. This will inevitably help to decide on which parameters to use.

A solution would be to make use of heavily insulated wire such as below

However this will result in a very bulky Helmholtz coils. The above design has less than 50 turns. The Helmholtz coil will have turns on the order of 10^2. Thus such heavy insulation may not be feasible since we want the coil to fit around the air bearing but within the frame. Also enamel coated wire may or may not do the job.

Taking all of this into consideration will effectively assist in parameter specification, as well as reducing the time spent in construction.

Earth Magnetic Field Simulator(EMFS) – Future Goals

Given current accomplishments the following are the goals ACS has with respect to the Helmholtz coil.

- Finalize specifications on coils based on cost and available resources
- Build Engineering Model
- Propose and build structure to mount to frame of air bearing
- Perform Tests

6.3 CODE (VARIOUS)

[The code may be found in Section 1.1 of the Fileshare as …]